

ПРИМЉЕНО: 28-04-2025			
Рад.јед.	б р о ј	Арх.шифра	Прилог
0801	664/1		

Наставном већу Института за физику Београд

Београд, 25.04.2025.

Предмет:

Молба за покретање поступка за реизбор у звање научни сарадник

С обзиром да испуњавам критеријуме прописане од стране Министарства просвете, науке и технолошког развоја за реизбор у звање Научни сарадник, молим Научно веће Института за физику у Београду да покрене поступак за мој реизбор у наведено звање.

У прилогу достављам:

1. Мишљење руководиоца пројекта са предлогом чланова комисије за реизбор у звање
2. Стручну биографију
3. Преглед научне активности
4. Елементе за квалитативну и квантитативну оцену научног доприноса са доказима
5. Списак објављених научних радова и њихове копије
6. Податке о цитираности
7. Диплома
8. Копије објављених радова и других публикација

Са поштовањем,

Марија Пуач

Др Марија Пуач

ПРИМЉЕНО:			
Рад.јед.	б р о ј	Датум	Прилог
0801-	004/2	28.04.2025	

Наставном већу Института за физику Београд

Београд, 25.04.2025.

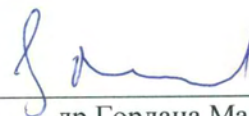
Предмет:**Мишљење руководиоца пројекта о реизбору др Марије Пуач у звање научни сарадник**

Др Марија Пуач је запослена у Лабораторији за неравнотежне процесе и примену плазме, у оквиру Националног центра изузетних вредности за неравнотежне процесе Института за физику у Београду. Др Пуач је ангажована у области пробоја у радиофреквенцијским пољима и њихово моделовање Монте Карло техником, што представља наставак рада којим је успешно одбранила докторску дисертацију. Додатно је активност проширила на изградњу модела еквивалентног електричног кола за диелектрична баријерна пражњења на атмосферском притиску, који одговарају експериментима развијеним у Лабораторији за неравнотежне процесе и примену плазме.

С обзиром да испуњава све предвиђене услове у складу са Правилником о поступку, начину вредновања и квантитативном исказивању научноистраживачких резултата истраживача МПНТР, сагласна сам са покретањем поступка за реизбор др Марије Пуач у звање научни сарадник.

За састав комисије за избор др Марије Пуач у звање научни сарадник предлажем:

- (1) др Драгана Марић, научни саветник, Институт за физику у Београду
- (2) др Никола Шкоро, научни саветник, Институт за физику у Београду
- (3) проф. Горан Попарић, редовни професор Физичког факултета Универзитета у Београду



др Гордана Маловић

научни саветник

Института за физику у Београду

Биографија др Марије Пуач

Др Марија Пуач (рођена Савић) је рођена 10.06.1985. године у Параћину.

Електротехнички факултет – модул Физичка електроника, смер Наноелектроника, оптоелектроника и ласерска техника уписала је 2004. године на Универзитету у Београду и завршила са просечном оценом 8,89. Дипломирала је 28.10.2008. године са темом „Анализа интегрисаних таласовода специфичне геометрије са шупљим језгром“ са оценом 10 под менторством проф. др Петра Матавуља.

Мастер академске студије уписала је на Електротехничком факултету Универзитета у Београду на смеру Наноелектроника, оптоелектроника и ласерска техника и завршила их 2009. године са просечном оценом 10. Мастер рад на тему „Монте Карло симулација пробоја у гасовима“ одбранила је 22.12.2009. године под менторством проф. др Зорана Љ. Петровића.

Докторске студије на Електротехничком факултету Универзитета у Београду – смер Наноелектроника и фотоника уписала је 2009. године. Докторску дисертацију под називом „Моделовање пробоја у гасовима Монте Карло техником“ одбранила је 10.07.2019. на Електротехничком факултету у Београду.

Марија Пуач је у радном односу од 30.10.2008. године у Институту за физику у Београду у Лабораторији за неравнотежне процесе и примену плазме под менторством проф. др Зорана Љ. Петровића и руководством др Гордане Маловић.

У звање научни сарадник изабрана је 20.12.2019. године. У периоду од 14.07.2020. до 13.07.2021. године је била на породилском одсуству.

Коаутор је тринаест научних радова објављених у међународним часописима као и већег броја радова на научним конференцијама, укључујући више уводних предавања.

Преглед научне активности др Марије Пуач

Кандидаткиња Марија Пуач се бави физиком јонизованих гасова и плазми у Лабораторији за неравнотежне процесе и примену плазме под руководством др Гордане Маловић у Институту за физику у Београду. Њен рад се може груписати у две целине.

Основно истраживање је нумеричког типа и односи се на моделовање пробоја у гасовима Монте Карло техником. Пробој у радиофреквенцијским (РФ) електричним пољима представља фокус истраживања и помоћу модела кандидаткиња је у потпуности објаснила физичку позадину РФ пробоја. Издвојени су физички процеси одговорни за формирање РФ плазми. Испитан је њихов стварни утицај на облик и положај напонске пробојне криве у U - p равни. Карактеристична особина РФ пробојних криви где једном пробојном притиску одговарају два пробојна напона уочена је и објашњена повећаним губицима на површинама током осциловања облака електрона између две напајане електроде.

Облик напонске пробојне криве испитиван је и у случају гасова са израженим процесом захвата електрона, као још један механизам губитка електрона. Кроз анализу функције расподеле енергије електрона објашњено је зашто је утицај захвата електрона јасно уочљив у десној грани напонске пробојне криве у кисеонику, док у левој не игра велику улогу.

Анализа је даље урађена за различите фреквенције, растојања између напајаних електрода, као и гасове. Модел РФ пробоја је употпуњен моделом површина електрода, са свим процесима на њиховим површинама, и укључивањем тешких честица и фотона. Као коначна примена израђеног модела, анализирани су смеше гасова: синтетички ваздух и атмосфера Марса.

Други део истраживања кандидаткиње је укључен у пројект „Atmospheric pressure plasmas operating in wide frequency range – a new tool for production of biologically relevant reactive species for applications in biomedicine - APPerTAin-BIOM“ програм Идеје Фонда за науку (2022 – 2024). У току трајања пројекта, али и након њега, област истраживања кандидаткиње је проширен на одређивање модела еквивалентног електричног кола за диелектрично баријерно прањење на атмосферском притиску.

Моделовањем измерених таласних облика струје и напона у присуству плазме и без ње, приликом диелектричног баријерног пражњења на атмосферском притиску, кандидаткиња је одредила еквивалентно електрично коло које описује електричне карактеристике експеримента. На основу кола се може одредити режим рада пражњења али и утицај мете (материјала) који се третира плазмом. Анализом кола и предате снаге може се одредити које карактеристике плазме, као и трајање третмана, су најбоље за конкретне случајеве.

Истраживачки рад и научни резултати које је до сада остварила др Марија Пуач могу се груписати у следеће теме:

- Развијање модела РФ пробоја и одговарајуће рачунарске симулације која описује све релевантне физичке процесе,
- Одређивање природе РФ пробоја; издвајање физичких процеса одговорних за пробој и квантификовање њиховог утицаја на одређене делове РФ напонске пробојне криве,
- Закон скалирања РФ пробојних напонских кривих,
- Квантификација утицаја материјала од ког су израђене електроде на облик РФ пробојне напонске криве,
- Утицај захвата електрона у гасу на РФ напонску пробојну криву, као последице природе молекула коришћеног гаса,
- Утицаја тешких честица, односно емисије секундарних електрона са површина електрода услед удара тешких честица, на формирање другог минимума на РФ напонској пробојној криви,
- Верификација развијеног модела његовом применом на смеше гасова као што су синтетички ваздух и атмосфера Марса,
- Анализа метода за одређивање брзина дрифта из измерених пробојних напонских кривих.
- Моделовање еквивалентног електричног кола за диелектрично баријерно пражњење на атмосферском притиску.

Елементи за квалитативну оцену научног доприноса

1. Квалитет научних резултата

1.1 Значај научних резултата

Најзначајнији рад др Марије Пуач је:

Marija Puac, Antonije Đorđević and Zoran Lj Petrovic: *Monte Carlo simulation of RF breakdown in oxygen - the role of attachment* - The European Physical Journal D (2020), Vol. 74, 72
M23, DOI: <https://doi.org/10.1140/epjd/e2020-100526-1>, IF(2020) = 1.425

У наведеном раду кандидаткиња је испитивала утицај захвата електрона на пробојни напон радиофреквенцијског пражњења у кисеонику при фреквенцији од 13,56 MHz. Користила је код базиран на Монте Карло техници који је модификовала тако да укључује процес захвата електрона, као један од механизма губитка електрона. Анализирана је пробојна напонска крива, која је поређена са доступним експерименталним резултатом.

Да би се одредио утицај захвата електрона на пробојни напон анализирани су и временски разложене просторне расподеле концентрације и средње енергије електрона, еластичних судара, јонизације и захвата електрона. Уочено је да захват електрона има значајан утицај на вишим притисцима, десној грани пробојне криве, што води повећању пробојног напона.

Да би одредила разлог већег утицаја захвата електрона на десну грану пробојне криве, кандидаткиња је посматрала функције расподеле енергије електрона у тачкама пробоја дуж криве. Имајући на уму да је максимум пресека за процес захвата електрона у судару две честице на енергији од око 6,6 eV, и посматрајући функције расподеле енергије електрона, може се закључити да на већим притисцима постоји значајније преклапање тог максимума са средњом енергијом електронског облака, самим тим и процес захвата електрона је учесталији на већим притисцима (његов утицај је већи). Што се тиче процеса дисоцијативног захвата електрона, његов утицај је мали на пробојни напон дуж целе пробојне криве јер пресека има максимум на ниским енергијама.

У поменутом раду представљено је и поређење пробојних кривих кисеоника и аргона, као два представника гаса са израженим процесима захвата електрона и без њих (аргон).

1.2 Параметри квалитета часописа

Кандидаткиња др Марија Пуач је објавила укупно 2 рада у међународним часописима и то:

- 1 рад у међународном часопису изузетних вредности (M21) Plasma Sources Science and Technology (IF=3,3 SNIP= 1,373),
- 1 рад у истакнутом међународном часопису (M23) The European Physical Journal D (IF= 1,425 SNIP=0,64),
Укупан импакт фактор објављених радова др Марије Пуач је 4,725.

Додатни библиометријски показатељи према упутству о начину писања извештаја о изборима у звања које је усвојио Матични научни одбор за физику су:

	ИФ	М	SNIP
Укупно	4,725	11	2,013
Усредњено по чланку	2,3625	5,5	1,0065
Усредњено по аутору	1,135	2,6	0,4879

1.3 Подаци о цитираности научних радова кандидаткиње

Према бази Google Scholar Citations радови др Марије Пуач су цитирани 213 пута. Према овој бази Хиршов индекс кандидаткиње је 7 а i10 индекс је 7. Према бази Web of Science радови др Марије Пуач су цитирани 148 пут. Према овој бази Хиршов индекс кандидаткиње је 7.

2. Нормирање броја коауторских радова

Према Правилнику о стицању истраживачких и научних звања, радови др Марије Пуач се признају са пуним бројем поена.

Број коаутора на раду из категорије M23 је 3. Рад се бави нумеричким рачунарским симулацијама где се са пуном тежином признаје број коаутора до 5. Рад из категорије M21 (5 коаутора) се бави експерименталним мерењима и моделовањем, где се пун број поена прихвата до 7 коаутора. Укупан нормиран број бодова је непромењен и износи 19,5 што је више од захтеваних 16 бодова за реизбор у звање научног сарадника.

3. Учешће на пројектима МПНТР

Др Марија Пуач је учествовала на следећим пројектима Министарства просвете, науке и технолошког развоја:

2008-2010: „Физичке основе примене неравнотежних плазми у нанотехнологијама и третманима материјала“ (141025),

2010-2019: „Фундаментални процеси и примене транспорта честица у неравнотежним плазмама, траповима и наноструктурама“ ОН171037,

2010-2019: „Примене нискотемпературних плазми у биомедицини, заштити човекове околине и нанотехнологијама“ (ИИИ41011).

2021-2024: „Atmospheric pressure plasmas operating in wide frequency range – a new tool for production of biologically relevant reactive species for applications in biomedicine - APPerTAin-BIOM“ програм Идеје Фонда за науку.

2021-2023: „Карактеризација радиофреквентног гасног пражњења које се примењује за третмане површина“ – пројекат билатералне сарадње између Републике Србије и Републике Мађарске.

4. Активности у научним и научно-стручним друштвима

4.1. Рецензије научних радова

Др Марија Пуач је била рецензент рада у часопису Plasma Sources Science and Technologies.

4.2. Предавања по позиву на међународним конференцијама

Др Марија Пуач је одржала 2 предавања по позиву:

Progress report на међународном скупу 31th Summer School and International Symposium on the Physics of Ionized Gases (SPIG 2022) 5-9 септембар 2022, Београд, Србија.

Предавање по позиву на међународном скупу XXVI Europhysics Conference on the Atomic and Molecular Physics of Ionized Gases (ESCAMPIG XXVI), 9-13 јул 2024, Брно, Чешка.

5. Утицај научних резултата

Утицај научних резултата се огледа у броју цитата који су наведени у тачки 1.3. овог одељка, а значај резултата је описан у тачки 1.

6. Конкретан допринос кандидата у реализацији радова у научним центрима у земљи и иностранству

Кандидаткиња је научну активност реализовала у Институту за физику у Београду, у Лабораторији за неравнотежне процесе и примену плазме, а у сарадњи са Електротехничким факултетом Универзитета у Београду и Српском академијом наука и уметности.

Бавила се моделовањем електричног пробоја у гасовима, са посебним фокусом на пробој у присуству радиофреквенцијског електричног поља. У овој области рада је имала кључну улогу у свим фазама истраживања – од дефинисања теме и разматрања критичних проблема, развоја и прилагођавања модела и детаља нумеричких симулација, обраде и анализе резултата, до писања радова и комуникације са уредницима и рецензентима часописа.

Током истраживања диелектричних баријерних пражњења на атмосферском притиску, у склопу пројекта APPerTAin-BIOM програм ИДЕЈЕ Фонда за науку Републике Србије, самостално је водила и успешно реализовала рад на теми моделовања еквивалентног електричног кола пражњења. У свим фазама припреме, писања и објављивања радова, била је одговорна за овај део истраживања.

Током свог рада, др Марија Пуач је развила све елементе потребне да јој омогуће самосталан научни рад у даљим фазама рада и ту је показала завидан ниво самосталности и способности за научни рад.

Елементи за квантитативну оцену научног доприноса др Марије Пуач

Остварени М-бодови по категоријама публикација

Категорија	М-бодова по публикацији	Број публикација	Укупно М бодова	Нормирани број М бодова
М21	8	1	8	8
М23	3	1	3	3
М31	3.5	1	3.5	3.5
М32	1.5	1	1.5	1.5
М34	0.5	5	2.5	2.5

Поређење оствареног броја М-бодова са минималним условима потребним за избор у звање научног сарадника

		Остварено	Остварено (нормирано*)
Укупно	16	19.5	19.5
М10+М20+М31+М32+М33+М41+М42	10	19.5	19.5
М11+М12+М21+М22+М23	6	11	11

* Нормирање броја бодова извршено је у складу са Прилогом 1 Правилника о поступање и начину вредновања и квантитативном исказивању научно-истраживачких резултата истраживача.

Списак публикација др Марије (Савић) Пуач од избора у звање научни сарадник

Рад у међународним часописима (M21):

1. Nikola Škoro, Kinga Kutasi, **Marija Puač**, Zoran Lj Petrović, Nevena Puač: Effect of target material on electrical properties of a two-electrode dielectric barrier helium plasma jet – Plasma Sources Sciences and Technology (2024), **33** 045015
DOI 10.1088/1361-6595/ad3d83

Рад у међународним часописима (M23):

1. **Marija Puač**, Antonije Dordevic and Zoran Lj Petrovic: Monte Carlo simulation of RF breakdown in oxygen - the role of attachment - The European Physical Journal D (2020), Vol. 74, pp. 72
DOI: <https://doi.org/10.1140/epjd/e2020-100526-1>

Предавање по позиву са међународног скупа штампано у изводу (M31):

1. **Marija Puač** and Zoran Lj Petrović: Nature of radio-frequency breakdown in argon viewed through electron energy distribution functions modeled by Monte Carlo technique – XXVI Europhysics Conference on the Atomic and Molecular Physics of Ionized Gases (ESCAMPIG XXVI), Brno, Czech Republic, July 9-13, 2024. pp. 12-15.

Предавање по позиву са међународног скупа штампано у изводу (M32):

1. **Marija Puač**, Zoran Lj Petrović: Modeling of radio-frequency breakdown by Monte Carlo technique – 31st Summer School and International Symposium on the Physics of Ionized Gases (SPIG 2022), Publ. Astron.Obs. Belgrade, 5-9 September, 2022. Serbia, pp.168
ISSN 0373-3742

Саопштење са међународног скупа штампано у целини (M33):

1. Jelena Marjanović, Dragana Marić, **Marija Puač**, Antonije Đorđević, Zoran Lj Petrović: RF breakdown in argon at low-pressures: Experiment and modelling – 32nd Summer School and International Symposium on the Physics of Ionized Gases (SPIG 2024), Publ. Astron.Obs. Belgrade No. 103, August 26-30, 2024, Belgrade Serbia, pp.138-141
ISSN 0373-3742

Саопштење са међународног скупа штампано у изводу (M34):

1. **Marija Puač**, Nikola Škoro, Kinga Kutasi, Nevena Puač: The equivalent electrical circuit for describing the dielectric barrier discharge plasma jet - 10th International Conference on Plasma Medicine & 9th International Workshop on Plasma for Cancer Treatment (ICPM&IWPCT), 8-13 September 2024, Portorož, Slovenia, Thu-P-16, pp 186
2. **M. Puač**, N. Skoro, K. Kutasi, N. Puač: Equivalent electrical circuit modeling of He dielectric barrier discharge plasma jet – Plasma Thin Film International Union Meeting (PLATHINIUM), 11-15 September 2023. Antibes, France. PLATH00195
3. A. Derzsi, B. Horvath, K. Kutasi, K. Spasić, **M. Puač**, N. Puač and N. Škoro: Properties of low-pressure rf discharges suitable for treatment of absorbants – XXIV Symposium on Application of Plasma Processes and XIII EU-Japan Symposium on Plasma Processing, 27 Jan – 1 Feb, 2023, Štrbske Pleso, Slovakia
https://neon.dpp.fmph.uniba.sk/sapp/download/SAPP_XXIV_JSPP_XIII_Book_of_Contributed_Papers.pdf
4. D. Marić, **M. Puač**, A. Đorđević, J. Marjanović, G. Malović, Z. Lj. Petrović; Breakdown in rf and dc fields; 73rd Annual Gaseous Electronics Virtual Conference (GEC); October, 5-9. 2020, San Diego, USA, UR2.00005, Bulletin of the American Physical Society (2020)
<https://meetings.aps.org/Meeting/GEC20/Session/UR2.5>
5. Zoran Lj Petrović, **Marija Puač**, Antonije Đorđević: Modeling of RF breakdown in different atmospheres – 72nd Annual Gaseous Electronics Conference, American Physical Society, College Station, Texas, USA, October 28 – November 1, 2019, DT3.00004,
<http://meetings.aps.org/Meeting/GEC19/Session/DT3.4>

Списак публикација др Марије (Савић) Пуач

ПРЕ избора у звање научни сарадник

Рад у тематском зборнику међународног значаја (M14):

1. Zoran Lj Petrović, Jelena Sivoš, **Marija Savić**, Nikola Škoro, Marija Radmilović-Radjenović, Saša Gocić, Dragana Marić: New phenomenology of gas breakdown in DC and RF fields – *Journal of Physics: Conference Series* (2014), Vol. 514, pp. 012043.
DOI: 10.1088/1742-6596/514/1/012043
ISBN 978-86-7025-782-5

Рад у међународним часописима изузетних вредности (M21a):

1. **Marija Puač**, Dragana Marić, Marija Radmilović-Radjenović, Milovan Šuvakov and Zoran Lj Petrović: Monte Carlo modeling of radio-frequency breakdown in argon – *Plasma Sources Sci. Technol.* (2018), Vol. 27, pp. 075013.
ИФ 3.939 DOI: 10.1088/1361-6595/aacc0c
ISSN 0963-0252

Рад у врхунским међународним часописима (M21):

1. Zoran Lj Petrović, Dragana Marić, **Marija Savić**, Srđan Marjanović, Saša Dujko, Gordana Malović: Using swarm models as an exact representation of ionized gases – *Plasma Process Polymers* (2016), Vol. 14, pp. 1600124, број хетероцитата 6.
ИФ 2.846 DOI: 10.1002/ppap.201600124
ISSN 1612-8850

Рад у истакнутим међународним часописима (M22):

1. Dragana Marić, **Marija Savić**, Jelena Sivoš, Nikola Škoro, Marija Radmilović-Radjenović, Gordana Malović and Zoran Lj. Petrović: Gas breakdown and secondary electron yields: – *Eur. Phys. J. D* (2014), Vol. 68, pp. 155, број хетероцитата 32.
ИФ 1.240 DOI: 10.1140/epjd/e2014-50090-x
ISSN 1434-6060

2. **M. Savić**, M. Radmilović-Radjenović, M. Šuvakov, S. Marjanović, D. Marić and Z. Lj. Petrović: On Explanation of the Double-Valued Paschen-Like Curve for RF Breakdown in argon – *IEEE Trans. Plasma Sci.* (2011), Vol. 39, pp. 2556-2557, број хетероцитата 10.
ИФ 1.174 DOI: 10.1109/TPS.2011.2159244
ISSN 0093-3813

3. Srđan Marjanović, Milovan Šuvakov, Ana Banković, **Marija Savić**, Gordana Malović, Stephen J. Buckman, and Zoran Lj. Petrović: Numerical Modeling of Thermalization of Positrons in Gas-Filled Surko Traps – *IEEE Trans. Plasma Sci.* (2011), Vol. 39, pp. 2614-2615, број хетероцитата 10.
ИФ 1.174 DOI: 10.1109/TPS.2011.2159129
ISSN 0093-3813

Рад у међународним часописима (M23):

1. Marija Radmilović-Radjenović, Branislav Radjenović, **Marija Savić**: Microwave field strength computing for the resonator designs and filters – Acta Physica Polonica A (2016), Vol 129, pp. 289-292.

ИФ 0.469 DOI: 10.12693/AphysPolA.129.289

ISSN 0587-4246

2. Š. Matejčik, M. Klas, B. Radjenović, M. Durian, **M. Savić** and M. Radmilović-Radjenović: The Role of the Field Emission Effect in the Breakdown Mechanism of Direct-Current Helium Discharges in Micrometer Gaps – Contrib. Plasma Phys. (2013), Vol. 53, pp. 573-579, број хетероцитата 4.

ИФ 0.983 DOI: 10.1002/ctpp.201300032

ISSN 0863-1042

3. M. Radmilović-Radjenović, B. Radjenović and **M. Savić**: The surface charging effects in three-dimensional simulation of the profiles of plasma-etched nanostructures – International Journal of Numerical Modelling: Electronic Networks, Devices and Fields (2011), Vol. 24, pp. 535-544, број хетероцитата 5.

ИФ 0.600 DOI: 10.1002/jnm.798

ISSN 0894-3370

4. A. Bojarov, M. Radmilović-Radjenović and **M. Savić**: Influence of the secondary electron emission on the characteristics of radio frequency plasmas – Hemijska Industrija (2011), Vol. 65, pp. 1-8.

ИФ 0.205 DOI: 10.2298/HEMIND100810063B

ISSN 0367-598X

5. **Marija B. Savić**, Marija Radmilović-Radenović: Modelovanje proboja u gasovima na niskim pritiscima Monte Karlo tehnikom (Gas discharges modeling by Monte Carlo technique) – Hemijska Industrija (2010), Vol. 64, pp. 171-175.

ИФ 0.137 DOI: 10.2298/HEMIND091221022S

ISSN 0367-598X

6. Marija Radmilović-Radjenović, Branislav Radjenović, **Marija Savić**: Breakdown phenomena in water vapor microdischarges – Acta Physica Polonica A (2010), Vol. 117, pp. 752-755.

ИФ 0.467 DOI: 10.12693/APhysPolA.117.752

ISSN 0587-4246

Предавање по позиву са међународног скупа штампано у изводу (M32):

1. Zoran Lj Petrović, Saša Dujko, Dragana Marić, Gordana Malović, Nevena Puač, Danko Bošnjaković, Olivera Šašić, **Marija Puač**, Jelena Sivoš, Milovan Šuvakov and Nikola Škoro: Non-Equilibrium in Ionized Gases Determined by Charge Particle Collisions with Molecules – POSMOL 2019, 18-21 July 2019, Belgrade, Serbia.

ISBN 978-86-7025-819-8

2. Zoran Lj Petrović, Antonije Djordjević, **Marija Puač**, Jana Petrović, Jelena Sivoš, Gordana Malović, Dragana Marić: Measurements and simulations of RF breakdown in gases – 7th

International Conference on Advanced Plasma Technologies, Plasmadis Ltd, Teslova ulica 30, 1000 Ljubljana, Slovenia, 24th February – 1st March 2019. Hue, Vietnam
ISBN 978-961-290-061-8

3. **Marija Puač**, Dragana Marić, Zoran Lj Petrović: The effect of attachment on rf breakdown – XXII Symposium on Application of Plasma Processes and XI EU-Japan Symposium on Plasma Processing, 18-24 January 2019, Štrbske Pleso, Slovakia.

4. Zoran Petrović, Antonije Djordjević, Jana Petrović, Jelena Sivoš, **Marija Puač**, Gordana Malović, Dragana Marić: RF Breakdown as a Swarm Experiment – 82nd IUVSTA Workshop, Osaka University, Japan, Bankoku Shinryokan, Okinawa, Japan, 4. - 7. Dec, 2017, pp. O2

5. Zoran Lj Petrović, Srdjan Marjanović, **Marija Savić**, Saša Dujko, Ilija Simonović, Dragana Marić: Transport theory as a foundation of nonequilibrium plasma models – 81st IUVSTA Workshop on Response of Biological Materials to Plasma Treated Medium, 12-16. March 2017, Slovenia, pp. 22-23
ISBN 978-961-285-628-1

6. Saša Dujko, Gordana Malović, Dragana Marić, Srdjan Marjanović, Zoran Lj Petrović, Marija Radmilović-Radjenović, **Marija Savić**, Ilija Adžić, Antonije Djordjević: Avalanches of electrons and positrons in Atmospheres of Planets and Satellites of the Solar System: Basic Phenomenology and Application to Gas Breakdown in DC and RF Fields – National Symposium on Plasma Science and Technology & International Conference on Plasma Science and Technology (PLASMA 2014), Mahatma Gandhi University, 8-11. Dec.2014. India, pp. 18.

7. Zoran Lj Petrović, Saša Dujko, Jasmina Mirić, Danko Bošnjaković, Ana Banković, Srdjan Marjanović, Dragana Marić, Jelena Sivoš, Nikola Škoro, **Marija Savić**, Olivera Šašić, Gordana Malović: Cross Sections for Scattering of Electrons and Positrons in Modeling of Ionized Gases and Non-Equilibrium Plasmas – International Symposium on Non-equilibrium Plasma and Complex-System Sciences (IS-NPCS), Osaka University, Icho Kaikan, Osaka, Japan, 26. - 28. Feb, 2014.

8. Z. Lj. Petrović, M. Radmilović-Radjenović, **M. Savić**, D. Marić, M. Šuvakov, N. Škoro and S. Dujko: Basic phenomenology and experimental techniques for gas breakdown from DC to RF and from few cm to micrometers – High Frequency Gas Breakdown Workshop Laboratoire de Physique des Plasmas, Ecole Polytechnique, 91128 Palaiseau, France, 4. Oct. 2010 France, pp. 4

9. Marija Radmilović-Radjenović, Zoran Lj Petrović, **Marija Savić**, Milovan Šuvakov: Modelling of a breakdown phenomena in radio-frequency discharges in micro gaps, 6th International Workshop on Microplasmas – 6th International Workshop on Microplasmas, CNRS and Universite Parys-Sud, Orsay, France, 3. - 6. Apr. 2011, pp. 33

10. Branislav Radjenović, Marija Radmilović-Radjenović, **Marija Savić**: Two-dimensional simulations of the microhollow cathode discharges in argon at atmospheric pressures – VI International Workshop on Microplasmas, Laboratoire de Physique des Gaz et des Plasmas CNRS& University of Paris-Sud, Orsay, France, 3. - 6. Apr, 2011, pp. 94-94

11. Zoran Lj Petrović, Jelena Sivoš, **Marija Savić**, Nikola Škoro, Marija Radmilović-Radjenović, Dragana Marić: New phenomenology in description of Townsend discharges and gas breakdown: from standard size to micro discharges – The 4th International Conference on Plasma Nanotechnology and Science (IC-PLANTS), Plasma Nanotechnology Research Center, Nagoya University, Gifu, Japan, 10. - 12. Mar, 2011, pp. I-07_1 - I-07_2.

12. D. Marić, **M. Savić**, S. Marjanović, N. Škoro, M. Šuvakov, M. Radmilović-Radjenović, G. Malović and Zoran Lj. Petrović: Plasma breakdown: Experiments and simulation – 38th EPS Conference on Plasma Physics, European Physical Society & Institute for Magnetic Fusion Research, 27. 06. - 01. 07. 2011. Strasbourg, France, pp. I4.316

Саопштење са међународног скупа штампано у целини (M33):

1. **Marija Puač**, Zoran Lj Petrović: Modeling of radio-frequency breakdown by Monte Carlo technique, 22nd International Conference on Gas Discharges and their Applications, 2nd to 7th September 2018. Novi Sad, Serbian Academy of Science and Arts, pp. 335-338.

2. **Marija Puač**, Dragana Marić, Zoran Lj Petrović: Electron energy distribution functions in a radio-frequency argon discharge - Monte Carlo simulations -29th Summer School and International Symposium on the Physics of Ionized Gases, University of Belgrade, Faculty of Physics, Serbia

Belgrade, Serbia, 22. Aug - 1. Sep, 2018, pp. 218-221.

ISSN 978-86-7306-146-7

3. **Marija Savić**, Dragana Marić, Zoran Lj Petrović: Monte Carlo simulation of radio-frequency breakdown in air and oxygen – 28th Summer School and International Symposium on the Physics of Ionized Gases, University of Belgrade, Faculty of Physics, Serbia

Belgrade, Serbia, 29. Aug - 2. Sep, 2016, pp. 312-315.

ISSN 978-86-84539-14-6

4. **Marija Savić**, Marija Radmilović-Radjenović, Milovan Šuvakov, Zoran Lj Petrović: Modeling of the radio frequency breakdown Paschen like curves by Monte Carlo technique –

27th Summer School and International Symposium on the Physics of Ionized Gases (SPIG 2014), Institute of Physics, Belgrade, 26.-29. Aug. 2014. Serbia, pp. 411-414

ISSN 978-86-7762-600-6

5. **Marija Savić**, Marija Radmilović-Radjenović, Milovan Šuvakov, Dragana Marić, Zoran Lj Petrović: Monte Carlo simulation of radio-frequency breakdown in argon – 20th International

Conference on Gas Discharges and their Applications, Orleans, France, 6.-11. Jul 2014, pp. 28511, sciencesconf.org:gd2014:28511

6. **Marija Savić**, Marija Radmilović-Radjenović, Milovan Šuvakov, Zoran Lj Petrović: The influence of the surface effects on argon radio-frequency discharge characteristics –3rd National Conference on Electronic, Atomic, Molecular and Photonic Physics, University of Belgrade, Faculty of Physics, Serbia, 25. - 25. Aug, 2013, pp. 25-28

ISBN 978-86-84539-10-8

7. **Marija Savić**, Marija Radmilović-Radjenović, Branislav Radjenović: Theoretical Predictions of the Microwave Breakdown Field – 26th Summer School and International

Symposium on the Physics of Ionized Gases, University of Novi Sad, Zrenjanin, Serbia, 27. - 31. Aug, 2012, pp. 325-328

8. **Marija Savić**, Marija Radmilović-Radjenović, Dragana Marić, Milovan Šuvakov, Zoran Lj Petrović: Monte Carlo simulations of RF breakdown – 26th Summer School and International Symposium on the Physics of Ionized Gases, University of Novi Sad, Zrenjanin, Serbia, 27. - 31. Aug, 2012, pp. 329-332

9. **Marija Savić**, Marija Radmilović-Radjenović, Milovan Šuvakov, Zoran Lj Petrović: Modeling of breakdown behavior in radio-frequency argon discharges – International Conference on Advanced Plasma, Slovenian Society for Vacuum Technique, Strunjan, Slovenia, 9. - 13. Sep, 2011, pp. 144-147

10. **Marija Savić**, Marija Radmilović-Radjenović, Milovan Šuvakov, Zoran Lj Petrović: The breakdown voltage curves and spatial profiles of ionization rates in argon rf discharges – 30th International Conference on Phenomena in Ionized Gases, Queen's University Belfast Belfast, Northern Ireland, UK, 28. Aug - 2. Sep, 2011, pp. C9-149-1 – C9-149-3

11. Marija Radmilović-Radjenović, **Marija Savić**, Milovan Šuvakov, Branislav Radjenović, Stefan Matejček, M. Klas: The breakdown voltage curves in argon dc and rf discharges from large to small gap sizes – 18th Symposium on Application of Plasma Processes Workshop on Plasmas as a Planetary Atmosphere Mimics, Comenius University in Bratislava; Society for Plasma Research and Applications, Vratna, Mala Fatra, Slovakia, 15. - 20. Jan, 2011, invited lecture, pp. 70-74.

12. **Marija Savić**, Marija Radmilović-Radjenović: Modelovanje interakcija plazme sa površinama – Naučni skup Physics 2010 BL, Prirodno-matematički fakultet, Banja Luka, Republika Srpska, Bosna i Hercegovina, 22. - 24. Sep, 2010, str. 101-110.
ISSN: 978-99955-21-21-9

13. **Marija Savić**, Marija Radmilović-Radjenović, Zoran Lj Petrović: The effect of metastable atoms on the secondary electron production in argon – 25th Summer School and International Symposium on the Physics of Ionized Gases, Astronomical Observatory of Belgrade, Donji Milanovac, Serbia, 30. Aug - 3. Sep, 2010, No 89, pp. 269-272.
ISSN 0373-3742

Саопштење са међународног скупа штампано у изводу (M34):

1. **Marija Puač**, Dragana Marić, Gordana Malović, Jelena Sivoš and Zoran Lj Petrović: Comparison of RF breakdown in argon and oxygen – Monte Carlo simulation – POSMOL 2019, 18-21 July 2019, Belgrade, Serbia. EMS 51 pp 133.
ISBN 978-86-7025-819-8

1. **Marija Puač**, Antonije Djordjević, Zoran Lj Petrović: The role of electron-electrode collisions and secondary electrons in radio-frequency breakdown – 71st Annual Gaseous Electronics Conference, American Physical Society, Portland, Oregon, USA, 5 - 9. Nov. 2018, poster ID: GT1.00071.
http://www.apsgec.org/gec2018/all_GEC18.pdf

2. **Marija Savić**, Dragana Marić, Marija Radmilović-Radjenović, Zoran Lj Petrović: Monte Carlo simulation of radio-frequency breakdown in oxygen and air – 69th Annual Gaseous Electronics Conference, American Physical Society, Bochum, Germany, 10. - 14. Oct, 2016, poster ID: BAPS.2016.GEC.MW6.74.

<http://meetings.aps.org/link/BAPS.2016.GEC.MW6.74>

3. **Marija Savić**, Marija Radmilović-Radjenović, Zoran Lj Petrović: The rf breakdown voltage curves-similarity law – 66th Annual Gaseous Electronics Conference, American Physical Society, USA, 30. Sep - 4. Oct, 2013, pp. CT1.23
ISSN 0003-0503

4. **Marija Savić**, Marija Radmilović-Radjenović, Milovan Šuvakov, Zoran Lj Petrović: First steps in obtaining Monte Carlo model of RF breakdown – ESCAMPIG XXI, Instituto de Plasmas e Fusão Nuclear from Instituto Superior Técnico, Universidade Técnica de Lisboa, Universidade do Porto, Universidade do Minho and Universidade da Madeira Portugal, 10. - 14. Jul, 2012, pp. T6-296-1 – T6-296-2

5. **Marija Savić**, Marija Radmilović-Radjenović, Zoran Lj Petrović: Monte Carlo simulations of breakdown in radio-frequency discharges – 64th Annual Gaseous Electronics Conference, Bulletin of the American Physical Society, Salt Lake City, Utah, 14. - 18. Nov, 2011, pp. 36-36

6. **Marija Savić**, Marija Radmilović-Radjenović, Milovan Šuvakov, Zoran Lj Petrović: Monte Carlo simulation of RF discharges – 2nd National Conference on Electronic, Atomic, Molecular and Photonic Physics, Institute of Physics, Belgrade, Serbia, 21. - 25. Jun, 2011, pp. 134-134

7. **Marija Savić**, Marija Radmilović-Radjenović, Zoran Lj Petrović: Modeling of low pressure breakdown by Monte Carlo technique – 20th European Conference on the Atomic and Molecular Physics of Ionized Gases, European Physical Society, Novi Sad, Serbia, 13. - 17. Jul, 2010, pp P2.58
ISSN 2-914771-63-0

GET MY OWN PROFILE



Marija (Savic) Puac

Institute of Physics
University of Belgrade, Serbia
plasma physics

	All	Since 2020
Citations	213	107
h-index	7	6
i10-index	7	5

0 articles 2 articles

not available available

Based on funding mandates

TITLE	CITED BY	YEAR
Gas breakdown and secondary electron yields D Marić, M Savić, J Sivoš, N Škoro, M Radmilović-Radjenović, G Malović, ... The European Physical Journal D 68, 1-7	77	2014
Monte Carlo modeling of radio-frequency breakdown in argon MŠZLP Marija Puač, Dragana Marić, Marija Radmilović-Radjenović Plasma Sources Science and Technology 27 (7), 075013	31	2018
On explanation of the double-valued Paschen-like curve for RF breakdown in Argon M Savic, M Radmilovic-Radjenovic, M Suvakov, S Marjanovic, D Maric, ... IEEE Transactions on Plasma Science 39 (11), 2556-2557	27	2011
Using Swarm Models as an Exact Representation of Ionized Gases GM Zoran Lj. Petrović, Dragana Marić, Marija Savić, Srđan Marjanović, Saša Dujko Plasma Processes and Polymers 14 (1-2)	19 *	2016
Numerical modeling of thermalization of positrons in gas-filled surko traps S Marjanovic, M Suvakov, A Bankovic, M Savic, G Malovic, SJ Buckman, ... IEEE Transactions on Plasma Science 39 (11), 2614-2615	16	2011
The Role of the Field Emission Effect in the Breakdown Mechanism of Direct-Current Helium Discharges in Micrometer Gaps ŠMMKBRMDMSMR Radjenović Contributions to Plasma Physics 53 (8)	12	2013
Monte Carlo simulation of RF breakdown in oxygen—the role of attachment M Puač, A Đorđević, ZL Petrović The European Physical Journal D 74, 1-8	10	2020
New phenomenology of gas breakdown in DC and RF fields SGDM Zoran Lj Petrović, Jelena Sivoš, Marija Savić, Nikola Škoro, Marija ... Journal of Physics: Conference Series 514, 012043	7 *	2014
The surface charging effects in three-dimensional simulation of the profiles of plasma-etched nanostructures BRMS M Radmilović-Radjenović International Journal of Numerical Modelling: Electronic Networks, Devices ...	6	2011
Breakdown Phenomena in Water Vapor Microdischarges BRMS M. Radmilović-Radjenović	4	2010

TITLE	CITED BY	YEAR
ACTA PHYSICA POLONICA A 117, 752-755		
Effect of target material on electrical properties of a two-electrode dielectric barrier helium plasma jet N Škoro, K Kutasi, M Puač, ZL Petrović, N Puač Plasma Sources Science and Technology 33 (4), 045015	1	2024
Microwave Field Strength Computing for the Resonator Designs and Filters BRMS M. Radmilović-Radjenović ACTA PHYSICA POLONICA A 129 (3), 289-292	1	2016
The breakdown voltage curves and spatial profiles of ionization rates in argon rf discharges M Savić, M Radmilović-Radjenović, M Šuvakov, ZL Petrović 30th ICPIG, August 28th–September 2nd, Belfast, Northern Ireland, UK, 1	1	2011
Influence of the secondary electron emission on the characteristics of radio frequency plasmas MS A Bojarov, M Radmilović-Radjenović Hemijska industrija 65 (1), 1-8	1	2011
RF BREAKDOWN IN ARGON AT LOW-PRESSURES: EXPERIMENT AND MODELLING J MARJANOVIĆ, D MARIĆ, M PUAČ, A ĐORĐEVIĆ, ZLJ PETROVIĆ SPIG 2024, 138		2024
Modeling of Radio-Frequency Breakdown by Monte Carlo Technique M PUAČ, ZLJ PETROVIĆ		2022
Electron Energy Distribution Functions during the RF Breakdown Z Petrovic, M Puač, A Djordjević APS Annual Gaseous Electronics Meeting Abstracts, KW81. 052		2021
Modelovanje proboja u gasovima Monte Karlo tehnikom M Puač PQDT-Global		2019
Modeling of RF breakdown in different atmospheres Z Petrovic, M Puač, A Đorđević APS Annual Gaseous Electronics Meeting Abstracts, DT3. 004		2019
Comparison of RF Breakdown in Argon and Oxygen–Monte Carlo Simulation M Puač, D Marić, G Malović, J Sivoš, ZL Petrović POSMOL 2019, 133		2019

Marija Puač

<https://www.webofscience.com/wos/author/rid/R-4697-2019>

Web of Science ResearcherID: [R-4697-2019](#)

Publication Metrics

For manuscripts published from date range April 2011 - April 2025

7	147
H-index	Sum of Times Cited
18	0
Total Publications	Web of Science Core Collection Publications

For all time

7	148
H-index	Sum of Times Cited
21	0
Total Publications	Web of Science Core Collection Publications

Publications

For manuscripts published from date range April 2011 - April 2025 (16)

Times Cited
(All time)

RF BREAKDOWN IN ARGON AT LOW-PRESSURES: EXPERIMENT AND MODELLING

Authors (5): Jelena Marjanović; Dragana Marić ... Zoran Lj. Petrović

Published: Sep 2024 in Summer School and International Symposium on the Physics of Ionized Gases

DOI: 10.69646/AOB103P138

Not indexed in
the Web of
Science

The equivalent electrical circuit for describing the dielectric barrier discharge plasma jet

Authors (4): Marija Puač; Nikola Škoro ... Nevena Puač

Published: Sep 2024

Not indexed in
the Web of
Science

<p>Nature of radiofrequency breakdown in argon viewed through electron energy distribution functions modeled by the Monte Carlo technique</p> <p>Authors (1): Marija Puač</p> <p>Published: Jul 2024</p>	<p>Not indexed in the Web of Science</p>
<p>Effect of target material on electrical properties of a two-electrode dielectric barrier helium plasma jet</p> <p>Authors (5): Skoro, Nikola; Kutasi, Kinga ... Puac, Nevena</p> <p>Published: Apr 2024 in Plasma Sources Science and Technology</p> <p>DOI: 10.1088/1361-6595/AD3D83</p>	<p>0</p>
<p>Equivalent electrical circuit modeling of He dielectric barrier discharge plasma jet</p> <p>Authors (4): Marija Puač; Nikola Škoro ... Nevena Puač</p> <p>Published: Sep 2023</p>	<p>Not indexed in the Web of Science</p>
<p>Properties of low-pressure rf discharges suitable for treatment of absorbants</p> <p>Authors (7): Aranka Derysi; B. Horvath ... Nikola Škoro</p> <p>Published: Jan 2023</p>	<p>Not indexed in the Web of Science</p>
<p>Breakdown in rf and dc fields</p> <p>Authors (6): Dragana Marić; Marija Puač ... Zoran Lj Petrović</p> <p>Published: Oct 2020</p>	<p>Not indexed in the Web of Science</p>
<p>Monte Carlo simulation of RF breakdown in oxygen - the role of attachment</p> <p>Authors (3): Puac, Marija; Dordevic, Antonije; Petrovic, Zoran Lj</p> <p>Published: Apr 2020 in The European Physical Journal D</p> <p>DOI: 10.1140/EPJD/E2020-100526-1</p>	<p>4</p>
<p>Modeling of RF breakdown in different atmospheres</p> <p>Authors (3): Zoran Lj Petrović; Marija Puač; Antonije Đorđević</p> <p>Published: Oct 2019</p>	<p>Not indexed in the Web of Science</p>
<p>Monte Carlo modeling of radio-frequency breakdown in argon</p> <p>Authors (5): Puac, Marija; Maric, Dragana ... Petrovic, Zoran Lj</p> <p>Published: Jul 2018 in Plasma Sources Science and Technology</p> <p>DOI: 10.1088/1361-6595/AACC0C</p>	<p>22</p>
<p>Using Swarm Models as an Exact Representation of Ionized Gases</p> <p>Authors (6): Petrovic, Zoran Lj.; Maric, Dragana ... Malovic, Gordana</p> <p>Published: Jan 2017 in Plasma Processes and Polymers</p> <p>DOI: 10.1002/PPAP.201600124</p>	<p>14</p>
<p>Gas breakdown and secondary electron yields</p> <p>Authors (7): Maric, Dragana; Savic, Marija ... Petrovic, Zoran Lj</p> <p>Published: Jun 2014 in The European Physical Journal D</p> <p>DOI: 10.1140/EPJD/E2014-50090-X</p>	<p>51</p>

New phenomenology of gas breakdown in DC and RF fields	7
Authors (8): Petrovic, Zoran Lj; Sivos, Jelena ... Maric, Dragana Published: May 2014 in Journal of Physics: Conference Series DOI: 10.1088/1742-6596/514/1/012043	
<hr/>	
The Role of the Field Emission Effect in the Breakdown Mechanism of Direct-Current Helium Discharges in Micrometer Gaps	10
Authors (6): Matejcik, S.; Klas, M. ... Radmilovic-Radjenovic, M. Published: Sep 2013 in Beitrage Aus der Plasmaphysik-contributions to Plasma Physics DOI: 10.1002/CTPP.201300032	
<hr/>	
On Explanation of the Double-Valued Paschen-Like Curve for RF Breakdown in Argon	21
Authors (6): Savic, Marija; Radmilovic-Radjenovic, Marija ... Petrovi, Zoran Lj Published: Nov 2011 in IEEE Transactions on Plasma Science DOI: 10.1109/TPS.2011.2159244	
<hr/>	
Numerical Modeling of Thermalization of Positrons in Gas-Filled Surko Traps	15
Authors (7): Marjanovic, Srdjan; Suvakov, Milovan ... Petrovic, Zoran Lj. Published: Nov 2011 in IEEE Transactions on Plasma Science DOI: 10.1109/TPS.2011.2159129	
<hr/>	



Република Србија
Универзитет у Београду

Оснивач: Република Србија

Дозволу за рад број 612-00-02666/2010-04 од 12. октобра 2011.
године је издало Министарство просвете и науке Републике Србије

Електротехнички факултет, Београд

Оснивач: Република Србија

Дозволу за рад број 612-00-588/2008-04 од 17. новембра 2008.
године је издало Министарство просвете Републике Србије

УБ



Диплома

Марија, Бојан, Пуач

рођена 10. јуна 1985. године, Параћин, Република Србија, уписана школске 2009/2010.
године, а дана 10. јула 2019. године завршила је докторске академске студије,
шреће сачењена, на студијском програму Електротехника и рачунарство, обима
180 (сто осамдесет) бодова ЕСПБ са просечном оценом 9,80 (девет и 80/100).

Наслов докторске дисертације је: „Моделовање робота у часовима Монте Карло техника“.

На основу тога издаје јој се ова диплома о сачењеном научном називу
доктор наука - електротехника и рачунарство

Број: 13277200

У Београду, 1. марта 2022. године

Декан
Проф. др Дејан Гвоздић

Ректор
Проф. др Владан Ђокић

00132975



31st Summer School and International Symposium on the Physics of Ionized Gases

Dr. Marija Puač

Belgrade, April 7th, 2022

Dear Dr. Puač,

On behalf of the Scientific and Organizing Committees, it is our pleasure to invite you to attend the *31st Summer School and International Symposium on the Physics of Ionized Gases* (SPIG 2022) and present a **Progress report**.

The SPIG 2022 will be held from September 5th to 9th, 2022 in Belgrade, Serbia. The details of the conference are available at official website: <http://spig2022.ipb.ac.rs/>. Please note that due to the limited conference budget, the SPIG2022 organizers will try to provide partial support to students and early stage researchers, as well as colleagues from economically less privileged countries. Thank you for your understanding and support.

We look forward to welcoming you to Belgrade.

Yours sincerely,

Dragana Ilić
(Co-Chair of the Scientific Committee)

Bratislav Obradović
(Co-Chair of the Loc. Org. Committee)

Vladimir Srećković
(Co-Chair of the Scientific Committee)

Jovan Cvetić
(Co-Chair of the Loc. Org. Committee)

SPIG 2022 Organizers:

University of Belgrade - School of Electrical Engineering

University of Belgrade - Faculty of Physics

Serbian Academy of Science and Arts



**31st Summer School and
International Symposium on
the Physics of Ionized Gases**

Belgrade, Serbia,
September 5 - 9, 2022

CONTRIBUTED PAPERS
&
**ABSTRACTS of INVITED LECTURES,
TOPICAL INVITED LECTURES and PROGRESS REPORTS**

Editors:
**Dragana Ilić, Vladimir Srećković,
Bratislav Obradović and Jovan Cvetić**



**БЕОГРАД
2022**

**31st Summer School and
International Symposium on
the Physics of Ionized Gases**



September 5 – 9, 2022, Belgrade, Serbia

S P I G 2022

CONTRIBUTED PAPERS

&

ABSTRACTS OF INVITED LECTURES,
TOPICAL INVITED LECTURES AND
PROGRESS REPORTS

Editors

Dragana Ilić, Vladimir Srećković,
Bratislav Obradović and Jovan Cvetić

University of Belgrade –
School of Electrical
Engineering

University of Belgrade –
Faculty of Physics
Serbian Academy of
Sciences and Arts

Belgrade, 2022

PUBLICATIONS OF THE ASTRONOMICAL OBSERVATORY OF BELGRADE
FOUNDED IN 1947

EDITORIAL BOARD:

Dr. Srdjan SAMUROVIĆ, Editor-in-Chief (Astronomical Observatory, Belgrade)

Dr. Rade PAVLOVIĆ (Astronomical Observatory, Belgrade)

Dr. Miroslav MIĆIĆ (Astronomical Observatory, Belgrade)

Dr. Branislav VUKOTIĆ (Astronomical Observatory, Belgrade)

All papers in this Publication are peer reviewed.

Published and copyright © by Astronomical Observatory, Volgina 7, 11060 Belgrade
38, Serbia

Director of the Astronomical Observatory: Dr. Gojko Djurašević

Typesetting: Tatjana Milovanov

Internet address <http://www.aob.rs>

ISSN 0373-3742

ISBN 978-86-82296-02-7

Number of copies / tiraž : 200

Production: Skripta Internacional, Mike Alasa 54, Beograd

CIP - Каталогизација у публикацији - Народна библиотека Србије, Београд

537.56(082)

539.186.2(082)

539.121.7(082)

533.9(082)

**SUMMER School and International Symposium on the Physics of Ionized Gases
(31 ; 2022 ; Belgrade)**

Contributed papers & abstracts of invited lectures, topical invited lectures and progress reports / 31st Summer School and International Symposium on the Physics of Ionized Gases - SPIG 2022, September 5-9, 2022, Belgrade, Serbia ; editors Dragana Ilić ... [et al.]. - Belgrade : Astronomical Observatory, 2022 (Beograd : Skripta Internacional). - 302 str. : ilustr. ; 24 cm. - (Publications of the Astronomical Observatory of Belgrade, ISSN 0373-3742)

Na nasl. str.: University of Belgrade, School of Electrical Engineering; University of Belgrade, Faculty of Physics; Serbian Academy of Sciences and Arts. - Tiraž 200. - Str. 17-18: Preface / editors Dragana Ilić ... [et al.]. - Bibliografija uz svaki rad. - Registar.

ISBN 978-86-82296-02-7

1. Ilić, Dragana, 1978- [urednik] [аутор додатног текста]

а) Јонизовани гасови – Зборници б) Атоми – Интеракција – Зборници в) Плазма – Зборници

COBISS.SR-ID 72751881

SPIG 2022

SCIENTIFIC COMMITTEE

D. Ilić (Co-chair), Serbia
V. Srećković (Co-chair), Serbia

A. Antoniou, Greece
D. Borka, Serbia
J. Burgdörfer, Austria
J. Cvetić, Serbia
V. Guerra, Portugal
M. Ivković, Serbia
K. Kutasi, Hungary
I. Mančev, Serbia
D. Marić, Serbia
N. J. Mason, UK
A. Milosavljević, France
V. Milosavljević, Serbia
K. Mima, Japan
Z. Mišković, Canada
L. Nahon, France
B. Obradović, Serbia
G. Poparić, Serbia
P. Roncin, France
I. Savić, Serbia
Y. Serruys, France
N. Simonović, Serbia
M. Škorić, Japan
M. Trtica, Serbia
S. Tošić, Serbia
R. White, Australia

ADVISORY COMMITTEE

D. Belić
N. Bibić
M. S. Dimitrijević
S. Đurović
N. Konjević
M. M. Kuraica
J. Labat
G. Malović
B. P. Marinković
Z. Mijatović
M. Milosavljević
Z. Lj. Petrović
L. Č. Popović
J. Purić
B. Stanić

ORGANIZING COMMITTEE

J. Cvetić (Co-chair)
B. Obradović (Co-chair)

M. Ignjatović (Co-secretary)
L. Gavanski (Co-secretary)

N. Konjević
N. Cvetanović
T. Gajo
I. Krstić
N. Sakan

CONTENTS

Dragana Ilić, Vladimir Srećković, Bratislav Obradović and Jovan Cvetić <i>Preface</i>	17
--	----

Section 1. ATOMIC COLLISION PROCESSES

Invited Lectures

Sergio Diaz-Tendero <i>Ultrafast Dynamics of Ionized Molecules and Molecular Clusters in the Gas Phase</i>	21
---	----

Darryl B. Jones <i>Electron Spectroscopies for Probing Electronic Structure and Collision Dynamics</i>	22
---	----

James Sullivan <i>Experiments with Positrons - From Fundamental to Applied Science</i>	23
---	----

Topical Invited Lectures

G. J. Boyle, M. J. E. Casey, D. G. Cocks, R. D. White and R. J. Carman <i>Thermalisation Time of Electron Swarms in Noble Gases for Uniform Electric Fields</i>	24
--	----

Saša Dujko, Danko Bošnjaković, Ilija Simonović and Christoph Köhn <i>Electron Transport, Transient Plasmas and High-Energy Phenomena in Planetary Atmospheres</i>	25
--	----

Teodora Kirova and Jelena Tamulienė <i>Numerical Investigations of the Impact of the Magnetic Field of Radiation on Amino Acids</i>	26
--	----

Minna Patanen <i>Electron-Ion Coincidence Experiments with Electron and Photon Ionization</i>	27
--	----

L. Schwob, J. Leroux, A. Kotobi, S. Dörner, K. Schubert, I. Unger, K. Atak, V. Zamudio-Bayer, J. T. Lau and S. Bari <i>X-Ray Action Spectroscopy of Gas-Phase Biomolecular Ions</i>	28
---	----

Progress Reports

Danilo Delibašić <i>Relative Importance of the Electron Continuum Intermediate State in Single-Electron Capture into Any State of Fast Protons from Helium- Like Atomic Systems</i>	29
--	----

S. Ganguly and S. Maclot <i>Fragmentation of Core-Ionized Adamantane Molecule</i>	30
--	----

M. Roy Chowdhury, G. A. Garcia, E. Rouquet, H. Hrodmarsson, J. C. Loison and L. Nahon <i>VUV Photoionization and Fragmentation of Cyano-Pahs</i>	31
--	----

Contributed Papers

J. Atić, D. Bošnjaković, I. Simonović, Z. Lj. Petrović and S. Dujko <i>Formation and Propagation of Streamers in CF_3I-SF_6 Gas Mixtures</i>	33
--	----

S. Dujko, D. Bošnjaković, M. Vass, I. Korolov, P. Hartmann, N. Pinhao, D. Loffhagen and Z. Donko <i>Electron Transport Coefficients in CO: Scanning Drift Tube Measurements and Kinetic Computations</i>	37
--	----

Nenad Milojević, Danilo Delibašić and Ivan Mančev <i>Single-Electron Capture From He by Fast Alpha Particles</i>	41
---	----

Ž. Nikitović and Z. Raspopović <i>Reduced Mobility of H^+ Ions in n-Butanol Gas</i>	45
---	----

I. Simonović, D. Bošnjaković, Z. Lj. Petrović and S. Dujko <i>Third-Order Transport Coefficients for Electrons in C_3F_8</i>	49
--	----

N. S. Simonović, D. B. Popović and A. Bunjac <i>Photoelectron Energy Spectra in Sequential Two-Photon Ionization of Hydrogen by Gaussian and Half-Gaussian Laser Pulses</i>	53
--	----

V. Stanković, M. Ristić, R. Ranković, M. Aoneas, M. Vojnović and G. B. Poparić <i>Dissociation of N_2 by Electron Impact in RF Electric Field</i>	57
--	----

Violeta V. Stanković, Mirjana M. Vojnović, Miroslav M. Ristić, Sava M. D. Galijaš and Goran B. Poparić <i>Excitation of $^1\Sigma^+_U$ and $^1\Pi_u$ States and Ionization of CO_2 in DC Electric Field.....</i>	61
Natalia Tańska, Kuba Wójcik, Sylwia Dylnicka, Elżbieta Ptasińska-Denga, Czesław Szmytkowski and Paweł Możejko <i>Total Cross Section Measurements for Electron Scattering on Methyl Formate ($HCOOCH_3$) Molecule: Methylation Effect.....</i>	65
M. M. Vojnović, M. M. Ristić and D. S. Belić <i>Rate Coefficients for O_3^+ Dissociation to O^+ and O_2^+ by Electron Impact.....</i>	69
Section 2. PARTICLE AND LASER BEAM INTERACTIONS WITH SOLIDS	
Invited Lecture	
J. Bonse, K. Wasmuth, H. Voss, J. Krüger and S. Gräf <i>Laser-Induced Periodic Surface Structures, Mechanisms, Applications, and Unsolved Problems.....</i>	75
Topical Invited Lectures	
J. Limpouch <i>High-Power Laser Interactions with Low Density Porous Materials and Their Applications.....</i>	76
Progress Reports	
Jovan Ciganović, Miloš Momčilović, Sanja Živković, Jelena Stasić and Milan Trtica <i>Action of Pulsed Lasers on Titanium Target: Surface Effects.....</i>	77
M. Hadžijojić and M. Ćosić <i>Study of Two Dimensional Crystals by Rainbow Scattering Effect.....</i>	78
Violeta N. Nikolić <i>Spectroscopic Investigation of the Influence of NO_3^- Anions on the Crystallization of SiO_2 Matrix.....</i>	80

D. M. Popovic, A. Kushima, A. A. Zekic, B. Kasalica, J. Stasic, J. Ciganovic, M. Bogdanovic and M. Trtica <i>Picosecond Pulsed Laser Ablation of Silicon Single Crystal</i>	81
N. Starčević <i>Ion-Crystal Rainbow Interaction Potential in Channeling</i>	82
Contributed Papers	
N. A. Bosak, A. N. Chumakov, L. V. Baran, V. V. Malyutina-Bronskaya, T. F. Raichonok, A. A. Ivanov, V. V. Kiris, E. M. Dyatlova, A. A. Shevchenok, A. V. Buka and A. S. Kuzmitskaya <i>Investigation of Properties of Yttrium Vanadate YVO₄ Films</i>	83
A. N. Chumakov, V. V. Lychkovsky and I. S. Nikonchuk <i>Features of Silicon Ablation in Air Under the Influence of Nd:YAG Laser Harmonics</i>	87
A. N. Chumakov, V. V. Luchkouski and I. S. Nikonchuk <i>Silicon Spalling Destruction and Ablation in Air Under Bichromatic Laser Radiation</i>	91
M. Ćosić, M. Hadžijojić and N. Nešković <i>Bohmian Dynamics of Positrons Channeled Through a Chiral Carbon Nanotubes</i>	95
H. Delibašić Marković, V. Petrović and I. Petrović <i>Analytical Prediction and Numerical Analysis of Plasma Mediated Ablation of Skin Tissue Samples with Nanosecond-to-Femtosecond Laser Pulses</i>	101
S. M. D. Galijaš, V. M. Milosavljević and G. B. Poparić <i>The Time-Symmetric Description of Electron Exchange in Ion-Ion Collision</i>	105
V. K. Goncharov, G. A. Gusakov and M. V. Puzyrev <i>Influence of Carbon Ions of Different Multiplicity on Regimes of Promising Laser Technologies for the Deposition of Diamond-Like Carbon Nanocoatings</i>	109
M. Hadžijojić and M. Ćosić <i>Study of Graphene by Rainbow Scattering Effect</i>	113

A. Kalinić, I. Radović, L. Karbunar, V. Despoja and Z. L. Mišković <i>Analytical Expression for Stopping Force Acting on a Slow Charged Particle Moving Parallel to a Thick Graphene-Sapphire-Graphene Structure</i>	117
M. D. Majkić, N. N. Nedeljković and M. A. Mirković <i>Effect of the Ionic Type on the Shape of the Nanostructures Created by an Impact of Slow Highly Charged Ions on Gold Surface</i>	121
N. N. Nedeljković, M. D. Majkić, M. A. Mirković, I. Stabrawa and D. Banaś <i>The Influence of the Ion-Target Parameters on the Size of the Surface Nanohillocks Created by an Impact of Highly Charged Ions</i>	125
Natalie Tarasenko, Vladislav Kornev, Alena Nevar, Mikhail Nedel'ko, Anton Radomtsev and Nikolai Tarasenko <i>Combining Plasma-Assisted Synthesis of Metal Oxide Nanoparticles with Thin Films Deposition</i>	129
Natalie Tarasenko, Vladislav Kornev, Svetlana Pashayan and Nikolai Tarasenko <i>Pulsed Laser Assisted Fabrication of Co-doped ZnO Nanocrystalline Layers on a Glass Substrate</i>	133
I. Traparić, M. Jovanović, M. Kuzmanović and M. Ivković <i>Elemental Analysis of Austenitic Steel by Calibration-Free Laser-Induced Breakdown Spectroscopy (CF-LIBS)</i>	137
Nora Trklja Boca, Žarko Z. Mišković, Radivoje M. Mitrović, Bratislav M. Obradović and Milorad M. Kuraica <i>Treatment of Steel 16MnCr5 and Steel 42CrMo4 by Plasma Flow Generated in Magnetoplasma Compressor</i>	141
M. Trtica, J. Stasic, X. Chen and J. Limpouch <i>ODS+Hf and AISI 316L Steel Surface Variations at High Laser Intensity, 10^{13} W/cm², in Air and Vacuum: Comparative Study</i>	145
S. Živković, J. Petrović, M. Momčilović, M. Radenković, N. Krstulović, J. Car, D. Palasti, F. Casian Plaza and G. Galbács <i>Perspective on the Use of Nanoparticles to Improve the TEA CO₂ Based LIBS Analytical Performances: Copper Nanoparticles for NELIBS Analysis of Polypropylene</i>	149

Section 3. LOW TEMPERATURE PLASMAS

Invited Lectures

Ryo Ono

Measurement and Simulation of Atmospheric-Pressure Streamer Discharge..... 155

L. J. Overzet, A. Press, K. Hernandez, J. Poulouse and M. J. Goeckner
Measurements of RF Plasma Re-Ignition: RF-IV and Proes..... 156

Topical Invited Lectures

S. Béchu, J. L. Lemaire, M. Mitrou, N. De Oliveira and P. Svarnas
Investigation of the Ro-Vibrational Levels of H₂/D₂ Molecules by VUV-Absorption Spectroscopy for the Production of H/D Negative Ions for Fusion Application..... 157

M. T. Belmonte, P. R. Sen Sarma, C. P. Clear, F. Concepcion, M. Ding, J. C. Pickering and S. Mar
What Can Plasma Spectroscopy Do for Astronomers? Measuring Atomic Parameters of Astrophysical Importance..... 158

A. Derzsi
Surface Processes in Low-Pressure Capacitively Coupled Plasmas.... 159

P. Dvořák, R. Žemlička, R. Příbyl, M. Tkáčik, J. Pálenik, P. Vašina, P. Skopal, Z. Navrátil and V. Buršíková
Higher Harmonic Frequencies of Discharge Voltage and Current in Capacitively Coupled Discharges..... 160

C. Fromentin, T. C. Dias, T. Silva, V. Guerra, E. Baratte and O. Guaitella
Coupled Kinetics in CO₂-N₂ Plasmas..... 161

Mohammed Koubiti

Application of Machine-Learning to Spectroscopic Line Emission by Hydrogen Isotopes in Fusion Devices for Isotopic Determination and Prediction..... 162

Mikhail Pinchuk, Olga Stepanova, Mikhail Gromov and Anton Nikiforov

Control of Guided Streamer Propagation and Interaction with Substrate in Helium Atmospheric Pressure Plasma Jet..... 163

Djordje Spasojević, Nikola V. Ivanović, Nikodin V. Nedić, Luka Rajačić, Nikola M. Šišović and Nikola Konjević <i>On the Application of Iterative Kinetic Model for Diagnostics of Abnormal Glow Discharges in Noble Gases.....</i>	164
--	-----

Progress Reports

Dejan Dojić, Miloš Skočić and Srdjan Bukvić <i>Measurements of Continuous Optical Spectrum During Nanosecond Laser Pulse Interaction with Metallic Target.....</i>	165
---	-----

Milan Ignjatovic <i>The Influence of Corona Discharge on the Lightning Surge Propagation Along the Transmission Lines.....</i>	166
---	-----

Amit Kumar, Nikola Škoro, Wolfgang Gernjak, Suzana Živković and Nevena Puač <i>Design, Development, and Characterization of Atmospheric Plasma System for Wastewater Treatment.....</i>	167
---	-----

Marija Puač and Zoran Lj. Petrović <i>Modeling of Radio-Frequency Breakdown by Monte Carlo Technique.....</i>	168
--	-----

Leo Sala and Jaroslav Kočišek <i>Interaction of Ionizing Radiation with DNA Nanostructures.....</i>	169
--	-----

N. Selaković, D. Maletić, N. Puač, G. Malović and Z. Lj. Petrović <i>Mass Spectrometry of Plasma Jet and Application of Electrical Discharges Operating at Atmospheric Pressure in Biomedicine.....</i>	170
--	-----

M. M. Vasiljević and Dj. Spasojević <i>Determination of the Electric Field Strength in Glow Discharges Using Argon Spectral Lines.....</i>	171
---	-----

Contributed Papers

O. Asvany, S. Thorwirth, P. C. Schmid, T. Salomon and S. Schlemmer <i>High-Resolution Spectroscopy of Astrophysically Relevant Molecular Ions.....</i>	173
--	-----

I. I. Filatova, V. A. Lyushkevich, S. V. Goncharik, U. I. Torchyk, Y. V. Kandratau and M. O. Slesarenka <i>The Effect of Plasma Seed Treatment on Germination and Early Growth of Thuja Koraiensis Nakai Plants</i>	175
Nikola Goleš, Neda Babucić, Nenad M. Sakan and Milivoje Ivković <i>Self-Mixing Interferometry for Plasma Diagnostics</i>	179
Miroslav Gulan and Vladimir Milosavljević <i>Characterization of the Dielectric Barrier-Free Atmospheric Plasma System</i>	183
Naveen Gupta <i>Laser Driven Electron Acceleration by q-Gaussian Laser Pulse in Plasma: Effect of Self Focusing</i>	187
Milan Ignjatovic, Jovan Cvetic, Vera Protic and Nemanja Grbic <i>Corona Model for Surge Wave Propagation Along the Transmission Lines</i>	191
N. V. Ivanović, N. V. Nedić, I. R. Videnović and D. Spasojević <i>Polarization Spectroscopy of Neon Lines for Electric Field Distribution Measurement in the Cathode Sheath of a Grimm-Type Glow Discharge</i>	195
Jovica Jovović and Gordana Lj. Majstorović <i>The Gas Temperature Diagnostics by Means of $AlO (B^2\Sigma^+ - X^2\Sigma^+)$ Molecular Band System from the Upgraded Atmospheric Pressure Pulsed Discharge Source in Argon</i>	199
V. V. Luchkouski and A. N. Chumakou <i>Formation and Heating of Silicon Plasma in Air Under Pulsed Bichromatic Laser Irradiation</i>	203
Jelena Marjanović, Dragana Marić, Gordana Malović and Zoran Lj. Petrović <i>Breakdown in Saturated Water Vapor</i>	207
N. V. Nedić, N. V. Ivanović, I. R. Videnović, D. Spasojević and N. Konjević <i>Looking Behind the Negative Glow Plasma: Estimating Cathode Sheath Parameters by End-On Optical Emission Spectroscopy in a Grimm-Type Glow Discharge Source</i>	211

B. M. Obradović, N. Cvetanović, I. B. Krstić and M. M. Kuraica <i>Detection of Fast Nitrogen and Oxygen Atoms via Emission Spectroscopy</i>	215
M. S. Rabasovic, B. P. Marinkovic and D. Sevic <i>Analysis of Printed Circuit Board LIBS Data Using Deep Learning</i>	219
Nenad M. Sakan, Milica L. Vinić, Vladimir A. Srećković, Ivan Traparić and Milivoje R. Ivković <i>Application of Artificial Neural Network in the Analysis of the Spectra from Laser Ablation Combined with Fast Pulse Discharge</i>	223
L. V. Simonchik and A. V. Kazak <i>Features of the HeI 492.2 nm Line Profile Registered at Diagnostics of DC and Streamer Discharges</i>	227
Miloš Skočić, Nikodin Nedić, Dejan Dojčić, Luka Rajačić and Srdjan Bukvić <i>Temperature Estimation in the Early Stage of Laser Induced Plasma Formation Relaying on Black Body Radiation</i>	231
G. B. Sretenović, P. S. Iskrenović, V. V. Kovačević, B. M. Obradović and M. M. Kuraica <i>Study of Plasma-Flow Interaction in Low Temperature Plasma Jets</i>	235
Biljana Stankov, Marijana R. Gavrilović Božović, Jelena Savović and Milivoje Ivković <i>Spectroscopic Characterization of Laser-Induced Plasma on Doped Tungsten</i>	239
Irinel Tapalaga, Ivan Traparić, Nora Trklja Boca, Jagoš Purić and Ivan P. Dojčinović <i>Modeling of Stark Spectral Line Broadening by Machine Learning Algorithms</i>	243
M. M. Vasiljević, G. Lj. Majstorović, I. R. Videnović and D. Spasojević <i>Spectroscopic Determination of the Degree of Dissociation of Hydrogen in the Glow Discharge</i>	247

Tatiana Vasilieva, Elena Nikolskaya, Michael Vasiliev, Nikita Yabbarov, Maria Sokol, Mariia Mollaeva and Margarita Chirkina <i>Comparison of Biocompatibility of Organic Polymers Modified in Various Types of Non-Temperature Plasmas</i>	251
---	-----

Section 4. GENERAL PLASMAS

Invited Lecture

Sven Thorwirth, Oskar Asvany and Stephan Schlemmer <i>Action-Spectroscopic Studies of Transient Carbon-Rich Molecular Ions</i>	257
---	-----

Topical Invited Lectures

J. Rosato, Y. Marandet, I. Hannachi and R. Stamm <i>Line Shape Modeling for Magnetic Fusion and Astrophysical Plasmas: An Overview of Recent Results</i>	258
---	-----

Progress Reports

Antonios Antoniou, Emmanuel Danezis, Dimitrios Stathopoulos, Evagelia Lyratzi and Dimitrios Tzimeas <i>Describing the Matemathical Methods for Calculating Basic Physical Parameters of the Gaussian-Rotational (GR) Model</i>	259
--	-----

A. Cinins, M. S. Dimitrijević, V. A. Srećković, K. Miculis, N. N. Bezuglov and A. N. Klyucharev <i>Analysis of Adiabatic Processes in Multilevel N-pod Quantum Systems from the Perspective of Riemannian Geometry</i>	260
--	-----

Milena Jovanović <i>Matter Distribution in Nearby Galaxies</i>	261
---	-----

V. Radović, A. Kovačević, D. Ilić, R. Street, L. Č. Popović, M. Nikolić, N. Andrić Mitrović and I. Čvorović-Hajdinjak <i>Development of a Time-Domain Pipeline for Detecting Binary Supermassive Black Holes in the Upcoming Legacy Survey of Space and Time (LSST)</i>	262
---	-----

T. Salomon, S. Brackertz, O. Asvany, I. Savić, D. Gerlich and S. Schlemmer <i>Recent Progress on Action Spectroscopy of Loosely Bound Hydrogen-Helium Complexes</i>	263
--	-----

Contributed Papers

A. Arsenić, D. Borka, P. Jovanović and V. Borka Jovanović <i>Winged Dragn Source From Leahy's Atlas: 3C 315</i>	265
--	-----

S. Das and D. C. Das <i>Higher Order Non-Linear Dust Ion Acoustic (DIA) Solitary Waves in Plasmas with Weak Relativistic Effects in Electrons and Ions</i>	269
---	-----

J. Kovačević-Dojčinović, I. Dojčinović, M. Lakićević and L. Č. Popović <i>Decomposition of the Blended $H\alpha$+$[N II]$ Lines in Spectra of the Active Galactic Nuclei Type 1.8-2</i>	271
--	-----

Amit Kumar and Jyotsna Sharma <i>The Effect of Negative Ions on Weibel Instability in the Presence of Large Amplitude Electrostatic Waves</i>	275
--	-----

V. A. Srećković, L. M. Ignjatović, V. Vujčić and M. S. Dimitrijević <i>The Chemi-Recombination Processes in Alkali-Metal Astrophysical and Low-Temperature Laboratory Plasmas: Rate Coefficients</i>	277
---	-----

The Workshop on X-ray and VUV Interaction with Biomolecules in Gas Phase (XiBiGP)

M. Berholts, P. H. W. Svensson, L. Pihlava, A. Vladyka, J. Niskanen, I. Unger, K. Kooser, C. Stråhlman, P. Eng-Johnsson, L. Schwob, A.-L. Vieli, O. Björneholm, C. Coleman, R. Lindblad and E. Kukk <i>Photofragmentation of the Radiation Therapy Enhancers: Can We Make Better Ones?</i>	283
---	-----

L. Carlini, P. Bolognesi, J. Chiarinelli, G. Mattioli, A. Casavola, M. C. Castrovilli, V. Valentini, A. De Stefanis, E. M. Bauer, E. Molteni, D. Sangalli and L. Avaldi <i>The "Lego Bricks" of Life: A Gas-Phase Study of Dipeptides</i>	284
--	-----

M. Di Fraia <i>Ultrafast Dynamics of Photo-Excited Molecules at Fermi Free Electron Laser</i>	286
--	-----

Bratislav P. Marinković <i>European Synchrotron and FEL User Organisation: Current Challenges and Prospects (COST Actions)</i>	287
Alexandra Mocellin, R. R. T. Marinho, O. Bjorneholm and A. Naves De Brito <i>Surface Propensity of Small Organic Biomolecules in Vapour-Water Interface by XPS</i>	288
Authors' Index.....	289
Programme of the SPIG 2022.....	293

MODELING OF RADIO-FREQUENCY BREAKDOWN BY MONTE CARLO TECHNIQUE

MARIJA PUAČ¹ and ZORAN LJ. PETROVIĆ²

¹*Institute of Physics, University of Belgrade, Pregrevice 118 Belgrade
E-mail smarija@ipb.ac.rs*

²*Serbian Academy Of Science And Arts, Knez Mihailova 35, Belgrade*

Abstract. Plasmas ignited by radio-frequency (RF) electric fields are widely used in many applications. Accordingly, scientific research is ranges, from experimental setups through mathematical models, relevant data and applications. Defining information for any application of RF plasmas are its breakdown voltage and related gas pressure. Monte Carlo proved to be a reliable technique for modeling voltage breakdown curves of RF plasmas. Recent research explained double valued nature of RF breakdown voltage curves and scaling law of those curves (Savić et al 2011), gave an insight of the physical nature of the RF breakdown (Puač et al 2018) and the role of attachment in presence of oxygen (Puač et al 2020). In this paper we review our findings on the underlying physics of RF breakdown and we present a versatile numerical tool for simulation that has no inherent limitations.

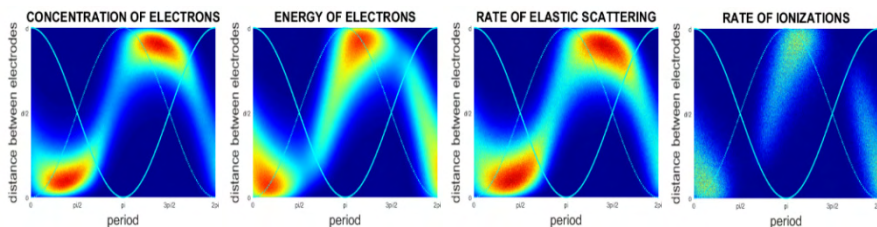


Figure 1: Spatial profiles of electron concentration, energy, and rates of elastic scattering and ionization. Background gas is helium, pressure and voltage are 1.13Torr and 330V, gap between electrodes is 23mm and frequency is 13.56MHz.

References

- Savić, M., Radmilović-Radjenović, M., Šuvakov, M., Marjanović, S., Marić, D., Petrović, Z. Lj: 2011, *IEEE Trans. Plasma Sci.*, **39**, 2556.
 Puač, M, Marić, D., Radmilović-Radjenović, M., Šuvakov, M., Petrović, Z. Lj: 2018, *Plasma Sources Science and Technologies*, **27**, 075013.
 Puač, M., Đorđević, A., Petrović, Z. Lj: 2020, *The European Physical Journal D*, **74**, 72.

SPIG 2022 PROGRAMME

Belgrade, Serbia, September 05 – 09, 2022

All indicated times are given in the Central European Summer Time (CEST) zone.

Monday 5th September 2022

SPIG 2022 (day 1)

XiBiGP Workshop	
09:00-09:30	<i>Registration</i>
09:30-09:40	Hall B: Opening and Introduction Aleksandar Milosavljević and Christophe Nicolas (SOLEIL)
09:40-10:00	<i>European Synchrotron and FEL User Organisation: Current Challenges and Prospects (COST Actions)</i> Bratislav Marinković , Institute of Physics Belgrade, Serbia [Regular]
	<i>Session 1, Hall B, Chair: Aleksandar Milosavljević</i>
10:00-10:20	<i>Ultrafast dynamics of photo-excited molecules at FERMI Free Electron Laser</i> Michele di Fraia , Elettra-Sincrotrone Trieste, Italy [Virtual]
10:20-10:40	<i>UV-induced processes in DNA</i> Lara Martínez-Fernandez , Universidad Autónoma de Madrid, Spain [Virtual]
10:40-11:00	<i>The 'LEGO bricks' of life: a gas-phase study of dipeptides</i> Laura Carlini , CNR-ISM, Italy [Virtual]
11:00-11:20	<i>Photofragmentation of the radiation therapy enhancers: can we make better ones?</i> Marta Berholts , Tartu University, Estonia [Virtual]
11:20-12:00	<i>Coffee break</i>
	<i>Session 2, Hall B, Chair: Sergio Diaz-Tendero</i>
12:00-12:30	<i>Plasmon-induced chemical reactions on noble metal nanoparticles studied by synchrotron XPS and surface-enhanced Raman scattering</i> Ilko Bald , University of Potsdam, Germany [Virtual]
12:30-12:50	<i>Valence band structure of isolated biomolecule-functionalized gold nanoparticles</i> Jelena Pajović , Faculty of Physics, University of Belgrade, Serbia [Regular]
12:50-13:10	<i>Determination of the Adenine-Thymine binding energy</i> Sebastian Hartweg , Synchrotron SOLEIL, France [Virtual]
13:10-13:30	<i>In the search of peptide prebiotic building blocks: Studying the fragmentation of photoionized Diketopiperazines</i> Darío Barreiro-Lage , Universidad Autónoma de Madrid, Spain [Regular]
13:30-15:30	<i>Lunch break</i>
	<i>Session 3, Hall B, Chair: Lucas Schwob</i>
15:30-16:00	<i>VUV and soft X-ray interactions with trapped biomolecular ions</i> Thomas Schlathöler , University of Groningen, Netherlands [TBC]
16:00-16:20	<i>Covalent bond formation within clusters: a pathway for the synthesis of complex molecules in the interstellar medium</i> Yoni Toker , Bar Ilan University, Israel [Regular]
16:20-16:40	<i>To be announced</i> Kaja Schubert , DESY, Germany [Virtual]
16:40-17:00	<i>X-ray absorption spectroscopy and mass spectrometry of protonated ATP molecule</i> Aleksandar Milosavljevic , Synchrotron SOLEIL, France [Regular]
17:00-17:30	<i>Coffee break</i>
	<i>Session 4, Hall B, Chair: Christophe Nicolas</i>
17:30-18:00	<i>An overview on the recent liquid-jet PES developments</i> Bernd Winter , Fritz Haber Institute of the Max Planck Society, Germany [Virtual]

18:00-18:20	<i>Surface propensity of small organic biomolecules in vapour-water interface by XPS</i> Alexandra Mocellin , Institute of Physics, Brasil [Virtual]
18:20-18:40	<i>Electronic structure and solvation effects from core and valence photoelectron spectroscopy of serum albumin</i> Jean Philippe Renault , University Paris Saclay, France [Virtual]
18:40-19:00	<i>First (e,e) coincidence measurements at PLEIADES beamline on solvated benzoate in water using a new magnetic bottle time-of-flight spectrometer</i> Jerome Palaudoux , Sorbonne Université, France [Virtual]
19:30-22:00	<i>Welcome cocktail (Gallery of Science and Technology, SASA)</i>

All indicated times are given in the Central European Summer Time (CEST) zone.

Tuesday 6th September 2022		
SPIG 2022 (day 2)		
<i>PL – Plenary lecture: 35+10 min</i>	<i>TL – Topical lecture: 25+5 min</i>	<i>PR – Progress Report: 15+5 min</i>
08:45-09:00	Opening, Chairs: V. Srećković, D. Ilić, B. Obradović, J. Cvetić	
	Plenary Session 1, Hall A, Chair: V. Srećković & D. Ilić	
09:00-09:45	Sven Thorwirth (Germany), Action-spectroscopic studies of transient carbon-rich molecular ions [Regular]	
09:45-10:30	Sergio Diaz-Tendero (Spain), Ultrafast dynamics of ionized molecules and molecular clusters in the gas phase [Regular]	
10:30-11:00	Break & Chat Room	
	Plenary Session 2, Hall A, Chair: B. Obradović	
11:00-11:45	Ryo Ono (Japan), Measurement and simulation of atmospheric-pressure streamer discharge [Virtual]	
11:45-14:30	Break	
	Hall A - Parallel Session: Chair: N. Simonović	Hall B - Parallel Session Chair: D. Borka
14:30-15:00	Stojan Madzunkov (USA), Utilization of Electric Dipole Fields in protection from GCR and SEPs [Regular]	Jiri Limpouch (Czech Republic), High-power laser interactions with low density porous materials and their applications [Virtual]
15:00-15:30	Gregory Boyle (Australia), Thermalisation time of electron swarms in Noble gases for uniform electric fields [Virtual]	Minna Patanen (Finland), Electron-ion coincidence experiments with electron and photon ionization [Virtual]
15:30-16:00	Mikhail Pinchuk (Russia), Control of guided streamer propagation and interaction with substrate in helium atmospheric pressure plasma jet [Regular]	Violeta N. Nikolic (Serbia), Spectroscopic investigation of the influence of NO ₃ ⁻ anions on the crystallization of the SiO ₂ matrix [15:30-15:50] [Regular]
16:00-16:30	Aranka Derzsi (Hungary), Surface processes in low-pressure capacitively coupled plasmas [Regular]	Dejan Dojčić (Serbia), Measurements of continuous optical spectrum during nanosecond laser pulse [15:50-16:10] [Regular] Milivoje Hadžijojić (Serbia), Study of two dimensional crystals by rainbow scattering effect [16:10-16:30] [Regular]
16:30-17:00	Break & Chat Room	
	Hall A - Parallel Session Chair: S. Tošić	Hall B - Parallel Session Chair: M. Trtica

17:00-17:30	Vasco Guerra (Portugal), Coupled kinetics in CO ₂ -N ₂ plasmas [Regular]	Nikola Starčević (Serbia), Ion-crystal rainbow interaction potential in channeling [17:00-17:20] [Regular]
17:30-18:00	Teodora Velcheva Kirova (Latvia), Numerical investigations of the impact of the magnetic field of radiation on amino acids [Regular]	Jovan V. Čiganović (Serbia), Action of pulsed lasers on titanium target: surface effects [17:20-17:40] [Regular]
18:00-18:30	Lucas Schwob (Germany), X-ray action spectroscopy of gas-phase biomolecular ions [Virtual]	Dušan Popović (Serbia), Picosecond pulsed laser ablation of silicon single crystal [17:40-18:00] [Virtual]
18:30-20:00	<i>Poster session (1)</i> Poster presentation – <i>Hall A</i> (Chair: <i>D. Borka</i>)	

All indicated times are given in the Central European Summer Time (CEST) zone.

Wednesday 7th September SPIG 2022 (day 3)		
<i>PL</i> – Plenary lecture: 35+10 min	<i>TL</i> – Topical lecture: 25+5 min	<i>PR</i> – Progress Report: 15+5 min
<i>Plenary Session 3, Hall A, Chair: D. Marić</i>		
09:00-09:45	Darryl Jones (Australia), Electron spectroscopies for probing electronic structure and collision dynamics [Virtual]	
09:45-10:30	James Sullivan (Australia), Experiments with positrons - from fundamental to applied science [Virtual]	
10:30-11:00	<i>Break & Chat Room</i>	
	<i>Hall A - Parallel Session</i> Chair: <i>G. Poparić</i>	<i>Hall B - Parallel Session</i> Chair: <i>V. Srečković</i>
11:00-11:30	Nicolina Pop (Romania), Dissociative recombination and excitation of molecular cations by electron-impact in cold plasmas: Application to H ²⁺ , BeH ⁺ and their isotopomers [Regular]	Stéphane Béchu (France), Investigation of the ro-vibrational levels of H ₂ /D ₂ molecules by VUV-absorption spectroscopy for the production of H-/D- negative ions for fusion application [Virtual]
11:30-12:00	Saša Dujko (Serbia), Electron transport, transient plasmas and high-energy phenomena in planetary atmospheres [Regular]	Joel Rosato (France), Line shape modeling for magnetic fusion and astrophysical plasmas: an overview of recent result [Virtual]
12:00-12:20	Milan Ignjatovic (Serbia), The influence of corona discharge on the lightning surge propagation along the transmission lines [Regular]	N. N. Bezuglov (Russia), Analysis of adiabatic processes in multilevel n-pod quantum systems from the perspective of riemannian geometry [Virtual]
12:30-14:30	<i>Break /SPIG Committee meeting at 13h</i>	
	<i>Hall A - Parallel Session</i> Chair: <i>V. Milosavljević</i>	<i>Hall A - Parallel Session</i> Chair: <i>L. Č. Popović</i>
14:30-15:00	Djordje Spasojević (Serbia), On the application of iterative kinetic model for diagnostics of abnormal glow discharges in noble gases [Regular]	Teresa Belmonte Sainz-Ezquerro (Spain), What can plasma spectroscopy do for astronomers? Measuring atomic parameters of astrophysical importance [Virtual]

15:00-15:20	Danilo Delibasic (Serbia), Relative importance of the electron continuum intermediate state in single-electron capture into any state of fast protons from helium-like atomic systems. [Regular]	Antonios Antoniou (Greece) , Describing the Mathematical Methods for Calculating Basic Physical Parameters of the Gaussian-Rotational (Gr) Model [Virtual]
15:20-15:40	Leo Sala (Czech Republic), Interaction of ionizing radiation with DNA nanostructures [Regular]	Thomas Salomon (Germany), Recent Progress on Action Spectroscopy of loosely bound Hydrogen-Helium complexes [Regular]

All indicated times are given in the Central European Summer Time (CEST) zone.

Thursday 8th September 2022		
SPIG 2022 (day 4)		
<i>PL – Plenary lecture: 35+10 min</i>	<i>TL – Topical lecture: 25+5 min</i>	<i>PR – Progress Report: 15+5 min</i>
<i>Plenary Session 4, Hall A, Chair: M. Trtica</i>		
09:00-09:45	Jorn Bonse (Germany), Laser-induced periodic surface structures, mechanisms, applications, and unsolved problems [Virtual]	
09:45-10:30	Marie-Lise Dubernet (France), Towards a Global Network for Laboratory Astrophysics Activities and Data [Virtual]	
10:30-11:00	Break & Chat Room	
<i>Plenary Session 3, Hall A, Chair: V. Guerra</i>		
11:00-11:45	Lawrence Overzet (USA), Measurements of RF plasma re-ignition: RF-IV and PROES [Virtual]	
11:45-14:00	Break	
	<i>Hall A - Parallel Session Chair: M. Škorić</i>	<i>Hall B - Parallel Session Chair: J. Cvetić</i>
14:00-14:30	Nathan Garland (Australia), When fusion plasmas get cool: A need for more atomic physics in classical fusion models [TBC]	Pavel Dvorak (Czech Republic), Higher harmonic frequencies of discharge voltage and current in capacitively coupled discharges [Regular]
14:30-15:00	Mohammed Koubiti (France), Application of machine-learning to spectroscopic line emission by hydrogen isotopes in fusion devices for isotopic determination and prediction [Virtual]	Milica Vasiljević (Serbia), Determination of the electric field strength in glow discharges using argon spectral lines. [Regular] 14:30-14:50
15:00-15:40	Break & Chat Room	
	<i>Hall A - Parallel Session Chair: V. Milosavljević</i>	<i>Hall B - Parallel Session Chair: D. Ilić</i>
15:40-16:00	Amit Kumar (Serbia), Design, development and characterization of atmospheric plasma system for wastewater treatment [Regular]	Viktor Radovic (Serbia), Development of a time-domain pipeline for detecting binary supermassive black holes in the upcoming Legacy Survey of Space and Time (LSST) [Virtual]

16:00-16:20	Nenad Selaković (Serbia), Mass spectrometry of plasma jet and application of electrical discharges operating at atmospheric pressure in biomedicine [Regular]	Milena Jovanovic (Serbia), Matter distribution in nearby galaxies [Virtual]
16:20-17:00	Break & Chat Room	
	Hall A - Parallel Session <i>Chair: I. Savić</i>	Hall B - Parallel Session <i>Chair: I. Mančev</i>
17:00-17:20 CET	Marija Puač (Serbia), Modeling of radio frequency breakdown by Monte Carlo technique [Regular]	Smita Omkarnath Ganguly (Sweden), Fragmentation of core-ionized adamantane molecule [Regular]
17:20-17:40 CET	Madhusree Roy Chowdhury (France), VUV Photoionization and Fragmentation of cyano-PAHs [Regular]	Dale Muccignat (Australia) , Simulating the feasibility of using liquid micro-jets for determining electron-liquid scattering cross-sections [Virtual]
17:40-20:00	Poster session (2) - Virtual poster presentations - Hall A (<i>Chair: N. Cvetanović</i>) [*Optional: 3min presentation per poster]	
20:30 -	Conference dinner and Closing	

Friday 9th September 2022	
SPIG 2022 (day 5)	
10:00-17:00	Excursions (optional, info at registration desk)
17:00	Departure

LIST OF POSTERS

No	Session	Title	Authors
1.	1.1.	Total cross section measurements for electron scattering on methyl formate (HCOOCH ₃) molecule: methylation effect	Natalia Tańska, Kuba Wójcik, Sylwia Dylnicka, Elżbieta Ptasińska-Denga, Czesław Szymkowski and Paweł Możejko
2.	1.1.	Dissociation of N ₂ by electron impact in RF electric field	V. Stanković, M. Ristić, R. Ranković, M. Aoneas, M. Vojnović and G. B. Poparić
3.	1.1.	Rate coefficients for O ₃ ⁺ dissociation to O ⁺ and O ₂ ⁺ by electron impact	M. M. Vojnović, M. M. Ristić and D. S. Belić
4.	1.1.	Photoelectron energy spectra in sequential two-photon ionization of hydrogen by gaussian and half-gaussian laser pulses	N. S. Simonović, D. B. Popović, A. Bunjac
5.	1.2.	Single-electron capture from He by fast alpha particles	Nenad Milojević, Danilo Delibašić Ivan Mančev

6.	1.3.	Reduced mobility of H ⁺ ions in n-butanol gas	Željka Nikitović and Zoran Raspopović
7.	1.3.	Excitation of $^1\Sigma_u^+$ and $^1\Pi_u$ states and ionization of CO ₂ in DC electric field	Violeta V. Stanković, Mirjana M. Vojnović, Miroslav M. Ristić, Sava M.D. Galijaš and Goran B. Poparić
8.	1.3.	Formation and propagation of streamers in CF ₃ I-SF ₆ gas mixtures	J. Atić, D. Bošnjaković, I. Simonović, Z.Lj. Petrović and S. Dujko
9.	1.3.	Electron transport coefficients in CO: Scanning drift tube measurements and kinetic computations	S. Dujko, D. Bošnjaković, M. Vass, I. Korolov, P. Hartmann, N. Pinhao, D. Loffhagen and Z. Donko
10.	1.3.	Third-order transport coefficients for electrons in C ₃ F ₈	I. Simonović, D. Bošnjaković, Z.Lj. Petrović and S. Dujko
11.	2.1.	The time-symmetric description of electron exchange in ion-ion collision	S. M. D. Galijaš, V. M. Milosavljević and G. B. Poparić
12.	2.1.	Analytical expression for stopping force acting on a slow charged particle moving parallel to a thick graphene-sapphire-graphene structure	Ana Kalinić, Ivan Radović, Lazar Karbunar, Vito Despoja and Zoran L. Mišković
13.	2.1.	Bohmian dynamics of positrons channeled through a chiral carbon nanotube	M. Ćosić, M. Hadžijojić, and N. Nešković
14.	2.1.	Study of graphene by rainbow scattering effect	M. Hadžijojić and M. Ćosić
15.	2.1.	The influence of the ion-target parameters on the size of the surface nanohillocks created by an impact of highly charged ions	N. N. Nedeljković, M. D. Majkić, M. A. Mirković, I. Stabrawa, D. Banaš
16.	2.1.	Effect of the ionic type on the shape of the nanostructures created by an impact of slow highly charged ions on gold surface	M. D. Majkić, N. N. Nedeljković M. A. Mirković,
17.	2.2.	Influence of carbon ions of different multiplicity on regimes of promising laser technologies for the deposition of diamond-like carbon nanocoatings	V.K.Goncharov, G.A.Gusakov, M.V.Puzyrev
18.	2.3.	Elemental analysis of austenitic steel by calibration-free laser-induced breakdown spectroscopy (CF-LIBS)	I. Traparić, M. Jovanović, M. Kuzmanović, M. Ivković

19.	2.3.	ODS+Hf and AISI 316L steel surface variations at high laser intensity, 1013 W/cm ² , in air and vacuum: comparative study	M. Trtica, J. Stasic, X. Chen and J. Limpouch
20.	2.3.	Silicon spalling destruction and ablation in air under bichromatic laser radiation	A.N. Chumakov, V.V. Luchkouski and I.S. Nikonchuk
21.	2.3.	Features of silicon ablation in air under the influence of Nd:YAG laser harmonics	A.N. Chumakov, V.V. Lychkovsky, I.S. Nikonchuk
22.	2.3.	Investigation of properties of yttrium vanadate YVO ₄ films	N.A. Bosak, A.N. Chumakov, L.V. Baran, V.V. Malyutina-Bronskaya, T.F. Raichonok, A.A. Ivanov, V.V. Kiris, E.M. Dyatlova, A.A. Shevchenok, A.V. Buka, A.S. Kuzmitskaya
23.	2.3.	Treatment of steel 16MnCr5 and steel 42CrMo4 by plasma flow generated in magnetoplasma compressor	Nora Trklja Boca, Žarko Z. Mišković, Radivoje M. Mitrović, Bratislav M. Obradović, Milorad M. Kuraica
24.	2.3.	Combining plasma-assisted synthesis of metal oxide nanoparticles with thin films deposition	Natalie Tarasenko, Vladislav Kornev, Alena Nevar, Mikhail Nedel'ko, Anton Radomtsev and Nikolai Tarasenko
25.	2.3.	Perspective on the use of nanoparticles to improve the tea CO ₂ based LIBS analytical performances: copper nanoparticles for NELIBS analysis of polypropylene	S. Živković, J. Petrović, M. Momčilović, M. Radenković, N. Krstulović, J. Car, D. Palasti, F. Casian Plaza and G. Galbács
26.	2.3.	Analytical prediction and numerical analysis of plasma mediated ablation of skin tissue samples with nanosecond-to-femtosecond laser pulses	H. Delibašić, Marković, V. Petrović and I. Petrović
27.	2.3.	Pulsed laser assisted fabrication of Co-doped ZnO nanocrystalline layers on a glass substrate	Natalie Tarasenko, Vladislav Kornev, Svetlana Pashayan, and Nikolai Tarasenko
28.	3.1.	The gas temperature diagnostics by means of AIO (B ² Σ ⁺ –X ² Σ ⁺) molecular band system from the upgraded atmospheric pressure pulsed discharge source in argon	Jovica Jovović, Gordana Lj. Majstorović
29.	3.1.	High-resolution spectroscopy of astrophysically relevant molecular ions	O. Asvany, S. Thorwirth, P. C. Schmid, T. Salomon, and S. Schlemmer

EUROPHYSICS CONFERENCE ON THE ATOMIC AND MOLECULAR PHYSICS OF IONIZED GASES

SINCE 1973

INTERNATIONAL SCIENTIFIC COMMITTEE

C. D. Pintassilgo, Portugal, Chair	F. Krčma, Czech Republic
R. Brandenburg, Germany	T. Minea, France
C. Costin, Romania	N. Škoro, Serbia
A. Derszi, Hungary	E. Stamate, Denmark
A. Fillipov, Russia	F. Taccogna, Italy
V. Herrero, Spain	E. Wagenaars, UK

Institute of Physics
University of Belgrade
Pregrevica 118, 11080 Belgrade, Serbia

10th October 2023

Dear Dr. Marija Puac

On behalf of the International Scientific Committee of the **Europhysics Conference on the Atomic and Molecular Physics of Ionized Gases (ESCAMPIG)**, it is my great pleasure to invite you to give a topical invited lecture on the next ESCAMPIG, which will be held in Brno, Czech Republic, from 9th to 13th July 2024.

The indicative title proposed by the Committee for your talk is

“Radio-frequency discharges - Monte Carlo breakdown fundamentals and simulation of electrical circuits of rf discharges”

The time devoted to a topical talk is 30 minutes, including questions and discussion.

We should be greatly honoured if you would accept our invitation. We are convinced that your presence at the Conference will contribute to the success of ESCAMPIG 2024.

Please let us know as soon as possible if you are able to accept this invitation.

Yours sincerely,



Carlos Daniel Pintassilgo
Chair of the International Scientific Committee of the ESCAMPIG

Prof. Carlos D Pintassilgo cdp@fe.up.pt

Faculdade de Engenharia da Universidade do Porto
Departamento de Engenharia Física
R Dr Roberto Frias,
4200-465 Porto
Portugal

Instituto de Plasmas e Fusão Nuclear
Instituto Superior Técnico
Av. Rovisco Pais
1049-001 Lisboa
Portugal



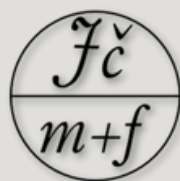
ESCAMPIG 2024

9- 13 JULY 2024, BRNO, CZECH REPUBLIC

26th Europhysics Conference on Atomic and Molecular Physics
of Ionized Gases

BOOK OF ABSTRACTS

MUNI Department of Plasma
Physics and Technology
SCI



CEPLANT

escampig2024@physics.muni.cz

**Department of Plasma Physics and Technology and CEPLANT
Faculty of Science
Masaryk University**

In collaboration with Jednota českých matematiků a fyziků

Local Organizing Committee

Chairman: Zdeněk Bonaventura (MUNI)

Co-chairman: Tomáš Hoder (MUNI)

Bohumila Tesaříková (MUNI)

František Krčma (BUT)

Ondřej Jašek (MUNI)

Pavel Dvořák (MUNI)

Realization/Support

Eliška Vrzalová (MUNI)

Anežka Winklerová (MUNI)

Pavel Kunovský (MUNI)

Monika Stupavská (MUNI)

Tereza Schmidtová (MUNI)

Radka Kunovská (MUNI)

Jan Vondra (JČMF)

International Scientific Committee

Chairman: Carlos Pintassilgo (Portugal)

Ronny Brandenburg (Germany)

Claudiu Costin (Romania)

Aranka Derszi (Hungary)

Anatoly Filippov (Russia)

Victor Herrero (Spain)

Nikola Škoro (Serbia)

Tiberiu Minea (France)

Eugen Stamate (Denmark)

Francesco Taccogna (Italy)

František Krčma (Czech Republic)

Erik Wagenaars (United Kingdom)

Edited by Ondřej Jašek

Postconference edition, 26.8. 2024, Brno

ESCAMPIG 2024 supported by

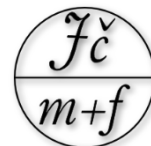


Table of Content

About Escampig Conference	4
Conference program overview	5
Conference Workshops	6
Social Events	7
Detailed Program, Tuesday July 9th	8
Detailed Program, Wednesday July 10th	8
Poster Session 1, Wednesday July 10th	26
Detailed Program, Thursday July 11th	182
Poster Session 2, Thursday July 11th	213
Detailed Program, Friday July 12th	364
Detailed Program, Saturday July 13th	383
Conference participants and Author Index	399
ESCAMPIG 2024 Participation statistics	404
Conference photo	405
Best Poster Prizes	406
Escampig Herald	407
Sponsors	420

About ESCAMPIG Conference

The history of the ESCAMPIG conference dates back to 1973, when the first ESCAMPIG conference was held in Versailles. Since 1974, the ESCAMPIG conference has been held every two years, with the exception of 2020, when the event was postponed for two years due to the pandemic. The community of conference participants increased since the first conference and settled at a stable value of around 200 participants, leading experts worldwide focusing on atomic and molecular processes in ionized gases, basic and applied plasma research, diagnostic methods, plasma-surface interactions, plasma sources, and technologies. During half a century of ESCAMPIG history, this conference has been organized in many countries of Western and Eastern Europe. In 2024, ESCAMPIG will be held in the Czech Republic for the first time in history.

Dear Participants,

On behalf of the Local Organization Committee and the Realization/Support team, I would like to extend our heartfelt thanks for your participation in ESCAMPIG 2024!

The friendly and enthusiastic atmosphere that, I believe, we all experienced during the conference is a testament to the vitality of the ESCAMPIG community. The significant number of young researchers attending is also a very promising sign for the future of the field. Let's hope we will have plenty of opportunities to meet and exchange ideas at events to come. It was our great pleasure to host you at ESCAMPIG 2024!

Zdenek Bonaventura, Chairman of LOC

1973	Versailles	France	2016	Bratislava	Slovakia
1974	Innsbruck	Austria	2018	Glasgow	United Kingdom
1976	Bratislava	Czechoslovakia	2022	Paris	France
1978	Essen	West-Germany (F.R.G.)	2024	Brno	Czech Republic
1980	Dubrovnik	Yugoslavia			
1982	Oxford	United Kingdom			
1984	Bari	Italy			
1986	Greifswald	East-Germany (G.D.R.)			
1988	Lisbon	Portugal			
1990	Orléans	France			
1992	St. Petersburg	Russia			
1994	Noordwijkerhout	The Netherlands			
1996	Poprad	Slovak Republic			
1998	Malahide	Ireland			
2000	Lillafüred	Hungary			
2002	Grenoble	France			
2004	Constanta	Romania			
2006	Lecce	Italy			
2008	Granada	Spain			
2010	Novi Sad	Serbia			
2012	Viana do Castelo	Portugal			
2014	Greifswald	Germany			



Conference Program Overview

Tuesday July 9		Wednesday July 10		Thursday July 11		Friday July 12		Saturday July 13	
		8:20	OPENING						
		8:35	H. Kersten	8:30	G. D. Stancu			8:30	J. Országh
		9:20	M. Puač	9:15	C. Vitelaru	9:15	L. Vialetto	9:15	F. Cichocki
		9:50	F. Sobczuk	9:50	Y. Guo	9:45	M. Baeva	9:45	Crookes Prize X.Tu
		10:10	O. Tarvainen	10:05	C.L. da Silva	10:05	Z. Kozáková		
		10:30	Coffee Break	10:30	Coffee Break	10:30	Coffee Break	10:30	Coffee Break
		11:00	P. Bruggeman	11:00	K. Kutasi	11:00	L.L. Alves	11:00	J. de Urquijo
		11:45	A. Stancampiano	11:45	M. Jimenez Redondo	11:45	A. Gómez-Ramírez	11:20	F.J. Morales-Calero
		12:15	V. Guerra	12:15	M. Rutigliano	12:15	C. Ionita	11:40	A. Cobos-Luque
		12:35	E. Wagenaars	12:35	J. Teunissen	12:35	T. Osawa	12:00	Q. Delavière-Dellion
		12:55	Lunch	13:10	Lunch	12:55	Lunch	12:20	CLOSING
								12:50	
		14:30	Poster Session 1	14:30	Poster Session 2	14:30	Excursions		
16:30	Registration	16:30	Coffee Break	16:30	Coffee Break				LEGEND
									General Invited Talk
									Topical Invited Talk
									Oral Presentation
									Hot Topic Talk
									Workshops
									IUPAP Early Career Prize
18:00	Welcome Party	17:00	A. Nelson, V. Guerra, M.Becker, M. Kushner	17:00	A. Dogariu	17:00			
				17:30	A. Gerakis				
				18:00	P. Dvořák	18:00	Lab tour MUNI		
				18:30	J.-P. van Helden	19:00	Garden Party MUNI		
		19:00		19:00					
				20:00	Conference dinner				
21:30				1:00		21:30			

Workshop 1

Predictive and practical simulations of plasma systems and plasma processes

Chairman: Adam Obrusnik (MUNI, PlasmaSolve, Czech Republic)

This topical workshop explores the evolution of plasma modeling and simulation over the past 10-20 years, highlighting both success stories and challenges. It features four renowned speakers from the field of low-temperature plasma, each with distinct primary expertise: calculating fundamental data for models, engineering plasma chemistry, modeling of industrial low-pressure systems, and elucidating new plasma mechanisms. The workshop will commence with each expert sharing their insights and experiences regarding plasma process simulation and their future outlook on the topic. This will be followed by a panel discussion, during which the audience, facilitated by the moderator, is encouraged to pose questions related to the workshop's theme. The workshop will be moderated by Adam Obrusnik who is a researcher dedicated to the development of plasma models for various applications, such as material deposition and plasma catalysis but also an entrepreneur who operates a company providing simulation solutions to diverse industries utilizing plasma.

SPEAKERS

Anna Nelson (United Kingdom), Vasco Guerra (Portugal), Marcus Becker (Germany), Mark J. Kushner (USA)

Workshop 2

Advancements in non-equilibrium plasma laser diagnostics

Chairman: Gabi Daniel Stancu (CentraleSupélec, France)

Non-equilibrium plasmas are complex reactive environments driven by multiphysics interactions that are employed or studied to meet numerous societal goals. Given the high intricacy of these systems, laser diagnostics remain essential to the advancement of plasma knowledge and engineering. Their exceptional features enable probing with high sensitivity, selectivity, spatial and temporal resolutions crucial plasma parameters such as nonequilibrium temperatures, densities of key reactive species, velocity and flux distributions and fields. The workshop will expose recent progresses achieved in advanced laser diagnostics for the investigation of non-equilibrium plasmas. Fundamental properties of non-equilibrium plasmas are tackled here by resonant or non-resonant, single or multiphoton and multi-wave techniques, including cavities and ultrashort lasers with wavelengths from ultraviolet to the THz spectroscopic domain. Principles, challenges, examples of studies of non-equilibrium plasmas and perspectives will be addressed.

SPEAKERS

Jean-Pierre van Helden (Germany) - Atomic oxygen measurements with THz absorption spectroscopy, ps-TALIF, and CRDS: A comparison

Alexandros Gerakis (Luxembourg) - Non-resonant four wave mixing diagnostics for the determination of nonequilibrium in plasmas

Pavel Dvořák (Czech Republic) - LIF studies of hybrid dissociation in electric discharges

Arthur Dogariu (USA) - Non-equilibrium thermometry in gases and plasmas using hybrid CARS

EXCURSIONS

Friday July 12th, 2024

ŠPILBERK CASTLE

Špilberk Castle has dominated Brno's skyline since the mid-13th century. Historically, it served not only as a symbol of safety and protection but also, at times, inspired fear and represented oppression for the city's citizens. A sightseeing tour of the castle includes the Casemates prison, historical fortifications, and a lookout tower.

BRNO UNDERGROUND

Water tanks Žlutý kopec: Mysterious underground cathedrals from the years 1874, 1894, and 1917 Two brick and one concrete water tank, unparalleled in Europe, whose visit will take your breath away! This Brno "must-see" is located under the unassuming grassy area of a revitalized park on Žlutý kopec and offers an experience akin to that of another world from a long-lost civilizations. Three colossal underground tanks are a unique architectural monument and a testament to exceptional technical industrial architecture in its pristine form.

VILLA TUGENDHAT

Villa Tugendhat, designed by the renowned German architect Ludwig Mies van der Rohe, was constructed in 1929–1930. It quickly became an icon of modern architecture in Europe, particularly noted for its revolutionary approach to space and the use of industrial building materials. The villa's history is as captivating as its cultural significance. In 2001, Villa Tugendhat was inscribed on the UNESCO World Heritage List, cementing its status as a pivotal work of architecture.

SOCIAL EVENTS

WELCOME RECEPTION/PARTY

Tuesday July 9th, 2024

The welcome reception will take place at the conference venue on Tuesday, July 9, from 6 p.m. The reception will feature a performance by the University Folk Song and Dance Ensemble Pořana Brno, along with their folk dance school.

CONFERENCE DINNER

Thursday July 11th, 2024

The conference dinner will take place at the Brewery House Poupě (Dominikánská 342, Brno) on Thursday, July 11, 2024, at 8 p.m. A buffet-style dinner offering a wide selection, including non-alcoholic beverages, beer, and wine, is planned. This dinner is included in the conference fee.

GARDEN PARTY AND LAB TOURS

Friday July 12th, 2024 from 5 p.m.

The garden party will be held on Friday, July 12, from 6 p.m. at the Botanic Garden of Masaryk University (Kotlářská 2, Brno). A BBQ-style dinner will be available, including soft drinks, beer, and wine. Guests will have the opportunity to visit the greenhouses of the Botanic Garden. Additionally, lab tours at the Department of Plasma Physics and Technology will be possible prior to the Garden Party.

ACCOMPANYING PERSONS

Optional programs for accompanying persons will be prepared and could additionally be arranged with the LOC upon request.

Detailed conference program Tuesday 9th, 2024

16:30	REGISTRATION
18:00	Welcome Party
21:30	

Detailed conference program Wednesday 10th, 2024

8:00	REGISTRATION		
8:20	OPENING - Carlos Pintassilgo, Zdeněk Bonaventura		
Morning Session Chairman: Ronny Brandenburg			
8:35	General invited	H. Kersten	On the combination of common and non-conventional probe diagnostics for process plasmas
9:20	Topical invited	M. Puač	Nature of radiofrequency breakdown in argon viewed through electron energy distribution functions modeled by the Monte Carlo technique
9:50	Oral	F. Sobczuk	Enhancing Low-Temperature Plasma Diagnostics: Ultra-High Resolution Spectroscopy with Signal Amplification
10:10		O. Tarvainen	Space charge compensation of pulsed high-current negative and positive hydrogen ion beams
10:30	Coffee Break		
Midday Session Chairman: Nikola Škoro			
11:00	General invited	P. Bruggeman	Plasma-liquid interactions: overview and perspectives
11:45	Topical invited	A. Stancampiano	Plasma in interaction with water droplets
12:15	Hot topic	V. Guerra	Deep Learning for Low-Temperature Oxygen-Based Plasmas Modelling
12:35		E. Wagenaars	Formation of O and H radicals in an atmospheric-pressure nanosecond pulsed discharge in helium with water vapour admixtures
12:55	Lunch		
14:30	Poster Session 1		
16:30	Coffee Break		
17:00	Workshop 1	A. Nelson, V. Guerra, M. Becker, M. Kushner	Predictive and practical simulations of plasma systems and plasma processes (Panel discussion)
19:00			

Nature of radiofrequency breakdown in argon viewed through electron energy distribution functions modeled by the Monte Carlo technique

Marija Puač¹ and Zoran Lj Petrović^{2,3}

¹ *Institute of Physics, University of Belgrade, 11080 Zemun, Serbia*

² *Serbian Academy of Science and Arts, 11001 Belgrade, Serbia*

³ *Department of Electrical Engineering Ulster University,*

(*) *smarija@ipb.ac.rs*

This paper investigates radiofrequency breakdown in argon by analyzing the electron energy distribution functions obtained from a Monte Carlo code. Energy gain is determined by the external AC field and applied frequency of 13.56 MHz while losses are due to many collisions between electrons and the background gas and electrons and infinite parallel electrodes. Two points on the breakdown voltage curve with the same breakdown pressure of 0.2 Torr and different voltages of 94 V and 447 V highlighted the need of increasing the number of electron – background gas collisions to maintain the discharge, which led to increase of pressure, hence the double valued nature of rf breakdown voltage curve. On the other hand, presence of Ramsauer minimum in the cross section for elastic scattering is responsible for fast collapse of EEDF peak for some combinations of breakdown voltage and breakdown pressure.

Radiofrequency (RF) breakdown has been analyzed in our recent papers [1], [2] as well as the role of attachment process in oxygen gas on the breakdown curve as the loss mechanism in the gas volume between two electrodes [3]. Now we have employed Monte Carlo code to investigate electron energy distribution functions (EEDFs). Background gas is argon and the applied frequency is 13.56 MHz. Electron dynamics is defined only by the external AC field and electron-gas molecule collisions. When electron reaches one of the electrodes it is being deleted from the simulation.

In Fig. 1 we have presented EEDFs along the breakdown voltage curve. As expected, mean energies are higher at high voltages (left-hand side of the curve). Electrons can also gain more energy from the AC field along their path uninterrupted with collisions, due to small pressures (background gas density). At the same time, there is a difference between EEDF sampled at different times in one period of AC field (lines in various colors in the same plot). When the AC field passes through zero, the EEDF has its maximum peak value because electrons gain small amounts of energy from the field and the low energy electrons are dominant. At the AC field maximum EEDF has the longest “tail”, electrons gain more energy, as expected. Right-hand side of the breakdown voltage curve has almost uniform EEDF over time period (from zero to 2π). Electrons mean energy has small deviation from the mean value. It is because the energy gain from the AC field gets “interrupted” by numerous collisions and EEDF doesn’t change much over one period.

Double valued nature of RF breakdown voltage curve [1] can be analyzed by focusing on the energy balance. Fig. 2 shows the differences between two breakdown points that have the same breakdown pressure of 0.2 Torr and different voltages of 94 V and 447 V (plots A and D from Fig. 1). In Fig. 2a there is comparison of mean energies. Minimum values of both energy plots are similar but maximum energies and means are quite different. Mean value for point A is around 20 eV while for D point is around 8 eV. We know that pressure is the same and it can be assumed that electrons experience the same number of collisions with background gas in both points (assuming that the collision frequency is not strongly dependent on the energy). Hence losses in the gas volume do not play a deciding role in energy balances for those two points. It is very likely that the high voltage in the second (‘upper’) curve is due to the high voltage that pushed electrons towards the electrode and thus increased the losses at

same point allowed electron to gain enough energy to ionize before colliding with the electrode. That allowed for achieving selfsustained conditions again for the same pressure.

The main difference is in energy that electron can obtain from the field between two collisions, presented in Fig. 2b. At the higher voltage that energy is around 1.5 eV while at lower voltage that energy drops almost 100 times. It means that electron needs to experience 100 times more elastic collisions to acquire enough energy to perform ionization, compared to the electron at 447 V. As both points are in region of low pressures and small number of collisions with the background gas, we can conclude that higher voltage point has more efficient ionizations.

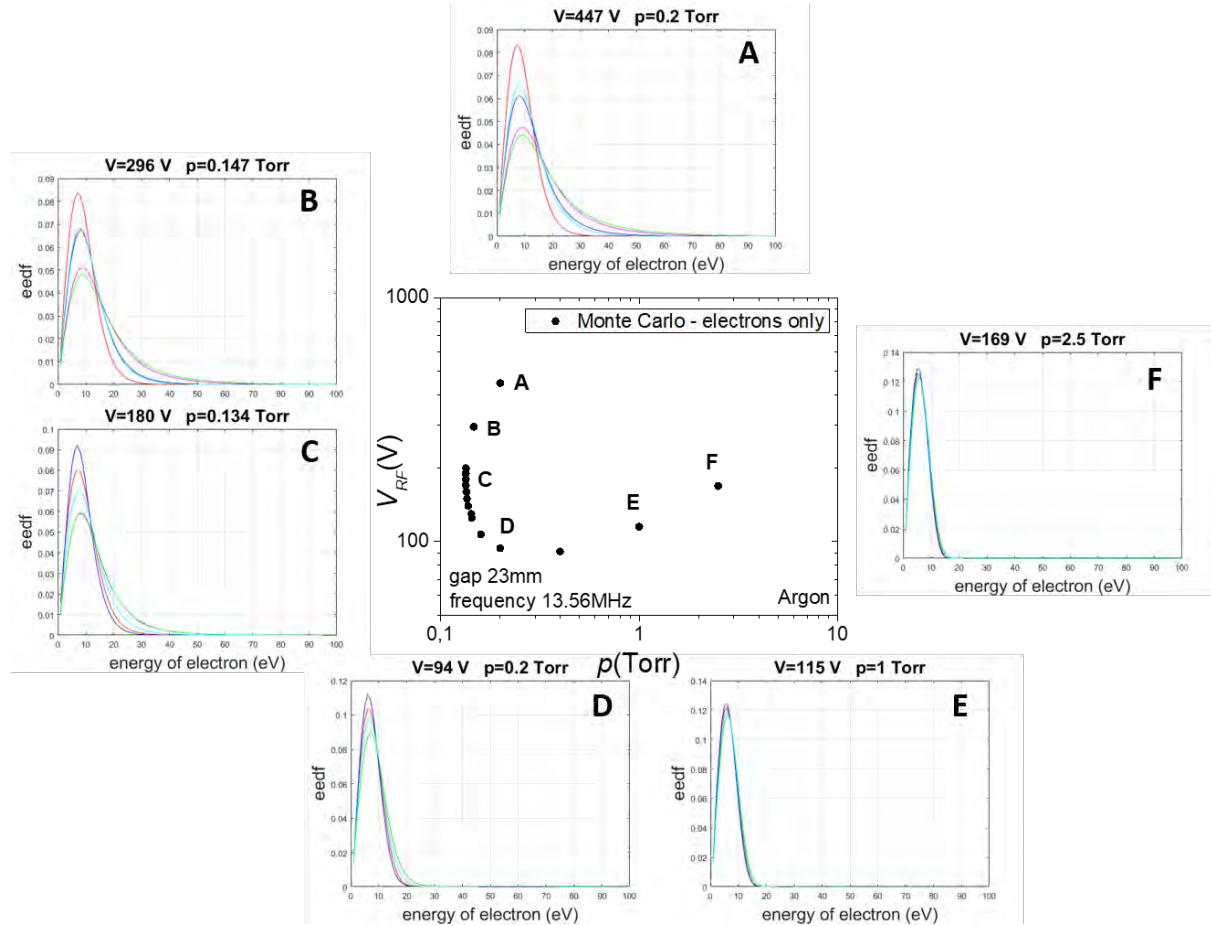


Fig. 1: Electron energy distribution functions (EEDFs) along breakdown voltage curve. Different lines at the same plot represent EEDF sampled at different times (from zero to 2π). Background gas is argon, frequency is 13.56 MHz and gap is 23 mm.

How the EEDFs are linked to the number of collisions can be seen in Fig. 3. In Fig. 3a EEDFs in the volume of the gas over one half period of time for the already mentioned points A and D from Fig. 1 are presented. We can see that at higher voltage there is a narrow peak with long tail that indicates presence of high energy electrons. At lower voltage peak is wider and tail is much shorter than at 447 V. Both peaks are slightly delayed compared to the field minima at $\pi/2$ which is a consequence of the inability of energy to relax at applied frequency of 13.56 MHz. Also, the difference in time necessary for the peak to form and to diminish can be observed. To investigate this peak “cycle” we have presented relaxation of 95% EEDF peak value over half period of time in Fig. 3b with applied AC field in light blue colored line. Value of 95% of the peak is chosen to avoid statistical fluctuations that the 100% of the peak has. Fig. 3c shows number of elastic collisions. As can be seen in Figure 3b, there is a steep slope that characterizes peak decline, which is more pronounced at the higher voltage. Decline in EEDF

means that electrons obtain energy fast which is in a good agreement with the peak in number of elastic collisions. Peak in the number of collisions (Fig. 3c) has to be a consequence of the peak in argon cross section set. That leads to a conclusion that at point A after the EEDF peak, the majority of the electrons have the energy that corresponds to the energy of the Ramsauer minimum and at the same time they gain energy fast.

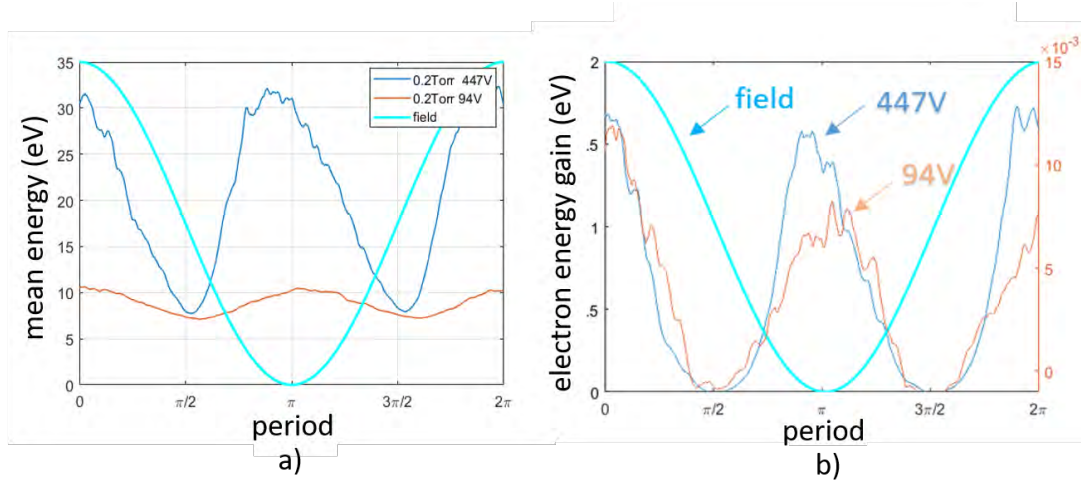


Fig. 2: a) mean energies for point A and D from Fig. 1, b) Gain of energy transferred from AC field to the electron between two collisions for points A and D (Fig. 1) with the same breakdown pressure of 0.2 Torr and different voltages: 447 V and 94 V. Background gas is argon, frequency is 13.56 MHz and gap is 23 mm.

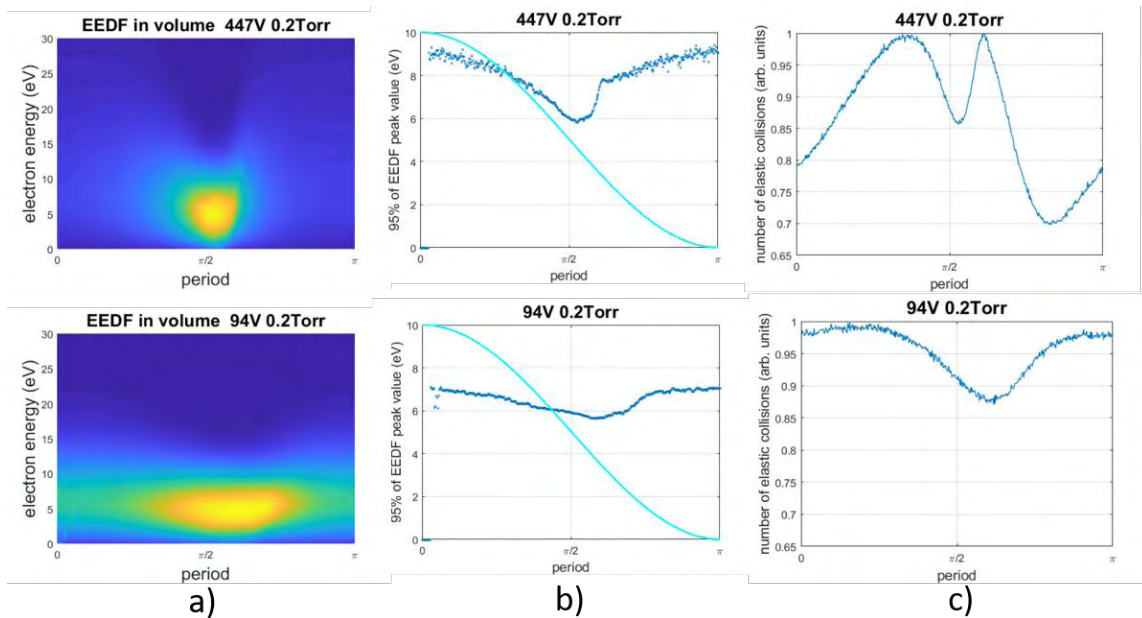


Fig. 3: a) EEDF over half period of time in 2D plots for points A and D (Fig. 1) with the same breakdown pressure of 0.2 Torr and different voltages: 447 V and 94 V. b) Relaxation of the 95% EEDF peak value over one half period for the same points as in Fig. 3a. Light blue line presenting applied AC field. c) Number of elastic collisions over one half of the period. All features do not present values but only how their shape is changing over half period of time (all are normalized to have maximum at 1). Background gas is argon, frequency is 13.56 MHz and gap is 23 mm.

The moment when discharge induced by the applied AC field ignites, as we know, is a balance of electron production via ionization and losses at electrode surfaces by absorption. Behind rough counting of electron number over time [1, 2] there is a neat energy balance that needs to be fulfilled. When voltage

breakdown curve moves towards high voltages and low pressures, number of collisions with the background gas decreases, breakdown voltage has a steep rise in its value and the amount of energy that electron can get from the AC field between two collisions has a steep growth as well. Rapid increase in electron energy is restricted by the point where electron crosses the gap between two electrodes too fast with insufficient number of collisions to perform ionization and they are being absorbed by the electrode, no matter how high their energy is. At that point, increase in number of collisions is required to randomize electron movement and to increase probability for them to experience ionization before they reach the electrode. Their portions of energy gained from the AC field between two collisions are being reduced but still big enough to overcome ionization threshold before they are lost at the electrode.

Acknowledgments: This research was supported by the Science Fund of the Republic of Serbia, 7739780, APPerTAIN-BIOM project and MSTDI-451-03-68/2022-14/200024. Zoran Lj Petrović is grateful to the SASA project F155.

References:

- [1] Savić M, Radmilovic-Radjenovic M., Šuvakov M., Marjanović S., Marić D., Petrović Z. Lj, *IEEE T Plasma Sci.* **39** (2011) 2556.
- [2] Puač M., Marić D., Radmilović-Radjenović M., Šuvakova M., Petrović Z. LJ, *Plasma Sources Sci. Technol.* **27** (2018) 075013.
- [3] Puač M., Đorđević A., Petrović Z. Lj. *European Physical Journal D:* **74** (2020) 74:72.

Monte Carlo simulation of RF breakdown in oxygen – the role of attachment[★]

Marija Puač^{1,a}, Antonije Đorđević^{2,3}, and Zoran Lj Petrović^{1,2}

¹ Institute of Physics, University of Belgrade, Pregrevica 118, 11080 Belgrade, Serbia

² Serbian Academy of Sciences and Arts, Knez Mihailova 35, 11001 Belgrade, Serbia

³ School of Electrical Engineering, University of Belgrade, Bulevar kralja Aleksandra 73, 11001 Belgrade, Serbia

Received 25 October 2019 / Received in final form 22 February 2020

Published online 14 April 2020

© EDP Sciences / Società Italiana di Fisica / Springer-Verlag GmbH Germany, part of Springer Nature, 2020

Abstract. Breakdown in oxygen, in external radio-frequency (RF) electric field is analyzed by employing a Monte Carlo simulation (MCS). Results were obtained for 13.56 MHz and distance between electrodes of 15 mm. Physical background of an oxygen RF breakdown is explained by observing time-resolved spatial distributions of electron concentration, mean energy, elastic scattering rate, ionization rate and attachment. The role of attachment is investigated in cases when these processes are included and when they are not. Especially influence of the attachment is highlighted by comparing oxygen and argon breakdown-voltage curves and spatial profiles. The electron losses induced by attachment extend the motion of the electron prebreakdown swarm much closer to electrodes to achieve a greater production; hence, spatial profiles at high values of the product pd where p is the pressure and d is the gap between electrodes, become more similar to those at the minimum of the breakdown curve. The most striking difference between the breakdown curves in argon and in oxygen is in the high increase of the breakdown voltage for high pd in oxygen.

1 Introduction

Considering the applicability of radio-frequency (RF) plasmas and their wide presence in industry, from integrated circuit (nanoelectronics) processing [1,2] all the way to the non-equilibrium (cold) plasma applications in medicine and agriculture [3,4], one would expect an equivalent interest in fundamental properties of RF breakdown and discharges. The basic understanding of RF plasmas that has been reached recently [5,6] is in principle relevant when the so called alpha regime is considered. However these studies start from a formed plasmas and consider the final profile of the self-consistent electric field. Thus those papers are not directly relevant for the breakdown which occurs in pristine gas without space charge and without preexisting excited species (that is the basic definition of the gas background in swarm studies). Since the operating voltage for formed plasmas may be quite different from the breakdown condition and since the whole art of producing the non-equilibrium plasmas at atmospheric pressure

depends very much on controlling the breakdown condition it is important that the understanding of RF plasma operation is being matched by the studies of RF breakdown [7–10] that have been undertaken recently.

While the RF discharges have been studied for quite some time by the likes of Tesla, Hittorf, Pupin and others, the swarm limit that is relevant for the breakdown conditions has not been considered for some time, although motivation existed in propagation of the electromagnetic waves through the ionosphere. In 1946 Holstein published a research on electron energy distribution in high-frequency gas discharge [11]. This study falls to the category of swarm physics and is thus directly relevant for breakdown but in itself is not a study of breakdown conditions. Later, the basic research of high-frequency breakdown was done by Margenau and Hartman and was published in their four papers named “Theory of high-frequency gas discharges”, including calculations of electron distribution functions, breakdown at low pressures and similarity laws [12–15]. At the same time, von Engel was investigating the starting potentials of high-frequency gas discharges and he proposed a theory (though we could use the term phenomenology in its literal meaning) of the high-frequency breakdown that has not been significantly changed almost to the present day [16,17]. The basic idea in the proposed explanation by von Engel and coworkers is that the condition for breakdown coincides with

[★] Contribution to the Topical Issue “Low-Energy Positron and Positronium Physics and Electron-Molecule Collisions and Swarms (POSMOL 2019)”, edited by Michael Brunger, David Cassidy, Saša Dujko, Dragana Marić, Joan Marler, James Sullivan, Juraĵ Fedor

^a e-mail: smarija@ipb.ac.rs

the condition that in one half period electrons may drift from one electrode to the other and then drift back as the field changes direction. One of the reasons for the absence of RF breakdown research is probably the existence of only a few experiments that could measure breakdown-voltage curves with reasonable precision providing reliable and well defined results that could be used in modeling. One of the experimental setups that has produced a lot of results of breakdown-voltage curve measurements in different gases in recent times, is the experiment of Lisovskiy and coworkers [18]. In the analysis these authors directly apply von Engel's phenomenology and extract even drift velocities under assumption of a sinusoidal time dependence of the drift velocity with changing E/N (t). Recently, two more elaborate experiments have been constructed by Korolov and colleagues [9,10] and Đorđević et al. [19,20]. Hence, now there exists a better starting point to build models of RF breakdown.

Basic physical description of RF breakdown has already been provided in our previous papers [7,8] in case of argon as a background gas. Also, the shape of the breakdown-voltage curve with a double-valued region at low pressures and similarity law were explained. While argon was easy to analyze due to its simpler set of collisional processes, in this paper we chose oxygen as a target. Motivation for focusing on oxygen is that it is an important constituent of the atmosphere that adds attachment (two and three-body processes) as a new non-conservative channel for electron losses. Attachment, on the other hand defines breakdown (dielectric properties) and behavior of most atmospheric discharges (both natural and man-made).

Oxygen has (similar to nitrogen, the other dominant atmospheric gas) a number of rotational and vibrational excitations in addition to electronic excitations. As a consequence, losses of electron energy in gas are significant [21] at all energies as compared to argon. From the breakdown point of view, the attachment represents electron loss mechanism in the volume (in addition to the electron losses by electrode absorption). In oxygen it all occurs also in the background of higher energy losses but distribution function has to adjust to the conditions when ionization can overcome all the losses and thus breakdown has to occur at considerably higher E/N as compared to argon. In order to explain the role of the non-conservative electron losses on the breakdown in RF fields in the presence of vibrational excitation energy losses we shall compare the anatomy of the profiles of emission, energy and ionization to those of argon.

2 Model and Monte Carlo simulation

Monte Carlo (MC) code that we have used has been explained elsewhere [22,23]. In general, the code can keep track of any kind of particles (electrons, ions, neutrals, metastables and photons) and at any time it registers fundamental characteristics of those particles, including their location, components of velocity and energy. At the beginning of simulation, electrons are initiated from the middle of the gap between the two electrodes and they start to

move according to the applied external electric field. Electrons can experience collisions but, eventually, they hit electrodes and get absorbed (or possibly reflected). While colliding, electrons may produce new electrons through ionization. At the same time, ions are produced as well. At this point, any heavy particle (ions, metastables or neutrals) can be observed in the same manner as electrons. On the other hand, production of secondary electrons at electrodes (as consequence of heavy particles collisions with electrodes) is not needed to sustain RF discharges and breakdown due to electrons only is the basic mode of breakdown. Hence, we shall for the moment neglect the effect of heavy particles and also of photons. The fast neutrals and ions that play a critical role in the DC breakdown are of importance in RF only for very special circumstances. For most of the pd range the breakdown is purely determined by electrons only. Breakdown occurs in principle in the pristine, unperturbed, gas and thus populations of vibrationally excited molecules and metastables are negligible. On the other hand simulations for ions and other energetic heavy particles are quite demanding as for the computational time (due to order of magnitude different time scales required) with very little effects and only in a very narrow range of conditions. The role of heavy particles in RF breakdown will be addressed separately.

Apart from processes that occur in the gas volume, there are processes at surfaces of electrodes. Our code can include two types of surface collisions of electrons: reflections (elastic and inelastic, described by the reflection coefficient R), and the electron-induced secondary electron emission. Production of electrons by other processes may be quantified by gamma coefficients (yields) that can be, in theory, decomposed into a sum of contributions by ions, metastables, fast neutrals and photons [24]. Presently, however, these surface effects are neglected.

The cross sections for electron scattering in oxygen have been taken from Itikawa [21] with addition of the three-body attachment cross section that was taken from Phelps' LxCat database [25]. Results obtained by Itikawa's cross sections are presented in [26,27] while influence of the three-body attachment was analyzed in [28]. The pressure for simulations has been taken as 1 Torr. The results should be independent of the pressure (taking into account the frequency-pressure scaling), although with the three-body scaling for attachment there could be some pressure dependence and differences in profiles [28]. For the present conditions we could not find any significant effects due to the three-body attachment when pressure was varied from 1 Torr to 760 Torr.

3 Results and discussion

3.1 RF breakdown-voltage curve and time-resolved spatial distributions

The procedure used to determine breakdown conditions represented by the gas pressure and the corresponding breakdown voltage is explained in [7,8]. By employing that method, we have obtained the breakdown-voltage curve for oxygen presented in Figure 1a. The frequency

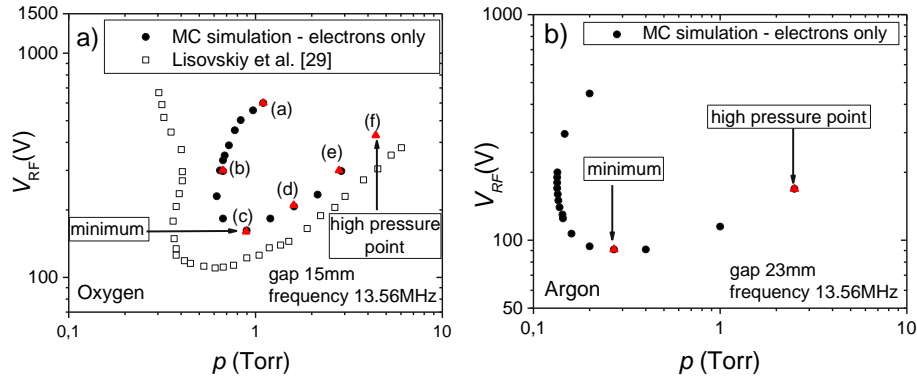


Fig. 1. Breakdown-voltage curves for RF breakdown at frequency of 13.56 MHz in different gases: (a) oxygen at electrode distance of 15 mm with available experimental data [29]; (b) argon at electrode distance of 23 mm [8]. Only electrons are included in MC simulation and there are no surface effects at electrodes, apart from absorption. Points in figure (a) marked from (a) to (f) are used as conditions for sampling presented in Figure 2.

of the external electric field is 13.56 MHz and the distance between the electrodes is 15 mm. Only electrons are included and their movement in gas and in the applied RF electric field is observed. As there are no surface effects, electrons are removed from the simulation when they reach an electrode. Regarding the three-body attachment, it has been scaled with pressure (in Torr). As can be seen in Figure 1a, the breakdown curve has its characteristic “U” shape with a distinctive double-valued region where two breakdown voltages correspond to one breakdown pressure. Nature of this double-valued area is discussed and explained (for argon) in our previous papers [7,8].

In Figure 2 we present time-resolved spatial distributions of electron concentration, mean energy and rates of elastic scattering, ionizations and attachment for conditions marked with (a)–(f) in Figure 1a. Light blue lines describe the applied electric field. Having a closer look at the concentration of electrons, we can see that the swarm of electrons nicely follows the applied electric field and changes its direction of motion when the field changes its sign (passes through zero). Also, if we observe the changes from point (a) to point (f), electrons are being slowly pushed away from the electrodes, causing a smaller and smaller area of the electron cloud profile to overlap with the electrodes (the overlap represents losses at electrodes). This change leads to a decrease in electron losses by electrode absorption, which is manifested as a decrease in the breakdown voltage in the curve in Figure 1a. As expected, rates of elastic scattering and ionization follow the profiles of the mean energy. By comparing the ionization and concentration, we can see that an increase in concentration is a direct consequence of the maximum in the number of ionizations. The rate of attachment that includes both two- and three-body processes has a small interruption when the applied field is zero, while the ionization is perturbed much more.

By looking at Figures 1a and 2 it is easy to understand the shape of the RF breakdown-voltage curve in oxygen. If we move from the minimum of the curve, as an optimal breakdown condition, to lower pressures, there is a sharp

increase in voltage. This increase exists due to a bigger and bigger overlap of the electron cloud with the electrodes, leading to larger and larger electron losses. Moving towards higher pressures from the minimum point, there is also an increase of breakdown voltage, but this increase is less dependent on the losses at electrodes and more on the losses in the gas volume due to the electron attachment.

3.2 Comparison of RF breakdown in argon and oxygen

A good way to understand how the attachment affects the oxygen RF breakdown is to compare these results to those obtained in argon [8]. To do so, we will first look at the breakdown-voltage curves for these two gases, presented in Figures 1a and 1b. Both curves are calculated for the applied frequency of 13.56 MHz. Despite the different distances between the two electrodes, 23 mm for argon and 15 mm for oxygen (chosen to be in accordance with some of the available experiments), they are close enough and conclusions could be drawn. The curves for both gases have a similar shape and distinctive minimums, but there is a considerable difference in the pd value and the breakdown voltage corresponding to the minimum. Oxygen discharge demands higher breakdown voltages and pressures to be maintained due to more electron excitation and vibrational collisions, requiring a higher E/N for electrons to reach the same mean energy. Of course, the presence of the attachment will push the breakdown towards even higher voltages to compensate for the resulting electron losses. The other difference is in the slope of the right-hand branch. From argon analysis [8] we know that at high pressures electrons are concentrated in the middle of the gap and losses at electrodes are very small. It is expected that the attachment, as a loss mechanism (together with the vibrational excitation as an energy loss), can be responsible for a sharp increase in breakdown voltages and the slope of the curve as a function of pd in the case of oxygen. We will verify this further by examining various time-resolved spatial profiles of the properties of the electron swarm (Figs. 3–5) and later on by analyzing electron energy distribution functions (Fig. 6).

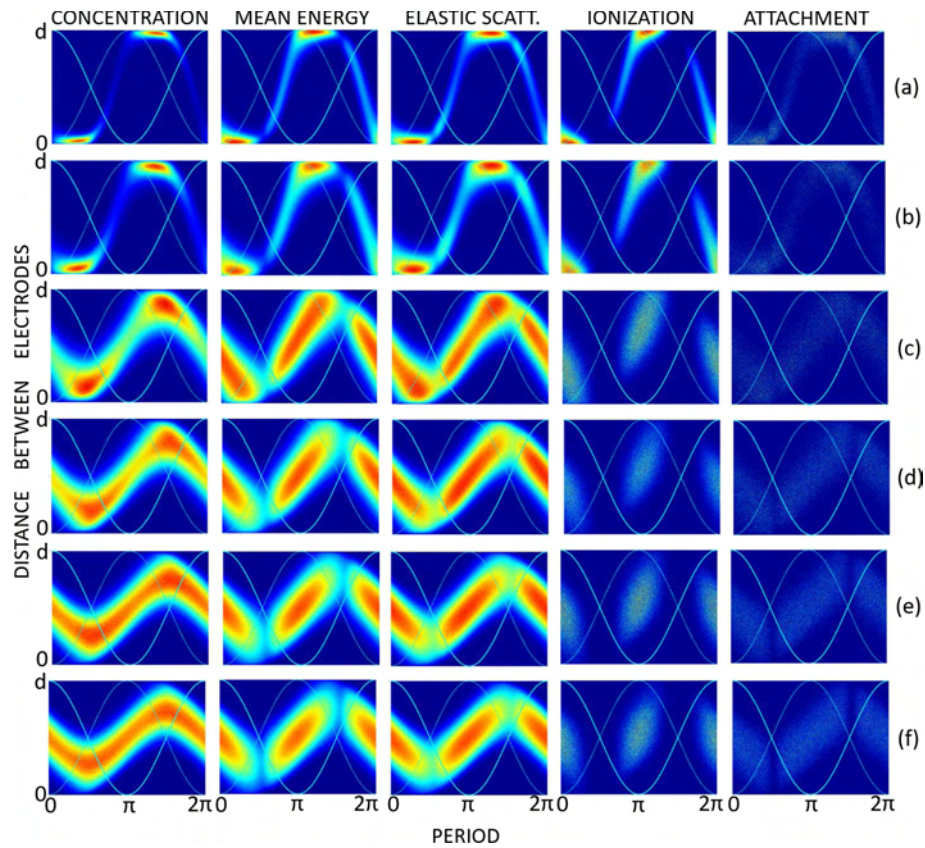


Fig. 2. Time-resolved spatial profiles of electron concentration, mean energy, elastic scattering, ionization and attachment rates for conditions marked in Figure 1. Light blue solid line represents applied field and light blue dotted line is the negative version of field profile to indicate direction of force on electrons. X -axis of plots are periods of time from 0 to π , while y -axis are distances between electrodes from 0 to $d = 15$ mm. Background gas is oxygen, frequency of external electric field is 13.56 MHz and gap is 15 mm. Sampling time of all plots is the same so that qualitative and quantitative conclusions can be made.

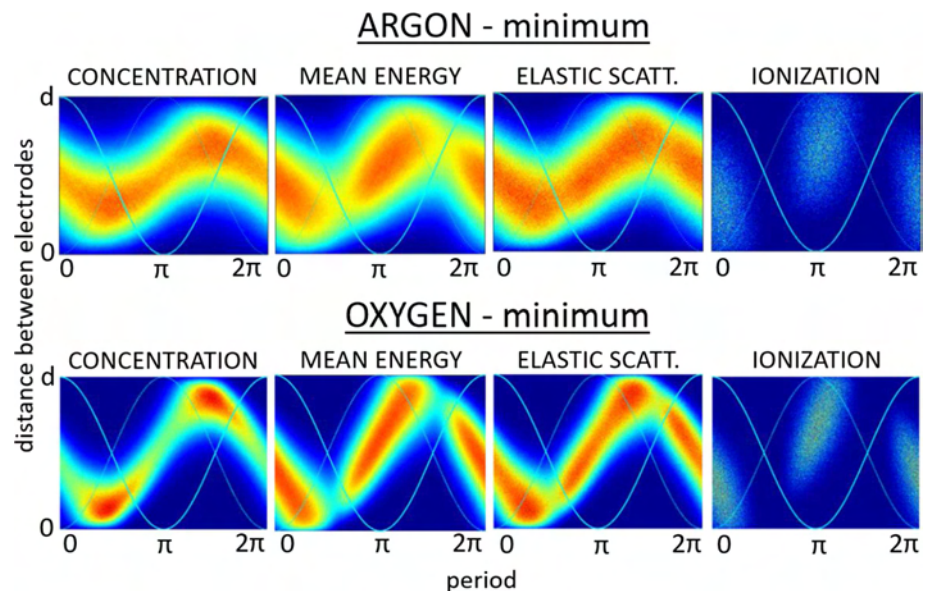


Fig. 3. Comparison of spatial profiles of electron concentration, mean energy and rates of elastic scattering and ionizations for two points that are minima of the breakdown-voltage curves (Fig. 1). Argon minimum: $V = 91$ V and $p = 0.27$ Torr; oxygen: $V = 160$ V and $p = 0.89$ Torr. X -axis of plots are periods of time from 0 to π , while y -axis are distances between electrodes from 0 to $d = 15$ mm. In both cases sampling time is the same, so that quantitative comparison can be made.

In Figures 3 and 4 a comparison is presented of time-resolved spatial profiles for argon and oxygen at distinctive points of the breakdown-voltage curves, labeled in Figure 1 as “minimum” and “high pressure point”. If we observe plots for conditions in minimums in Figure 3, they have similar modulations. In both cases the swarm of electrons is migrating from one electrode to the other one according to the applied field and only brushes the electrodes. Yet for oxygen, due to a higher pressure and higher losses, the growth towards the electrodes is more pronounced and the density peak is much sharper. Plots of the mean energy and elastic collision rate follow this, as explained earlier. The main difference is in the ionization plots. Significantly larger numbers of ionizations are required for the discharge to be maintained in the case of oxygen due to the attachment. At the same time a higher field is required to compensate for the energy losses due to vibrational excitation. On the other hand, if we compare the plots for the far high pressure points in Figure 4, even on the first sight, they are quite different. While electrons in argon are concentrated equally at both halves of the gap at the same time and do not depart far from the center of the gap, in oxygen they are still almost reaching electrodes and form a continuous “zigzag” line. This is a consequence of a few times higher voltage required in the case of oxygen that leads to a much stronger force that pushes electrons. Also, small cut-offs in plots of the electron mean energy (and also to a lesser degree for elastic collisions) can be seen when the field changes its sign due to a more efficient energy relaxation in the molecular gas.

Finally, if we wish to isolate only the effect of attachment then we need to make simulation with oxygen with and without electron losses due to attachment. These results are shown in Figure 5. While differences are not as obvious as in the comparison between argon and oxygen it is clear that attachment narrows down the channel of electrons and of course the operating voltage needs to be higher. The electron losses remove electrons that are below the threshold of ionization. Electrons that are not accelerated by the field directly but go in the perpendicular or backward directions are more likely to be lost. One needs to bear in mind that all this occurs when electron energies are overlapping with ionization and thus only dissociative attachment with its high threshold is relevant and in competition with ionization.

3.3 Electron energy distribution functions

In Figure 6 electron energy distribution functions (EEDF) are presented for various initial conditions (p, V) along the breakdown-voltage curve for oxygen. Differently colored lines in the same figure (figures are marked with capital letters A–F) indicate different moments within one period of the RF field. Starting from A, there are obvious modulations of EEDFs at different phases of one period. As we move all the way to F, these modulations are still present, but less observable. A larger modulation from A to C can be explained by electron losses at electrodes, with varying times of arrival and numbers of electrons arriving at electrodes. The losses of electrons reaching the walls are for

the highest energy electrons and, hence, a greater modulation of the EEDF develops.

For conditions related to the points D, E and F the swarm of electrons merely brushes the electrodes and only a small number of them is lost. At the same time their energies are low. Thus modulations of the EEDFs are less expressed (Fig. 6).

In Figure 6A at some instants of one time period the high energy tail of EEDFs reaches high energies. Due to a high applied voltage (Fig. 6A), there is a large energy transfer from the electric field to electrons. Also, as the pressure is low, electrons experience a small number of collisions in which they can lose energy. As a consequence, electrons gain a lot of energy very fast resulting in the long EEDF high-energy tail. Moving along the breakdown curve, the EEDF tails shrink from A to F. If we compare voltages at points A and F, they are not that much different. What really makes a difference is the pressure that is 4 times higher at the point F as compared to A. This leads to a higher number of collisions with oxygen molecules and more rapid energy relaxation.

Another valuable information that can be derived from the EEDF plots are the values of the electron mean energy and energy span. At point A the mean energy is around 10 eV and decreases as we move to F, where mean energy is close to 6 eV. These energies include the answer why the effect of the attachment is more obvious in the right-hand branch of the breakdown-voltage curve. As we know, the peak in the cross section for the two-body attachment process is around 6.6 eV. In the right-hand side of the breakdown-voltage curve, the peak of the cross section overlaps with the energies of the majority of electrons. In the left-hand side of the curve, due to a wider energy span, a significant number of electrons have energies above the peak of the cross sections for dissociative attachment and influence of that process is reduced. At the same time the effect of the three-body attachment, that peaks at low energies, is small for all conditions covered here [28].

One may conclude from Figure 6 that the crossover distributions indicated as C are more similar to those for the high pressure branch (D, E and F). Similar could be concluded for the spatial profiles shown in Figure 2 when it comes to the relative population of the electrons as they cross from one electrode to the other. Simply speaking growth as electrons cross the gap in 2c is small and more similar to the growth and radial extent in 2d–2f. On the other hand in 2c the overlap of the electron ensemble with electrodes is easily observed, it is sharp and similar to the lower pressure profiles 2a and 2b. Such overlap indicates a large number of electrons colliding with the surface and significant electron losses. As point 2c shows transition from one set of curves to the other in two major aspects it is a true transition point which leads to it being at the local minimum of the breakdown curves.

4 Conclusions

Since von Engel’s theory of high-frequency breakdown, understanding of RF breakdown has not changed much. Von Engel explained the breakdown at low pressures when

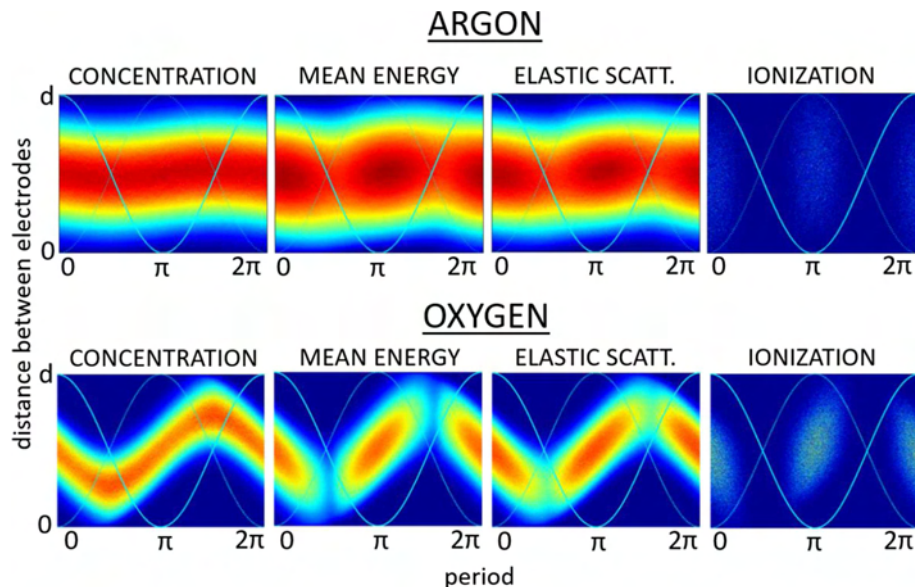


Fig. 4. Comparison of spatial profiles of electron concentration, mean energy and rates of elastic scattering and ionizations for two high pressure points presented in Figure 1. Argon: $V = 169$ V and $p = 2.5$ Torr; oxygen: $V = 430$ V and $p = 4.4$ Torr. X-axis of plots are periods of time from 0 to π , while y-axis are distances between electrodes from 0 to $d = 15$ mm. In both cases sampling time is the same, so that quantitative comparison can be made.

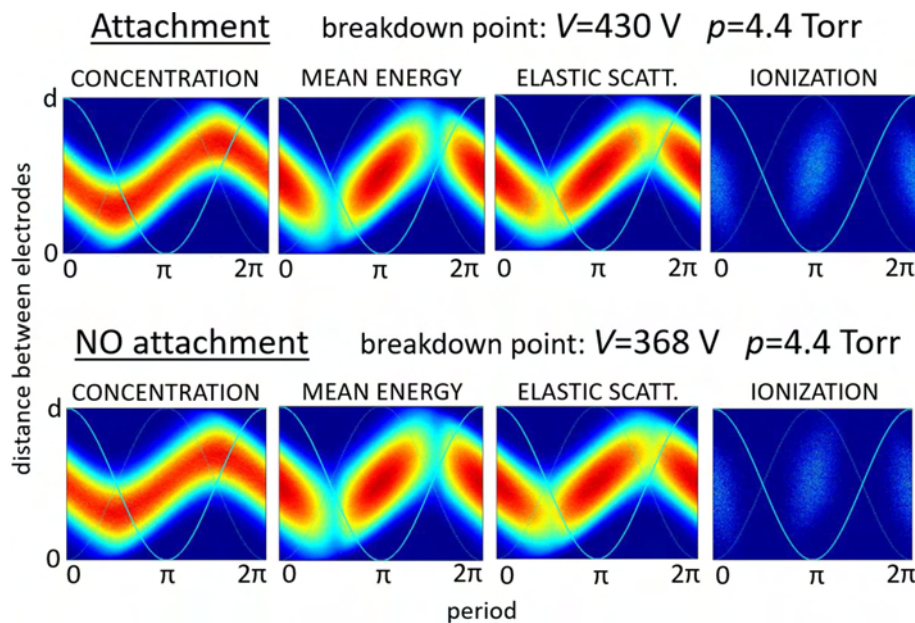


Fig. 5. Comparison of the attachment influence on the breakdown conditions observed in two cases: when attachment processes are included (breakdown conditions are $V = 430$ V and $p = 4.4$ Torr) and when there are no attachments (breakdown conditions $V = 368$ V and $p = 4.4$ Torr). Background gas is oxygen, frequency is 13.56 MHz and distance between electrodes is 15 mm.

electrons are reaching the electrodes, but at the same time he only superficially mentioned the influence of electrodes on the breakdown, with a conclusion that a more detailed swarm analysis is needed in the regions where electrons are not in contact with electrodes. We have tried to perform such an analysis in the case of argon in our previous papers [7,8]. We have done so by employing a Monte Carlo computational code and by using the fact that the

beginning of the breakdown can be observed as a growth of an electron swarm in a time-varying electric field. RF breakdown in oxygen is an obvious step towards understanding the breakdown in electronegative gases. Comparison with argon pointed out differences between the two gases (one of which is electronegative). It was shown that vibrational energy losses change the operation of the RF breakdown considerably. To the left of the breakdown

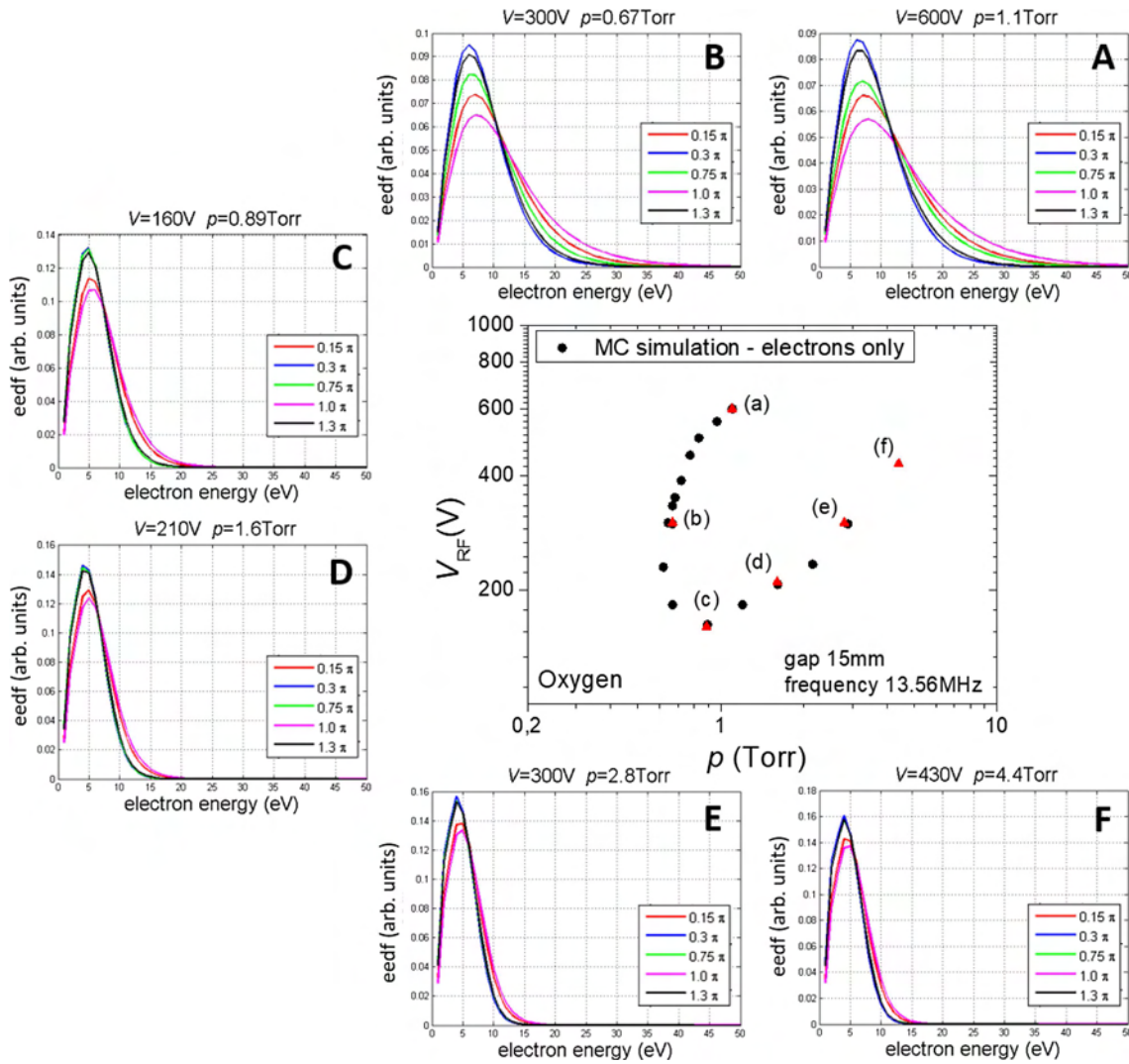


Fig. 6. EEDFs along breakdown-voltage curve for oxygen as background gas at frequency of 13.56 MHz and distance between electrodes of 15 mm. Different curves represent different phases of RF period and their variation indicates modulation in the distribution at different energies.

curve minimum one can observe similar behavior in two gases as most of the ionization occurs right in front of the electrodes and with significant losses to the electrodes. At pressures higher than those for the minimum a combination of vibrational energy losses and attachment drives breakdown to higher voltages and at the same time the required distance to achieve sufficient ionizations is longer and electrons approach closer to the electrodes while their radial width is smaller as the electrons going in perpendicular direction and backwards are more likely to be lost in attachment. Yet even under those conditions the number of electrons being lost at the electrodes is small. Finally, by observing EEDFs at different points on the breakdown curve and at different times over one period, processes of attachment have been indicated as responsible for a significant increase of the voltage in the right-hand side branch of the breakdown curve. At the same time the attachment has negligible influence on the left-hand side branch.

Electron energies at high pressures overlap much more with cross sections for attachment, while at low pressures, the peak of EEDF exceeds energies where attachment has the greatest probability.

While the definition of the breakdown coincides with the conditions of the predominance of swarms, the study of the breakdown has a relevance for application of RF plasmas including pulsing [30,31] in processing and production of non-equilibrium (cold) plasmas at the atmospheric pressure [4,32] and [33]. In both examples, the presence of electronegative gases is unavoidable and conditions for the breakdown will significantly affect the required power supplies and operation of plasma devices. At the same time, the continued growth from the breakdown towards the formation of plasma may be followed by a more complex tools such as PIC [5,34] and [35]. By the same logic, the understanding of the afterglow has the same importance and requires a similar, albeit inverted, sequence of modeling.

The authors acknowledge support from the Serbian Ministry of Education, Science and Technological Development under project numbers OI 171037 and III 41011. ZLjP is grateful to Serbian Academy of Sciences and Arts and its project F155 for its partial support.

Author contribution statement

Marija Puač – put together the computational code and performed computational analysis, analysed the results and wrote the first draft of the manuscript. Antonije Đorđević – helped in planning, in the analysis of the results and worked on finalization of the manuscript. Zoran Lj Petrović – defined the plan of research, defined algorithms for the Monte Carlo code and worked on development of the RF breakdown model. He supervised the studies and analysis of the results, organization and finalization of the manuscript.

Publisher's Note The EPJ Publishers remain neutral with regard to jurisdictional claims in published maps and institutional affiliations.

References

1. I. Adamovich, S.D. Baalrud, A. Bogaerts, P.J. Bruggeman, M. Cappelli, V. Colombo, U. Czarnetzki, U. Ebert, J.G. Eden, P. Favia, D.B. Graves, S. Hamaguchi, G. Hieftje, M. Hori, I.D. Kaganovich, U. Kortshagen, M.J. Kushner, N.J. Mason, S. Mazouffre, S. Mededovic Thagard, H.-R. Metelmann, A. Mizuno, E. Moreau, A.B. Murphy, B.A. Niemira, G.S. Oehrlein, Z.Lj. Petrović, L.C. Pitchford, Y.-K. Pu, S. Rauf, O. Sakai, S. Samukawa, S. Starikovskaia, J. Tennyson, K. Terashima, M.M. Turner, C.M.M. van de Sanden, A. Vardelle, *J. Phys. D: Appl. Phys.* **50**, 323001 (2017)
2. T. Makabe, Z.Lj. Petrović, in *Plasma Electronics: Applications in Microelectronic Device Fabrication*, 2nd edn. (CRC Taylor & Franics Group, Boca Raton, USA, 2015)
3. N. Puač, N. Škoro, K. Spasić, S. Živković, M. Milutinović, G. Malović, Z.Lj. Petrović, *Plasma Process Polym.* **15**, e1700082 (2017)
4. N. Puač, M. Gherardi, M. Shiratani, *Plasma Process Polym.* **15**, e1700174 (2018)
5. Z. Donko, *Plasma Sourc. Sci. Tech.* **20**, 024001 (2011)
6. M.J. Kushner, *J. Phys. D: Appl. Phys.* **42**, 194013 (2009)
7. M. Savić, M. Radmilovic-Radjenovic, M. Šuvakov, S. Marjanović, D. Marić, Z.Lj. Petrović, *IEEE Trans. Plasma Sci.* **39**, 2556 (2011)
8. M. Puač, D. Marić, M. Radmilović-Radjenović, M. Šuvakova, Z.Lj. Petrović, *Plasma Sources Sci. Technol.* **27**, 075013 (2018)
9. I. Korolov, A. Derzsi, Z. Donko, *J. Phys. D: Appl. Phys.* **47**, 475202 (2014)
10. I. Korolov, Z. Donko, *Phys. Plasmas* **22**, 093501 (2015)
11. T. Holstein, *Phys. Rev.* **70**, 367 (1946)
12. H. Margenau, *Phys. Rev.* **73**, 297 (1948)
13. H. Margenau, L.M. Hartman, *Phys. Rev.* **73**, 309 (1948)
14. H. Margenau, *Phys. Rev.* **73**, 326 (1948)
15. L.M. Hartman, *Phys. Rev.* **73**, 316 (1948)
16. E.W. Gill, A. von Engel, *Proc. R. Soc. A* **192**, 446 (1948)
17. E.W. Gill, A. von Engel, *Proc. R. Soc. A* **197**, 107 (1949)
18. V.A. Lisovskiy, V.D. Yegorenkov, *J. Phys. D: Appl. Phys.* **31**, 3349 (1998)
19. Z.Lj. Petrović, A. Đorđević, J. Petrović, J. Sivoš, M. Puač, G. Malović, D. Marić, in *82nd IUVSTA Workshop* (Okinawa, Japan, 2017), p. O2
20. J. Petrović, A. Đorđević, D. Marić, Z.Lj. Petrović, in *XXIV ESCAMPIG* (Glasgow, Scotland, 2018), p. 381
21. Y. Itikawa, *J. Phys. Chem. Ref. Data* **38**, 1 (2009)
22. Z. Ristivojevic, Z.Lj. Petrović, *Plasma Sources Sci. Technol.* **21**, 035001 (2012)
23. Z.Lj. Petrović, S. Bzenic, J. Jovanovic, S. Durovic, *J. Phys. D: Appl. Phys.* **28**, 2287 (1995)
24. A.V. Phelps, Z.Lj. Petrović, *Plasma Sources Sci. Technol.* **8**, R21 (1999)
25. PHELPS database, www.lxcat.net (Retrieved on May 29, 2015)
26. R.D. White, R.E. Robson, K.F. Ness, T. Makabe, *J. Phys. D: Appl. Phys.* **38**, 997 (2005)
27. S. Dujko, R.D. White, Z.Lj. Petrović, R.E. Robson, *Plasma Sources Sci. Technol.* **20**, 024013 (2011)
28. S. Dujko, U. Ebert, R.D. White, Z.Lj. Petrović, *Jpn. J. Appl. Phys.* **50**, 08JC01 (2011)
29. V. Lisovskiy, J.-P. Booth, K. Landry, D. Douai, *J. Phys. D: Appl. Phys.* **39**, 660 (2006)
30. K. Maeshige, G. Washio, T. Yagisawa, T. Makabe, *J. Appl. Phys.* **91**, 9494 (2002)
31. T. Ohmori, T.K. Goto, T. Makabe, *Appl. Phys. Lett.* **83**, 4637 (2003)
32. N. Škoro, N. Puač, S. Živković, D. Krstić-Milošević, U. Cvelbar, G. Malović, Z.Lj. Petrović, *Eur. Phys. J. D* **72**, 2 (2018)
33. E. Traldi, M. Boselli, E. Simoncelli, A. Stancampiano, M. Gherardi, V. Colombo, G.S. Settles, *EPJ Tech. Instrum.* **5**, 4 (2018)
34. M.M. Turner, A. Derzsi, Z. Donko, S.J. Kelly, T. Laffeur, T. Massenbrock, *Phys. Plasmas* **20**, 013507 (2013)
35. Z. Donko, *Phys. Rev. E* **57**, 7126 (1998)

Effect of target material on electrical properties of a two-electrode dielectric barrier helium plasma jet

Nikola Škoro^{1,*} , Kinga Kutasi² , Marija Puač¹ , Zoran Lj Petrović^{3,4} 
and Nevena Puač¹ 

¹ Institute of Physics, University of Belgrade, Pregrevica 118, 11080 Belgrade, Serbia

² HUN-REN Wigner Research Centre for Physics, Konkoly-Thege Miklós út 29-33, Budapest, 1525, Hungary

³ Serbian Academy of Sciences and Arts, Knez Mihailova 35, 11000 Belgrade, Serbia

⁴ School of Engineering, Ulster University, Jordanstown, Co., Antrim BT37 0QB, United Kingdom

E-mail: nskoro@ipb.ac.rs

Received 29 December 2023, revised 12 March 2024

Accepted for publication 11 April 2024

Published 22 April 2024



Abstract

In this paper we present electrical characterization of a dielectric barrier discharge plasma jet operating with He (2 slm and 3 slm) as working gas and interacting with Cu, polyethylene terephthalate and distilled H₂O targets. We used a plasma jet with two copper electrodes wrapped around a glass tube. One electrode was powered by a high-voltage sinusoidal signal of 30 kHz, whereas the other electrode and the target holder were grounded. We have performed detailed investigation of the voltage and current waveforms, phase differences, volt–current (*V–I*) characteristics, calculated impedances and power deposition. The aim was to determine the influence of different target materials and their conductivity on the plasma properties. We calculated the total harmonic distortion factor that showed that the current through grounded electrode depends on the conductivity of the target. We also calculated the power delivered to the plasma core and the plasma plume regions and observed that the change in the target conductance influenced the power in both plasma regions. The experimentally characterized electrical circuit was simulated by a model of equivalent electrical circuit corresponding to the plasma-off and plasma-on regime. Voltage controlled current source was added as model of a streamer formed in plasma-on regime.

Supplementary material for this article is available [online](#)

Keywords: atmospheric pressure plasma jet, electrical measurements, conductive target, dielectric target, equivalent electrical circuit

1. Introduction

Cold (non-thermal) plasmas at the atmospheric pressure have been proven to be very prospective and useful in a variety of different applications. In some cases, applications of these plasmas are as successful as of plasmas at low pressures [1–3].

The key feature of non-thermal plasmas at atmospheric pressure is the ability to provide a chemically reactive environment in a room-temperature gas and this has facilitated development of numerous plasma applications in biomedicine [4–7]. In this area of applications, one of the most used sources of non-thermal atmospheric-pressure plasma is the plasma jet [8, 9]. Generally speaking, a plasma jet is a technically simple device comprising of a dielectric tube that directs the buffer gas to flow through a limited volume of space where a high

* Author to whom any correspondence should be addressed.

electric field is applied. The volume with the high electrical field is usually formed by bringing a high-voltage signal to a conductive wire inserted into the tube or to a conductive surface attached to the outer side of the tube—to serve as a powered electrode. Since in the latter case the electrodes are separated from the plasma region by a dielectric this type of source is called a dielectric barrier discharge (DBD) jet. The other electrode of the jet may be positioned somewhere at the tube or in the vicinity of the tube ending and may serve as a substrate holder. The core plasma is formed inside the tube and as plasma plume exits the tube, it mixes with the air, providing a flux of neutral species (reactive and others), ions, metastables and UV photons. The active species are sustained by the streamer leaving the glass tube and extending deep into the outer region. Outside the tube, from the mixing of the plasma with the surrounding air, different reactive oxygen and nitrogen species [10–12] are produced. Plasma sources are particularly advantageous for a number of biomedical and biotechnology applications as they produce small amounts of active species sufficient to induce chains of biochemical events but insufficient to change the entire environment into toxic.

In all applications, plasma jet is positioned in front of the target that is exposed to the flux of reactive particles generated by the plasma [13]. The insertion of a target into the plasma plume region affects the gas flow and, consequently, affects the mixing of the working gas with the air [14]. This, in turn, changes the properties of the plasma and in most situations significantly modifies the delivery of the reactive species to the target.

In cases where a DBD jet has only the powered electrode, target surface connected to the ground also serves as the grounded electrode. The target, then, obviously represents a part of the electrical circuit, thus influencing the plasma. For plasma jets with the grounded electrode positioned at the tube, the plasma is created between two electrodes in the noble gas [15]. Therefore, location of electrodes producing the active plasma is far from the target. However, if the plasma region comes close to or in contact with the target surface, it will start behaving as an additional electrode, changing the electrical circuit, and thereby altering plasma properties similar to a jet with a single (powered) electrode and a grounded target.

As a result, the second important parameter affecting the properties of the plasma produced by jets is the target conductivity [16–18]. It was experimentally shown by observing the optical emission spectra that the target conductivity impacts the densities of excited species in plasma [19–23]. Computational research of the influence of the target conductivity demonstrated that the variation of the conductivity influences electron temperature and densities of charged and neutral species in the plasma effluent [24]. In addition, the dependence of the impact force of an atmospheric-pressure non-equilibrium plasma jet on different target types has been recently measured [25].

Clearly, target conductivity presents a crucial parameter when it comes to applications. Hence, measurements related to treatments have been conducted, using appropriate targets or their models treated by specific plasma jet configurations [26–28]. In that way, valuable data related to applications have

been acquired. However, in most situations, authors studied pin/needle electrode jets or DBD jets with pulsed power. The configuration of a DBD jet with one continuously powered and one grounded electrode is a frequently encountered configuration used in many biomedical applications, as well in the treatment of liquids [29]. Thus, we believe that investigation of the influence of the target conductivity on plasma parameters in this jet configuration is of interest.

Power dissipation is one of the key properties when it comes to the treatment of biological samples and water, as it is connected to the stability and reproducibility of the plasma treatment and the heat transfer to the target [16]. The significance of the power as one of the most important parameters is visible especially in the fields of plasma medicine and plasma agriculture where the comparison of different plasma sources and their efficacy is important. This fact has been recognized by several groups of authors [16, 30–32], so the procedure to establish power given to the plasma requires further research and development of appropriate protocols. The power dissipation in plasma is encountered as one of the open issues in plasma diagnostics. As a rule, the actual power dissipated in the plasma is often quite different from the input power. Especially, the case of DBD plasma jets with two electrodes is intricate since the power dissipated in the effluent that interacts with the target surface is different than the power in the plasma core. Introducing the target produces a power outflux from the plasma [33, 34], whose accurate determination can be a challenging task since suitable signal waveforms cannot be monitored easily.

The principal aim of this work is to investigate the effect of the conductivity and the type of the target surface on the properties of a continuously powered DBD type atmospheric-pressure plasma jet that is operated in front of three different targets: a copper plate, a polyethylene terephthalate (PET) plate and a distilled-water surface. The measurements presented in this paper clarify the link between the conductivity of the targets and the electrical characteristics, namely the voltage–current ($V-I$) characteristics and power. For all three types of targets, we conducted comprehensive measurements of the average power dissipated between the powered and the grounded electrode, as well as measurements of the average power delivered from the plasma to the grounded target, aiming at determining the power portion directed towards the target. Also, a Simulink MATLAB model was developed to describe an equivalent electrical circuit of the DBD jet. With this model we have given an insight of the electrical circuits (and components) that are describing plasma-off and plasma-on regime, with consideration of three different targets. We present the results of voltage and current waveforms and $V-I$ characteristics obtained for different targets and gas flows. Additionally, power dissipation is discussed with respect to the target type.

2. Experimental setup

The studies presented here have been conducted with a two-electrode DBD jet with He as the working gas. The schematic of the experiment is shown in figure 1(a). The jet consists of a

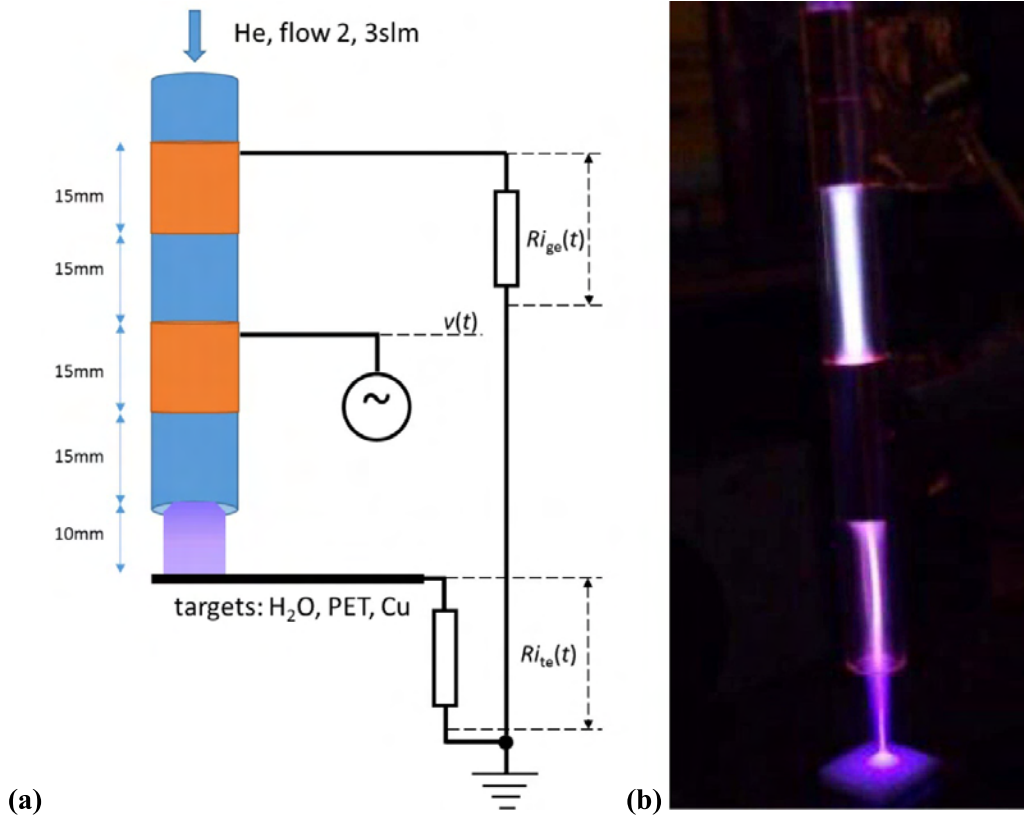


Figure 1. (a) Schematics of the experimental setup. Dashed lines present the measurement points of the supplied voltage $v(t)$. Voltages on $R = 100 \text{ k}\Omega$ resistors are used for monitoring the grounded electrode current $i_{ge}(t)$ and the target current $i_{te}(t)$. (b) Image of He plasma jet operating.

20 cm long glass tube, with 6 mm outer and 4 mm inner diameters. To produce a high-voltage signal, a 30 kHz sine signal is sent from a signal generator (PeakTech 4025) to a ‘home-built’ amplifier and then to a transformer. This high-voltage signal is then supplied to the powered electrode made of a copper (Cu) foil tightly wrapped and glued around the glass tube. The width of the powered electrode is 15 mm and it is positioned 15 mm from the end of the glass tube. The grounded electrode made of the Cu foil is wrapped around the tube 15 mm away from the powered electrode. The flows of 2 slm or 3 slm of Helium are introduced into the tube through a flow controller. In all experiments the jet is positioned vertically, and the target surfaces are placed below the jet tube ending at the distance of $d = 10 \text{ mm}$ (see figure 1(a)). We have used a Cu plate (thickness 1 mm), PET plates (thickness 2 mm) and 22 ml of distilled water (dH₂O) in a glass Petry dish ($\varnothing 5.5 \text{ cm}$) as target surfaces. In the case of the PET target, we have used 3 plates in a stack (total thickness of 6 mm).

For all measurements presented here the plasma plume was touching the target surface (see figure 1(b)). Plasma was in a glow regime if looked at by a naked eye for all plasma operating conditions. In case of all three targets with the voltage increase one conductive channel was formed along the tube axis with its emission intensity increasing with the voltage. Even for maximum applied voltages and for Cu target we did not see the formation of separate filaments. Nevertheless, the

time resolved ICCD images show for this type of APPJ that depending on the conditions like water vapour percentage, percentage of surrounding air mixing with helium, applied power, we could detect formation and propagation of Pulsed Atmospheric-pressure Plasma Streamers (PAPS) [15, 35].

All three targets were grounded through a resistor ($R = 100 \text{ k}\Omega$). The electrical conductivity and relative permittivity for the targets are given in table 1 [36–39]. The general relation between the permittivity and conductivity is the following:

$$\varepsilon(\omega) = \varepsilon'(\omega) + j\varepsilon''(\omega) = \varepsilon_r(\omega)\varepsilon_0 + j\frac{\sigma(\omega)}{\omega}, \quad (1)$$

where $\varepsilon_r(\omega)$ is relative permittivity, ε_0 is vacuum permittivity, ω is frequency and $\sigma(\omega)$ is the conductivity. As seen from table 1, in case of Cu target, the conductivity is the one responsible for the system behaviour while in the case of PET it is the permittivity. As it should be expected, in the case of water both parameters are almost equally influencing the system behaviour.

The Cu plate exposed to the ambient air was unprocessed and unpolished before it was used as a target, so one may presume that an oxide layer, whose conductivity is relatively low (in the range of that for semiconductors), is formed on the surface.

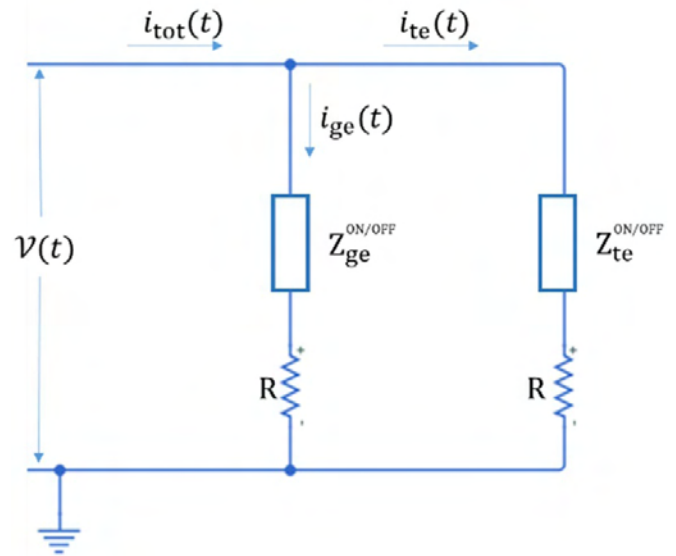
Table 1. Electrical conductivity and relative permittivity of the targets.

Target	Electrical conductivity, σ (S m ⁻¹)	Relative permittivity, ϵ_r	E'	ϵ''	Dominant term in equation (1)
Cu plate [36]	$6 \cdot 10^7$	1	$\sim 10^{-12}$	$\sim j10^2$	Im part i.e. conductivity
Distilled H ₂ O [37, 38]	$5 \cdot 10^{-6}$	80	$\sim 10^{-10}$	$\sim j10^{-11}$	Both Re and Im
PET plate [36, 39]	10^{-21}	3–4.5	$\sim 10^{-11}$	$\sim j10^{-26}$	Re part i.e. permittivity

Nevertheless, we perform treatment of the surfaces by plasma before measurements to remove organic and other complex contaminants, to clean the surface from deposited materials and to make the surface more uniform without hoping that we have removed completely the oxide layer on the surface [40, 41]. After the plasma treatment of the surface the influence of possible variations of the properties of the surface layer on the plate conductivity is negligible. Similarly, clean PET plates are exposed to the preconditioning treatment before each measurement set and no visible change of the plate surface after the measurement has been observed. For dH₂O samples, the water conductivity was determined before the measurements and it did not change during the short duration of the measurements. We used Hanna Instruments (HI76312) conductivity probe with Hanna Instruments controller HI5521 to monitor the conductivity of the water target. Therefore, the stability of target surfaces is adequate so that it does not affect the plasma during measurements in all cases.

The electrical measurements were done at three points in the electrical circuit (see figure 1(a)). The voltage signal supplied to the jet $v(t)$ was measured with a high-voltage probe (Tektronix 6015A) attached to the powered electrode of the jet. Both currents, from the grounded electrode $i_{ge}(t)$ and the target $i_{te}(t)$, were monitored by measuring the voltage drops (Agilent 10076 C) on the 100 k Ω resistors and are recorded separately. These recordings allowed observing electrical waveforms during plasma operation, to obtain the RMS values of the voltage and currents and, eventually, to calculate the power transmitted to the plasma. All measurements were repeated, and we have obtained stable and reproducible operation of the plasma in the whole range of conditions investigated.

During initial measurements we monitored the humidity in the gas flow by using a dew point meter (Vaisala DMT 143). The abundance of the H₂O vapour proves to be an important parameter that influences the plasma conditions [42, 43]. We observed that after 10–15 min of operation, the humidity dropped to ~ 15 ppm and stayed at that value throughout the experiment. Thus, we adopted a procedure for preconditioning the jet before each measurement set that includes 10 min of plasma operation with an appropriate target at a moderate value of the applied voltage.


Figure 2. Experimental equivalent electrical circuit of DBD plasma jet.

3. Results and discussion

3.1. Equivalent electrical circuit

In general, the electrical circuit of the DBD plasma jet can be represented as shown in figure 2. Impedance Z_{ge} represents total impedance in the first branch (plasma core) of electrical circuit consisting of two electrodes wrapped around the glass tube. Z_{te} represents total impedance in the second branch (plasma plume) of electrical circuit with the target. Both Z_{ge} and Z_{te} can be calculated from the V – I characteristics. The ON and OFF annotations represent plasma on (discharge working in stable mode) and plasma off (no discharge) cases.

To better understand the behaviour of the plasma system we have developed a more detailed model of equivalent electrical circuit by using Matlab Simulink. The schematics of the circuit is shown in figure 3. All elements are denoted in similar manner as the impedances in figure 2. The first branch represents electrical properties of the powered and grounded electrode wrapped around the glass tube (capacitance C_{ge} and resistance

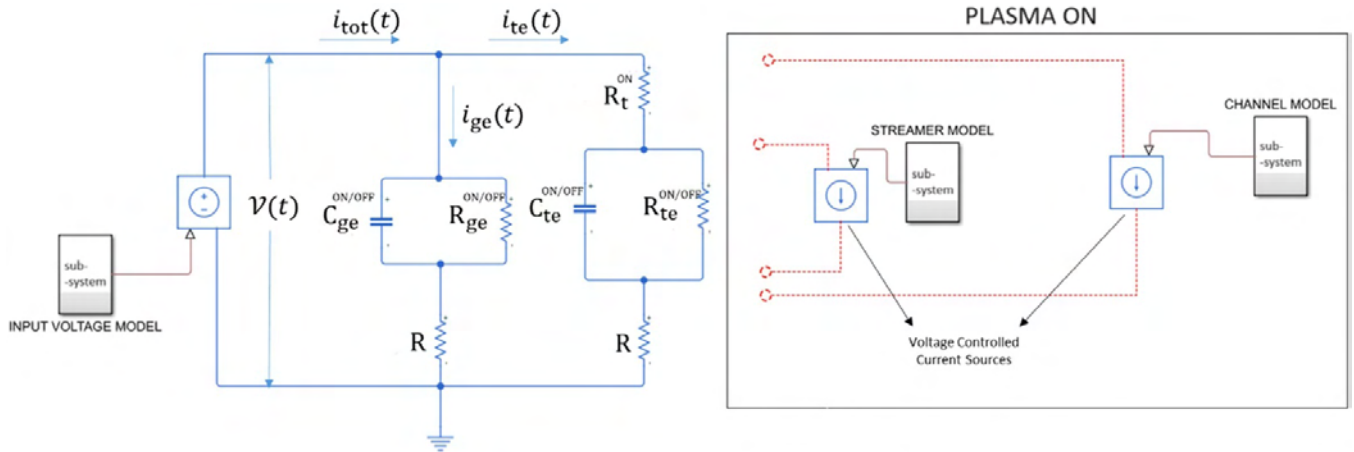


Figure 3. Detailed model of the equivalent electrical circuit made in MATLAB Simulink. When plasma is ignited, additional voltage controlled current sources must be added due to the occurrence of PAPS (streamer). Then the additional elements to the circuit are shown on the right-hand side in the schematics denoted with PLASMA ON.

Table 2. Parameters of equivalent electrical circuit.

		R (M Ω)	R_{ge} (M Ω)	C_{ge} (pF)	R_t (M Ω)	R_{te} (M Ω)	C_{te} (pF)
Plasma OFF	Cu	0.10	6.80	1.50	/	10	1.00
	dH ₂ O	0.10	6.80	1.50	/	13	0.75
	PET	0.10	6.80	1.50	/	11	0.85
Plasma ON	Cu	0.10	2.20	1.50	2.80	7	1.50
	dH ₂ O	0.10	2.10	1.70	3.50	7	1.25
	PET	0.10	2.20	1.35	3.50	/	1.40

R_{ge} in parallel) and second represents the target (capacitance C_{te} and resistance R_{te} in parallel).

Electrical components of the equivalent circuit and their values are presented in table 2. The values obtained from the equivalent electrical circuit model give the current and voltage waveforms that are in 99% agreement with the measured ones. When applied voltage $v(t)$ is below the breakdown threshold for plasma ignition (Plasma-OFF), equivalent electrical circuit of the DBD jet is shown in the left-hand side of the figure 3. In Plasma-OFF regime, if we change the target, thus changing the electrical properties, the electrical circuit representing the core of plasma does not change (C_{ge} , R_{ge}). This is an expected behaviour because a two-electrode DBD jet is basically a simple capacitor filled with gas. The capacitance C_{ge} represents the capacitance due to the dielectric material of the tube (C_{wall}) and also due to the volume of the discharge tube (C_{gas}). The change of target material influences only part of the electrical circuit that includes the target where we can see small changes in C_{te} and R_{te} .

Plasma ignition (Plasma-ON) introduces significant changes to the circuit in both branches. The capacitances of both branches (plasma core and plasma plume) are changed depending on the electrical characteristics of the targets and formation of the plasma sheaths. At the same time the resistances (R_{ge} , R_{te}) are decreased due to the breakdown and plasma ignition. When target is PET, the almost ideal insulator, target is represented only as capacitor C_{te} (R_{te} is zero). In plasma plume branch after plasma ignition, we have a

new element R_t representing mainly the energy dissipation in plasma plume and trough the target. The appearance of PAPS is modelled by the voltage controlled current source [44–46] shown in right-hand side of figure 3 (streamer model). The PAPS appear only in the positive half-period of the voltage signal [15, 35]. In similar DBD jet configuration, in negative half-period of the voltage signal we did not observe PAPS, but a formation of a continuous plasma channel that starts at the target and spreads towards powered electrode of DBD jet [47]. This plasma channel is modelled by the second voltage controlled current source figure 3 (channel model).

3.2. Electrical measurements

We have performed full electrical characterization of the DBD jet with a grounded target surface positioned underneath. Three different signals were monitored in time: the voltage supplied to the powered electrode $v(t)$, the current flowing between powered and grounded electrode $i_{ge}(t)$ and the current passing through the plasma plume into the target $i_{te}(t)$. As the current $i_{ge}(t)$ effectively describes the region between the electrodes, we may attribute these values to the plasma core, while the other current, $i_{te}(t)$, provides an insight into the plasma plume, the region of the plasma between the core and the target.

In figure 4 we show waveforms obtained at 2 slm of He and three different targets. These waveforms were obtained for each target when the discharge is ignited by the same voltage

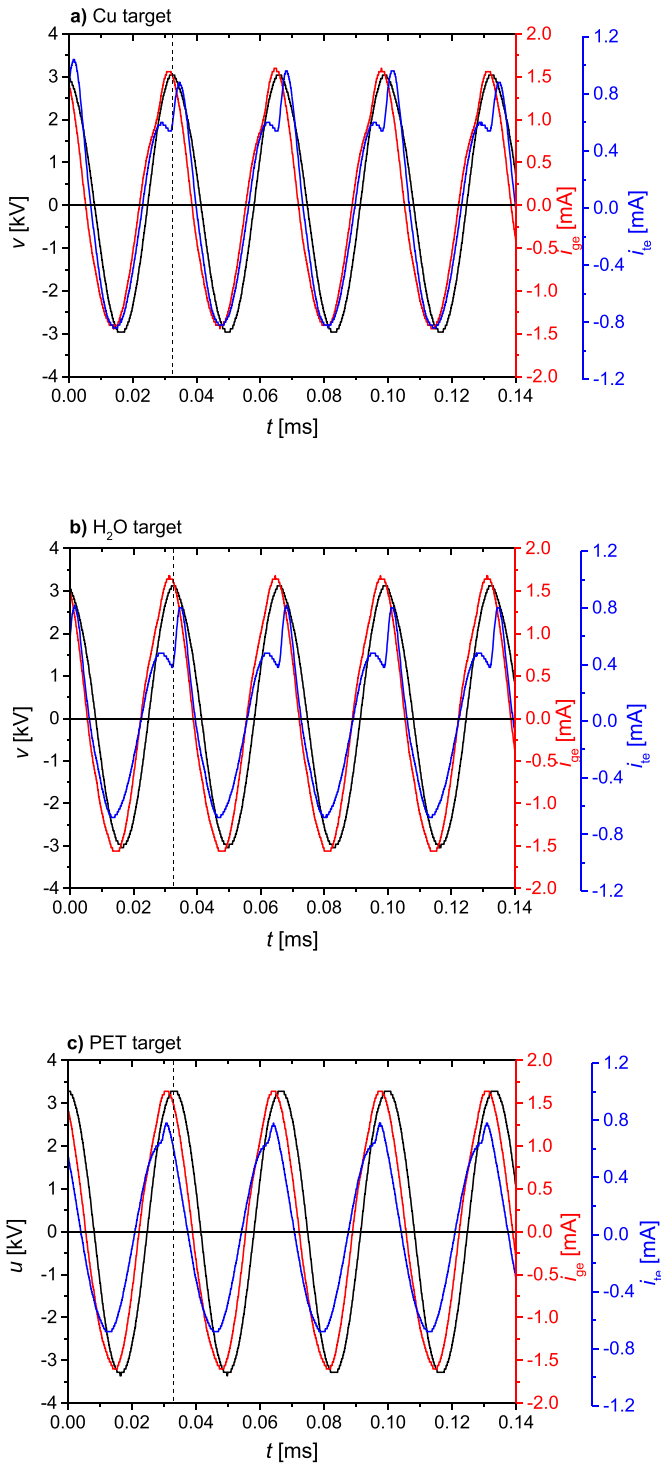


Figure 4. Waveforms of voltage $v(t)$ (left-hand side), grounded electrode current $i_{ge}(t)$ and target electrode current $i_{te}(t)$ (right-hand side) recorded for three different targets and flow of 2 slm of He. Vertical dashed lines mark the time-point of one maximum of the $v(t)$ signal.

as indicated at the signal generator. The left-hand side y-axis shows values of $v(t)$, while the right-hand side shows values of $i_{ge}(t)$ and $i_{te}(t)$. Vertical dashed lines in the plots mark the time-point of one maximum of $v(t)$ signal to assist the observation

of the time-shift between the voltage and current signals. The period of the $v(t)$ signal is $T = 33 \mu\text{s}$.

For all three targets the current signals ($i_{ge}(t)$, $i_{te}(t)$) precede the voltage signal indicating that this is a predominantly capacitive system. This is even more pronounced when the plasma is not ignited. In that case both currents, that pass through the grounded wrapped electrode and through the target, precede the voltage waveform and they are influenced mainly by the geometry of the electrodes and position of the target. The phase differences in the plasma-off case are $\sim 55^\circ$ for the grounded electrode and $\sim 50^\circ$ for the target electrode. These values differ from the 90° phase difference that is expected for a purely capacitive impedance, due to resistance of the components of the electrical circuit and the plasma jet.

When the discharge is ignited, the current $i_{ge}(t)$ through the grounded electrode precedes the voltage signal for $\Delta\tau = 2.55 \mu\text{s}$, which corresponds to the phase shift of $\sim 28^\circ$. This phase shift is not influenced by the type of target indicating that the parameters of the plasma core inside the tube are mainly governed by the inter-electrode distance and geometry. On the other hand, the current passing through the target is highly influenced by the type of target and its characteristics, as expected. The phase differences between $i_{te}(t)$ and $v(t)$ are $\sim 14^\circ$, $\sim 28^\circ$ and $\sim 41^\circ$ for the Cu, dH₂O and PET target, respectively. The increase in the phase shift corresponds to the decrease in the conductivity of the target.

3.2.1. V - I characteristics. To get a clearer picture of the non-linearity that plasma introduces into the system, we have analysed the signals in the frequency domain by using the Fast Fourier transform. When plasma is not ignited, all three signals for all three targets have only the fundamental harmonic (1st harmonic), as expected. When plasma is ignited, the non-linearity introduced into the system by the plasma can be evaluated through the total harmonic distortion factor (THD). THD is calculated as

$$\text{THD} = \frac{\sqrt{\sum_{n=2}^{\infty} V_{n,\text{RMS}}^2}}{V_{\text{fund,RMS}}} \cdot 100 (\%) \quad (2)$$

where $V_{n,\text{RMS}}$ are root mean square (RMS) values of the higher harmonics ($n = 2, 3, \dots$) and $V_{\text{fund,RMS}}$ is the RMS value of the fundamental harmonic at $f = 30 \text{ kHz}$. The same formula was used for I_{ge} and I_{te} .

The calculated THD values are shown in table 3. While the voltage waveform is not distorted, the THD percentage for the current going through the grounded electrode (I_{ge}) depends on the conductivity of the target. In table 3 we can see that the highest distortion ($\text{THD}_{I_{ge}}$) in the signal is obtained for the Cu target and generally it increases when target's conductivity increases. The situation with I_{te} is somewhat different, as it is in correlation with the effective conductivity, which also depends on the stability of the material of the target surface and/or fluctuations in plasma-surface interactions. The highest THD was obtained for the dH₂O target. This indicates that during the plasma operation the target surface is changing

Table 3. THD percentages for voltage and current signals.

Target	THD_V (%)	$THD_{I_{ge}}$ (%)	$THD_{I_{te}}$ (%)
Cu	0	18.2	38.2
dH ₂ O	0	13.4	46
PET	0	7.3	13.5

significantly due to the helium gas flow, evaporation, and the plasma-water interface interactions. The high instability of the dH₂O surface results in the appearance of a large number of significant harmonics (up to $n = 14$) present in the signal. On the other hand, for the Cu target there are $n = 6$ significant harmonics and for PET only $n = 3$ (n includes the 1st harmonic). The appearance of the higher harmonics can also be anticipated since there is a visible variation in the I_{te} signal shape at positive peak value.

To facilitate the comparison of time-varying signals, the RMS values of waveforms should be calculated. In case of the voltage, the RMS values were calculated using:

$$V_{RMS} = \sqrt{\frac{1}{nT} \int_0^{nT} v^2(t) dt}. \quad (3)$$

Calculation of the RMS values for the currents was conducted in a similar manner. In all calculations, seven periods were used ($n = 7$).

In figure 5 we show $V-I$ characteristics of the DBD jet measured for three targets and 2 slm of the He flow. Figures 5(a)–(c) show the dependence of the voltage on the current flowing through the grounded electrode (I_{ge}), and figures 5(d)–(f) present the $V-I$ characteristics depending on the current through the target (I_{te}). The measurements are performed starting with voltages lower than the breakdown voltage and then increasing gradually to the maximum voltage of the power supply (shown in solid symbols). Then, from the maximum voltage of the power supply it is decreased to the starting voltage (shown with open symbols). The increment and decrement of the applied voltage is accomplished in steps, sweeping over the same values.

The $V-I$ characteristics for low voltages, when the plasma is not ignited, are linear since the impedance depends only on the characteristics of the electrode system, mainly on its capacitance. In all $V-I$ characteristics there is a drop of the V_{RMS} values at the point where plasma is ignited. As expected, the current flowing through the grounded electrode is higher than the current through the target. After ignition, the main plasma core is constrained inside the jet, between the electrodes wrapped around the jet tube. Here, the gas mixture consists of helium with only a small amount of air impurities in which the breakdown occurs. Then plasma spreads towards the end of the tube where the percentage of air in the mixture is higher. Having crossed some distance in the external region, the plasma gets in contact with the grounded target surface.

From figures 5(a)–(c) we can see that the impedance is not constant for the whole range of the applied voltages due to the changes introduced by plasma. The nonlinearity of the

impedance is more evident in the $V-I$ curves for the grounded target (figures 5(d)–(f)), especially for the Cu and dH₂O targets. For lower applied voltages and currents the plasma plume is a glow type. With an increase in the applied voltage an apparent conductive channel is formed whose emission intensity increases with the voltage. After the channel formation, the applied voltage increases slower than the current through the plasma plume. This is represented in the $V-I$ curves as a change of the impedance to a lower value. The plasma behaviour and $V-I$ points do not change in measurements when the input voltage is decreased (figures 5(a)–(f), open symbols). The only difference with respect to the increasing-voltage case is that the plasma stays ignited till lower voltages are reached, thus producing a hysteresis effect. The hysteresis as shown in figure 5 is often observed for plasma discharges. What is interesting here is that the hysteresis depends strongly on the material of the target and seems to be the largest for water target.

For a better comparison, the $V-I$ characteristics obtained for the different targets are presented together in figure 6. The voltage dependence on the current through the grounded electrode are given in figure 6(a) and the dependence on the current through the target in figure 6(b). The points acquired after the plasma ignition are marked by open symbols and connected with a line to make the data more legible.

The data points obtained without plasma for the targets fall on top of each other, as shown in figure 6(a). Obviously, before the breakdown, the impedance is the same for all three targets ($Z_{ge} = 3.3 \text{ M}\Omega$) and this is also confirmed by components (C_{ge} , R_{ge}) obtained by Simulink model. As observed in the previous section, after the plasma ignition, the voltage drops significantly for all the targets and regimes of operation, i.e. the voltage and current obviously depend on the type of the target. For the Cu target, the plasma after ignition initially operates at around 1700 V, while the current flowing between electrodes is around 700 μA . This is the lowest plasma operation voltage and current for all three targets. The reason lies in the high conductivity of the target that enables efficient breakdown and discharge operation. For the case of the PET target, the voltage after ignition is around 1830 V and the current is at 800 μA (see figure 6(a)). A similar operating voltage of around 1800 V is also obtained with the dH₂O target, while the current immediately goes to around 850 μA .

Slopes of the $V-I$ characteristics of the core plasma after plasma ignition change in a different manner, depending on the target (figure 6(a)). The curves obtained for the PET and dH₂O targets both change the slope in the 0.9 mA–1 mA interval, while for the Cu target the change is observed around 0.8 mA. By assessing the recorded waveforms that are used to obtain points of the $V-I$ characteristics we could observe only variation in the amplitude of the waveforms. The slope change

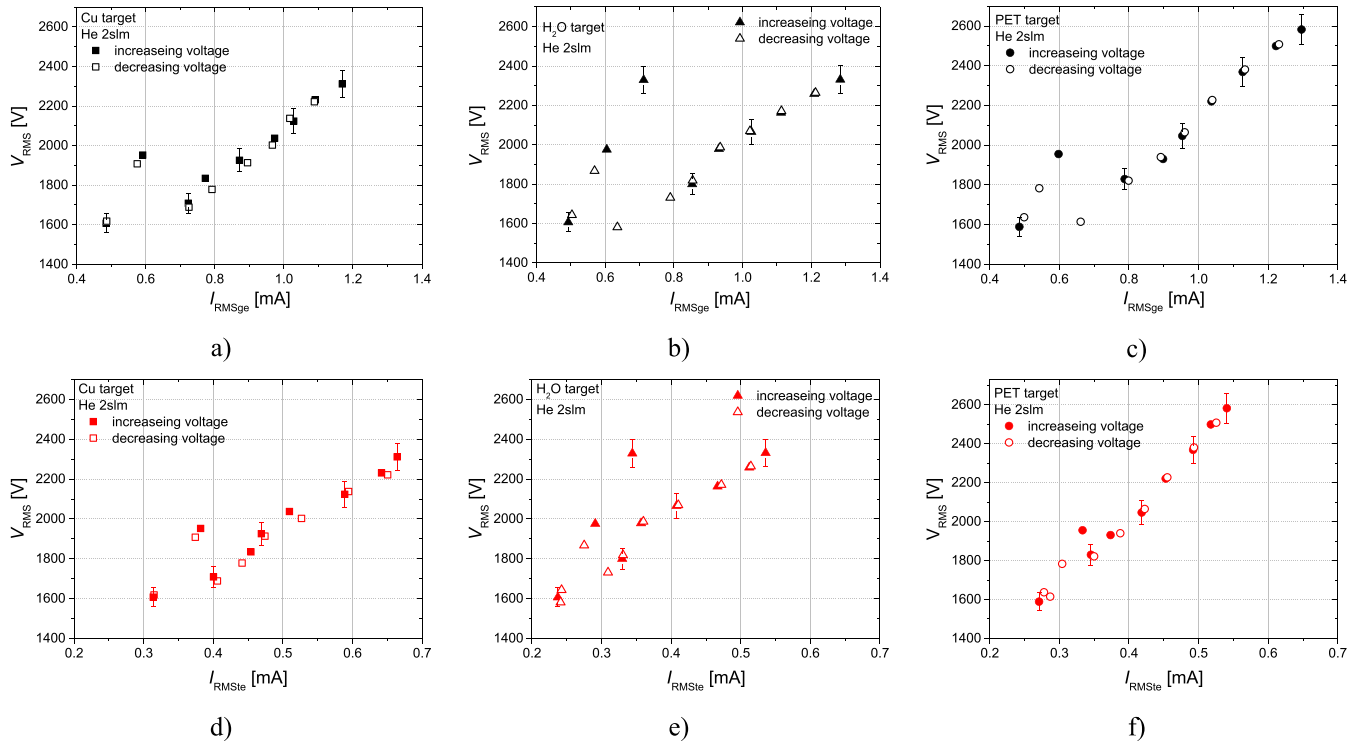


Figure 5. V - I characteristics of the He DBD jet plasma in contact with 3 different targets. Solid symbols are points obtained by increasing the input voltage, while open symbols are obtained by decreasing the voltage. Plots (a)–(c) present the dependence of the RMS voltage on the current through the grounded electrode I_{RMSge} and (d)–(e) the dependence on the current through the target I_{RMSste} .

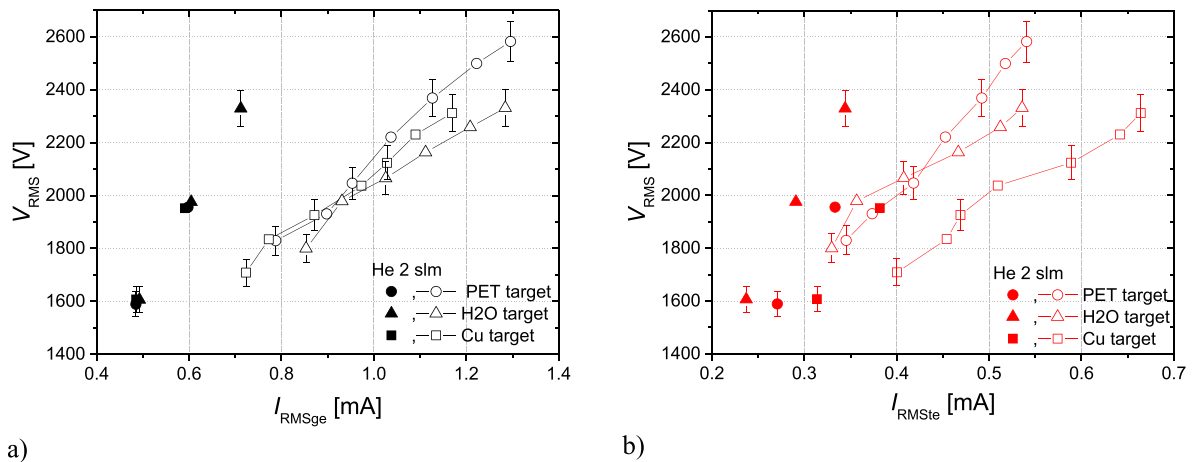


Figure 6. V - I characteristics of the DBD jet in contact with 3 different targets. The dependence of V_{RMS} is plotted against (a) grounded electrode current, (b) target current. The open symbols are measured with the plasma ignited and they are connected by lines to improve legibility.

(i.e. the impedance change) is due to the nonlinear changes of charge densities in the plasma that may originate from different reaction kinetics in the gas phase and/or effects of the surface charges [48, 49]. We could not observe any additional distortion of the waveforms that has been detected by other authors in the case of the plasma mode transition [50–52].

The points of the plasma plume V - I characteristics obtained before plasma ignition differ significantly with the targets used (figure 6(b)). After ignition, the highest RMS current values (I_{te}) are recorded for the Cu target. This can be

explained by a considerable amount of charged particles that are efficiently transferred to the plasma plume. In the case of PET and dH_2O targets the maximal measured currents are similar. However, the RMS voltages depend on the target’s conductivity. For the PET target the impedance is constant for all applied voltages. However, for the dH_2O and Cu targets the impedances change and this corresponds to an appearance of a stronger, more intense, conductive plasma channel.

In figure 7 we show the V - I characteristics obtained for the PET and dH_2O targets at two different He flow rates: 2 slm and

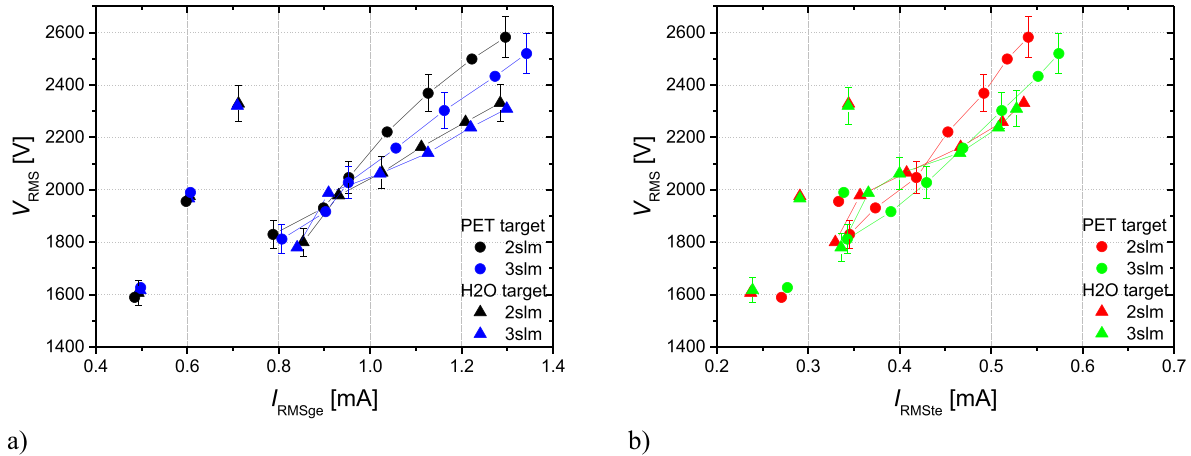


Figure 7. V – I characteristics of the DBD jet in contact with PET and dH₂O targets at two He flow rates. The dependence of V_{RMS} is plotted against (a) grounded electrode current, (b) target current. Lines connect the points obtained when plasma is ignited to improve legibility.

3 slm. Points obtained with ignited plasma are connected by lines. The variations in He gas flow affect the V – I characteristics for these two targets, but they do not introduce significant changes for the Cu target. With the Cu target the plasma plume impinges on a highly conductive surface, which may result in the occurrence of a stronger gas flow of He between the jet tube and the target [14, 53]. Thus, relatively small changes in the gas flow rate (between 2 slm and 3 slm) cannot modify the electrical properties of the jet.

For the V – I characteristics of the plasma core part, i.e. for the voltage dependence on the current through the grounded electrode, in the case of the water target there is a very small difference between the operating points obtained at different flow rates (figure 7(a)). For the currents below 1.1 mA the curves are indistinguishable, while at higher currents the difference is of the order of the voltage measurement error (around 20 V). However, for the PET target there are bigger differences in the operating voltages at different flow rates. For jet currents above 0.9 mA, voltages may be different as much as 100 V. The V – I characteristic of the plume region, i.e. the voltage dependence on the current through the target, shown in figure 7(b), has a similar dependence as in figure 7(a). In the plume region the V – I characteristics in the case of dH₂O do not change with the gas flow, while for the PET target the operating voltages become different for the currents above 4 mA. Hence, the pronounced difference in the V – I characteristics of both regions measured at different flow rates is observed only for the PET target. Since the effect of the surface charges is pronounced on the PET target, these results indicate that the surface charges can affect both the plasma plume region and the plasma core. This has been thoroughly studied in the case of the pulse-powered jets [24, 26, 54]. In papers [18, 55] it has been shown that for low-permittivity dielectric targets (such as PET) there is a rapid charging of the surface and formation of surface ionization waves. Additionally, properties of the dielectric target influence not only the density of electrons, i.e. the electric field, but also the density of radicals in the plume region [56]. In our case of continuous power supply, the same processes occur, but may be diminished due

to short plasma-off time in comparison to the low-duty cycle pulsed discharges. Nevertheless, a strong influence of the low-permittivity PET target on both the electron and neutral species in the plasma plume is reflected in the plasma core, resulting in visible differences in the V – I characteristics obtained with the two He flow rates. For the case of a pulse-powered jet in contact with high-permittivity dielectric (H₂O target), authors discuss the existence of a return stroke (or ‘third’ discharge) due to the high electron production and enhancement of the electric field adjacent to the substrate surface [18, 56]. On the other hand, in the situation with continuously powered jet against a grounded conductive target, the appearance of anode directed streamers has been observed but only in a narrow range of operating conditions [47].

3.2.2. Power transmitted to the discharge. Another important parameter that describes interactions between the plasma and the target is the power delivered to the discharge and then forwarded to the target. In this study, as the first step in power assessment, time-dependent power signals are obtained. The instantaneous power is calculated from the voltage and current waveforms (as shown in figure 4). Since we recorded both the current between powered and grounded electrode $i_{ge}(t)$ and the current passing through the plasma plume into the target $i_{te}(t)$, powers delivered to the core of the plasma and from the plume to the target could be calculated. The following formula is used for calculation:

$$p(t) = v(t) \cdot i_k(t) \quad (4)$$

providing the appropriate current waveform is used (denoted by index k).

The instantaneous power calculated using plasma-on waveforms also contains the power losses in the plasma jet circuitry [57]. To separate this part, several approaches could be used. For instance, at a specific current, the input power without plasma could be measured allowing an estimate of the power losses [57, 58]. Another approach applied here is to subtract the effect of the displacement current, assuming only

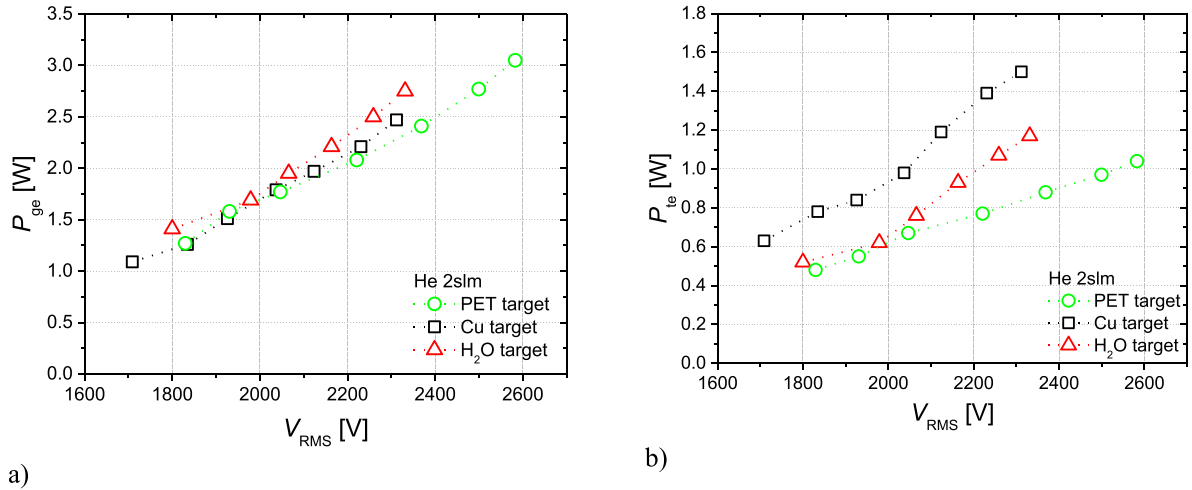


Figure 8. The average power as a function of the RMS voltage in the case of Cu, dH₂O and PET targets at 2 slm of He. (a) Average power dissipated between the powered and grounded electrode (plasma core region) and (b) average power dissipated from the plume to the grounded target (plasma plume region).

stray capacitance of the plasma source from calculated circuit impedance [59]. Then, the time-averaged power is obtained from the equation:

$$P_k = \frac{1}{nT} \int_0^{nT} p(t) dt. \quad (5)$$

The calculated powers are plotted against the RMS voltages for the Cu, dH₂O and PET targets at 2 slm of He in figure 8. P_{ge} shown in figure 8(a) is the average power dissipated between powered and grounded electrode (in the plasma core region), while in figure 8(b) we calculated P_{te} as the average power delivered from the plasma to the grounded target (plasma plume region). The lowest plasma core power of 1.1 W is obtained for the Cu target at the lowest operating voltage of 1700 V. The highest power is for the PET target, i.e 3 W at 2580 V RMS (figure 8(a)). The powers calculated for all three targets in the RMS voltage range from 1900 V to 2100 V are very similar. For higher voltages, the discrepancy is more pronounced. The highest power dissipated at a specific voltage is for the water target and the lowest power is for the PET target. These results are in accordance with the $V-I$ characteristic (figure 6(a)). In the plume region, the lowest power of 0.5 W is measured for the PET target and the highest power of 1.5 W is obtained for the Cu target (figure 8(b)). Unlike the power dissipated in the plasma core (figure 8(a)), here the lowest and the highest powers are not correlated with the extreme values of operating voltages. These results agree well with the $V-I$ characteristic in figure 6(b)—at a particular operating voltage, the highest current is achieved for the Cu target and hence the highest powers in figure 8(b) are also obtained for this target. The power from the plasma plume dissipated to the target (P_{te}) strongly depends on the target type, with a difference between the minimal and maximal power of more than 40% at around 2300 V. For voltages below 2100 V powers measured for a high-permittivity dielectric (dH₂O)

and a low-permittivity dielectric (PET) are almost the same. Concerning the dependence of P_{ge} and P_{te} on the respected currents, as slopes of the $V-I$ characteristics obtained for all 3 targets showed similar rising tendency (figure 6), the dependence of power P_{ge} on grounded electrode current and power P_{te} on target current would be similar to the dependences on voltages plotted in figure 8 with slightly different slopes. Calculated P_{ge} values would correspond to the RMS values of grounded electrode current from 0.7 mA to 1.3 mA while for P_{te} values the target current range would be from 0.35 mA to 0.65 mA.

To estimate the efficiency of transferring the power from the plasma core to the plasma effluent in contact with the target, we calculated the ratio of the average power dissipated between the powered and the grounded electrodes to the average power delivered from the plume to the grounded target. This power transfer efficiency as a function of the RMS voltage is shown in figure 9. The obtained values clearly show the changes in plasma behaviour related to the target conductance.

For the copper target, more than 50% of the plasma core power is delivered to the plume region and the target, while for the dielectric targets (PET and dH₂O) these percentages are around 35%. The reason for this is twofold. One is the combination of a strong conductive channel impinging upon conductive material results in high power delivered to the target. This is also visible in the $V-I$ measurements plotted with I_{te} (figure 6(b)) where the current obtained for Cu target is higher than for other two materials. The highest conductivity led to the highest currents. Apart from the current and voltage amplitudes their phase difference will determine the average power delivered to that part of the circuit. In case of Cu target the phase, difference is 2 and 3 times smaller compared to the phase differences in case of dH₂O and PET, respectively. Thus, one can assume that there is a threshold conductivity of the target below which the power ratio appears to be the same regardless of the conductivity.

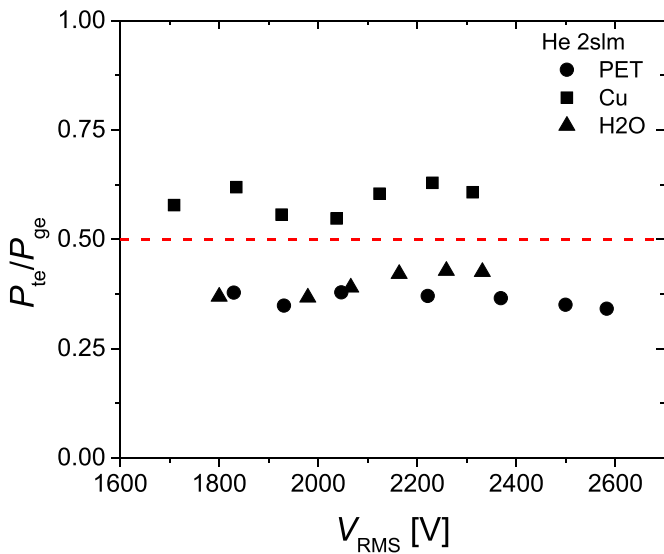


Figure 9. Ratio of the power dissipated in the plume (passing through the target) and the power in the plasma core region for three different targets: PET, Cu and dH₂O. The results are obtained for 2 slm of He.

Values of the power ratio for the Cu target oscillate, i.e the efficiency curve presented in figure 9 has inflections. In the case of the water and PET targets, the ratios are nearly the same below 2100 V. Above that voltage, the ratio for dH₂O stays around 40%, while the values for PET decrease slightly reaching 35%. This difference between the dielectric targets at higher voltages is also visible in figures 6(b) and 8(b). Considering the presented results, the efficiency of the power transfer is one of the important parameters that should be considered when performing treatments with conductive or dielectric substrates.

4. Conclusion

In this paper we presented detailed electrical characterization of a DBD plasma jet in contact with three different types of targets: a conductive Cu plate, a PET plate (low electrical-permittivity sample) and distilled H₂O (high-permittivity sample). The analysis included an equivalent electrical circuit model that emphasizes differences between plasma-off and plasma-on regime (by including voltage controlled current source representing a streamer with a leading ionization and tail back to the electrode). Small changes in electrical elements corresponding to the target's electrical properties (C_{te} , R_{te} and R_i) are also observed.

The experimental setup allowed us to record the high-voltage signal supplied to the jet and two currents. One current was recorded at the grounded electrode $i_{ge}(t)$, while the other was in the line connecting the target and the ground $i_{te}(t)$. In both cases the currents were separately monitored by measuring the voltage on 100 kΩ resistors. In this way we were able to obtain waveforms from the core and plume regions of the plasma. Using the waveforms, plasma-induced nonlinearity in the sine signal was assessed and described using the *THD*

factor. The voltage waveform was not distorted, but the *THD* for the grounded electrode current (I_{ge}) was shown to depend on the conductivity of the target. The highest distortion in the I_{ge} signal is obtained for the Cu target and for other dielectric targets the distortion is increased with the increase of the target conductivity. For the current passing through the target (I_{te}), the situation was somewhat different and *THD* did not appear to be directly in correlation with the target conductivity, but with the target surface stability and/or plasma-surface interactions. Moreover, we assessed the phase shift between the voltage and currents waveforms. Only for I_{te} , the phase shift changed when we exchanged the target type. The observed increase in the phase shift corresponded to the decrease in the conductivity of the target.

Using the recorded time-varying signals, we calculated appropriate RMS values and plotted $V-I$ characteristics for two plasma regions: the plasma core and plasma plume. The $V-I$ characteristics were obtained for two gas flow rates. From plasma-off measurements we were able to calculate the impedance of the plasma source. The changes in slopes of the $V-I$ characteristics occurred due to the nonlinear variations of the charge density at different currents, which, in turn, affected the amplitudes of the waveforms and consequently RMS values. We could not observe any additional distortion in the waveforms that was detected by other authors in the case of plasma mode change. The influence of the He flow rate on the $V-I$ characteristics was clearly visible only for the PET target, while the effect is barely present for the dH₂O target. In the case of the Cu target we could not observe any change in the $V-I$ characteristics for the two flows investigated.

By calculating the instantaneous power, we obtained the average power delivered to the plasma core region P_{ge} and the plume region P_{te} . The values obtained for P_{ge} were similar for different targets, while the P_{te} values had considerable differences depending on the targets. The highest power was delivered to the conductive type of target, i.e the Cu plate. For dielectric targets the calculated powers were lower from 30% to 40% in comparison to the Cu target, showing weak dependence on operating voltage and the target. To estimate the power transfer efficiency between the core plasma and the plasma effluent that was in contact with the target, we calculated the ratio of powers in these two regions. The ratio of the average powers P_{te}/P_{ge} showed that the efficiency of the power transfer was higher for the Cu target and lower for PET and dH₂O targets, with similar ratios for these two dielectric targets.

Data availability statement

All data that support the findings of this study are included within the article (and any supplementary files).

Acknowledgments

K K was financially supported by the Hungarian Scientific Research Fund (Grant NKFIH-K132158). N P, N Š and M P are financially supported by the Science Fund, Republic of Serbia, 7739780, APPerTAin-BIOM Project and by the

MSTDI Republic of Serbia Grant Nos. 451-03-47/2023-01/200024. Z Lj P is grateful to the SANU Project F155 for partial support. We thank Ms. Vera Furtula for performing a part of the electrical measurements.

ORCID iDs

Nikola Škoro  <https://orcid.org/0000-0002-0254-8008>
 Kinga Kutasi  <https://orcid.org/0000-0001-6082-1853>
 Marija Puač  <https://orcid.org/0000-0002-6011-0434>
 Zoran Lj Petrović  <https://orcid.org/0000-0001-6569-9447>
 Nevena Puač  <https://orcid.org/0000-0003-1142-8494>

References

- [1] Adamovich I et al 2022 *J. Appl. Phys.* **55** 373001
- [2] Ostrikov K, Cvelbar U and Murphy A B 2011 *J. Phys. D: Appl. Phys.* **44** 174001
- [3] Makabe T and Petrovic Z L 2016 *Plasma Electronics: Applications in Microelectronic Device Fabrication* 2nd edn (CRC Press)
- [4] Stoffels E, Flikweert A J, Stoffels W W and Kroesen G M W 2002 *Plasma Sources Sci. Technol.* **11** 383–8
- [5] Graves D B 2017 *IEEE Trans. Radiat. Plasma Med. Sci.* **1** 281–92
- [6] von Woedtke T, Laroussi M and Gherardi M 2022 *Plasma Sources Sci. Technol.* **31** 054002
- [7] Miletić M, Mojsilović S, Okić Đorđević I, Maletić D, Puač N, Lazović S, Malović G, Milenković P, Petrović Z L and Bugarski D 2013 *J. Phys. D: Appl. Phys.* **46** 345401
- [8] Choi E H, Hong Y J and Kaushik N K 2021 *Appl. Sci. Converg. Tech.* **30** 118–36
- [9] Winter J, Brandenburg R and Weltmann K-D 2015 *Plasma Sources Sci. Technol.* **24** 064001
- [10] Stancampiano A, Selaković N, Gherardi M, Puač N, Petrović Z L and Colombo V 2018 *J. Phys. D: Appl. Phys.* **51** 484004
- [11] Gerber I C, Mihaila I, Hein D, Nastuta A V, Jijie R, Pohoata V and Topala I 2017 *Appl. Sci.* **7** 812
- [12] Oh J-S, Aranda-Gonzalvo Y and Bradley J W 2011 *J. Phys. D: Appl. Phys.* **44** 365202
- [13] Lu X, Naidis G V, Laroussi M, Reuter S, Graves D and Ostrikov K 2016 *Phys. Rep.* **630** 1–84
- [14] Robert E, Sarron V, Darny T, Riès D, Dozias S, Fontane J, Joly L and Pouvesle J-M 2014 *Plasma Sources Sci. Technol.* **23** 012003
- [15] Maletić D, Puač N, Malović G, Đorđević A and Petrović Z L 2017 *J. Phys. D: Appl. Phys.* **50** 145202
- [16] Hofmann S, Van Gils K, van Der Linden S, Iseni S and Bruggeman P 2014 *Eur. Phys. J. D* **68** 56
- [17] Do Nascimento F, Moshkalev S and Machida M 2017 *Braz. J. Phys.* **47** 278–87
- [18] Klarenaar B L M, Guaitella O, Engeln R and Sobota A 2018 *Plasma Sources Sci. Technol.* **27** 085004
- [19] Zaplotnik R, Biščan M, Kregar Z, Cvelbar U, Mozetič M and Milošević S 2015 *Spectrochim. Acta B* **103–104** 124–30
- [20] Kovačević V V, Sretenović G B, Slikboer E, Guaitella O, Sobota A and Kuraica M M 2018 *J. Phys. D: Appl. Phys.* **51** 065202
- [21] Yamada H et al 2016 *J. Phys. D: Appl. Phys.* **49** 394001
- [22] Nastuta A V, Pohoata V and Topala I 2013 *J. Appl. Phys.* **113** 183302
- [23] Shershunova E A, Moshkunov S I and Khomich V Y 2019 *IEEE Trans. Plasma Sci.* **47** 4909
- [24] Norberg S A, Johnsen E and Kushner M J 2015 *J. Appl. Phys.* **118** 013301
- [25] Li C, Pei X and Lu X 2017 *J. Appl. Phys.* **121** 203305
- [26] Darny T, Pouvesle J M, Puech V, Douat C, Dozias S and Robert E 2017 *Plasma Sources Sci. Technol.* **26** 045008
- [27] Sobota A, Guaitella O and Garcia-Caurel E 2013 *J. Phys. D: Appl. Phys.* **46** 5
- [28] Damany X, Pasquiers S, Blin-Simiand N, Bauville G, Bournonville B, Fleury M, Jeanney P and Sousa J S 2016 *Eur. Phys. J. Appl. Phys.* **75** 24713
- [29] Brandenburg R 2017 *Plasma Sources Sci. Technol.* **26** 053001
- [30] Marinov D and Braithwaite N S J 2014 *Plasma Sources Sci. Technol.* **23** 062005
- [31] Hofmann S, Van Gessel A F H, Verreycken T and Bruggeman P 2011 *Plasma Sources Sci. Technol.* **20** 065010
- [32] Golda J, Kogelheide F, Awakowicz P and Gathen V S V D 2019 *Plasma Sources Sci. Technol.* **28** 095023
- [33] Stoffels E, Sladek R E J, Kieft I E, Kersten H and Wiese R 2004 *Plasma Phys. Control. Fusion* **46** B167–77
- [34] Teschner T, Bansemer R, Weltmann K D and Gerling T 2019 *Plasma* **2** 348–59
- [35] Maletić D, Puač N, Selaković N, Lazović S, Malović G, Đorđević A and Petrović Z L 2015 *Plasma Sources Sci. Technol.* **24** 025006
- [36] Ohring M 1995 *Engineering Materials Science* (Academic)
- [37] MatWeb 1999 *MatWeb-Material Property Data* Water, H₂O (available at: www.matweb.com/) (Accessed 1 July 2019)
- [38] Malmberg C G and Maryott A A 1956 *Dielectric constant of water from 0° to 100° C* *J. Res. Nat. Bur. Stand.* **56** 2641
- [39] Engineering ToolBox 2008 *Dielectric constants of common liquids* (available at: www.engineeringtoolbox.com/liquid-dielectric-constants-d_1263.html) (Accessed 1 July 2019)
- [40] Phelps A V and Petrovic Z L 1999 *Plasma Sources Sci. Technol.* **8** R21
- [41] Panzner G, Egert B and Schmidt H P 1985 *Surf. Sci.* **151** 400–8
- [42] Bruggeman P, Iza F, Lauwers D and Gonzalvo Y A 2010 *J. Phys. D: Appl. Phys.* **43** 012003
- [43] Murakami T, Niemi K, Gans T, O'Connell D and Graham W G 2012 *Plasma Sources Sci. Technol.* **22** 015003
- [44] Fang Z, Shao T, Yang J and Zhang C 2016 *Discharge processes and an electrical model of atmospheric pressure plasma jets in argon* *Eur. Phys. J. D* **70** 3
- [45] Valdivia-Barrientos R, Pacheco-Sotelo J, Pacheco-Pacheco M, Benítez-Read J S and López-Callejas R 2006 *Plasma Sources Sci. Technol.* **15** 237–45
- [46] Fang Z, Ji S, Pan J, Shao T and Zhang C 2012 *IEEE Trans. Plasma Sci.* **40** 883–91
- [47] Maletić D 2018 *Development and diagnostics of atmospheric plasma jet and application on biological samples* *PhD Thesis* University of Belgrade, Belgrade
- [48] Golubovskii Y B, Maiorov V A, Behnke J and Behnke J F 2003 *J. Phys. D: Appl. Phys.* **36** 39–49
- [49] Liu S and Neiger M 2003 *J. Phys. D: Appl. Phys.* **36** 3144
- [50] Walsh J L, Iza F, Janson N B, Law V J and Kong M G 2010 *J. Phys. D: Appl. Phys.* **43** 075201
- [51] Brandenburg R, Navrátil Z, Jánský J, St' Ahel P, Trunec D and Wagner H E 2009 *J. Phys. D: Appl. Phys.* **42** 085208
- [52] Sobota A, Guaitella O and Rousseau A 2014 *Plasma Sources Sci. Technol.* **23** 025016

- [53] Darny T, Pouvesle J M, Fontane J, Joly L, Dozias S and Robert E 2017 *Plasma Sources Sci. Technol.* **26** 105001
- [54] Viegas P, Slikboer E, Obrusník A, Bonaventura Z, Sobota A, Garcia-Caurel E, Guaitella O and Bourdon A 2018 *Plasma Sources Sci. Technol.* **27** 094002
- [55] Simoncelli E, Stancampiano A, Boselli M, Gherardi M and Colombo V 2019 *Plasma* **2** 369–79
- [56] Yue Y, Pei X, Gidon D, Wu F, Wu S and Lu X 2018 *Plasma Sources Sci. Technol.* **27** 064001
- [57] Gerling T, Brandenburg R, Wilke C and Weltmann K D 2017 *Eur. Phys. J. Appl. Phys.* **78** 10801
- [58] Pipa A V, Koskulics J, Brandenburg R and Hoder T 2012 *Rev. Sci. Instrum.* **83** 115112
- [59] Puač N, Petrović Z L, Radetić M and Djordjević A 2005 *Mater. Sci. Forum* **494** 291–6



**32nd Summer School and
International Symposium on
the Physics of Ionized Gases**

Belgrade, Serbia,
August 26 - 30, 2024

CONTRIBUTED PAPERS
&
**ABSTRACTS of INVITED LECTURES,
TOPICAL INVITED LECTURES and PROGRESS REPORTS**

Editors:
**Bratislav Obradović, Jovan Cvetić,
Miroslav Kuzmanović and Nikola Cvetanović**



**БЕОГРАД
2024**

**32nd Summer School and
International Symposium on
the Physics of Ionized Gases**



August 26 – 30, 2024, Belgrade, Serbia

S P I G 2024

CONTRIBUTED PAPERS

&

ABSTRACTS OF INVITED LECTURES,
TOPICAL INVITED LECTURES AND
PROGRESS REPORTS

Editors

Bratislav Obradović, Jovan Cvetic,
Miroslav Kuzmanović and Nikola Cvetanović

University of Belgrade –
Faculty of Physical
Chemistry

Serbian Academy of
Sciences and Arts

Belgrade, 2024

PUBLICATIONS OF THE ASTRONOMICAL OBSERVATORY OF BELGRADE
FOUNDED IN 1947

EDITORIAL BOARD:

Dr. Srdjan SAMUROVIĆ, Editor-in-Chief (Astronomical Observatory, Belgrade)

Dr. Rade PAVLOVIĆ (Institute of Physics, Belgrade)

Dr. Miroslav MIĆIĆ (Astronomical Observatory, Belgrade)

Dr. Branislav VUKOTIĆ (Astronomical Observatory, Belgrade)

All papers in this Publication are peer reviewed.

Published and copyright © by Astronomical Observatory, Volgina 7, 11060 Belgrade 38, Serbia

Director of the Astronomical Observatory: Dr. Luka Č. Popović

Typesetting: Tatjana Milovanov

Internet address <https://publications.aob.rs>

ISSN 0373-3742

ISBN 978-86-82296-08-9

Financially supported by the Ministry of Science, Technological Development and Innovation of the Republic of Serbia

CIP - Каталогизacija у публикацији - Народна библиотека Србије, Београд

537.56(082)

539.186.2(082)

539.121.7(082)

533.9(082)

SUMMER School and International Symposium on the Physics of Ionized Gases (32 ; 2024 ; Beograd)

Contributed papers & abstracts of invited lectures, topical invited lectures and progress reports / 32nd Summer School and International Symposium on the Physics of Ionized Gases - SPIG 2024, August 26 – 30, 2024, Belgrade, Serbia ; editors Bratislav Obradović ... [et al.]. - Belgrade : Astronomical Observatory, 2024 (Beograd : Skripta Internacional). - 215 str. : ilustr. ; 24 cm. - (Publications of the Astronomical Observatory of Belgrade, ISSN 0373-3742)

Na nasl. str.: University of Belgrade, Faculty of Physical Chemistry; Serbian Academy of Sciences and Arts. - Tiraž 200. - Str. 17-18: Preface / editors Bratislav Obradović ... [et al.]. - Bibliografija uz svaki rad. - Registar.

ISBN 978-86-82296-08-9

1. Kuzmanović, Miroslav, 1967- [urednik] [autor dodatnog teksta]

a) Јонизовани гасови - Зборници b) Атоми - Интеракција - Зборници

v) Плазма - Зборници

COBISS.SR-ID 150439689

SPIG 2024

SCIENTIFIC COMMITTEE

J. Cvetić (Co-chair), Serbia
B. Obradović (Co-chair), Serbia

A. Antoniou, Greece
J. Burgdörfer, Austria
M. Ćosić, Serbia
V. Guerra, Portugal
M. Ivković, Serbia
J. Kovačević-Dojčinović, Serbia
K. Kutasi, Hungary
I. Mančev, Serbia
D. Marić, Serbia
N. J. Mason, UK
A. Milosavljević, France
V. Milosavljević, Serbia
D. Milošević, BH
K. Mima, Japan
L. Nahon, France
G. Poparić, Serbia
I. Radović, Serbia
P. Ranitovic, Serbia
P. Rousseau, France
I. Savić, Serbia
Y. Serruys, France
N. Simonović, Serbia
V. Srećković, Serbia
M. Škorić, Japan
S. Tošić, Serbia
M. Trtica, Serbia
R. White, Australia

ADVISORY COMMITTEE

D. Belić
N. Bibić
M. S. Dimitrijević
S. Đurović
D. Ilić
N. Konjević
M. M. Kuraica
J. Labat
G. Malović
B. P. Marinković
M. Milosavljević
Z. Mišković
Z. Lj. Petrović
L. Č. Popović
B. Stanić

ORGANIZING COMMITTEE

M. Kuzmanović (Chair)
M. Ristić (Co-secretary)
B. Stankov (Co-secretary)
N. Konjević
N. Cvetanović
D. Ranković
M. Milovanović
M. Marković
A. Šajić
I. Traparić

Reviewers for the Book of SPIG 2024

Jovan Cvetić, Full Professor, University of Belgrade, School of Electrical Engineering, Belgrade, Serbia

Marko Čosić, Associate research professor, Vinča Institute of Nuclear Sciences, Belgrade, Serbia

Milivoje Ivković, Principal Research Fellow, Institute of Physics, Belgrade, Serbia

Jelena Kovačević-Dojčinović, Associate research professor, Astronomical Observatory Belgrade, Serbia

Ivan Mančev, Full Professor, University of Niš, Faculty of Sciences and Mathematics, Niš, Serbia

Dragana Marić, Principal Research Fellow, Institute of Physics, Belgrade, Serbia

Aleksandar R. Milosavljević, Principal Research Fellow, Synchrotron SOLEIL, Saint-Aubin, France

Vladimir Milosavljevic, Full Professor, University of Belgrade - Faculty of Physics, Belgrade, Serbia

Dejan Milošević, Full Professor, University of Sarajevo – Faculty of Science, Sarajevo, Bosnia and Herzegovina

Bratislav Obradović, Full Professor, University of Belgrade - Faculty of Physics, Belgrade, Serbia

Goran Poparić, Full Professor, University of Belgrade - Faculty of Physics, Belgrade, Serbia

Ivan Radović, Principal Research Fellow, Vinča Institute of Nuclear Sciences, Belgrade, Serbia

Predrag Ranitović, Principal Research Fellow, University of Belgrade - Faculty of Physics, Belgrade, Serbia

Igor Savić, Full Professor, University of Novi Sad, Faculty of Sciences and Mathematics, Novi Sad, Serbia

Nenad Simonović, Principal Research Fellow, Institute of Physics, Belgrade, Serbia

Vladimir Srečković, Principal Research Fellow, Institute of Physics, Belgrade, Serbia

Miloš Škorić, Principal Research Fellow, Vinča Institute of Nuclear Sciences, Belgrade, Serbia

Sanja Tošić, Research Associate Assistant, Institute of Physics, Belgrade, Serbia

Milan Trtica, Principal Research Fellow, Vinča Institute of Nuclear Sciences, Belgrade, Serbia

CONTENTS

Bratislav Obradović, Jovan Cvetić, Miroslav Kuzmanović and Nikola Cvetanović <i>Preface</i>	17
Section 1. ATOMIC COLLISION PROCESSES	
Invited Lectures	
O. Asvany, P.C. Schmid, S. Thorwirth and S. Schlemmer <i>Missing Ions in Laboratory and Space</i>	21
Himadri Chakraborty <i>Impact Spectroscopy and Chronoscopy of Gas Phase Atoms, Molecules and Fullene</i>	22
Alicja Domaracka <i>Ion Processing of Molecular Systems: A Way to Form Complex Systems in Space</i>	23
Carla Figueira de Morisson Faria <i>Exploring Quantum Effects in the Attosecond Domain</i>	24
G. G. Paulus <i>Extreme UV Imaging with High Harmonics</i>	25
Xiao-Min Tong <i>Theory on Dynamics of Atoms in Strong Laser Field</i>	26
Topical Invited Lectures	
N. Pinhão <i>Description of Electron Swarms in an Electric Field: A Finite Elements Computation Including Third-order Transport Parameters</i>	27
Helgi Rafn Hrodmarsson <i>VUV Photionization of Interstellar Molecules: Making Sense of Our Beautifully Mysterious Universe, Molecule by Molecule</i>	28
Progress Reports	
Jasmina Atić and Saša Dujko <i>Electron Transport and Negative Ionization Fronts in Strongly Attaching Gases</i>	29

Daan Boer and Jan Van Dijk <i>LOKI-B C++: An Open-Source Boltzmann Solver for Reproducible Electron Boltzmann Calculations.....</i>	30
Danijela Danilović, Dušan K. Božanić, Aleksandar R. Milosavljević, Radovan Dojčilović and Vladimir Djoković <i>Synchrotron Radiation Photoelectron Spectroscopy Study of the Electronic Structure of Ag-Bi-I Rudorffite Nanoparticles.....</i>	31
M. Fournier, J. Palaudoux, R. Dupuy, F. Penent and C. Nicolas <i>Photoelectron Spectroscopy of Solvated Biological Interest Molecules in Liquid Jet Configuration.....</i>	32
D. Habibović and D. B. Milošević <i>Strong-field Processes Induced by Tailored Laser Fields.....</i>	33
Emilia Heikura, Christina Zindell, Denis Kargin, Aleksandar Milosavljevic, Andreas Hans, Rudolf Pietschnig and Arno Ehresmann <i>Towards Distant Dependent Inner-shell Photoelectron Circular Dichroism.....</i>	34
Laura Pille, Bart Oostenrijk, Juliette Leroux, Carlos Ortiz Mahecha, Robert Meißner, Debora Scuderi, Sadia Bari and Lucas Schwob <i>Exploring Biomolecular Properties in the Gas Phase by Using Advanced Light Sources.....</i>	35
M. Werl, T. Koller, P. Haidegger, S. Wrathall, L. Esletzbichler, A. Niggas, F. Aumayr, K. Tókési and R.A. Wilhelm <i>De-excitation Cascade Calculation for Highly Excited Hollow Atoms</i>	36
Posters	
Danko Bošnjaković, Ilija Simonović and Saša Dujko <i>Studies on Streamer Discharges in Ultra-low GWP Gases.....</i>	37
G. J. Boyle, N. A. Garland, R. P. Mceachran and R. D. White <i>Electron Transport in Simple Liquid Mixtures.....</i>	38
Saša Dujko, Ilija Simonović, Danko Bošnjaković, Jasmina Atić and Zoran Lj. Petrović <i>Electron Transport in Radio-Frequency Electric and Magnetic Fields in Ultra-low GWP Gases.....</i>	39
Saša Dujko, Ilija Simonović, Danko Bošnjaković, Zoran LJ. Petrović and J. De Urquijo <i>Studies on Electron Swarms and Streamer Discharges in Eco-friendly RPC Gases.....</i>	40

N. A. Garland, R. D. White, R. E. Robson and M. Hildebrandt <i>An Aliasing Method for Determination of Transport Data for Exotic Charged Particles in Crossed Electric and Magnetic Fields</i>	41
Mai Hao, Gerjan Hagelaar, Boya Zhang and Xingwen Li <i>Monte Carlo Simulation of Electron Swarms in Pulsed Townsend Experiment and Validation of the Swarm Data Derived from Waveform Analysis</i>	45
Jelena B. Maljković, Jelena Vukalović, Francisco Blanco, Gustavo Garcia and Bratislav P. Marinković <i>Investigation of Elastic Electron Scattering by Anaesthetic Molecules in Gaseous Phase</i>	46
Bratislav P. Marinković and Stefan Đ. Ivanović <i>Electron Scattering Cross Sections Represented in Belgrade Electron-atom/molecule Database (BEAM)</i>	47
Bratislav P. Marinković, Jozo J. Jureta and Lorenzo Avaldi <i>Ejected Electron Spectra of Krypton Studied by High and Low Energy Electrons</i>	48
Nenad Milojević, Ivan Mančev, Danilo Delibašić and Miloš Milenković <i>Post-prior Discrepancy in the CBI-4B Method for Single-electron Capture in Fast $\text{Li}^{3+} + \text{He}$ Collisions</i>	49
D. L. Muccignat, D. B. Jones, J. R. Gascooke, G. J. Boyle, N. A. Garland and R. D. White <i>Direct Electron-liquid Energy Loss Spectra Measurements Using a Liquid Micro-jet</i>	53
Željka Nikitović and Zoran Raspopović <i>Diffusion Coefficients of H_2^+ Ions in H_2 Gas</i>	57
T. Rook, L. Cruz Rodriguez and C. Figueira de Morisson Faria <i>Influence of Catastrophes and Hidden Dynamical Symmetries on Ultrafast Backscattered Photoelectrons</i>	61
Ilija Simonović, Danko Bošnjaković and Saša Dujko <i>Three-dimensional Streamer Model in the AMReX Environment</i>	62
Barbora Stachová, Juraj Országh and Štefan Matejčík <i>Excitation of Acetone Induced by Electron Impact</i>	63
Sanja Tošić, Vladimir Srećković and Veljko Vujčić <i>Small Molecules Essential to Astrophysics: Collisional and Radiative Processes</i>	64

Mirjana M. Vojnović, Miroslav M. Ristić, Violeta V. Stanković-Mališ and Goran B. Poparić <i>Dissociative Electron Attachment to CO₂ in Electric and Magnetic Fields.....</i>	65
Jelena Vukalović, Jelena B. Maljković, Francisco Blanco, Gustavo Garcia and Bratislav P. Marinković <i>Investigation of Elastic Electron Scattering from Desflurane Molecule at Intermediate Electron Energy.....</i>	66
Guanyu Wang, Boya Zhang and Xingwen Li <i>Transport Properties of Two-temperature SF₆ and Its Alternative Gases.....</i>	67
Section 2. PARTICLE AND LASER BEAM INTERACTIONS WITH SOLIDS	
Topical Invited Lectures	
Marija Gorjanc <i>Plasma Modification of Natural Fibres to Improve Adhesion in Bio-composites.....</i>	71
Milan Radović <i>Integrating Pulse Laser Deposition and Advanced Spectroscopy: Unveiling Hidden Phenomena in Transition Metal Oxides.....</i>	72
Progress Reports	
Hristina Delibašić-Marković <i>Characterizing Ionization and Electron Dynamics in Biological Materials: Theoretical and Numerical Insights into Pulsed Laser-induced Breakdown Processes.....</i>	73
Ana Kalinić, Ivan Radović, V. Despoja, Lazar Karbunar and Z. L. Mišković <i>Interaction of Ions with Graphene-insulator-graphene Composite Systems.....</i>	74
Violeta V. Stanković Mališ and Goran B. Poparić <i>Modeling the Surface Interaction of Cellulosic Materials with CO₂ Plasmas.....</i>	75
Posters	
Milivoje Hadžijojić and Marko Ćosić <i>Low Energy Heavy Ion Rainbow Scattering by Graphene.....</i>	76
Ana Kalinić, Ivan Radović, Lazar Karbunar and Z. L. Mišković <i>Interaction of Ions with Drift-current Biased Supported Graphene.....</i>	80

F. Komarov, O. Milchanin, M.V. Puzyrev and I.S. Rahavaya <i>Forming Nanocrystalline SnO₂ Films on Silicon and Silicon Dioxide by Laser-Plasma Deposition Method</i>	81
Dragan Ranković, Biljana Stankov, Ivan Traparić, Miroslav Kuzmanović and Milivoje Ivković <i>Target Selection for LIBS Studies of Hydrogen Isotope Retention</i>	85
Miroslav Ristić, Aleksandra Šajić, Jovana Babić and Miroslav Kuzmanović <i>Equilibrium Composition of Plasma Obtained by Laser Ablation of Glass</i>	86
Violeta V. Stanković Mališ and Goran B. Poparić <i>Semiquantum Simulation of Cellulosic Materials Interaction with CO₂ Plasmas</i>	87
Nikola Starčević and Srdjan Petrović <i>Rainbows in Transmission of Proton Through Thin Silicon Carbide Crystal</i>	88
N. Tarasenko, V. Kornev, M. Nedelko, A. Radomtsev, N. Tarasenko, Jovan Ciganovic, Sanja Zivkovic and Miloš Momcilovic <i>Properties of Cu/Zn Oxide Nanostructures Formed by Plasma-activated Electrolysis</i>	92

Section 3. LOW TEMPERATURE PLASMAS

Invited Lectures

Satoshi Hamaguchi <i>Opportunities and Challenges in Low-temperature Plasma Science for Atomic-layer Processing</i>	99
Jan van Dijk and Daan Boer <i>LXCat 3 and Beyond – Fostering Reproducibility in Low-temperature Plasma Science</i>	100

Topical Invited Lectures

Peter Hartmann <i>Using Dust Particles as Probes in Low Pressure Gas Discharges</i>	101
Mirjana Kostic, Ana Kramar, Bratislav Obradovic and Milorad Kuraica <i>Atmospheric Pressure Plasma in Processing of Cellulose Fibers: From Surface Cleaning to Tailored Properties</i>	102
Violeta Lazic <i>LIBS Spectroscopy: What We Can Measure, and How?</i>	103

C. Lazzaroni, A. Remigy, M. Jacquemin, H. Kabbara, S. Kasri, B. Menacer, K. Gazeli, V. Mille and G. Lombardi <i>Micro Hollow Cathode Discharges in Argon/Nitrogen Used for Boron Nitride PECVD</i>	104
P. Maguire, N. Hendaway, H. Mcquaid and D. Mariotti <i>Liquid Microdroplets in a Microplasma: Phenomena and Technological Applications</i>	105
Peter Papp, Samuel Peter Kovár, Ladislav Moravský and Štefan Matejčík <i>Ion Induced Reactions in IMS Studied by DFT</i>	106
G. Primc, M. Zver, R. Zaplotnik, A. Filipič, D. Dobnik and M. Mozetič <i>Inactivation of Viruses in Water by Plasma Treatment</i>	107
Nevena Puač, Nikola Škoro, Sergej Tomić, Andjelija Marković, Neda Babucić, Olivera Jovanović, A. Morina, Gordana Malović, Miodrag Čolić and Zoran Lj. Petrović <i>Diagnostics and Applications of Atmospheric Pressure Plasmas for Triggering of Cell Mechanisms</i>	108
Progress Reports	
A. P. Jovanović, H. Höft, D. Loffhagen, T. Gerling and M. M. Becker <i>Fluid Modelling of Single-filament DBD and Self-pulsing Discharges at Atmospheric Pressure Using FEDM</i>	109
Sanja Pavlovic and Goran Poparić <i>Thermal and Acoustic Properties of Cellulose Fibrous Materials</i>	110
M. Stankov, M. M. Becker, L. Bröcker, C.-P. Klages and D. Loffhagen <i>Analysis of Dielectric Barrier Discharges in Ar-monomer Mixtures Using a Standardized Fluid Modelling Approach</i>	111
Olga Stepanova, Vadim Snetov, Oleg Grushko, Dmitry Subbotin, Ilya Ruchkin and Mikhail Pinchuk <i>“Air-plasma-water” Electrophysical System Based on DBD Plasma Jet: Prospects and Problems</i>	112
Ivan Traparić <i>Application of Machine Learning and Artificial Intelligence in Plasma Spectroscopy</i>	113

Posters

- E.N. Bocharnikova, O.N. Tchaikovskaya, S.A. Chaykovsky,
V.I. Solomonov, A.S. Makarova and I.V. Sokolova
*Luminescent Analysis of E-beam Induced Transformation of Phenol in
the Presence of Humic Substances.....* 114
- N.N. Bogachev, A.S. Bakshaev, L.V. Kolik, E.M. Konchekov and
A.S. Kon'kova
*Compact Piezotransformer Source of the Cold Atmospheric Plasma
with Three Types of Discharges.....* 118
- N.N. Bogachev, I.L. Bogdankevich, V.I. Zhukov, D.M. Karfidov,
V.P. Stepin and N.G. Gusein-Zade
*Ionization of a Plasma Antenna Channel in a Dielectric
Gas-discharge Tube.....* 119
- Nikola Cvetanović, Saša S. Ivković and Bratislav M. Obradović
*Estimation of Nitrogen Impurity Level in Helium Atmospheric
Discharge via Emission Spectroscopy.....* 120
- Lazar Gavanski, Nataša Simić and Stevica Djurović
*Measurement of the Velocity of the Plasma Jet Appearing from a Wall
Stabilized Arc.....* 121
- Jovica Jovović
*The Measurement of Pulsed Gas Discharge Parameters by Means of
Fe I Lines in Argon and Argon-hydrogen Mixture.....* 125
- E.M. Konchekov, N.G. Gusein-Zade, D.V. Yanykin, L.V. Kolik,
Yu.K. Danileiko, V.I. Lukanin, K.F. Sergeichev, I.V. Moryakov,
V.D. Borzosekov, V.V. Gudkova, M.E. Astashev and S.V. Gudkov
*Low-temperature Plasma and Plasma-activated Liquids in Solving
Agricultural Problems: Experimental Technique.....* 129
- A. Kropotkin, A. Chukalovsky, A. Kurnosov, T. Rakhimova and
A. Palov
*Modelling of an ICP Discharge in Oxygen with Full Kinetics Scheme
with Newly Calculated VV/VT Rate Constants.....* 130
- Vitaly Kuzmenko, Andrey Miakonkikh and Konstantin Rudenko
*The Formation of Microneedles Structures from Silicon Using Plasma
Etching in SF₆/O₂ Mixture in Inductively Coupled Plasma.....* 134
- James Lalor and Vladimir Milosavljević
*Investigating the Thermal Profile of an Atmospheric Pressure Argon
Plasma Jet on a Conductive and Insulating Mesh Surface.....* 135

Zlatko Majlinger <i>Stark Width Estimates for the Most Prominent Ce II Spectral Lines Important for Astrophysical Investigations.....</i>	136
Zlatko Majlinger, Milan S. Dimitrijević and Vladimir A. Srećković <i>Stark Widths of Several Te II Spectral Lines for Investigation of Astrophysical Spectra.....</i>	137
Jelena Marjanović, Dragana Marić, Marija Puač, Antonije Đorđević and Zoran Lj. Petrović <i>RF Breakdown in Argon at Low-pressures: Experiment and Modelling.....</i>	138
Milica Marković, Dragan Ranković and Miroslav Kuzmanović <i>The Effect of Acids on Pig Bone Estimated by LIBS.....</i>	142
A. Miakonkikh, V. Kuzmenko and K. Rudenko <i>Fluorocarbon Polymerizing Plasmas Etching Processes for Structures of Microelectronics.....</i>	143
Nikodin V. Nedić, Nikola V. Ivanović, Ivan R. Videnović, Djordje Spasojević and Nikola Konjević <i>Cathode Sheath Diagnostics by Integral End-on Optical Emission Spectroscopy in an Analytical Glow Discharge Source in Argon.....</i>	144
S.A. Poniaev, P.A. Popov, N.A. Monakhov, T.A. Lapushkina and M.A. Kotov <i>The Use of Thermoelectric Radiation Detectors for Heat Flux Measurements in Shock-tubes with Gas Ionization.....</i>	145
Aleksandra Šajić, Dragan Ranković, Miroslav Ristić and Miroslav Kuzmanović <i>Determination of Unknow Analyte Concentration in Glass Samples Using the LIBS Method.....</i>	146
Biljana Stankov, Marijana R. Gavrilović Božović, Dragan Ranković, Jelena Savović and Milivoje Ivković <i>Fast Photography in the Service of Spatially and Temporally Resolved LIBS Diagnostics of Doped Tungsten.....</i>	147
Desanka Topalović, Neda Babucić, Nikola Škoro and Nevena Puač <i>Measurements of Reactive Oxygen and Nitrogen Species in Plasma Activated Water by Microwave Discharge.....</i>	148
Ivan Traparić, Biljana Stankov and Milivoje Ivković <i>Detection of Rhenium in Tungsten Using LIBS with Additional Fast Pulse Discharge.....</i>	152

Ivan Traparić, Biljana Stankov, Nikola Vujadinović, Milica Vinić and Milivoje Ivković <i>Influence of the Ablation Angle Change on Spectral Line Intensities in LIBS Experiments.....</i>	153
V.V. Voevodin, O.I. Korzhova, V.Yu. Khomich, V.A. Yamschikov, N. Yu. Lysov and A.V. Klubkov <i>Influence of Interelectrode Distance on the Characteristics of Three-electrode Pulsed SDBD.....</i>	154
Veljko Vujčić, Vladimir A. Srećković, Ognjan Kounchev and Felix Iacob <i>A&M Datasets for LTP Treatment of Plants.....</i>	158
Section 4. GENERAL PLASMAS	
Invited Lecture	
Andreja Gomboc <i>How Stars Get Thorn Apart by Supermassive Black Holes.....</i>	161
Paola Marziani <i>Super-Eddington Quasars: From Atomic Physics to Cosmology.....</i>	162
Luca Volpe <i>Current Situation and Future Prospectives of the European IFE Program, Technology Development, Science and Related Applications.....</i>	163
Topical Invited Lectures	
M. D. Christova, Milan S. Dimitrijević and S. Sahal-Bréchet <i>Astrophysical Applications of Stark Broadening of Spectral Lines.....</i>	164
A. Cinins, Milan S. Dimitrijević, Vladimir A. Srećković, K. Miculis, I. I. Beterov and N. N. Bezuglov <i>Penning and Photo Ionizations of Cold Rydberg Alkali-metal Atoms Under Föster Resonance Conditions.....</i>	165
Ugo Jacovella <i>Exploring the Importance of Interstellar Ions in the Enigma of Diffuse Interstellar Bands.....</i>	166
G. La Mura, G. Mulas, M. A. Iatì, C. Cecchi-Pestellini, S. Rezaei and R. Saija <i>Interstellar Dust as a Dynamic Environment.....</i>	167
S.V. Ryzhkov <i>Magneto-inertial Fusion and Powerful Installations.....</i>	168

C. Suzuki, F. Koike, N. Tamura, T. Oishi, Y. Kawamoto, T. Kawate, M. Goto, N. Nakamura and I. Murakami <i>Comprehensive Z-dependence Analysis of Soft X-ray Spectra from Highly Charged Heavy Ions Using Magnetically Confined High-temperature Plasmas.....</i>	169
Miroslava Vukcevic <i>On the Conditions for Soliton Formation in the Galactic Enviroment</i>	170
Progress Reports	
B. Z. Djordjević, D. J. Strozzi, C. A. Walsh, J. D. Moody, C. R. Weber, S. A. Maclaren and G. B. Zimmerman <i>Integrated Radiation-magneto-hydrodynamic Simulations of Magnetized Burning Plasmas.....</i>	171
M. Drissi, G.A. Garcia, L. Nahon, S. Boye-Peronne, B. Gans, H.R. Hrodmarsson, H.L. Le, M.-X. Jiang and J.-C. Loison <i>Photoelectron Spectroscopy of Radicals of Astrochemical Interest.....</i>	172
Felix Iacob <i>Electron NS^+ Collisions in Cold Plasma.....</i>	173
Aleksandra Kolarski <i>Properties of Earth's Lower Ionospheric Plasma Perturbed by Solar Flares.....</i>	174
Petar Kostić <i>Supernova Remnants in Clumpy Medium: Hydrodynamic and Radio Synchrotron Evolution.....</i>	175
Nikola Veselinović, Mihailo Savić, Aleksandar Dragić, Dimitrije Maletić, Dejan Joković, Radomir Banjanac, Miloš Travar and Vladimir Udovičić <i>Fluctuations in the Flux of Energetic Protons in Heliosphere Before and During Sudden Decreases in Galactic Cosmic Ray Intensity.....</i>	176
Vladimir Zeković <i>SLAMS-enhanced Particle Acceleration at High-Mach Number Astrophysical Shocks: TeV in a Blink of Supernova.....</i>	177
Posters	
Edi Bon, Paola Marziani and Nataša Bon <i>Variability Along the Main Sequence of Quasars.....</i>	178
Andjelka B. Kovačević, Dragana Ilić, Luka Č. Popović, Marina Pavlović, Aman Raju, Momčilo Tošić and Iva Čvorović-Hajdinjak <i>Advanced Nonlinear Analysis for Detecting Binary Quasars and Transient Events in the LSST Era.....</i>	182

Jelena Kovačević-Dojčinović, Ivan Dojčinović and Luka Č. Popović <i>Two-component Model of Fe II Lines in Spectra of Active Galactic Nuclei</i>	183
Nenad M. Sakan, Zoran Simić, Vladimir A. Srećković and Momchil Dechev <i>The Complex Emmitter Inside Dense Plasma, Continuation of a Coulomb Cut-off Approach, Argon Case</i>	184
Vladimir A. Srećković, Nicolina Pop, Milan Dimitrijević and Magdalena Christova <i>Investigation of Chemistry of Hydrogen, Helium and Lithium Molecular Ions in the Early Universe</i>	185
Vladimir A. Srećković, Nicolina Pop, Milan S. Dimitrijević, Magdalena D. Christova and Veljko Vujčić <i>Dataset for Photodissociation of Small Molecular Ions</i>	186
Vladimir A. Srećković, Nicolina Pop and Veljko Vujčić <i>New Molecular Data for Confined Molecular Systems and Astrochemical Modelling</i>	187
 2nd Workshop on Swarm Physics and Gaseous Dielectrics (2nd SPGD)	
G. J. Boyle, D. L. Muccignat, M. J. E. Casey, R. D. White, H. Vemulapilli, M. M. van Rijn and C. M. Franck <i>Analysis of Current Waveforms in the Pulsed-Townsend Experiment</i>	191
N. A. Garland, D. L. Muccignat, G. J. Boyle and R. D. White <i>Rapidly Exploring and Designing Electron Transport Quantities in Dielectric Gas Insulator Mixtures with Approximation Theories</i>	192
Satoru Kawaguchi, Kazuhiro Takahashi and Kohki Satoh <i>Physics-informed Neural Networks for Studies on Electron Swarms in Gases</i>	193
Marnik Metting van Rijn, Stephen F. Biagi and Christian M. Franck <i>Electron Scattering Cross Sections of 1,1,1,2-Tetrafluoroethane (R134a)</i>	194
D. L. Muccignat, G. J. Boyle, N. A. Garland and R. D. White <i>Advances in Machine Learning Methods for the Determination of Electron Scattering Cross-section Sets</i>	195
L.G. Pérez, O. González and J. De Urquijo <i>Three-body Electron Attachment Processes In H₂O, CO₂, and Their Mixtures</i>	196

N. Pinhão <i>Fitting of Electron Collision Cross Sections from Swarm Data Using a Genetic Algorithm</i>	197
M. Ranković, R. Kumar T P, P. Nag, J. Kočišek and J. Fedor <i>Electron Induced Processes in Dielectric Insulation Gases</i>	198
Jacob Stephens, Max Flynn and Andreas Neuber <i>Multi-term Boltzmann Models: Engineering Tools for the Pulsed Power Community</i>	199
L. Vialetto <i>Particle Propagation and Electron Transport in Gases</i>	200
Boya Zhang, Mai Hao, Peiqiong Liu and Xingwen Li <i>Deriving Swarm Parameters from Ion Kinetics and Determining Collision Cross Sections Through Data-driven Methods for Eco-friendly Insulating Gases</i>	201
Authors' Index.....	203
Programme of the SPIG 2024.....	207

RF BREAKDOWN IN ARGON AT LOW-PRESSURES: EXPERIMENT AND MODELLING

JELENA MARJANOVIĆ¹ , DRAGANA MARIĆ¹ , MARIJA PUAC¹ ,
ANTONIJE ĐORĐEVIĆ²  and ZORAN LJ. PETROVIĆ² 

¹*Institute of Physics, University of Belgrade, Pregrevica 118, 11080 Belgrade, Serbia*

E-mail sivosj@ipb.ac.rs

²*Serbian Academy of Sciences and Arts, Kneza Mihaila 35, 11001 Belgrade, Serbia*

Abstract. We present results for RF breakdown in argon discharge at low pressures, obtained experimentally and using Monte Carlo code for a frequency of 13.56 MHz. Experimental measurements are conducted at an interelectrode distance (d) of 0.7 cm for pressures (p) ranging from 0.9 to 29 Torr. In our experiment, we employ a technique that eliminates issues related to displacement current. This technique is based on the use of a balanced capacitive bridge, enabling precise breakdown detection and time-domain tracking.

1. INTRODUCTION

Low-temperature plasmas generated using RF power in the frequency range of 1 to 100 MHz find widespread applications in various industrial processes. These applications, such as plasma etching and deposition in the integrated circuit industry, electric propulsion in aerospace, materials processing, surface cleaning, and thin-film deposition, are closely tied to the breakdown itself and the underlying processes. However, when it comes to the breakdown in RF fields, there have been limited attempts to correlate experimentally measured parameters with elementary processes, as is commonly done in the case of direct current (DC) breakdown and discharge. Despite attracting considerable attention from researchers in the past period, the study of RF breakdown faces challenges due to the need to isolate minute breakdown currents from the displacement current. In this study, we present results from RF breakdown measurements at 13.56 MHz in argon and compare them with results from the Monte Carlo simulation, aiming to provide insights that can enhance the efficiency and reliability of these industrial processes.

2. EXPERIMENTAL SET-UP

Breakdown is achieved between two plane-parallel copper electrodes placed inside a tightly fitting borosilicate glass cylinder. This arrangement prevents

long-path electric discharges towards the metal parts of the housing while allowing the recording of the emission intensity distribution along the axis of the chamber. The electrodes' diameter is 3.5 cm, and their gap is adjustable. For this work, it was set at 0.7 cm. One electrode is excited, while the other remains at zero potential. The discharge chamber is housed in a special metal box to eliminate interference with the extremely sensitive balance of the capacitive bridge. The box has only openings for recording the emission distribution using an ICCD camera (Figure 1a). The chamber is first evacuated to low pressure ($<10^{-6}$ Torr), and argon is introduced into the system and kept at a slow flow rate to maintain the required gas purity during measurements. Electrodes were treated and stabilized using an argon discharge at 1 Torr for approximately 60 minutes. The treatment is done at a pressure corresponding to conditions in the left-hand branch of the breakdown curve, where ions receive enough energy from the electric field to reach electrodes and remove impurities and oxides from electrode surfaces through bombardment. Throughout the electrode treatment, we monitored changes in the discharge voltage. The process is terminated when further treatment no longer results in a change in the discharge voltage.

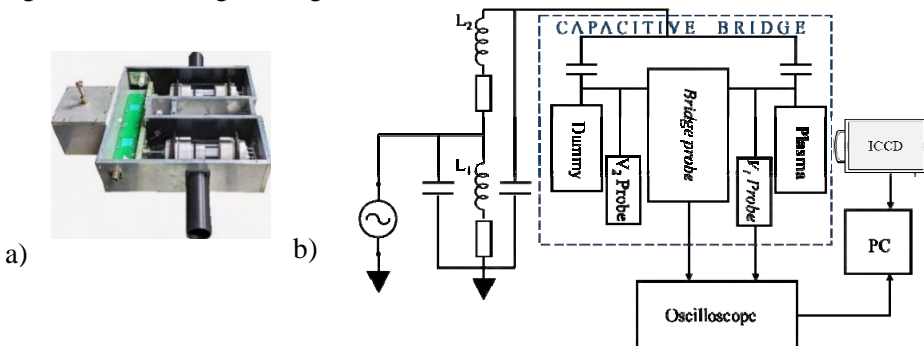


Figure 1: a) Photo of the capacitive bridge, b) schematic of the experimental set-up.

The schematic of the experimental set-up is shown in Figure 1b. The entire electrical circuit is housed in an aluminum box to protect against interference and losses. We utilized a Rigol DG5102 RF signal generator for the power source, which provides a sine signal set to a frequency of 13.56 MHz. This signal is then amplified by a linear amplifier, specifically the Barthel RFA-0.1/50-100 BOO. Coils L_1 and L_2 are part of an inductive coupling and represent a resonant transformer that operates exclusively at 13.56 MHz. This resonant transformer raises the generator voltage to the kilovolt range. The capacitive bridge comprises four capacitors, two of which are physically identical discharge chambers. While the 'Dummy' remains inactive and functions solely as a capacitor, the 'Plasma' acts as the active chamber where the discharge is observed. We monitor the voltage signal from the bridge diagonal using the 'Bridge probe'. Before taking measurements, we calibrated probe V_1 , which we use to measure the voltage on the discharge chamber. When the bridge is in balance, the signal from the diagonal is

minimal. We detect the moment of breakdown in the gas using an oscilloscope (Keysight Infiniium DSO9104A). The amplitude of the voltage signal from the diagonal of the bridge increases sharply. In other words, the bridge suddenly goes out of balance due to a change in impedance when the breakdown occurs.

3. RESULTS AND DISCUSSION

Figure 2 compares radio frequency (RF) breakdown curves for argon discharge obtained at 13.56 MHz. The curves are derived from measurements (represented by full circles) and Monte Carlo simulations (represented by open circles). The breakdown curve, obtained at the electrode distance of 0.7 cm, covers a range from 0.65 Torr cm to 20 Torr cm. Monte Carlo (MC) code was described and explained elsewhere (Raspopović et al., 1999). These simulations were carried out with only electrons, and their movement is determined by the external electric field (Puač, et al., 2018). The set of cross-sections consists of momentum transfer, two excitations and an ionization cross-section and has been tested for argon swarms in our group (Petrović et al., 2007). Physical processes on the electrodes and the effects of the heavy particles were modelled by factors of reflection $R = 0.4$ and $\gamma = 0.07$. These values were chosen to modify the breakdown voltage curve to better correspond to the measured curve. Breakdown points were determined in two ways. For the right-hand branch, pressure was fixed, and voltage was slowly increased until the number of electrons in time didn't get a positive slope (Savić et al., 2011). Similarly, points in the left-hand branch were determined by fixing the voltage and increasing the pressure until the breakdown occurred. The RF breakdown curves are expected to have the characteristic 'S' shape. However, for small interelectrode distances the curves are distorted (Lisovskiy, Yegorenkov, 1998), in such a way that the left-hand branch is somewhat flattened, which is also observed in both of our curves (experiment and MC).

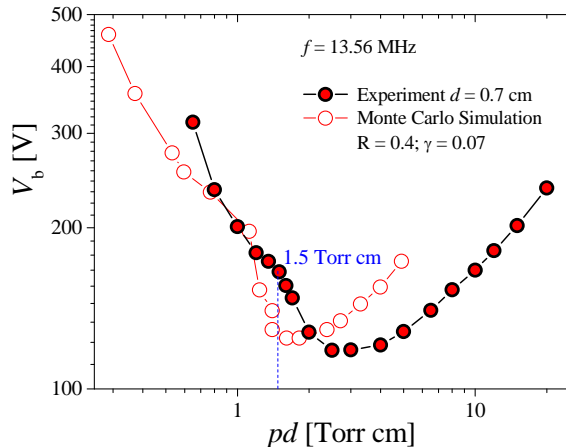


Figure 2: RF breakdown curves for Ar discharge at $f = 13.56$ MHz. Comparison of experimental results for electrode gap of 0.7 cm (full circles) and MC simulation (open circles) when the secondary electron yield is $\gamma = 0.07$, and the reflection is assumed to be $R = 0.4$.

Analyzing the breakdown behavior at high pd values, we observe that the breakdown voltage decreases with decreasing pressure (p) (the electrode gap (d) is fixed). At $pd+ = 2.5$ Torr cm, the minimum breakdown voltage occurs. Beyond this point, the breakdown voltage increases as pressure decreases further. In the left-hand branch of the curve, an inflexion point appears at 1.5 Torr cm. This inflexion can be attributed to conditions where the amplitude of electron oscillations in the RF field becomes comparable to the interelectrode distance (d), leading to increased losses. From this point on, the breakdown is conditioned by a balance between losses at the surface of electrodes and the gain of energy from the increasing field and numerous electrons crossing the threshold for ionization. Thus, the secondary electron yield at the electrodes becomes significant.

Acknowledgements

This research was supported by the Science Fund of the Republic of Serbia, Grant No. 7749560, project EGWIn. Zoran Lj. Petrović is grateful to the SASA project F155 and Antonije Đorđević to the project F133.

References

- Burm, K.T.A.L.: 2005, *Contrib. Plasma Phys.* **45**, 54.
Conrads H., Schmidt M. : 2000, *Plasma Sources Sci. Technol.* **9**, 441.
Mahony C. M. O., Gans T., Graham W. G., Maguire P. D., Petrović Z. Lj. :2008, *Appl. Phys. Lett.*, **93**, 011501.
Makabe, T., Petrovic, Z. Lj.: 2006, *Plasma Electronics: Applications in Microelectronic Device Fabrication (1st ed.)*, CRC Press.
Lee H.C.: 2018, *Appl. Phys. Rev.* **5**, 011108.
Lisovskiy A. V., Yegorenkov V. D.: 1998, *J. Phys. D, Appl. Phys.*, **31**, 3349.
Korolov I., Donkó Z. : 2015, *Phys. Plasmas*, **22**, 093501.
Petrović Z. Lj., Šuvakov M., Nikitović Ž., Dujko S., Šašić O., Jovanović J., Malović G., Stojanović V.: 2007, *Plasma Sources Sci. Technol.*, **16**, S1–S12.
Puač M., Marić D., Radmilović-Radjenović M., Šuvakov M., Petrović Z. Lj.: 2018, *Plasma Sources Sci. Technol.*, **27**, 075013.
Raspopović Z. M., Sakadžić S., Bzenić S. A., Petrović Z. Lj.: 1999, *IEEE Trans. Plasma Sci.* **27**, 1241.
Savić M., Radmilović-Radjenović M., Šuvakov M., Marjanović S., Marić D., Petrović Z. Lj.: 2011, *IEEE Trans. Plasma Sci.* **39**, 2556.

SPIG 2024 PROGRAMME

Belgrade, Serbia, August 26 – 30, 2024

All indicated times are given in the Central European Summer Time (CEST) zone.

Monday 26 th August 2024		
Workshops		
	<i>2nd SPGD Workshop</i>	<i>LIBS4fusion Workshop</i>
09:20-09:30	Opening and Introduction: Saša Dujko	Opening: Milivoje Ivković
	<i>Session 1, Hall A</i>	<i>Session 1, Hall B</i>
09:30-10:00	Miloš Ranković (Czech Republic) Electron-induced processes in dielectric insulation gases	Volker Naulin (Denmark) Fusion: from science fiction to science fact
10:00-10:30	Jaime de Urquijo (Mexico) Three-body electron attachment processes in H ₂ O, CO ₂ , and their mixtures	Radomir Panek (Czech Republic) EUROfusion, the consortium coordinating European fusion research
10:30-11:00	Boya Zhang (China) Deriving Swarm Parameters from Ion Kinetics and Determining Collision Cross Sections through Data-Driven Methods for Eco-friendly Insulating Gase	Miloš Škorić (Serbia) to be confirmed Fusion related research at the University of Belgrade
<i>11:00-11:30</i>	<i>Coffee break</i>	
	<i>Session 2, Hall A</i>	<i>Session 2, Hall B</i>
11:30-12:00	Jacob Stephens (USA) Multi term Boltzmann models: Engineering Tools for the Pulsed Power Community	Corneliu Porosnicu (Romania) Plasma-wall interaction studies within the EUROfusion Consortium
12:00-12:30	Luca Vialetto (USA) Particle propagation and electron transport in gases and plasmas	V. Alimov (Russia) to be confirmed Diagnostics of the fusion reactor wall
12:30-13:00	Satoru Kawaguchi (Japan) Physics-informed neural networks for studies on electron swarms in gases	Violeta Lazić (Italy) Deployments of Laser Induced Breakdown Spectroscopy
<i>13:00-15:00</i>	<i>Lunch break</i>	
	<i>Session 3, Hall A</i>	<i>Session 3, Hall B</i>
15:00-15:30	Dale Muccignat (Australia) Advances in machine learning methods for the determination of electron scattering cross-section sets	Milivoje Ivković (Serbia) NOVA2LIBS4fusion
15:30-16:00	Greg Boyle (Australia) Analysis of current waveforms in the pulsed-Townsend Experiment	Dragan Ranković (Serbia) TEA CO ₂ laser LIBS
16:00-16:30	Nuno Pinhão (Portugal) Fitting of Electron Collision Cross Sections from Swarm Data using a Genetic Algorithm	15:50 Biljana Stankov (Serbia) Stark parameters of beryllium spectral lines 16:10 Miroslav Kuzmanović (Serbia) Problem of LIBS surface and depth elemental analysis of PFC materials
<i>16:30-17:00</i>	<i>Coffee break</i>	
	<i>Session 4, Hall A</i>	<i>Session 4, Hall B</i>
17:00-17:30	Nathan Garland (Australia) Rapidly exploring and designing electron transport quantities in dielectric gas	Ivan Traparić (Serbia) Hydrogen isotope retention diagnostics

	insulator mixtures with approximation theories	17:20 Marijana Gavrilović Božović (Serbia)
17:30-18:00	Marnik Metting Van Rijn (Switzerland) Electron scattering cross sections of 1,1,1,2-Tetrafluoroethane (R134a)	17:40 Milivoje Ivković (Serbia) In-situ LIBS for fusion reactors surface diagnostics
18:00-20:00	SPIG 2024 Welcome Cocktail (Club of SASA)	18:00-18:30 Rounding table

All indicated times are given in the Central European Summer Time (CEST) zone.

Tuesday 27th August 2024

SPIG 2024 (day 2)

	PL – Plenary lecture: 35+10 min	TL – Topical lecture: 25+5 min	PR – Progress Report: 15+5 min
08:45-09:00	Opening, Chairs: Bratislav Obradović, Jovan Cvetic and Miroslav Kuzmanović		
	Plenary Session 1, Hall A, Chair: Dejan Milošević		
09:00-09:45	Xiao-Min Tong (Japan) Theory on dynamics of atoms in strong laser field		
09:45-10:30	Gerhard G. Paulus (Germany) Extreme UV imaging with high harmonics		
10:30-11:00	Coffee Break		
	Plenary Session 2, Hall A, Chair: Miloš Škorić		
11:00-11:45	Luca Volpe (Spain) Current situation and future perspectives of the European IFE program, technology development, science and related applications		
11:45-12:30	Andreja Gomboc (Slovenia) How stars get thorn apart by supermassive black holes		
12:30-14:30	Lunch Break		
	Hall A - Parallel Session: Chair: Bratislav Obradović	Hall B - Parallel Session Chair: Ivan Mančev	
14:30-15:00	Paul Maguire (United Kingdom) Liquid microdroplets in a microplasma: phenomena and technological applications 3	Peter Papp (Slovakia) Ion induced reactions in IMS studied by DFT 3	
15:00-15:30	Nevena Puač (Serbia) Diagnostics and applications of atmospheric pressure plasmas for triggering of cell mechanisms 3	Violeta Stanković Mališ (Serbia) Modeling the surface interaction of cellulosic materials with CO ₂ plasmas 2 (15:00-15:20) Ana Kalinić (Serbia): Interaction of ions with graphene-insulator-graphene composite systems 2 (15:20-15:40)	
15:30-16:00	Claudia Lazzaroni (France) Micro hollow cathode discharges in Ar/N ₂ used for boron nitride PECVD 3	Hristina Delibašić Marković (Serbia): Characterizing Ionization and Electron Dynamics in Biological Materials: Theoretical and Numerical Insights into Pulsed Laser-Induced Breakdown Processes 2 (15:40-16:00)	
16:30-17:00	Coffee Break		
	Hall A - Parallel Session Chair: Jovan Cvetic	Hall B - Parallel Session Chair: Ivan Radović	
17:00-17:30	Chihiro Suzuki (Japan) Comprehensive Z dependence analysis of soft X-ray spectra from highly charged heavy ions using magnetically confined high-temperature plasmas 4	Myriam Drissi (France) Photoelectron spectroscopy of radicals of astrochemical interest 4 (17:00-17:20)	
17:30-18:00	Sergei Ryzhkov (Russia) Magneto-inertial fusion and powerful installation 4	Matthias Werl (Austria) De-excitation cascade calculation for highly excited of hollow atoms 1 (17:20-17:40)	
18:00-18:20	Blagoje Djordjevic (USA): Integrated radiation-magneto-hydrodynamic simulations of magnetized burning plasmas	Jasmina Atić (Serbia) Electron transport and negative ionization fronts in strongly attaching gases 1 (17:40-18:00)	

		Danijela Danilović (Serbia) Synchrotron radiation photoelectron spectroscopy study of the electronic structure of Ag-Bi-I ruderffite nanoparticles 1 (18:00-18:20)
18:30-20:00	<i>Poster session 1</i> - SASA Gallery of Science and Technology (<i>Chair: Nikola Cvetanović</i>)	

All indicated times are given in the Central European Summer Time (CEST) zone.

Wednesday 28th August		
SPIG 2024 (day 3)		
<i>PL – Plenary lecture: 35+10 min</i>	<i>TL – Topical lecture: 25+5 min</i>	<i>PR – Progress Report: 15+5 min</i>
<i>Plenary Session 3, Hall A, Chair: Igor Savić</i>		
09:00-09:45	Stephan Schlemmer (Germany) Missing ions in laboratory and space	
09:45-10:30	Alicja Domaracka (France) Ion processing of molecular systems: a way to form complex systems in space	
10:30-11:00	<i>Coffee Break</i>	
<i>Plenary Session 4, Hall A, Chair: Dragana Marić</i>		
11:00-11:45	Jan van Dijk (Netherlands) LXCat 3 and Beyond – Fostering Reproducibility in Low-Temperature Plasma Science	
	<i>Hall A - Parallel Session</i> <i>Chair: Aleksandar Milosavljević</i>	<i>Hall B - Parallel Session</i> <i>Chair: Jelena Kovačević Dojčinović</i>
11:45-12:15	Nuno Pinhão (Portugal): Description of electron swarms in an electric field: a finite elements computation including third-order transport parameters 1	Nikolai N. Bezuglov (Russia): Penning and photoionizations of cold Rydberg alkali metal atoms under Förster resonance conditions 4
12:15-12:45	Marine Fournier (France): Photoelectron spectroscopy of solvated biological interest molecule in liquid-jet configuration 1 (12:15-12:35)	Giovanni La Mura (Italy): Interstellar dust as a dynamic environment 4
12:45-14:30	<i>Lunch Break / SPIG Committee meeting</i>	
	<i>Hall A - Parallel Session</i> <i>Chair: Sanja Tošić</i>	<i>Hall B - Parallel Session</i> <i>Chair: Vladimir Srečković</i>
14:30-15:00	Helgi Hroddmarsson (France): VUV photoionization of interstellar molecules: Making sense of our beautifully mysterious Universe molecule by molecule 1	Miroslava Vukčević (Serbia): On the conditions for soliton formation in the galactic environment 4
15:00-15:20	Dino Habibović (Bosnia and Herzegovina) Strong-field processes induced by tailored laser fields 1	Nikola Veselinovic (Serbia): Fluctuations in the Flux of Energetic Protons in Heliosphere before and during Sudden Decreases in Galactic Cosmic Ray Intensity 4
15:20-15:40	Daan Boer (Netherlands) LoKI-B C++: An open-source Boltzmann solver for reproducible electron Boltzmann calculations 1	Aleksandra Kolarski (Serbia): Properties of Earth's lower ionospheric plasma perturbed by solar flares 4
15:40-16:00	Emilia Jasmiina Heikura (Germany): Towards distant dependent inner-shell photoelectron circular dichroism 1	Vladimir Zeković (Serbia): SLAMS-enhanced particle acceleration at high-Mach number astrophysical shocks: TeV in a blink of a supernova 4
16:00-16:20	Laura Pille (Germany): Exploring biomolecular properties in the gas phase by using advanced light sources 1	Petar Kostić (Serbia): Supernova remnants in clumpy medium: hydrodynamic and radio synchrotron evolution 4
16:30	<i>Mini excursion (info at registration desk): Belgrade underground tour</i>	

All indicated times are given in the Central European Summer Time (CEST) zone.

Thursday 29th August 2024	
SPIG 2024 (day 4)	
<i>PL – Plenary lecture: 35+10 min</i>	<i>TL – Topical lecture: 25+5 min</i>
<i>PR – Progress Report: 15+5 min</i>	
	<i>Plenary Session 5, Hall A, Chair: Nenad Simonović</i>
09:00-09:45	Carla Faria (United Kingdom) Exploring quantum effects in the attosecond domain
09:45-10:30	Himadri Chakraborty (USA) Impact spectroscopy and chronoscopy of gas phase atoms, molecules and fullerenes
10:30-11:00	<i>Coffee Break</i>
	<i>Plenary Session 6, Hall A, Chair: Dragana Ilić</i>
11:00-11:45	Paola Marziani (Italy) Super-Eddington Quasars: from Atomic Physics to Cosmology
11:45-12:30	Satoshi Hamaguchi (Japan): Opportunities and challenges in low-temperature plasma science for atomic-layer processing
12:30-14:00	<i>Lunch Break</i>
	<i>Hall A - Parallel Session</i> <i>Chair: Vladimir Milosavljević</i>
14:00-14:30	Marija Gorjanc (Slovenia): Plasma modification of textile fibers for adhesion improvement in bio-composites 2
14:30-15:00	Mirjana Kostić (Serbia): Atmospheric pressure plasma in processing of cellulose fibres: from surface cleaning to tailored properties 3
15:00-15:30	Miran Mozetič (Slovenia): Inactivation of viruses in water by plasma treatment 3
	<i>Hall B - Parallel Session</i> <i>Chair: Marko Čosić</i>
	Magdalena D. Christova (Bulgaria): Astrophysical applications of Stark broadening of spectral lines 4
	Ugo Jacovella (France): Exploring the importance of interstellar ions in the enigma of diffuse interstellar bands 4
	Felix Jacob (Romania) Electron NS+ collisions in cold plasma 4 (15:00-15:20)
15:30-16:00	<i>Coffee Break</i>
	<i>Hall A - Parallel Session</i> <i>Chair: Predrag Ranitović</i>
16:00-16:30	Milan Radović (Switzerland) Pulse Laser Deposition and Advanced Spectroscopy: Key to Revealing Emerging Properties in Transition Metal Oxides 2
	<i>Hall B - Parallel Session</i> <i>Chair: Goran Poparić</i>
	Peter Hartmann (Hungary) Using dust particles as probes in low pressure gas 3
16:30-17:00	Violeta Lazić (Italy) LIBS spectroscopy: what we can measure, and how? 3
	Sanja Pavlović (Serbia) Thermal and acoustic properties of cellulose fibrous materials 3 (16:30-16:50)
17:00-17:20	Ivan Trparić (Serbia) Application of Machine Learning and Artificial Intelligence in Plasma Spectroscopy 3
	Marjan Stankov (Germany) Analysis of dielectric barrier discharges in Ar-monomer mixtures using a standardized fluid modelling approach 3 (16:50-17:10)
17:20-17:40	Olga Stepanova (Russia) Air-Plasma-Water Electrophysical System: prospects and problems 3
	Aleksandar Jovanović (Germany) Fluid modelling of single-filament DBD and self-pulsing discharges at atmospheric pressure using FEDM 3 (17:10-17:30)
17:50-19:00	<i>Poster session 2 - SASA Gallery of Science and Technology (Chair: Miroslav Kuzmanović)</i>
20:00-24:00	Conference dinner and closing

Friday 30th August 2024 SPIG 2024 (day 5)	
10:00-17:00	<i>Excursions (optional, info at registration desk): Belgrade sightseeing cruise (10 – 13:30)</i>
17:00	Departure

LIST OF POSTERS

No.	Section	Title	Authors
1	1.1.	Excitation of acetone induced by electron impact	Barbora Stachová, Juraj Országh and Štefan Matejčík
2	1.1.	Small molecules essential to astrophysics: collisional and radiative processes	S. Tošić, V. Srečković and V. Vujčić
3	1.1.	Investigation of elastic electron scattering from desflurane molecule at intermediate electron energy	J. Vukalović, J.B. Maljković, F. Blanco, G. Garcia and B.P. Marinković
4	1.1.	Ejected electron spectra of krypton studied by high and low energy electrons	B.P. Marinković, J.J. Jureta and L. Avaldi
5	1.1.	Electron scattering cross sections represented in Belgrade electron-atom/molecule database (beam)	B.P. Marinković and S.Đ. Ivanović
6	1.1.	Direct electron-liquid energy loss spectra measurements using a liquid micro-jet	D. L. Muccignat, D. B. Jones, J. R. Gascooke, G. J. Boyle, N. A. Garland and R. D. White
7	1.1.	Influence of catastrophes and hidden dynamical symmetries on ultrafast backscattered photoelectrons	T. Rook, L. Cruz Rodriguez and C. Figueira de Morisson Faria
8	1.1.	Dissociative electron attachment to CO ₂ in electric and magnetic fields	M. M. Vojnović, M. M. Ristić, V. V. Stanković-Mališ and G. B. Poparić
9	1.1	Investigation of Elastic Electron Scattering by Anaesthetic Molecules in Gaseous Phase	Jelena B. Maljović, Jelena Vukalović, Francisco Blanco, Gustavo Garcia and Bratislav P. Marinković
10	1.2.	Post-prior discrepancy in the CB1-4B method for single-electron capture in fast Li ³⁺ + He collisions	Nenad Milojević, Ivan Mančev, Danilo Delibašić and Miloš Milenković
11	1.3.	Diffusion coefficients of H ₂ ⁺ ions in H ₂ gas	Ž. Nikitović and Z. Raspopović
12	1.3.	Transport properties of two-temperature SF ₆ and its alternative gases	G.Wang, B. Zhang and X.Li
13	1.3.	Monte Carlo simulation of electron swarms in pulsed Townsend experiment and validation of the swarm data derived from waveform analysis	M. Hao, G. Hagelaar, B. Zhang and X. Li
14	1.3.	An aliasing method for determination of transport data for exotic charged particles in crossed electric and magnetic fields	N. A. Garland, R. D. White, R. E. Robson and M. Hildebrandt

15	1.3.	Studies on electron swarms and streamer discharges in eco-friendly RPC gases	S. Dujko, I. Simonović, D. Bošnjaković, Z.Lj. Petrović and J. De Urquijo
16	1.3.	Electron transport in radio-frequency electric and magnetic fields in ultra-low GWP gases	S. Dujko, I. Simonović, D. Bošnjaković, J. Atić and Z. Lj. Petrović
17	1.3.	Studies on streamer discharges in ultra-low GWP gases	D. Bošnjaković, I. Simonović and S. Dujko
18	1.3.	Electron transport in simple liquid mixtures	G. J. Boyle, N. A. Garland, R. P. Mceachran and R. D. White
19	1.3	Three-dimensional streamer model in the AMREX environment	I. Simonović, D. Bošnjaković and S. Dujko
20	2.1.	Interaction of ions with drift-current biased supported graphene	A. Kalinić, I. Radović, L. Karbunar and Z. L. Mišković
21	2.1.	Rainbows in transmission of protons through thin silicon carbide crystal	N. Starčević and S. Petrović
22	2.1.	Low energy heavy ion rainbow scattering by graphene	M. Hadžijojić and M. Čosić
23	2.2.	Forming nanocrystalline SnO ₂ films on silicon and silicon dioxide by laser-plasma deposition method	F. Komarov, O. Milchanin, M. V. Puzyrev and I. S. Rahavaya
24	2.3.	Equilibrium composition of plasma obtained by laser ablation of glass	M. Ristić, A. Šajić, J. Babić and M. Kuzmanović
25	2.3.	Semiquantum simulation of cellulosic materials interaction with CO ₂ plasmas	V. Stanković Mališ and Goran B. Poparić
26	2.3.	Properties of Cu/Zn oxide nanostructures formed by plasma-activated electrolysis	N. Tarasenko, V. Kornev, M. Nedelko, A. Radomtsev, N. Tarasenka, J. Ciganović, S. Živkovic and M. Momčilović
27	2.3.	Target selection for LIBS studies of hydrogen isotope retention	D. Ranković, B. Stankov, I. Traparić, M. Kuzmanović and M. Ivković
28	3.1.	Measurement of the velocity of the plasma jet appearing from a wall stabilized arc	L. Gavanski, N. Simić and S. Djurović
29	3.1.	The measurement of pulsed gas discharge parameters by means of Fe I lines in argon and argon-hydrogen mixture	J. Jovović
30	3.1.	Stark widths of several Te II spectral lines for a purpose in investigation of astrophysical spectra	Z. Majlinger, M.S. Dimitrijević and V. Srečković
31	3.1.	Stark width estimates for the most prominent Ce II spectral lines important for astrophysical investigations	Z. Majlinger
32	3.1.	Determination of unknow analyte concentration in glass samples using the LIBS method	A. Šajić, D. Ranković, M.Ristić and M. Kuzmanović
33	3.1.	Investigating the thermal profile of an atmospheric pressure argon plasma jet on a conductive and insulating mesh surface	J. Lalor and V. Milosavljević
34	3.1.	The use of thermoelectric radiation detectors for heat flux measurements in shock-tubes with gas ionization	S.A. Poniaev, P.A. Popov, N.A. Monakhov, T.A. Lapushkina and M.A. Kotov

35	3.1.	Detection of rhenium in tungsten using LIBS with additional fast pulse discharge	I. Traparić, B. Stankov and M. Ivković
36	3.1.	Estimation of nitrogen impurity level in helium atmospheric discharge via emission spectroscopy	N. Cvetanović, S.S. Ivković and B.M. Obradović
37	3.1.	The effect of acids on pig bone estimated by LIBS	M. Marković, D. Ranković and M. Kuzmanović
38	3.1.	Fast photography in the service of spatially and temporally resolved LIBS diagnostics of doped tungsten	B. Stankov, M. R. G. Božović, D. Ranković, J. Savović and M. Ivković
39	3.1.	Influence of the ablation angle change on spectral line intensities in LIBS experiments	I. Traparić, B. Stankov, N. Vujadinović, M. Vinić and M. Ivković
40	3.2.	Modelling of an icp discharge in oxygen with full kinetics scheme with newly calculated VV/VT rate constants	A. Kropotkin, A. Chukalovsky, A. Kurnosov, T. Rakhimova and A. Palov
41	3.2.	Influence of interelectrode distance on the characteristics of three-electrode pulsed sdbd	V. V. Voevodin, O. I. Korzhova, V. Yu. Khomich, V. A. Yamschikov, N. Yu. Lysov and A. V. Klubkov
42	3.2.	RF breakdown in argon at low-pressures: experiment and modelling	J. Marjanović, D. Marić, M. Puač, A. Đorđević and Z. Lj. Petrović
43	3.2.	Cathode sheath diagnostics by integral end-on optical emission spectroscopy in an analytical glow discharge source in argon	N. V. Nedić, N. V. Ivanović, I. R. Videnović, Dj. Spasojević and N. Konjević
44	3.3.	Luminescent analysis of e-beam induced transformation of phenol in the presence of humic substances	E. N. Bochamnikova, O. N. Tchaikovskaya, S. A. Chaykovsky, V. I. Solomonov, A. S. Makarova and I. V. Sokolova
45	3.3.	The formation of microneedles structures from silicon using plasma etching in SF ₆ /O ₂ mixture in inductively coupled plasma	V. Kuzmenko, A. Miakonkikh and K. Rudenko
46	3.3.	Fluorocarbon polymerizing plasmas etching processes for structures of microelectronics	A. Miakonkikh, V. Kuzmenko and K. Rudenko
47	3.3.	A&M datasets for LTP treatment of plants	V. Vujčić, V.A. Srečković, O. Kounchev and F. Iacob
48	3.3.	Low-temperature plasma and plasma-activated liquids in solving agricultural problems: experimental technique	E.M. Konchekov, N.G. Gusein-Zade, D.V. Yanykin, L.V. Kolik, Yu.K. Danileiko, V.I. Lukanin, K.F. Sergeichev, I.V. Moryakov, V.D. Borzosekov, V.V. Gudkova, M.E. Astashev and S.V. Gudkov
49	3.3.	Compact piezotransformer source of the cold atmospheric plasma with three types of discharges	N. N. Bogachev, A. S. Bakshaev, L. V. Kolik, E. M. Konchekov and A. S. Kon'kova
50	3.3.	Measurements of reactive oxygen and nitrogen species in plasma activated water by microwave discharge	D. Topalović, N. Babučić, N. Škoro and N. Puač
51	3.3.	Ionization of a plasma antenna channel in a dielectric gas-discharge tube	N. N. Bogachev, I. L. Bogdankevich, V. I. Zhukov, D. M. Karfidov, V. P. Stepin and N. G. Gusein-Zade

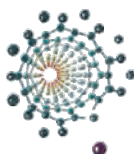
52	4.2.	Dataset for photodissociation of small molecular ions	V.A. Srečković, N. Pop, M.S. Dimitrijević, M.D. Christova and V. Vujčić
53	4.2.	Investigation of chemistry of hydrogen, helium and lithium molecular ions in the early Universe	V.A. Srečković, N. Pop, M.S. Dimitrijević and M.D. Christova
54	4.2.	New molecular data for confined molecular systems and astrochemical modelling	V.A. Srečković, N. Pop, and V. Vujčić
55	4.2.	The complex emitter inside dense plasma, continuation of a Coulomb cut-off approach, argon case	N.M. Sakan, Z. Simić, V.A. Srečković and M. Dechev
56	4.2.	Variability along the main sequence of quasars	E. Bon, P. Marziani and N. Bon
57	4.2.	Advanced nonlinear analysis for detecting binary quasars and transient events in the LSST era	A.B. Kovačević, D. Ilić, L.Č. Popović, M. Pavlović, A. Raju, M. Tošić and Iva Čvorović-Hajdinjak
58	4.2	Two-Component Model of Fe II Lines in Spectra of Active Galactic Nuclei	Jelena Kovačević-Dojčinović, Ivan Dojčinović and Luka Č. Popović

ACKNOWLEDGEMENT

32nd SUMMER SCHOOL AND INTERNATIONAL
SYMPOSIUM ON THE PHYSICS OF IONIZED GASES

is organized by

**University of Belgrade – Faculty of Physical Chemistry
Serbian Academy of Sciences and Arts**



**Faculty of Physical Chemistry
University of Belgrade**



**Serbian Academy
of Sciences and Arts**

and

with the support of the

**Ministry of Science, Technological Development and Innovation
Republic of Serbia**



Republic of Serbia
MINISTRY OF SCIENCE,
TECHNOLOGICAL DEVELOPMENT
AND INNOVATION

sponsored by



Telekom Srbija

technical organizer

PANACOMP - Zemlja čuda d.o.o.

icpm¹⁰
&
IWPCT

8 - 13 september, Portorose, Slovenia

BOOK OF ABSTRACTS

10TH INTERNATIONAL
CONFERENCE ON PLASMA
MEDICINE

&
9TH INTERNATIONAL
WORKSHOP ON PLASMA
FOR CANCER TREATMENT

8-13 September 2024
Portorose, Slovenia



BOOK OF ABSTRACTS

10th INTERNATIONAL CONFERENCE ON
PLASMA MEDICINE

&

9th INTERNATIONAL WORKSHOP ON PLASMA
FOR CANCER TREATMENT

Organized by: **Jozef Stefan Institute**

Date: **8 – 13 September, 2024**

Venue: **Conference centre LifeClass Hotels & Spa Portorož, Portorož, Slovenia**



Title: Book of abstracts – 10th International Conference on Plasma Medicine and 9th International Workshop on Plasma for Cancer Treatment

Editors: Urška Kisovec, Nataša Hojnik, Martina Modic, Uroš Cvelbar

Digital edition

URL: https://f6-ge.ijs.si/icpm10/?page_id=1269

Ljubljana, Jožef Stefan Institute

2024

Katalogni zapis o publikaciji (CIP)
pripravili v Narodni in univerzitetni
knjižnici v Ljubljani

[COBISS.SI-ID 205716995](https://nuk.uz.si/COBISS.SI-ID/205716995)

ISBN 978-961-264-293-8 (PDF)

WELCOME NOTE

Dear Participants,

On behalf of the organizing committee, it is with great excitement and anticipation that I welcome you to the 10th International Conference on Plasma Medicine (ICPM10), held in conjunction with the traditional summer school and the 9th International Workshop on Plasma for Cancer Treatment (IWPCT9).

ICPM10 and IWPCT9 continue the legacy of providing a vital platform for the exchange of knowledge and ideas in the multidisciplinary field of plasma biomedicine. As we gather in this beautiful setting, we aim to foster collaboration among experts from diverse fields such as plasma physics, medicine, biology, biochemistry, pharmacy, agriculture, and food science. Together, we will explore the cutting-edge developments and technological challenges in plasma medicine, a rapidly advancing field that promises significant therapeutic breakthroughs.

This conference offers a unique opportunity for professionals and researchers to engage in meaningful discussions, share insights, and establish international collaborations that will drive the future of plasma technology in medicine and beyond. We are confident that the knowledge and experiences shared during this event will contribute to the advancement of our field and inspire innovative solutions to the complex challenges we face. We hope you find this event both inspiring and rewarding.

Sincerely,

Prof. Dr. Uroš Cvelbar ,
head of the Organising Committee

SPONSORS



COMMITTEES

International Scientific Committee (ISPM Board)

- Gerrit Kroesen, *TU Eindhoven*, Chair
- Julia Bandow, *RUB*
- Sander Bekeschus, *INP Greifswald*
- Paula Bourke, *University College Dublin*
- Eun-Ha Choi, *Kwangwoon University*
- Cristina Canal, *UPC*
- Yuzuru Ikehara, *Chiba University*
- Petr Lukes, *Institute of Plasma Physics CAS*
- Alexander Fridman, *Drexel University*
- Matteo Gherardi, *University of Bologna*
- Satoshi Hamaguchi, *Osaka University*
- Eric Robert, *University of Orleans*
- Rob Short, *University of Sheffield*
- Katharina Stapelmann, *North Carolina State University*
- Zdenko Machala, *Comenius University*
- Vandana Miller, *Drexel University*
- Hiromasa Tanaka, *Nagoya University*
- Thomas von Woedtke, *INP Greifswald*

IWPCT Scientific Committee

1. Vandana Miller, Chair, *Drexel University*
2. Sander Bekeschus, *INP Greifswald*
3. Katharina Stapelmann, *North Carolina State University*
4. Audrey Glory, *University of Montreal*
5. Angela Privat Maldonado, *University of Antwerp*
6. Lars Boeckmann, *University Medical Center Rostock*
7. Shinya Toyokuni, *Nagoya University*

Organising Committee

1. Uroš Cvelbar, *Jožef Stefan Institute*, Chair
2. Maja Čemažar, *Institute of Oncology Ljubljana*
3. Nataša Hojnik, *Jožef Stefan Institute*
4. Martina Modic, *Jožef Stefan Institute*
5. Naomi Northage, *Jožef Stefan Institute*
6. Gregor Serša, *Institute of Oncology Ljubljana*
7. Vasyl Shvalya, *Jožef Stefan Institute*
8. Bojana Žegura, *National Institute of Biology*
9. James L. Walsh, *University of York and Jožef Stefan Institute*

11:45	Mon-O-2-3	Experimental Setup and Efficacy Assesment of a Non-Thermal Plasma System for Bioaerosol Decontamination <u>Silvia Giuditta Scaltriti</u> , Gabriele Neretti, Fabio Avino, Ivo Furno	36
12:00	Mon-O-2-4	Analysis of Cold Atmospheric Plasma Parameters for Effective Inactivation of <i>Aspergillus Flavus</i> and <i>Fusarium Keratoplasticum</i> <u>Jonathan Thomas</u> , Darby Roberts, Brian Gilger, Katharina Stapelmann	37

12:30 – 13:30 **Lunch Break**

Section: **PLASMA FOR CANCER THERAPY**

Hall: **IWPCT**

Chair: **Sander Bekeschus**

14:00	IT-2	Application of non-thermal plasma during tumorectomies: from the lab to the clinic <u>Audrey Glory</u> , Julie Lafontaine, Jean-Sébastien Boisvert, Sylvain Coulombe, Erica Patocskai, Philip Wong	9
14:45	Mon-O-1-3	Synergistic Effects of Plasma-Treated Water Solutions and Doxorubicin in Head and Neck Cancer Treatment <u>Vittoria Perrotti</u> , Marwa Balaha, Giulia Petrucci, Viviana di Giacomo, Roberto Gristina, Eloisa Sardella	22
15:00	Mon-O-1-4	Plasma Enhance Immunotherapy for Cancer Treatment <u>Zhitong Chen</u> , Qiujie Fang	23
15:15	Mon-O-1-5	Medical gas plasma technology synergizes with immune checkpoint blockade in the treatment of dermatologic malignancies <u>Lea Miebach</u> , Julia Berner, Eric Freund, Thomas von Woedtke, Klaus-Dieter Weltmann, Ramona Clemen, Sander Bekeschus	24
15:30	Mon-O-1-6	Revolutionizing pancreatic cancer therapy with the combination of chemotherapy and cold atmospheric plasma using the turkey in ovo model <u>Ruben Verloy</u> , Emma Peeters, Angela Privat-Maldonado, Sophie Rovers, Evelien Smits, Annemie Bogaerts	25
15:45	Mon-O-1-7	Implementation of Non-Thermal Plasma as an Immunogenic Therapy Addition to the Standard-of-Care for Head and Neck Squamous Cell Carcinoma <u>H. Verswyvel</u> , M. Bauwens, H. Zaryouh, G. Van Haesendonck, E. Cardenas De La Hoz, S. Koljenovic, C. Deben, A. Wouters, A. Lin, A. Bogaerts, E. Smits	26
16:00	Mon-O-1-8	Cold plasma endoscopy: investigating intrabody fluid issue for bile duct cancer local treatment <u>Korentin Géraud</u> , Manon Soulier, Marine Camus, Allan Pavy, Laura Fouassier, Thierry Dufour	27

Section: **PLASMA-BASED DECONTAMINATION AND STERILIZATION**

Hall: **ICPM Session 2**

Chair: **James L. Walsh**

14:00	Mon-O-2-5	Plasma-mediated decontamination of animal tissue samples: a novel approach towards antibiotic-free applications <u>Alexander Pogoda</u> , Yuanyuan Pan, Jürgen F. Kolb, Monika Röntgen, Sybille Hasse	38
14:15	Mon-O-2-6	Plasma Sterilization: Studies on Probable Mechanisms and Biochemical Actions behind Bacterial Inactivation <u>Tejal Barkhade</u> , Kushagra Nigam, G. Ravi, S. K Nema, Seema Rawat	39
14:30	Mon-O-2-7	Sterilization Mechanisms of <i>Saccharomyces cerevisiae</i> in O₂/SF₆ Low-Pressure Plasmas Rafael P. Ribeiro, Nilson C. Cruz, Tania A. Passeti, <u>Elidiane C. Rangel</u>	40

14:45	Mon-O-2-8	Liquid laboratory biowaste sterilization by cold plasma: prospects and obstacles <u>Aleksandra Lavrikova</u> , Fabio Avino, Rita Agus, Vivianne Padrun, Laurence Winkel, Andrew C. Oates, Ivo Furno	41
15:00	Mon-O-2-9	Air Sterilisation and Treatment by Non-Thermal Atmospheric Plasma <u>Naigui Shang</u> , Minkwan Kim, John Lawson, Bharathram Ganapathisubramani, Rodolphe Hervé, Charles W. Keevil	42
15:15	Mon-O-2-10	Advancing Bacterial Mitigation on Hospital Floors with a DBD Plasma Sheet Keerthana Dandamudi, Rachana Dandamudi, Bhavya Bellannagari, <u>Sohail Zaidi</u>	43
15:30	Mon-O-2-11	Implementation of Atmospheric Pressure Plasma-Activated Gaseous Media into Advanced Decontamination Processes <u>Zlata Kelar Tučeková</u> , Lukáš Vacek, Michal Pazderka, Jakub Kelar, Filip Růžička, Mirko Černák	44
15:45	Mon-O-2-12	<i>Candida albicans</i> biofilm eradication through cold atmospheric plasma: The impact of voltage and exposure time in the antifungal mode of action <u>Manca Lunder</u> , Rok Fink, Sebastian Dahle	45
16:00	Mon-O-2-13	Promoting the inactivation effects of non-thermal plasma on filamentous fungi using staining solutions <u>Eliška Lokajová</u> , Jana Jirešová, Vladimír Scholtz	46
16:15	Mon-O-2-14	Comparison between the Antimicrobial Effect of Plasma Activated Water on Amniotic Membrane Contaminated by <i>Klebsiella pneumoniae</i> and <i>Escherichia coli</i> <u>Felipe Almeida</u> , Anelise Doria, Luciana Sant'Anna	47

Section: **REGULATORY ISSUES AND STANDARDS IN PLASMA MEDICINE**

Hall: **ICPM Session 2**

Chair: **Eun-ha Choi**

16:30	Mon-O-3-1	DIN SPEC 91315 Revised – A New Method for Risk Assessment of Reactive Gas Species Emission by CAP Sources <u>Andreas Helmke</u> , Thomas Borchardt, Jannik Schulz, Wolfgang Viöl	49
-------	-----------	--	----

16:45 – 17:00 **Coffee Break**

Section: **PLASMA FOR CANCER THERAPY**

Hall: **IWPCCT**

Chair: **Audrey Glory**

17:00	IT-3	Physical Plasma in Clinics – Requirements, Tech-transfer, Acceptance <u>Martin Weiss</u>	10
17:30	Mon-O-1-9	Understanding the effects of plasma species on gap junction channels in the propagation of cancer cell death <u>Maria C. Oliveira</u> , Angela Privat-Maldonado, Annemie Bogaerts	28
17:45	Mon-O-1-10	Identification of gas plasma resistance mechanisms in human squamous cell carcinoma cells <u>Julia Berner</u> , Lea Miebach, Marcel Kordt, Kristian Wende, Brigitte Vollmar, Sander Bekeschus	29
18:00	Mon-O-1-11	Large-scale transcriptomic profiling of 35 cancer cell lines reveals similar gene sets predisposing for sensitivity to plasmas and H₂O₂ but not HOCl <u>Debora Singer</u> , Anke Schmidt, Thomas Von Woedtke, Klaus-Dieter Weltmann, Steffen Emmert, Sander Bekeschus	30

- 18:15 Mon-O-1-12 **Cold Plasma-based Redox Therapy for Breast-to-Bone Metastasis Tumor Growth Control** 31
Laura Bouret, Jean-Baptiste Billeau, Michael Weber, Derek Rosenzweig, Stephan Reuter
- 18:30 Mon-O-1-13 **Numerical modeling of plasma-induced immunogenic cell death** 32
Tomoyuki Murakami

Section: **REGULATORY ISSUES AND STANDARDS IN PLASMA MEDICINE**

Hall: **ICPM Session 2**

Chair: **Eun-ha Choi**

- 17:00 Mon-O-3-2 **By any other name: a search for optimal plasma nomenclature** 50
 Caroline Corcoran, Rachel Bennett, Vandana Miller, Fred C. Krebs, and Will Dampier
- 17:15 Mon-O-3-3 **Standardization in Plasma Medicine: From DIN Spec to IEC standard** 51
Kai Masur, Mareike Meister, Eun Ha Choi, Sybille Hassel, Thomas von Woedtke
- 17:30 Mon-O-3-4 **Standardized Treatment Procedures for In Vitro Analysis of Different Cold Plasma Technologies: Is It Even Possible?** 52
 Thoralf Bernhardt, Philipp Ficht, Anna Staffeld, Thomas Borchardt, Andreas Helmke, Mareike Meister, Sybille Hasse, Sander Bekeschus, Steffen Emmert, Lars Boeckmann

17:45 – 18.45 **Special Session on Regulatory issues**

PLENARY SESSION

Hall: **IWPCT**

Chair: Uroš Cvelbar

- 18:45 PL-2 **Star Wars in Dermatology – Plasma medicine** 3
Steffen Emmert, Alexander Thiem, Sander Bekeschus, Lars Boeckmann

19:30 – 21:30 **Welcome Reception**

Tuesday, 10 September 2024

PLENARY SESSION

Hall: **ICPM Session 1**

Chair: **Gerrit Kroesen**

- 10:00 PL-3 **Plasma for Biology and Medicine – Now and Next** 4
Sander Bekeschus, von Woedtke, Steffen Emmer, Klaus-Dieter Weltmann

Section: **PLASMA LIQUID INTERACTIONS, PLASMA-ACTIVATED LIQUIDS**

Hall: **ICPM Session 1**

Chair: **Annemie Bogaerts**

- 10:45 IT-5 **Plasma-Liquid Interactions in The Presence of Organic Matter – Including Chemical, Biological, and Electrical Interactions** 12
Katharina Stapelmann, Sophia Gershman, Vandana Miller
- 11:15 Tue-O-4-1 **Efficient Generation and Characterization of Plasma-Activated Water Using a Surface Dielectric Barrier Discharge System** 54
 Benedito Botan Neto, Michaela Shiotani Marcondes, Luan Gonçalves de Lima, Felipe de Souza Miranda, Douglas Marcel Leite, André Luis Pereira, Cristiane Yumi Koga-Ito, Rodrigo Sávio Pessoa

11:30	Tue-O-4-2	Exploring the Potential of Plasma-Activated Water: Impact of Gas Composition on Reactive Species Generation, Antimicrobial Efficacy, and Cytotoxicity <u>Felipe de Souza Miranda</u> , Victoria Kelly Fonseca Tavares, Diego Morais da Silva, Noala Vicensoto Moreira Milhan, Nilton Franccelosi Azevedo Neto, Rodrigo Sávio Pessoa, Cristiane Yumi Koga-Ito	55
11:45	Tue-O-4-3	Synergizing Dielectric Barrier and Gliding Arc Discharges: Advancements in Plasma-Activated Water Generation <u>Nilton F. Azevedo Neto</u> , Felipe S. Miranda, Pedro W. P. Moreira Junior, Clodomiro A. Junior, Cristiane Y. K. Ito, Rodrigo S. Pessoa	56
12:00	Tue-O-4-4	Chemical and Bactericidal Properties of Cell Culture Media DMEM and RPMI Modified by He/O₂ Plasma Treatment <u>Petr Lukeš</u> , Barbora Tarabová, Zuzana Kovalová, Vít Jirásek	57

Section: **PLASMA SURFACE INTERACTIONS/MODIFICATIONS FOR BIOMEDICAL APPLICATIONS**

Hall: **ICPM Session 2**

Chair: **Lenka Zajíčková**

10:45	Tue-O-5-1	Insights into the use of aerosolized precursors in atmospheric pressure plasma polymerization: process control and coating stability Giulia Laghi, Chiara Buganè, Gianmarco Rossi, Lucia Barbera, Riccardo Gallerani, Guglielmo Guido Condorelli, Romolo Laurita, <u>Matteo Gherardi</u>	68
11:00	Tue-O-5-2	Production of reactive oxygen species and its controlled delivery by functionalized thin films deposited by plasma technology <u>Paula Navascués</u> , Flaela Kalemi, Dirk Hegemann	69
11:15	Tue-O-5-3	Commercial Medical Applications of Surface Treatment by Cold Plasma <u>Amnon Lam</u>	70
11:30	Tue-O-5-4	Biomimetic surfaces for improved biological response <u>Ita Junkar</u> , Niharika Rawat, Metka Benčina, Janez Kovač, Katja Lakota, Polona Žigon, Valentina Puca, Rossella Grande, Vittoria Perrotti, Aleš Igljč	71
11:45	IT-6	Hydrogels in plasma medicine: focus on the chemical interaction between reactive species and biopolymers Francesco Tampieri, Alfio G. Arcoria, Albert Espona-Noguera, Cristina Canal	13

12:30 – 13:30 **Lunch Break**

14:00 – 16:45 **POSTER SESSION**

Tue-P-1	Plasma Jet Treatment of the Inner Wall of Montgomery Tracheal Implant (T-Tube) <u>Konstantin G. Kostov</u> , Ananias A. Barbosa, Paulo F. G. Cardoso, Antje Quade, Daniel Legendre, Diego M. Silva, Cristiane Y. Koga-Ito	81
Tue-P-2	Development of a decontaminating coating activated by cold plasma for biohazard control A. Baraze, C. Muja, F. Sainct, S. Allix, <u>T. Maho</u> , P. Guillot	82
Tue-P-3	Cold plasma enamel surface treatment to increase fluoride varnish uptake <u>Sara Fathollah</u> , Hossein Abbasi, Sadegh Akhoundi, Aboutorab Naeimabadi, Sahar Emamjome	83
Tue-P-4	Evaluation of the Antimicrobial Effect of Room Temperature and Refrigerated Plasma Activated Water <u>Felipe Almeida</u> , Anelise Doria, Luciana Sant'Anna	84

Tue-P-5	Inactivation of microorganisms on fabrics using plasma-activated nebulized mist driven by different plasma gases	85
	<u>Pengyu Zhao</u> , Sihong Ma, Yikang Jia, Li Guo	
Tue-P-6	Investigation of cold plasma treatment on antimicrobial peptides as strategy for selective bacterial targeting	86
	<u>D. Doll</u> , N. Nawrath, F. M. Fuchs, P. Awakowicz, A. R. Gibson, N. Metzler-Nolte	
Tue-P-7	Reduction in bacterial survival on the surface of F9 filters after being exposed to cold atmospheric plasma treatment	87
	<u>Ingrid Curril</u> , Andreas Helmke, Mrotzek, Julia, Schulz Jannik and Wolfgang Viöl	
Tue-P-8	Comparative Study on Bacterial Inactivation using O₂ and N₂-added He/Ar Plasma	88
	<u>Krishnaveni Parvataneni</u> , Sohail H. Zaidi	
Tue-P-9	The influence of non-thermal plasma on fungal growth on building materials	89
	<u>Jana Jirešová</u> , Eliška Lokajová, Kamila Zdeňková, Vladimír Scholtz	
Tue-P-10	Evaluation of Resistance Development in Bacteria Against Cold Atmospheric Plasma in Consequence of Repetitive Plasma Treatment Methods	90
	<u>Şeyma Ecem Irmak</u> , Utku Kürşat Ercan	
Tue-P-11	Plasma-activated liquids reduce the viability of biofilms associated with endodontic infections	91
	Ana <u>Bessa Muniz</u> , Lady Daiane Pereira Leite, Mariana Raquel da Cruz Vegian, Diego Morais da Silva, Noala Vicensoto Moreira Milhan, Felipe de Souza Miranda, Rodrigo Sávio Pessoa, Cristiane Yumi Koga-Ito	
Tue-P-12	Helium Cold Atmospheric Plasma Effectively Acts on Multispecies Cariogenic Biofilms Formed <i>in situ</i>	92
	<u>Leandro Wagner Figueira</u> , Ana Bessa Muniz, Maria Aparecida Rodrigues de Holanda, Thalita Mayumi Castaldelli Nishime, Konstantin Georgiev Kostov, Cristiane Yumi Koga-Ito	
Tue-P-13	The Effect of Bisphenol a Degraded by Non-Thermal Plasma on Yeast	93
	<u>Jana Makuková</u> , Ivana Kyzeková, Stanislav Kyzek, Oleksandr Galmiz, Dominik Juračka, Sára Pišteková, Michal Galamboš, Zdenko Machala, Andrea Ševčovičová	
Tue-P-14	Combined Antimicrobial Properties of Ultraviolet radiation and Plasma-Activated Water	94
	<u>Ramin Mehrabifard</u> , Bernard Gitura Kimani, Zdenko Machala	
Tue-P-15	Synergistic Enhancement of Antibiotic Efficacy Against Biofilms with Cold Plasma	95
	<u>Thomas P. Thompson</u> , Katie Harvey, Jordanne-Amee Maybin, Ross M. Duncan I, Paula Bourke, Noreen J. Hickok, Theresa A. Freeman, Brendan F. Gilmore	
Tue-P-16	Role of long living species in the inactivation of bacteria: comparison of different plasma sources	96
	<u>Leonardo Zampieri</u> , Rita Agus, Brayden Myers, Ivo Furno, Claudia Riccardi, Emilio Martines	
Tue-P-17	Antimicrobial Activity of SDBD Plasma Treatment on Planktonic and Biofilm Forms of Escherichia coli	97
	<u>Oleksandr Galmiz</u> , Bernard Gitura Kimani and Zdenko Machala	
Tue-P-18	Bacterial decontamination by a He plasma jet operating in different concentrations of O₂	98
	<u>Diego Morais da Silva</u> , Augusto Stancampiano, Sébastien Dozias, Konstantin Georgiev Kostov, Cristiane Yumi Koga-Ito, Eric Robert	
Tue-P-19	Electrical Characterization and Efficacy Assessment of a Cold Atmospheric Plasma System for Closed Environment Sanitization	99
	<u>Silvia Giuditta Scaltriti</u> , Gabriele Neretti, Fabio Avino, Ivo Furno	

Tue-P-20	Cold Plasma: A promising Approach to Mitigate Common Ragweed Pollen Allergens <u>Nataša Hojnik</u> , Janez Zavašnik, Vasyl Shvalya, Jernej Šribar, Igor Križaj, James Walsh	100
Tue-P-21	Toxicological characterisation of BPA and BPS and their transformation products formed after degradation with cold atmospheric pressure plasma <u>Martina Štampar</u> , Ana Kovačič, Martina Modic, Nataša Hojnik, Martin Rafael Gulin, Christina Nannou, Lelouda-Athanasia Koronaiou, David Heath, James L. Walsh, Dimitra Lambropoulou, Uroš Cvelbar, Ester Heath, Bojana Žegura	101
Tue-P-22	Cold plasma for the treatment of house dust mite allergens <u>Jernej Šribar</u> , Nataša Hojnik, Igor Križaj, James Walsh	102
Tue-P-23	Mitigating Bacteria from Hospital Floors: Plasma Approach Keerthana Dandamudi, <u>Rachana Dandamudi</u> , Sohail Zaidi	103
Tue-P-24	Non-thermal Plasma-Activated Water Against Candida auris Isolates from Healthcare-Associated Infections <u>Andra-Cristina Bostănaru-Iliescu</u> , Adrian Fifere, Adriana Elena Anița, Valentin Năstasă, Dragos Constantin Anița, Robert Capotă, Florica-Mirela Doroftei, Bogdan Minea, Eugen Hnatiuc, Mihai Mareș	104
Tue-P-25	Effect of NTP exposure on the electronic components <u>Ladislav Fišer</u> , Vladimír Scholtz, Jana Jirešová	105
Tue-P-26	Establishing the role of the stringent response in non-thermal plasma treatment <u>Lauren Walsh</u> , Felicity Tso, Vandana Miller, Donald C. Hall Jr	106
Tue-P-27	Cold Atmospheric Plasma Jet with Pulsed Voltage and Gold Nanoparticles Enhance Cytotoxic Anticancer Effect <u>I Schweigert</u> , M Biryukov, A Polyakova, N Krychkova, E Gorbunova, A Epanchintseva, I Pyshnaya, Dm Zakrevsky, E Milakhina, O Koval	107
Tue-P-28	Ferroptosis Drives Cell Death After Cold Atmospheric Plasma Treatment in Cervical Cancer Cells <u>Marcel Arnholdt</u> , Martin Weiss	108
Tue-P-29	Cold Plasma Deposition of Topotecan: A Novel Approach for Local Cancer Drug Delivery to Glioblastoma Cells <u>Beatriz Pinheiro Lopes</u> , Liam O'Neill, Fiona O'Neill, Paula Bourke, Daniela Boehm	109
Tue-P-30	Non-thermal plasma as a partner in crime for anti-cancer therapies: Optimization in the 3D spheroid tumor model for HNSCC <u>Bauwens M.</u> , Verswyvel H., De Waele J., Wouters A., Bogaerts A., Smits E.	110
Tue-P-31	Combination therapy of medical gas plasma and cisplatin enhances tumor toxicity and immunogenicity in human bladder cancer cells <u>Nadine Gelbrich</u> , Julia Edelmann, Martin Burchardt, Sander Bekeschus	111
Tue-P-32	Exploring the Therapeutic Potential of Surface DBD Plasma in B16F10 cells Treatment: A Comparative Study of Direct and Indirect Approaches <u>Luan Gonçalves de Lima</u> , Michaela Shiotani Marcondes, Rafaela Campos Queiroz, Dayane Batista Tada, Clodomiro Alves Júnior, Rodrigo Sávio Pessoa	112
Tue-P-33	Cold gas plasma alters tyrosine kinase activity in lung cancer cells <u>Paul Schulan</u> , Kristian Wende, Ramona Clemen, Sander Bekeschus	113
Tue-P-34	The impact of cold piezoelectric plasma on cancer cell viability: a study on cholangiocarcinoma <u>Manon Soulier</u> , Bouchra Lekbaby, Imane Houari, Henri Decauchy, Allan Pavy, Alexia Coumes, Laura Fouassier, Thierry Dufour	114
Tue-P-35	Combination Treatment of Head and Neck Cancer Cell Lines with Cold Plasma and Chemotherapeutics Elena A. Vochitu, Nishtha Gaur, Robert D. Short, <u>Sarah L. Allinson</u>	115

Tue-P-36	Machine Learning Assessment of Cold Atmospheric Plasma Efficacy on Breast Cancer: Exploring Receptor Status Correlations for Optimized Treatment Strategies Gizem Dilara Özdemir, <u>Fatoş Başdeli</u> , Zehra Ece Şen, Mehmet Akif Özdemir, Utku Kürşat Ercan	116
Tue-P-37	In Vitro Adaptive Plasma Cancer Treatment with Real-Time In-Situ Diagnostics using Impedance Measurements <u>Zichao Hou</u> , Taeyoung Lee, Michael Keidar	117
Tue-P-38	Evaluation of pyrazolopyrimidinones as anticancer prodrugs activated by cold atmospheric plasma <u>Natalia Bednarz</u> , Ciara McEvoy, Gemma K. Kinsella, Daniela Boehm, Paula Bourke, John C. Stephens, James Curtin	118
Tue-P-39	Novel combination therapy of non-thermal plasma and immune checkpoint inhibitors for melanoma <u>Lisa Van der Heyden</u> , Angela Privat-Maldonado, Evelien Smits, Annemie Bogaerts	119
Tue-P-40	Sensitization of vulvar cancer cells with ATM kinase inhibitor prior PAL treatment <u>Hortense Decool</u> , Johanna Renner, Martin Weiss	120
Tue-P-41	Impact of plasma-activated phosphate-buffered saline on viability of human cancer and non-cancerous cells <u>Darina Kužmová</u> , Helena Gbelcová, Zdenko Machala	121
Tue-P-42	Numerical modeling on the mechanism of plasma-induced cell death Ippei Saito, Motohiro Tomita, <u>Tomoyuki Murakami</u>	122
Tue-P-43	The beneficial effect of successive Cold Atmospheric Plasma treatments on in vitro behaviour of human gingival fibroblasts Andreea-Mariana Negrescu, Leonardo Zampieri, Anisoara Cimpean, <u>Emilio Martines</u>	123
Tue-P-44	A Minimally Invasive Surgical Platform Against Pancreatic and Biliary Tract Cancers Using Cold Atmospheric Plasma Vasilios Vavourakis, <u>Charalambos Anastassiou</u> , Thierry Dufour, Laura Fouassier, Panagiotis Svarnas	124
Tue-P-45	Effects of Cold Atmospheric Argon Plasma Jet Treatment on the Biological Activity of Human Gingival Fibroblasts Neusa Silva, Joana Marques, Mariana Brito da Cruz, Henrique Luís, António Mata, <u>Susana Sérgio</u>	125
Tue-P-46	Safety evaluation of plasma activated water on skin and breathing: an in-vivo study <u>Mahdiyeh Bakhtiyari-Ramezani</u> , Sara Hejri, Aboutorab Naeimabadi	126
Tue-P-47	Anti-yeast activity of transient spark PAW combined with UV-A and natural phenolics on planktonic yeast <i>Wickerhamomyces anomalus</i> <u>Bernard Gitura Kimani</u> , Ramin Mehrabifard, Zdenko Machala	127

16:45 – 17:00

Coffee Break

Section: **PLASMA LIQUID INTERACTIONS, PLASMA-ACTIVATED LIQUIDS**

Hall: **ICPM Session 1**

Chair: **Petr Lukeš**

17:00	Tue-O-4-5	Plasma-Generated Nitric Oxide Water for Biological Applications: Infection Control and Cosmetic Innovations <u>Nagendra Kumar Kaushik</u> , Neha Kaushik, Linh Nhat Nguyen, Tirtha Raj Acharya, Manorma Negi, Shweta Bharat Borkar, Paritosh Patel, Apurva Jaiswal, Eun Ha Choi	58
17:15	Tue-O-4-6	Assessing the antiviral effect of plasma-conditioned media against herpes simplex 1 infection in polarized vaginal epithelial cells <u>Caroline Corcoran</u> , Brian Wigdahl, Vandana Miller, Fred C. Krebs	59

17:30	Tue-O-4-7	Plasma activated water pre-treatment substantially enhances phage activity against <i>Proteus mirabilis</i> biofilms Akash Shambharkar, Thomas P. Thompson, <u>Laura McClenaghan</u> , Paula Bourke, Brendan, F. Gilmore, Timofey Skvortsov	60
17:45	Tue-O-4-8	The effects of plasma-activated liquid on urinary tract infection and colitis in mice <u>Zdenko Machala</u> , Michal Pastorek, Barbora Gromová, Slavomír Pásztor, Peter Celec, Lubomíra Tóthová, Barbora Konečná, Roman Gardlik	61
18:00	Tue-O-4-9	Plasma Activated Water is Effective against Redoubtable Nosocomial Microorganisms <u>Andra-Cristina Bostănaru-Iliescu</u> , Adrian Fifere, Valentin Năstasă, Laura-Elena Ursu, Florica-Mirela Doroftei, Bogdan Minea, Eugen Hnatiuc, Mihai Mareş	62
18:15	Tue-O-4-10	Inactivation pathways of <i>Escherichia coli</i> and <i>Staphylococcus aureus</i> induced by transient spark discharge in liquids <u>Karol Hensel</u> , Aleksandra Lavrikova, Helena Bujdáková	63
18:30	Tue-O-4-11	Decontamination of Healthcare Textiles Using Plasma-Activated Water <u>Markus Ahrens</u> , Sonja Böttl, Petra Mela	64
18:45	Tue-O-4-12	Utilizing the Potential of Plasma-Treated Water for Enhanced Maize Growth and Stress Tolerance <u>Zuzana Okruhlicová</u> , Zuzana Lukačová, Karol Hensel	65
19:00	Tue-O-4-13	Microbiological and pH Assessment in Pineapple Jams and Zucchini Preserves Treated with Plasma Activated Water Pedro Inácio Rodrigues Melo, Nathalia Cristina de Carvalho Sousa, Felipe Santos de Almeida, <u>Anelise Cristina Osório César Doria</u> , Sônia Khouri Sibelino	66

Section: **PLASMA MEDICAL APPLICATIONS – CLINICAL AND ANIMAL STUDIES**

Hall: **ICPM Session 2**

Chair: **Thomas von Woedtke**

17:00	Tue-O-6-1	Non-Invasive Physical Plasma (NIPP) Improves Conventional Wound Management of Cut and Bite Wounds in European Hedgehogs: Results of a Prospective, Non-Randomized Monocentric Wildlife Clinical Trial Jürgen Eichler, Björn Rulik, Alexander Abazid, <u>Matthias B. Stope</u>	73
17:15	Tue-O-6-2	Cold plasma enamel surface treatment to increase fluoride varnish uptake <u>J Sara Fathollah</u> , Hossein Abbasi, Sadegh Akhoundi, Aboutorab Naeimabadi, Sahar Emamjome	74
17:30	Tue-O-6-3	Cold Plasma Therapy for Venous Ulcers: Early Clinical Trial Outcomes <u>Ana Megía-Macías</u> , Osvaldo Daniel Cortázar, Bernardo Hontanilla	75
17:45	Tue-O-6-4	Safety and efficacy study of Plasma-activated Lactate Ringer's Solution (PAL) for application on animal and human skin <u>Kae Nakamura</u> , Katsumi Ebisawa, Masaaki Mizuno, Nobuhisa Yoshikawa, Hiromasa Tanaka, Kazunobu Hashikawa, Shinya Toyokuni, Masaru Hori, Yuzuru Kamei, Hiroaki Kajiyama	76
18:00	Tue-O-6-5	An Innovative Method for Molecular Introduction into Fish Eggs Using Surface Discharge Treatment <u>Yoshihisa Ikeda</u> , Takuro Doi, Yugo Kido, Taiju Saito, Masafumi Jinno	77
18:15	Tue-O-6-6	Treatment of psoriasis with an ALOE device: pilot research A.V. Kazak, <u>L.V. Simonchik</u> , S. A. Kazel	78
18:30	Tue-O-6-7	Cold atmospheric-pressure plasma and plasma treated liquids for veterinary applications <u>Kristína Trebulová</u> , Zdenka Kozáková, Kamila Klementová, Ivana Paličková, Alois Čížek, Jan Hrudka, Eric Robert, Augusto Stancampiano, Inna Orel, František Krčma	79

Wednesday, 11 September 2024

PLENARY SESSION

Hall: **ICPM Session 1**

Chair: **Masaru Hori**

- 10:00 PL-4 **Cold plasma as a combinatorial therapy to combat orthopaedic infection** 5
Carly J. Smith, Amanda Watkins, Autumn Melvage, Amanda Connelly, Thomas P. Schaer, Brendan Gilmore, Daniela Boehm, Paula Bourke, Noreen Hickok, Theresa A. Freeman

Section: **FUNDAMENTALS OF ATMOSPHERIC PLASMA**

Hall: **ICPM Session 1**

Chair: **Michael Keidar**

- 10:45 IT-7 **Innovative Solutions in Agriculture and Biomedicine: Leveraging Electrical Discharges in Gases for Plasma Applications** 14
Sabnaj Khanam, Madeeha Iqbal, Khadija Akter, Juie Rana, Anchal Bhatnagar, Young Jun Hong, Eun Ha Choi, Ihn Han
- 11:15 Wed-O-7-1 **Online diagnostics of the production of reactive species in a micropulsed plasma jet** 129
Leonardo Zampieri, Emilio Martines
- 11:30 Wed-O-7-2 **Establishing a set of measurements to monitor plasma source duplicates in collaborative groups through systematic investigation and correlation of parameters** 130
Helena Jablonowski, Ulfilas Hoffmann, Robert Bansemer, Katayoon Hadian Rasnani, Michael Schmidt, Raphael Rataj1, Sander Bekeschus, Torsten Gerling, Klaus-Dieter Weltmann, Thomas von Woedtke
- 11:45 Wed-O-7-3 **Development of A Long Tube Plasma Jet for Treating Pipeline-shape Structures and Its Affecting Factors Study** 131
Yajun Zhao, Kangkang Qiu, Li Zhang, Shanshan Jin, Zhi Fang
- 12:00 Wed-O-7-4 **Identification of relevant plasma components in plasma-induced microcirculation enhancement** 132
Thomas Borchardt, Ole Grams, Andreas Helmke, Steffen Emmert, Wolfgang Viöl

Section: **PLASMA-CELL AND PLASMA-TISSUE INTERACTIONS – BIOLOGICAL AND BIOCHEMICAL REACTIONS**

Hall: **ICPM Session 2**

Chair: **Kristian Wende**

- 10:45 Wed-O-8-1 **Combining Plasma, Micelles, and Chitosan into PCCM-125: Long-Term Nitric Oxide Delivery and Angiogenesis-Independent Wound Healing in Human Corneal Epithelial Cell Model** 134
Maher Hadaya, Jinjie He, Israel Ojalvo, Sindi Beqo, Mo Hadaya, Aarna Doshi, Alexander A. Fridman, Christopher M. Sales
- 11:00 Wed-O-8-2 **Using Principal Component Analysis to Investigate the Morphological Changes in Cells Exposed to Non-Thermal Plasma** 135
Amal Mathew, Hrushikesh Deshpande, Julia Sutter, Sophia Gershman, Mikhail Schneider, Fred Krebs, Katharina Stapelmann, Vandana Miller
- 11:15 Wed-O-8-3 **Plasma-treated hydrogels: manufacturing therapeutic 3D scaffolds for tissue regeneration** 136
Albert Espona-Noguera, Marina Valls, Francesco Tampieri, Milica Živanić, Cristina Canal
- 11:30 Wed-O-8-4 **Novel skin model for plasma medicine and cosmetics** 137
Lisa Hermans, Vinodini Vijayarangan, Angela Privat-Maldonado, Sebastien Dozias, Julien Lemaire, Eric Robert, Annemie Bogaerts, Augusto Stancampiano

11:45 Wed-O-8-5 **Multipetrode DBD Plasma Torch Design with Drug Delivery Option for Wound Healing and Sterilization** 138
Srida Aliminati, Sohail Zaidi

12:30 – 13:30 **Lunch Break**
13:45 – 21:30 **Excursion + Dinner**

Thursday, 12 September 2024

PLENARY SESSION

Hall: **ICPM Session 1**

Chair: **Hiromasa Tanaka**

10:00 PL-5 **From transient and localized plasma surface interaction to deep tissue biological effects in Plasma Medicine** 6
E. Robert, J.G. Bauzin, G. Collet, S. Dozias, P. Escot Bocanegra, A. Hocine, F. Prieur, J.M. Pouvesle, A. Rouillar1, A. Stancampiano, V. Vijayarangan

Section: PLASMA-CELL AND PLASMA-TISSUE INTERACTIONS – BIOLOGICAL AND BIOCHEMICAL REACTIONS

Hall: **ICPM Session 1**

Chair: **Steffen Emmert**

9:45 IT-8 **The Mechanisms of Cold Atmospheric Plasma in Promoting Healing of Infectious Wounds** 15
Lanlan Nie, Xi Chen, Xinpei Lu

10:15 IT-9 **Plasma Polymers as Surface Finishes for Tissue Engineering Materials** 16
Lenka Zajíčková, Lucie Janů, Martina Janůšová, Jiřina Medalová, Patrik Matušů, Jan Příbyl, Šimon Klimovič, Beáta Beliančinová, David Nečas

10:45 Thu-O-8-1 **Plasma-activated biogel for dermatological treatment** 140
Dingxin Liu, Hao Zhang, Jishen Zhang, Li Guo, Mingzhe Rong

11:00 Thu-O-8-2 **A Cold Atmospheric Plasma Jet – Composite Hydrogel Dressing for Controlled delivery of Platinum based Drugs into the Epithelium** 141
Hao Naing Tun Thet, Elena Vochitu, Nishtha Gaur, Sarah Allinson, Rob Short, Toby Jenkins

11:15 Thu-O-8-3 **CAP impact on the primary teeth enamel** 142
Joanna Pawłat, Michał Kwiatkowski, Piotr Terebun, Dawid Zarzeczny, Elżbieta Grządka, Agnieszka Starek-Wójcicka, Marta Krajewska, Monika Machoy, Agnieszka Mazur-Lesz

11:30 Thu-O-8-4 **Direct Cold Atmospheric Plasma Treatment vs Plasma-activated Hydrogels in Wound Treatment** 143
Nishtha Gaur, Naing Tun Thet, Sarah Allinson, Alex Robson, Toby Jenkins, Craig Williams, Gordon Ramage, Endre Szili, Rob Short

11:45 Thu-O-8-5 **Absorption of FD-150 into White Blood cells by Microplasma** 144
Jaroslav Kristof, Mahedi Hasan, Sadia Afrin Rimi, Abubakar Hamza Sadiq, Alam Md Jahangir, Kazuo Shimizu

12:00 Thu-O-8-6 **Pores and Filaments – The quest for a reliable and reproducibly patterned plasma-permeabilization of the skin** 145
Monika Gelker, Astrid Ichter, Robert Köhler, Wolfgang Viöl

Section: **FUNDAMENTALS OF ATMOSPHERIC PLASMA**

Hall: **ICPM Session 2**

Chair: **Uroš Cvelbar**

09:45	Thu-O-7-1	Portable and affordable cold air plasma source for biomedical applications Myron Klenivskiy, Josef Khun, Laura Thonová, Eva Vaňková, <u>Vladimír Scholtz</u>	154
10:00	Thu-O-7-2	Cold plasma systems for bioaerosol decontamination: scale-up of a portable room-scale device <u>Pasquale Isabelli</u> , K. De Baerdemaeker, Francesco Tomelleri ¹ , F. Devlieghere, Matteo Gherardi, Romolo Laurita	155
10:15	Thu-O-7-3	From Idea to Prototype – Clinic plasma treatment on-demand – the potential of the new portable device MOBIPLAS <u>Klaus-Dieter Weltmann</u> , Robert Bansemer, Hannes Bendt, Julia Berner, Sander Bekeschus, Thomas von Woedtke	156
10:30	Thu-O-7-4	Electrical, Optical and Thermal Characterization of Argon–Hydrogen Plasma Jets for Medical and Biomedical Applications Fellype do Nascimento, <u>Konstantin G. Kostov</u>	157
10:45	Thu-O-7-5	System for <i>In Situ</i> Measurements During Skin Wound Treatment by Cold Atmospheric Plasma Suneel Kumar, Dhruv Patel, Dnyaneshwari Rananavare, Jonathan Thomas, Jascha Brettschneider, Julia Sutter, Fred Krebs, Vandana Miller ³ , Katharina Stapelmann, <u>Francois Berthiaume</u>	158
11:00	Thu-O-7-6	Computational study of a pulsed atmospheric pressure dielectric barrier discharge interacting with liquid <u>Sarah Van Hove</u> , Ivan Tsonev, Annemie Bogaerts	159
11:15	Thu-O-7-7	Computational modelling of <i>in-vitro</i> treatment with a plasma jet: elucidating the effects of the treatment setup <u>Pepijn Heirman</u> , Annemie Bogaerts	160
11:30	Thu-O-7-8	Developing a conductive treatment method for pathological specimens using plasma for the diagnosis using electron microscopy Sanae Ikehara, Kazuhiko Azuma, Syota Ohki, Hiroki Kondo, Yoko Iizumi, Toshiya Okazaki, Masaru Hori, Komei Baba, <u>Yuzuru Ikehara</u>	161
11:45	Thu-O-7-9	Characterization of 3-pin Atmospheric Pressure Plasma Jet used for production of Plasma Activated Water by ICCD imaging Amit Kumar, Nikola Škoro, Gordana Malović, <u>Nevena Puač</u>	162
12:00	Thu-O-7-10	Multimodal linking of biological imaging data in plasma medicine <u>Mohsen Ahmadi</u> , Robert Wagner, Anke Schmidt, Sander Bekeschus, Markus M. Becker	163

12:30 – 13:30 **Lunch Break**

14:00 – 16:45 **POSTER SESSION**

Thu-P-1	Atmospheric Pressure Plasma Synthesis of Gold Nanoparticles for SERS Recognition of Bacterial DNA <u>Jelena Štrbac</u> , Vasyl Shvalya, Martina Modic, Janez Zavašnik, Damjan Vengust, Uroš Cvelbar	171
Thu-P-2	Label-Free SERS Detection of Carcinogens by Plasma-Made Nanostructures <u>Neelakandan M Santhosh</u> , Vasyl Shavlya, Martina Modic, Nataša Hojnik, Jaka Olenik, Janez Zavašnik, Martin Košiček, Uroš Cvelbar	172
Thu-P-3	The use of atmospheric pressure plasmas for the control of antibiotic- resistant bacteria in the agri-food sector <u>Z. Aliyeva</u> , T. Maho, P. Guillot, C. Muja	173

Thu-P-4	Treatment of fresh and marine water microalgae by combined gliding arc discharge plasma and pulsed electric field <u>Liutauras Marcinauskas</u> , Kamilė Jonynaitė, R. Celiešiūtė-Germanienė, Mindaugas Aikas, Žydrūnas Kavaliauskas, Rolandas Uscila, Skirmantas Keršulis, Arūnas Stirke, Antanas Strakšys, Voitech Stankevič	174
Thu-P-5	Characterizing Reactive Species Distribution in Plasma-Based Surface Decontamination for Enhanced Food Safety <u>Caterina Maccaferri</u> , Filippo Capelli, Ana Sainz García, Matteo Gherardi, Fernando Alba Elías, Romolo Laurita	175
Thu-P-6	Cold atmospheric microplasma mediated drug delivery through blood-brain barrier <u>Alam Md Jahangir</u> , Yamano Tomoki, Abubakar Hamza Sadiq Sadia Afrin Rimi, Mahedi Hasan, Jaroslav Kristof, Kazuo Shimizu	176
Thu-P-7	Study on the changes of cell membrane lipids for delivering large molecules drug by using microplasma irradiation <u>Sadia Afrin Rimi</u> , Mamun Md Al, Alam Md Jahangir, Abubakar Hamza Sadiq, Mahedi Hasan, Jaroslav Kristof, and, Kazuo Shimizu	177
Thu-P-8	Boosting transdermal drug penetration by cold plasma – insights on the molecular level <u>Kristian Wende</u> , Paula Marx, Johanna Striesow, Patricia Lopalco, Thomas von Woedtke, Sander Bekeschus	178
Thu-P-9	Development of a Cold Atmospheric Plasma Responsive Polyacrylate Hydrogel System for On-Demand Drug Delivery <u>Natasha Harwood</u> , Maciek Kopec, Toby Jenkins	179
Thu-P-10	Plasma-Designed Nanosensors for SERS Detection of Hazardous Chemicals <u>Martin Košiček</u> , Vasyl Shvalya, Damjan Vengust, Oleg Baranov and Uroš Cvelbar	180
Thu-P-11	Rapid Plasma-Driven Fabrication of Gas Sensors for Safety Against Hazardous Gases <u>Ardita Kurtishaj Hamzaj</u> , Edoardo Donà, Neelakandan M Santhosh, Vasyl Shvalya, Martin Košiček, Uroš Cvelbar	181
Thu-P-12	Synergistic Application of Cold Atmospheric Plasma and Vancomycin in MRSA biofilms <u>Katie Harvey</u> , Thomas P. Thompson, Paula Bourke, Noreen J. Hickok, Theresa A. Freeman, Brendan F. Gilmore	182
Thu-P-13	Comparative Studies of two Low Temperature Microwave Plasma Devices at Atmospheric Pressure for Medical Applications <u>Neda Babučić</u> , Kinga Kutasi, Nikola Škoro, Nevena Puač	183
Thu-P-14	Electrical and optical characterization of a plasma source for the biological decontamination of waste water in volume <u>Maria Saba</u> , Thomas Maho, Philippe Guillot	184
Thu-P-15	Comparative bio-application study of various non-thermal plasma generating devices using reference protocol <u>Anna Machková</u>	185
Thu-P-16	The equivalent electrical circuit for describing the dielectric barrier discharge plasma jet <u>Marija Puač</u> , Nikola Škoro, Kinga Kutasi and Nevena Puač	186
Thu-P-17	Experimental characterization of a flat DBD plasma source <u>Zhanel Aliyeva</u> , Cristina Muja, Thomas Maho, <u>Philippe Guillot</u>	187
Thu-P-18	Thrust force generated by surface dielectric barrier discharge <u>Juš Polanšek</u> , Uroš Cvelbar	188
Thu-P-19	Thermal Stress and its Role in Plasma Bacterial Inactivation: High resolution Characterization <u>A. Rouillard</u> , A. Stancampiano, S. Dozias, A. Devos, J.G Bauzin, A. Hocine, E. Robert, P. Escot Bocanegra	189
Thu-P-20	Scale-up of non-thermal plasma and photocatalysis for bacteria inactivation and VOCs removal <u>Thomas Vazquez</u> , Aleksandra Lavrikova, Dalimír Wiederman, Jan Babic, and Zdenko Machala	190

Thu-P-21	Characterization of a cold atmospheric air plasma jet supplied by microsecond voltage pulses <u>Gabriele Neretti</u> , Arturo Popoli, Andrea Cristofolini	191
Thu-P-22	Evaluating Antimicrobial Effects of Plasma-Activated Liquids Using Surface-Wave Microwave Plasma Jet: A Comparative Analysis of Deionized Water and Saline Solution <u>Michaela Shiotani Marcondes</u> , Luan Gonçalves de Lima, Lady Daiane Pereira Leite, Victória Kelly Fonseca Tavares, Clodomiro Alves Júnior, Felipe de Souza Miranda, Cristiane Yumi Koga Ito, Rodrigo Sávio Pessoa	192
Thu-P-23	Underwater Discharge Plasma for in situ Generation of Micro-nanobubbles <u>Mengying Zhu</u> , Mingyan Zhang, Dingxin Liu, Renwu Zhou	193
Thu-P-24	Application of plasma-activated water on oral pathogens <u>Li Guo</u> , Yikang Jia, Pengyu Zhao, Dingxin Liu	194
Thu-P-25	Plasma-activated medium for intraoperative adhesion prophylaxis <u>Franziska Kessler</u> , Martin Weiss	195
Thu-P-26	Proteomics and single-cell microscopy analysis for the investigation of plasma-activated water inactivation mechanism of <i>Escherichia coli</i> <u>Rita Agus</u> , Aleksandra Lavrikova, Fabio Avino, Brayden Myers, Ivo Furno	196
Thu-P-27	Development of a Plasma Functionalised Liquid for prevention and control of MRSA biofilm device-associated infections <u>Orla Nic Shiurdain</u> , Sean Kelly, Peter Dobbyn, Soukaina Barroug, Daniela Boehm, Paula Bourke	197
Thu-P-28	Addition of ROS scavengers provides an insight into the antimicrobial effect of plasma treated liquids <u>Moritz Wilch</u> , Rinat Ortmann, Monika Gelker, Wolfgang Viöl	198
Thu-P-29	Disinfection of <i>Enterococcus faecalis</i> on baby bottle nipples using atmospheric low-temperature plasma bubbled-up water <u>Taiki Osawa</u> , Ziyu Liu, Kai Fukuchi, Akane Yaida, Yuriko Matsumura, Atsuo Iwasawa, Norihiko Ito, Akitoshi Okino	199
Thu-P-30	Developing a Chicken Juice-Based Infection Model to Assess the Antimicrobial Effects, Mechanisms of Actions, and Modes of Delivery of Plasma Functionalized Liquid <u>Soukaina Barroug</u> , Orla Nic Shiurdain, Sean Kelly, and Paula Bourke	200
Thu-P-31	Antibacterial effect of Plasma Activated Water against <i>L. monocytogenes</i> and <i>E. Faecalis</i> <u>Ana Sainz-García</u> , Elisa Sainz-García, Félix Gallarta-González, Alpha Verónica Pernía Espinoza, Rodolfo Múgica-Vidal, Ignacio Muro-Fraguas, Ana González-Marcos, María López, Yolanda Sáenz, Fernando Alba-Elías	201
Thu-P-32	Evaluation of Plasma Activated Liquids for Decontamination of Flexible Endoscopes <u>Naomi Northage</u> , Vasyil Shvalya, Martina Modic, Malcolm J. Horsburgh, James L. Walsh	202
Thu-P-33	Investigation of toxicity effects of Plasma Activated Water on a water model plant <i>Lemna Minor</i> <u>Olivera Jovanović</u> , Arian Morina, Nikola Škoro and Nevena Puač	203
Thu-P-34	Effect of plasma-activated water produced in an Air-Operated DBD Coaxial Reactor on <i>Candida albicans</i> Biofilms <u>Victoria Kelly Fonseca Tavares</u> , Felipe de Souza Miranda, Augusto Stancampiano, Jean-Michel Pouvesl3, Pablo Escot Bocanegra, Eric Robert, Rodrigo Savio Pessoa, Cristiane Yumi Koga-Ito	204
Thu-P-35	The influence of Cold Atmospheric Plasma treatment on patient-derived 3-dimensional organoids <u>Jana Baroen</u> , Angela Privat-Maldonado, Evelien Smits, Annemie Bogaerts	205
Thu-P-36	Cold atmospheric plasma treatment of chronic wounds—investigation of the effects of reactive oxygen and nitrogen species on fibrosis-related cellular signaling pathways <u>Juliette Letellier-Bao</u> , Stephan Reuter, Caroline Boudoux, Anie Philip	206

Thu-P-37	Hemostasis by plasma treatment shortens the wound healing duration by bypassing the inflammatory response and proliferation of bone marrow-derived fibroblasts	207
	<u>Emiri Yamamoto</u> , Shinsuke Akita, Sanae Ikehara, Kazuhiko Azuma, Syota Ohki, Yoshihiro Nakano, Shigehito Sakai, Takashi Yamaguchi, Nobuyuki Mitsukawa, Emilio Martinez, Yuzuru Ikehara	
Thu-P-38	Enhancing Wound Healing with Bioprinted Chitosan Hydrogels Treated by Cold Atmospheric Plasma Jets	208
	<u>Noor Mohamad</u> , Masoumeh Ezati, Amir Hashemi, Kateřina Polášková, Inna Zumberg, Vratislav Čmiel, Jan Schäfer, Lenka Zajčková	
Thu-P-39	Using atmospheric-pressure plasma for precise and less invasive suture wounds	209
	<u>Ignacio Muro-Fraguas</u> , Rodolfo Múgica-Vidal, Ana Sainz-García, Elisa Sainz-García, Ana González-Marcos, Letricia Barbosa-Pereira, Ana Rodríguez-Bernaldo de Quirós, Patricia Vazquez-Loureiro, Antia Lestido-Cardama, Fernando Alba-Elías	
Thu-P-40	The <i>plasmACT</i> European Doctoral Network (2024-2027) – Plasma Medicine Against Actinic Keratosis	210
	<u>Sander Bekeschus</u> , Lars Boeckmann, Annemie Bogaerts, Steffen Emmert, Angela Privat-Maldonado, Eric Robert, Klaus-Dieter Weltmann, Thomas von Woedtke, Diana Albrecht, Evelien Smits, Augusto Stancampiano, Ana Sobota, Kristian Wende	
Thu-P-41	Non-thermal Plasma Induces Oxidative Stress Markers Relevant to Wound Healing	211
	<u>Gagana Karkada</u> , Julia Sutter, Jonathan Thomas, Suneel Kumar, Fred C. Krebs, Francois Berthiaume, Katharina Stapelmann, Vandana Miller	
Thu-P-42	The beneficial effect of successive Cold Atmospheric Plasma treatments on <i>in vitro</i> behaviour of human gingival fibroblasts	212
	<u>Andreea-Mariana Negrescu</u> , Leonardo Zampieri, Anisoara Cimpean, Emilio Martinez	
Thu-P-43	Mouse Skin Response to Cold Plasma	213
	<u>Andrea Jurov</u> , Špela Kos, Tanja Blagus, Ivana Sremački, Gregor Filipič, Nataša Hojnik, Anton Nikiforov, Christophe Leys, Maja Čemažar, Gregor Serša, Uroš Cvelbar	
Thu-P-44	Effect of plasma activated ringer lactate and saline solutions on the migration and proliferation of murine melanoma cells (B16F10)	214
	Diego V Neves, Kaique Hergesel, Daiane Lima, Maria Vitoria Fragoso, Keren Moura, Juliana Praxedes, Amanda Lima, Breno Ferrari, Fernando Pradela, Leonilda Santos, Elidiane C Rangel, Elaine Oliveira, <u>Nilson C Cruz</u>	
Thu-P-45	Plasma Controlled Nanogold for Detection and Recognition of Explosives with Machine Learning Assisted SERS	215
	<u>Jaka Olenik</u> , Vasyl Shvalya, Martina Modic, Damjan Vengust, Martin Košiček, Uroš Cvelbar, James L. Walsh	
Thu-P-46	The influence of extracellular DNA on the sensibility of antibiotic resistant bacteria to cold atmospheric plasma	216
	Ibtissam Courti, Thomas Maho, Florent P. Sainct, Philippe Guillot, <u>Cristina Muja</u>	
Thu-P-47	Reconstructed Epidermis Permeation Studies Using a Plasma Jet and Spray Device	217
	Vinodini Vijayaragan, Amaury Rouillard, Sebastien Dozias, <u>Augusto Stancampiano</u> , Pablo Escot-Bocanegra, Catherine Grillon, Eric Robert	
Thu-P-48	Role of plasma and the carrier gas on CO binding with human hemoglobin	218
	Inna Orel, Eloise Mestre, Titaina Gibert, Sebastien Dozias, Roberto Motterlini, <u>Claire Douat</u>	

16:45 – 17:00

Coffee Break

Section: **PLASMA-CELL AND PLASMA-TISSUE INTERACTIONS – BIOLOGICAL AND BIOCHEMICAL REACTIONS**

Hall: **ICPM Session 1**

Chair: **Theresa Freeman**

17:00	Thu-O-8-7	Effects of Cold Atmospheric Argon Plasma Jet Treatment on the Biological Activity of Human Gingival Fibroblasts	146
		<u>Neusa Silva, Joana Marques, Mariana Brito da Cruz, Henrique Luís, António Mata, Susana Sério</u>	
17:15	Thu-O-8-8	Modification of Cellular Receptors as a Potential Antiviral Mechanism of Non-Thermal Plasma	147
		<u>Julia Sutter, Keziah K. Adjei, Benjamin S. Haslund-Gourley, Stephen R. Jennings, Fred C. Krebs, Mary Ann Comunale, Brian Wigdahl, Vandana Miller</u>	
17:30	Thu-O-8-9	Plasma Patch Device for Skin Disease Therapy	148
		<u>Seunghun Lee, Ju-yeon Choi, Ki-Ho Baek, Sang-Hyun Kim, Sung-hoon Jung, Joo-young Park, Do-geun Kim</u>	
17:45	Thu-O-8-10	The Effect of Cold Atmospheric Plasma (CAP) and Plasma Activated Liquid (PAL) on the Proliferation of Mesenchymal Stem Cells (MSCs)	149
		<u>Sara Alsiyabi, Daniela Boehm</u>	
18:00	Thu-O-8-11	Plasma jet characteristics and treatment consequences depend on target properties of several hydrogel and vertebrate tissue models	150
		<u>Alice Martinet, Lea Miebach, Klaus-Dieter Weltmann, Thomas von Woedtke, Steffen Emmert, Sander Bekeschus</u>	
18:15	Thu-O-8-12	Oxidative damage in nucleic acids in human lung cancer cells irradiated with cold atmospheric pressure plasma	151
		<u>Hirofumi Kurita, Yuka Hijii, Khulan Bidbayasakh, Sumire Arai</u>	
18:30	Thu-O-8-13	Synergistic Enhancement of Antibiotic Efficacy Against Biofilms with Cold Plasma	152
		<u>Thomas P. Thompson, Katie Harvey, Jordanne-Amee Maybin, Ross M. Duncan, Paula Bourke, Noreen J. Hickok, Theresa A. Freeman, Brendan F. Gilmore</u>	

Section: **PLASMA FOR PHARMACEUTICAL APPLICATIONS, BIOCHEMICAL AND BIOMOLECULAR ENGINEERING**

Hall: **ICPM Session 2**

Chair: **Matteo Gherardi**

17:00	IT-9	Albumin aggregation by cold atmospheric plasma	17
		<u>Tetsuji Shimizu</u>	
17:30	Thu-O-9-1	Effects of OH radicals on Plasma Gene/Molecular Transfection	165
		<u>Takuto Tokura, Masaki Yamashita, Yoshihisa Ikeda, Susumu Satoh, Masafumi Jinno</u>	
17:45	Thu-O-9-2	Plasma deposition of anti-proliferative drugs for vascular stents	166
		<u>Fiona O'Neill, Chloe Frewen, Liam O'Neill, Paula Bourke</u>	
18:00	Thu-O-9-3	Plasma-activated Hydrogels: A Versatile Drug Delivery Platform for Multiple Clinical Indications	167
		<u>Nishtha Gaur, Naing T. Thet, Alexander Robson, Jontana Allkja, Craig Williams, Gordon Ramage, Toby Jenkins, Robert D. Short</u>	
18:15	Thu-O-9-4	Plasma-activated cryomicroneedles for transdermal drug delivery	168
		<u>Jishen Zhang, Dingxin Liu, Hao Zhang, Li Guo, Mingzhe Rong</u>	
18:30	Thu-O-9-5	Effect of low level of oxidation on protein structures and their function	169
		<u>Maryam Ghasemtarei, Tapio Ala Nissila, Annemie Bogaerts</u>	

20:00 – 22:00

Conference Dinner

Friday, 13 September 2024

Section: PLASMA AGRICULTURAL APPLICATIONS

Hall: **ICPM Session 1**

Chair: **Nevena Puač**

09:45	IT-11	Cold Atmospheric Pressure plasmas uses in the food sector	18
		<u>Romolo Laurita</u> , Alina Bisag, Filippo Capelli, Caterina Maccaferri, Giorgia Gozzi, Silvia Tappi, Beatrice Cellini, Pietro Rocculi, Marco Dalla Rosa, Lucia Vannini Junior Bernardo Molina-Hernandez, Jessica Laika, Lilia Neri, Clemencia Chaves-López, Antonella Ricci, Massimo Mozzon, Lama Ismaiel, Ancuta Nartea, Cinzia Mannozi, Luca Belleggia, Cristiana Cesaro, Roberta Foligni, Matteo Gherardi Vittorio Colombo	
10:15	Fri-O-10-1	Bactericidal and Plant-Growth Effects of Amino-Acid Solutions Irradiated by Electrically-Neutral Oxygen Radicals	220
		<u>Masafumi Ito</u> , Naoyuki Iwata, Kenji Ishikawa, Yasuhiro Nishikawa, Motoyuki Shimizu, Hironaka Tsukakoshi, Masashi Kato, Masaru Hori	
10:30	Fri-O-10-2	Modeling of <i>Aspergillus brasiliensis</i> growth and inhibition by non-thermal plasma	221
		<u>Zdeňková Kamila</u> , Lokajová Eliška, Jirešová Jana, Klenivskyi Myron, Vladimír Scholtz	
10:45	Fri-O-10-3	Potential of non-thermal plasma in the induction of adaptive response in plant seeds	222
		<u>Stanislav Kyzek</u> , Kristína Vargová, Júlia Serdahelyová, Matúš Chalachan, Veronika Medvecká, Petra Šrámková, Sára Pišteková, Jana Makuková, Ivana Kyzeková, Anna Zahoranová, Andrea Ševčovičová, Eliška Gálová	

Section: PLASMA FOR PHARMACEUTICAL APPLICATIONS, BIOCHEMICAL AND BIOMOLECULAR ENGINEERING

Hall: **ICPM Session 2**

Chair: **Eric Robert**

09:45	Fri-O-9-1	Plasma-oxidized proteins cause alterations in antigen-presenting cell maturation	224
		Ramona Clemen, Kevin Arlt, Thomas von Woedtke, <u>Sander Bekeschus</u>	
10:00	Fri-O-9-3	Genome Content Sensitive DNA Optical Analysis with Nanoplasmonics	226
		<u>Vasyl Shavlya</u> , Martina Modic, Cene Skubic, Janez Zavašnik, Uroš Cvelbar	
10:15	Fri-O-9-4	Plasmonic Sensors for small and large entities from Molecules to Monitoring of Biofilm Growth on Surfaces and Their Plasma Cleaning	227
		Aabha Bajaj, Mohammad Abutoama, Anand M. Srivastav, Marwan J. Abuleil, Martina Modic, Vasyl Shvalya, Uroš Cvelbar, <u>Ibrahim Abdulhalim</u>	
10:30	Fri-O-9-5	Boosting transdermal drug penetration by cold plasma – insights on the molecular level	228
		<u>Kristian Wende</u> , Paula Marx, Johanna Striesow, Patricia Lopalco, Thomas von Woedtke, Sander Bekeschus	
10:45	Fri-O-9-6	Expanding plasma-driven biocatalysis using unspecific peroxygenase from <i>Collariella virescens</i> and a capillary plasma jet	229
		<u>Sabrina Klopsch</u> , Tim Dirks, Davina Stoesser, Steffen Schüttler, Judith Golda, Julia E. Bandow	

11:00 Fri-O-9-7 **Local plasma jet application in the oral cavity to combat respiratory virus infections** 230
Thomas von Woedtke, Nancy Mounogou Kouassi, Sander Bekeschus, Ulfilas Hoffmann, Robert Bansemmer, Torsten Gerling, Veronika Hahn, Henry Skowski, Michael Schmidt, Raphael Rataj, Katayoon Hadian Rasnani, Helena Jablonowski, Manuel Hein, Jessica Akoh Arrey, Uwe Mamat, Klaus-Dieter Weltmann, Ulrich E. Schaible, Gülsah Gabriel

Section: **PLASMA LIQUID INTERACTIONS, PLASMA-ACTIVATED LIQUIDS**

Hall: **ICPM Session 1**

Chair: **Zdenko Machala**

11:00 Fri-O-4-1 **Metabolic Disorders in *E. coli* Induced by Electrically Neutral Oxygen Radicals Irradiation of Tryptophane-Containing Solutions** 232
Kenji Ishikawa, Masafumi Ito, Naoyuki Iwata, Yasuhiro Nishikawa, Motoyuki Shimizu, Hironaka Tsukakoshi, Masashi Kato, Masaru Hori, Hiromasa Tanaka

11:15 Fri-O-4-3 **Atmospheric pressure plasma – a chance for wastewater management in an industrial context?** 234
Michal Szulc, Carmen Kirner, Jochen Schein

11:30 Fri-O-4-4 **Combining sub-lethal doses of cold atmospheric plasma with vancomycin-loaded liposomes to eradicate MRSA biofilms** 235
Ross Duncan, Thomas P. Thompson, Vicky Kett, Brendan Gilmore

12:30 – 13:30 **Lunch Break**

14:00 – 15:00 **Closing**

The equivalent electrical circuit for describing the dielectric barrier discharge plasma jet

Marija Puač¹, Nikola Škoro¹, Kinga Kutasi² and Nevena Puač¹

¹Institute of Physics, University of Belgrade, Pregrevica 118, Belgrade, Serbia

²HUN-REN Wigner Research Centre for Physics, Konkoly Thege M. út 29-33, Budapest, Hungary

E-mail: smarija@ipb.ac.rs

The electrical characterization of an atmospheric pressure dielectric barrier discharge (DBD) complemented by the model of equivalent electrical circuit can significantly contribute to a better understanding of plasma behavior. The modeled DBD plasma jet operates with He gas and has two copper electrodes wrapped around a 20 cm long glass tube. The electrodes are 15 mm wide and separated 15 mm from each other. The lower electrode is 15 mm away from the tube end and is powered with high-voltage sinusoidal signal at 30 kHz frequency. The upper electrode and the target holder beneath the jet are grounded. The voltages measured on the $R=100\text{ k}\Omega$ resistors are used for monitoring the currents through grounded electrode and the target ($i_{ge}(t)$ and $i_{te}(t)$, respectively). Three targets with different electrical characteristics are analyzed: Cu, PET and H_2O .

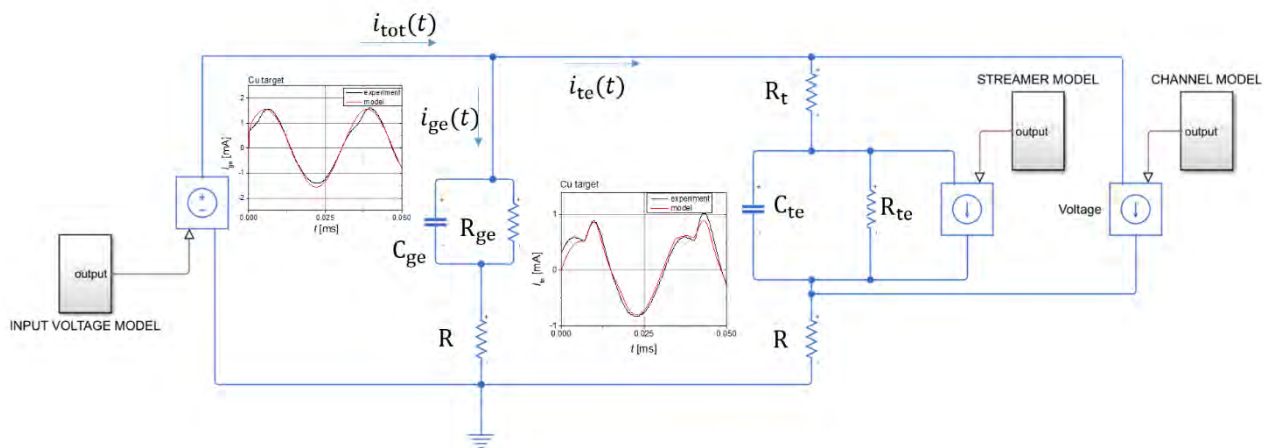


Fig. 1 Schematics of the equivalent electrical circuit representing DBD plasma jet when plasma is on. Waveforms inserted in the picture present comparison of the measured currents and modeled for copper target: left-hand side $i_{ge}(t)$ and right-hand side $i_{te}(t)$.

The model of the equivalent electrical circuit, when plasma is ignited, is presented in Fig.1. Circuit consists of the grounded branch and the target branch. Both have equivalent impedances that correspond to the recorded currents $i_{ge}(t)$ and $i_{te}(t)$, respectively (inserted waveform plots in Fig.1). The shape of the current $i_{te}(t)$ shows a peak appearing only in the last quarter of the positive part of the input voltage amplitude. The peak in the current waveform stem from streamer (bullet) formation and its width corresponds to the third harmonic, oscillating at 90 kHz, with some delay compared to the voltage waveform. That streamer is modeled with controlled current source. Its input port is connected to the mathematical sinusoidal signal with frequency of 90 kHz and predetermined delay. Also, there is a channel appearing only in the negative part of the target current affecting the waveform by increasing the current amplitude. The channel is added in the circuit model as a controlled current source with input port connected to the mathematical sinusoidal signal at 30 kHz with no delay compared to the voltage.

This research was supported by the Science Fund of the Republic of Serbia, 7739780, APPerTAin-BIOM project and MSTDI-451-03-68/2022-14/200024.



PLATHINIUM

PLASMA THIN FILM INTERNATIONAL UNION MEETING

Abstract book

11 - 15 September 2023 - Antibes, French Riviera

www.plathinium.com

Table of content

ORAL PRESENTATIONS.....	4
Tue. 12 Sept. – Morning	4
Auditorium Antipolis.....	4
Ella Fitzgerald room	10
Tue.12 Sept. – Afternoon	15
Auditorium Antipolis.....	15
Ella Fitzgerald room	22
Wed. 13 Sept. – Morning	32
Auditorium Antipolis.....	32
Ella Fitzgerald room	40
Wed. 13 Sept. – Afternoon	47
Auditorium Antipolis.....	47
Ella Fitzgerald room	52
Thu. 14 Sept. – Morning	61
Auditorium Antipolis.....	61
Ella Fitzgerald room	69
Thu. 14 Sept. – Afternoon	76
Auditorium Antipolis.....	76
Ella Fitzgerald room	85
Fri. 15 Sept. – Morning	92
Auditorium Antipolis.....	92
Ella Fitzgerald room	99
POSTER PRESENTATIONS.....	105
Session #1 – Tue. 12 Sept.....	106
Session #2 – Wed. 13 Sept.....	143



PLATHINIUM

PLASMA THIN FILM INTERNATIONAL UNION MEETING

ORAL PRESENTATIONS

- Tuesday 12 September
- Wednesday 13 September
- Thursday 14 September
- Friday 15 September

PROC-P1-195 • Equivalent electrical circuit modeling of a He dielectric barrier discharge plasma jet

M. Puač¹, N. Škoro¹, K. Kutasi², N. Puač¹

¹ *Institute of Physics, Pregrevača 118, University of Belgrade – Belgrade (RS)*

² *Wigner Research Centre for Physics, Budapest (HU)*

A model of an electrical circuit characterizing dielectric barrier discharge (DBD) jet is proposed. Characterization is done by analyzing waveforms, phase shifts and $V-I$ characteristics when plasma is interacting with three different targets: Cu, PET and H₂O, respectively. The schematics of the DBD jet is presented in Figure 1.a). The lower electrode is powered with high-voltage sinusoidal signal at 30 kHz frequency, while the other electrode and target holder are grounded. Scheme of the equivalent electric circuit is presented in Figure 1.b). Left-hand side scheme corresponds to the plasma OFF regime. The circuit is the same for all three targets, R_t is zero, and the grounded elements R_{ge} and C_{ge} do not change. As expected, small changes are observed only in the elements corresponding to the target electrical characteristics, R_{te} and C_{te} . As for the plasma ON regime, it is found that the shape of the $i_{te}(t)$ signal shows a streamer (bullet) appearing in the last quarter of the positive part of the input voltage amplitude. The shape of the streamer current corresponds to the third harmonic, oscillating at 90 kHz, with some delay compared to the voltage. Hence, the plasma ignition is reflected in the form of a large resistor R_t , in orders of $M\Omega$, and by voltage controlled current source in the additional branch of equivalent electric circuit representing streamer current (right-hand side of the Figure 1.b)).

Thanks/Acknowledgement

This research was supported by the Science Fund of the Republic of Serbia, 7739780, APPerTAin-BIOM project and MSTDI-451-03-68/2022-14/200024.

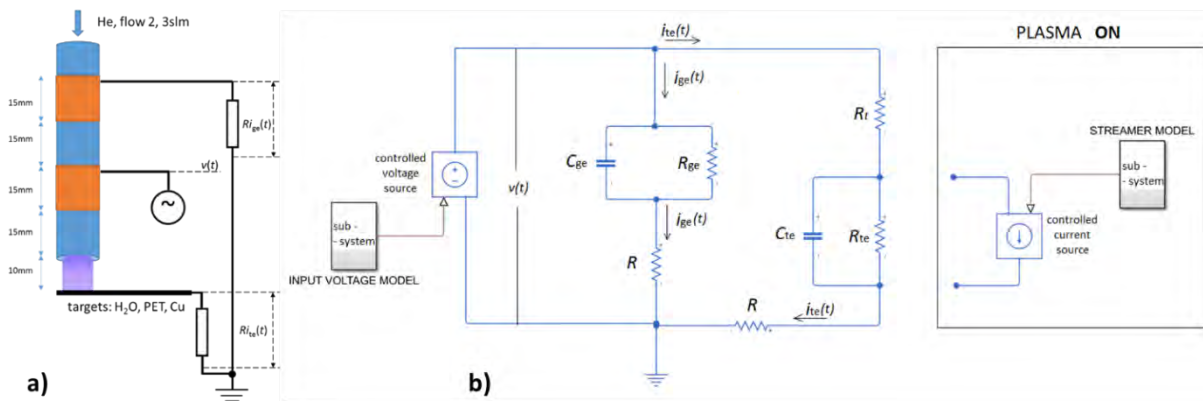


Figure 1. a) Schematics of the experimental setup. Voltages on $R=100\text{ k}\Omega$ resistors are used for monitoring the grounded electrode current $i_{ge}(t)$ and the target current $i_{te}(t)$; b) Schematics of the equivalent electrical circuit. Left-hand side of scheme corresponds to the plasma OFF regime, right-hand side corresponds to the plasma ON regime.



SAPP XXIV

24th Symposium on Application of Plasma Processes
and
13th EU-Japan Joint Symposium on Plasma
Processing

Book of Contributed Papers

Štrbské Pleso, Slovakia
27 Jan - 1 Feb, 2023

Edited by J. Országh, B. Stachová, D. Mészáros, P. Papp, Š. Matejčík



Book of Contributed Papers: 24th Symposium on Application of Plasma Processes and 13th EU-Japan Joint Symposium on Plasma Processing, Štrbské Pleso, Slovakia, 27 January – 1 February 2023.

Symposium organised by Department of Experimental Physics, Faculty of Mathematics, Physics and Informatics, Comenius University in Bratislava and Society for Plasma Research and Applications in hotel SOREA TRIGAN***.

Editors: J. Országh, B. Stachová, D. Mészáros, P. Papp, Š. Matejčík

Publisher: Society for Plasma Research and Applications, Bratislava, Slovakia

Issued: January 2023, Bratislava, first issue

ISBN: 978-80-972179-3-8

URL: <https://neon.dpp.fmph.uniba.sk/sapp/>

Local Organizers

Department of Experimental Physics

Faculty of Mathematics, Physics and Informatics

Comenius University in Bratislava

Mlynská dolina F2

842 48 Bratislava, Slovakia

URL: <http://www.fmph.uniba.sk/>

Tel.: +421 2 602 95 686

Fax: +421 2 654 29 980



Society for plasma research and applications

Faculty of Mathematics, Physics and Informatics

Comenius University Bratislava

Mlynská dolina F2

842 48 Bratislava, Slovakia

E-mail: spvap@neon.dpp.fmph.uniba.sk

Tel.: +421 2 602 95 686



Local Organizing Committee

Štefan Matejčík (chair)

František Krčma

Peter Papp

Juraj Országh

Ladislav Moravský

Veronika Medvecká

International Scientific Committee

24th Symposium on Application of Plasma Processes

Prof. J. Benedikt	Christian-Albrechts-University, Kiel, Germany
Dr. R. Brandenburg	INP, Greifswald, Germany
Dr. Z. Donkó	Hungarian Academy of Sciences, Budapest, Hungary
Dr. T. Field	Queen's University, Belfast, United Kingdom
Prof. S. Hamaguchi	Osaka University, Japan
Prof. F. Krčma	Brno University of Technology, Brno, Czech Republic
Prof. N. Mason	School of Physical Sciences, University of Kent, United Kingdom
Prof. Š. Matejčík	Comenius University in Bratislava, Slovakia
Prof. J. Pawlat	University of Technology, Lublin, Poland
Prof. M. Radmilović-Radjenović	Institute of Physics, Belgrade, Serbia
Prof. P. Scheier	Leopold-Franzens University, Innsbruck, Austria

13th EU-Japan Joint Symposium on Plasma Processing

Prof. S. Hamaguchi	Osaka University, Japan
Prof. N. Mason	School of Physical Sciences, University of Kent, United Kingdom
Prof. Z. Petrović	Institute of Physics, Belgrade, Serbia

Reading Committee

Prof. Š. Matejčík	Comenius University in Bratislava, Slovakia
Prof. F. Krčma	Brno University of Technology, Brno, Czech Republic
Prof. N. Mason	University of Kent, United Kingdom
Assoc. Prof. P. Papp	Comenius University in Bratislava, Slovakia
Assoc. Prof. J. Országh	Comenius University in Bratislava, Slovakia
Assoc. Prof. V. Medvecká	Comenius University in Bratislava, Slovakia

Conference Topics

1. Electrical discharges and other plasma sources
2. Elementary plasma processes and plasma-chemical reactions
3. Theory and modelling of plasmas and plasma processes
4. Plasma-surface interactions
5. Plasma surface treatment for applications
6. Plasmas for nanomaterials
7. Plasma diagnostics
8. Ion mobility and mass spectrometry

Table of Contents

INVITED LECTURES

IL-1	Kinga Kutasi	EFFICIENT DEPOSITION AND TRAPPING OF REACTIVE SPECIES IN LIQUIDS AND HYDROGELS	11
IL-2	Erik Képeš	SPATIOTEMPORAL SPECTROSCOPIC CHARACTERIZATION OF ASYMMETRIC LASER-INDUCED PLASMAS	14
IL-3	Jaroslav Kočišek	DNA ORIGAMI NANOSTRUCTURES FOR STUDIES OF RADIATION DAMAGE	16
IL-4	Jean-Michel Povesle	PLASMA JET INTERACTIONS WITH TARGETS: PHYSICS AND APPLICATIONS	17
IL-5	Nikola Škoro	DEVELOPMENTS OF PLASMA ACTIVATED LIQUIDS FOR AGRICULTURAL AND WATER TREATMENT APPLICATIONS	18
IL-6	Pankaj Attri	CONTRIBUTION OF NON-THERMAL PLASMA IN AGRICULTURE: FOCUS ON PRE-HARVEST TREATMENT	19
IL-7	Jozef Breka	TECHNOLOGICAL 3D PLASMA SOURCES SCALING AND COMPUTATION	20
IL-8	Zdenko Machala	TRANSPORT OF COLD PLASMA REACTIVE SPECIES INTO WATER AND BIO-RELEVANT EFFECTS OF PLASMA-ACTIVATED WATER	21
IL-9	Anna Zahoranová	COLD ATMOSPHERIC PRESSURE PLASMA TECHNOLOGY FOR ECOLOGICAL AGRICULTURE	22
IL-10	Mehrnoush Narimisa	DIAGNOSTICS AND CHARACTERIZATION OF A NOVEL MULTIPURPOSE RF ATMOSPHERIC PRESSURE PLASMA JET FOR MATERIAL PROCESSING	28
IL-11	Vahideh Ilbeigi	DETECTION OF PLANT HORMONES BY ION MOBILITY SPECTROMETRY	33
IL-12	Marián Lehotský	PLASMA ASSISTED POLYMER BIOFUNCTIONALIZATION	36
IL-13	Judith Golda	DIAGNOSTIC CHALLENGES IN ATMOSPHERIC PRESSURE PLASMAS FOR PLASMA CATALYSIS	38
IL-14	Ján Žabka	LABORATORY VERSION OF THE ORBITRAP MASS ANALYZER WITH SEVERAL TYPES OF ION SOURCES HANKA – SPACE INSTRUMENT	39
IL-15	Kanako Sekimoto	FUNDAMENTAL PROCESSES OF ATMOSPHERIC PRESSURE DARK-CURRENT DISCHARGE IONIZATION	40
IL-16	Manabu Tanaka	DEVELOPMENT OF THERMAL PLASMA SOURCES WITH DIODE-RECTIFICATION AND THEIR APPLICATIONS TO NANOMATERIAL FABRICATION	42

	HOT TOPICS	50	
HT-1	Tom Field	SPARK CHEMISTRY: CAN WE CONTROL THE ENERGY OF THE ELECTRONS?	51
HT-2	Michal Hlína	USAGE OF MICROWAVE PLASMA TORCH FOR TREATMENT OF DIFFERENT TYPES OF MATERIALS	52
HT-3	Mateusz Zawadzki	TIME-OF-FLIGHT DIFFERENTIAL ELECTRON SCATTERING FROM MOLECULAR TARGETS: BENCHMARK CROSS SECTIONS	54
HT-4	Piotr Śliwiński	EFFECT OF ELECTRON BEAM REMELTING OF PLASMA SPRAYED Ni-Cr-Re COATINGS	57
HT-5	Petr Dohnal	RECOMBINATION OF COLD MOLECULAR IONS WITH ELECTRONS	64
HT-6	Peter Čermák	COHERENCE TRANSFER SPECTROMETER FOR 2 μm RANGE	66
HT-7	Jan Benedikt	A COMPUTATIONALLY ASSISTED TECHNIQUE TO MEASURE MATERIAL-SPECIFIC SURFACE COEFFICIENTS IN CAPACITIVELY COUPLED PLASMAS BASED ON CHARACTERISTICS OF THE ION FLUX-ENERGY DISTRIBUTION FUNCTION	68
HT-8	Vlasta Štěpánová	DECONTAMINATION OF RASPBERRIES INOCULATED WITH ENTEROCOCCUS FAECIUM BACTERIA USING PLASMA-ACTIVATED GASEOUS MEDIA	71
	YOUNG SCIENTISTS' LECTURES	72	
YS-1	Aleksandra Lavrikova	EFFECTS OF AIR PULSED STREAMER CORONA DISCHARGE ON SINGLE AND MIXED SPECIES BIOFILMS OF S. AUREUS AND P. AERUGINOSA	73
YS-2	Oguz Han Asnaz	NOVEL METHOD FOR THE SYNTHESIS OF CORE-SHELL NANOPARTICLES FOR FUNCTIONAL APPLICATIONS	75
YS-3	Fayza Hassan	TIME RESOLVED SPECTROSCOPY OF DISCHARGES IN CONDUCTING LIQUIDS	76
YS-4	Maren Dworschak	SILICON NANOCRYSTAL SYNTHESIS WITH THE ATMOSPHERIC PLASMA SOURCE HELIXJET	78
YS-5	Kristína Trebulová	IMPACT OF CAPP ON THE YEAST CANDIDA GLABRATA	80
YS-6	Ján Ďurian	PIC/MCC STUDIES OF LOW PRESSURE HELIUM CAPACITIVELY COUPLED RADIOFREQUENCY DISCHARGES WITH A STRUCTURED ELECTRODE	84
YS-7	Ludmila Čechová	PLASMA ACTIVATED WATER: FROM THE SEED GERMINATION TO THE PLANT GROWTH	91
YS-8	Luka Hansen	CHALLENGES DURING THE DESIGN OF A DC MICROPLASMA CELL INTENDED FOR IN SITU TEM	94
YS-9	Ranna Masheyeva	ON THE IN-SITU DETERMINATION OF THE EFFECTIVE SECONDARY ELECTRON EMISSION COEFFICIENT IN LOW-PRESSURE CAPACITIVELY COUPLED RADIO FREQUENCY DISCHARGES	95

YS-10	Tristan Winze	UTILIZING VUV/UV-RADIATION FROM AN ATMOSPHERIC PRESSURE PLASMA JET TO INITIATE PHOTO-CHEMISTRY IN ORGANOSILICON PRECURSORS	99
YS-11	Rezvan Hosseini Rad	HIGH PRESSURE COAXIAL DIELECTRIC BARRIER DISCHARGE FOR CO ₂ SPLITTING BY COMBINED ACTION OF PACKED BED	101
YS-12	Ján Blaško	ELECTRON INDUCED FLUORESCENCE OF NITROGEN	106
POSTER PRESENTATIONS			111
P-01	David Trunec	ABSORPTION SPECTROSCOPY OF GASEOUS PRODUCTS GENERATED BY COPLANAR BARRIER DISCHARGE IN AIR AND N ₂ /O ₂ MIXTURES	112
P-02	Kerstin Sgonina	REACTORS FOR PLASMA-ASSISTED CATALYSIS AT ATMOSPHERIC PRESSURE	115
P-03	Benedek Horváth	EXPERIMENTAL AND COMPUTATIONAL INVESTIGATION OF SURFACE PROCESSES IN RADIOFREQUENCY HELIUM DISCHARGES	116
P-04	Aranka Derzsi	ELECTRON EXCITATION DYNAMICS IN LOW-PRESSURE CAPACITIVELY COUPLED ARGON-OXYGEN PLASMAS	121
P-05	Kamila Shojaa	TIME-RESOLVED SPECTROSCOPY OF DISCHARGES IN CsCl SOLUTIONS	123
P-06	Mária Mat'ášová	CHARACTERIZATION OF MICROGAP VACUUM BREAKDOWNS GENERATED BY PULSED ELECTRIC FIELD	124
P-07	Matej Klas	FIELD EMISSION PARAMETERS OF LARGE AREA PALLADIUM ELECTRODES IN A VACUUM	128
P-08	Piotr Terebun	ANALYSIS OF THE NUMBER AND LENGTH OF GLIDING ARCS FOR DIFFERENT COMPOSITIONS AND FLOW RATES OF THE WORKING GAS	131
P-09	Mateusz Zawadzki	MOLECULAR HYDROGEN MASS STOPPING POWERS FOR LOW-ENERGY ELECTRONS	132
P-10	Dawid Zarzeczny	PLASMA TREATMENT FOR CONDITIONING OF JUICE	134
P-11	Juraj Országh	EXCITATION OF ACETONE INDUCED BY ELECTRON IMPACT	135
P-12	Barbora Stachová	ELECTRON IMPACT EXCITATION OF CARBON MONOXIDE	138
P-13	Dušan Mészáros	LOW ENERGY ELECTRON ATTACHMENT TO CARBON TETRACHLORIDE CLUSTERS	142
P-14	René Cartaya	ELECTRON-INDUCED DEPROTONATION OF ACETIC ACID CH ₃ COOH CLUSTERS EMBEDDED IN ARGON AND OLIGOMERS FORMATIONS	145
P-15	Mate Vass	EFFECT OF GAS TEMPERATURE ON THE ELECTRON DYNAMICS IN AN ATMOSPHERIC PRESSURE RF PLASMA JET BASED ON A HYBRID MODEL	148
P-16	Pankaj Pareek	PRODUCTION MECHANISM OF HYDROGEN PEROXIDE IN TRANSIENT SPARK DISCHARGE AND ELECTROSPRAY SYSTEM	152

P-17	Kateřina Šindelková	CHARACTERIZATION OF PLASMA ACTIVATED WATER FOR BIO-APPLICATIONS	156
P-18	Věra Mazánková	PLASMA POLYMERIZATION OF ANTIBACTERIAL THIN FILMS FROM PROPANE-BUTANE MIXTURE IN ATMOSPHERIC PRESSURE DISCHARGE	159
P-19	Zuzana Měšťánková	USE OF DIRECT APPLICATION OF PLASMA FOR THERAPEUTIC PURPOSES	163
P-20	Sandra Ďurčányová	PREPARATION OF PROTECTIVE HYDROPHOBIC LAYERS ON ALUMINUM USING PLASMA POLYMERIZATION AT ATMOSPHERIC PRESSURE	166
P-21	Aranka Derzsi	PROPERTIES OF LOW-PRESSURE RF DISCHARGES SUITABLE FOR TREATMENT OF ABSORBANTS	169
P-22	Martin Kuřka	MODIFICATION OF MICROPOROUS POLYPROPYLENE MEMBRANES BY PLASMA-INITIATED GRAFTING OF ACRYLIC ACID	170
P-23	František Krčma	SURFACE CLEANING OF ARCHEOLOGIC LEAD BY LOW PRESSURE PLASMA	175
P-24	Joanna Pawłat	COLD ATMOSPHERIC PLASMA FOR PRESERVATION OF BREAD	176
P-25	Jana Šimečková	INFLUENCE OF PAW APPLICATION ON WATER AGGREGATE STABILITY OF SOIL – CONTAINER EXPERIMENT	178
P-26	Martin Muller	PLASMA MODIFICATION OF METAL OXIDE NANOWIRES FOR Zn-AIR BATTERIES	182
P-27	Masoomah Mahmoodi-Darian	COMPARISON OF CONTINUOUS AND PULSED LOW POWER DC SPUTTERED Ti THIN FILMS	183
P-28	Nevena Puac	MASS SPECTROMETRY OF LARGE ASYMETRICAL CCP OXYGEN DISCHARGE	184
P-29	Ladislav Moravský	ATMOSPHERIC PRESSURE CHEMICAL IONIZATION STUDY OF SULPHUR-CONTAINING COMPOUNDS BY ION MOBILITY SPECTROMETRY AND MASS-SPECTROMETRY	186
P-30	Emanuel Matáš	DETECTION OF NO ₂ GENERATED BY APPJ IN ARGON USING IMS	189
P-31	Bartosz Michalczuk	LOW ENERGY ELECTRON ATTACHEMNT BY FLUOROSILANES	194
P-32	Marija Radmilović-Radjenović	SIMULATION STUDIES OF SURGICAL ELECTRODE DESIGN TO PREVENT SPARKING ENHANCED BURNS	196

PROPERTIES OF LOW-PRESSURE RF DISCHARGES SUITABLE FOR TREATMENT OF ABSORBANTS

A. Derzsi¹, B. Horváth¹, K. Kutasi¹, K. Spasic², M. Puač², N. Puač²
and N. Škoro²

¹*Wigner Research Centre for Physics, Budapest, Hungary*

²*Institute of Physics, Belgrade, Serbia*

E-mail: derzsi.aranka@wigner.hu

Particle-in-Cell/Monte Carlo Collisions simulations are performed to provide a detailed characterization of low-pressure capacitively coupled radiofrequency gas discharge plasmas suitable for treatment of absorbants. Based on the simulations, discharge characteristics such as particle densities, and particle flux and energy distributions at the surfaces relevant for treatment of Zeolite are determined.

Zeolite has long been recognized as a mineral with excellent absorptive properties. This material, made up of arrays of aluminum, silica, and oxygen, has been recently introduced as a novel microporous material suitable for application in water decontamination. Since it is a porous material, the absorption process results in not only capturing particles between grains, but also insertion of the particles into its pores. Due to its high effective surface area, desorption is typically performed using suitable solutions. However, this way of Zeolite regeneration proved to be ineffective for some adsorbed pharmaceuticals. Experimental investigations performed so far showed that in this case regeneration can be efficiently performed by plasma treatment which also represents an efficient and ecologically responsible procedure. These procedures are based on the interaction of adsorbed particles and chemically active species created in the plasma. However, the desirable effects can be achieved only for a narrow range of treatment conditions. For the reliable, knowledge-based optimization of the applications, a detailed characterization of the plasma reactor used for surface treatment is required, including information on the plasma properties and surface processes. In this work, one-dimensional in space and three dimensional in velocity space (1d3v) Particle-in-Cell/Monte Carlo Collisions (PIC/MCC) simulations are performed in low-pressure capacitively coupled plasmas in Argon, under conditions corresponding to the experiments for treatment of Zeolite (4.5 cm electrode gap, driving frequency of 13.56 MHz, pressures < 600 mTorr, voltage amplitudes < 450 V). For these conditions, the voltage-current characteristics, as well as the power and emission spectrum for the discharge are available from the experiments. In the simulations, electrons, Ar⁺ ions, and fast Ar atoms are traced. As surface processes, secondary electron emission due to heavy particles and elastic reflection of electrons are considered. The PIC/MCC simulations provide information on many plasma parameters and distributions of interest, such as densities of the traced particles and their flux and energy distribution at the surfaces, the spatiotemporal distribution of the electric field, the power absorption and energy of particles, as well as the ionization and excitation dynamics in the discharge.

Acknowledgement: This work was supported by the grant 2019-2.1.11-TÉT-2020-00162 “Characterization of radiofrequency gas discharges applied for surface treatment” of the Hungarian National Research, Development and Innovation Office and bilateral project Hungary-Serbia (2021-2023).

Bulletin of the American Physical Society

73rd Annual Gaseous Electronics Virtual Conference

Volume 65, Number 10

Monday–Friday, October 5–9, 2020; Time Zone: Central Daylight Time, USA.

Session UR2: Modeling and Simulation: Breakdown and Kinetics

1:00 PM–2:45 PM, Thursday, October 8, 2020

Chair: Matthew Hopkins, Sandia National Laboratories NM

Abstract: UR2.00005 : Breakdown in rf and dc fields*

2:00 PM–2:30 PM Live

[Preview Abstract](#)

[← Abstract →](#)

Author:

Dragana Maric

(Institute of Physics Belgrade, University of Belgrade, Serbia)

In this presentation new developments in measurements of the breakdown in radiofrequency fields will be presented together with results of Monte Carlo simulations that reveal physical causes for the features of breakdown curves, scaling and the importance of surface processes and of attachment of electrons will be examined. It has been found that in the two valued branch of the breakdown curve in one end electrons never reach region close to electrodes while for the higher voltages they dominantly collide with electrodes where they may disappear or be reflected. The nature of the dominant ionization is different in two branches. A new technique for the detection of the rf breakdown at low pressures, based on a balanced capacitive bridge will also be presented. The technique eliminates common problems in rf breakdown measurements and enables a precise time-domain tracking of the breakdown process. The presentation will be completed by the results of studies of dc breakdown and high E/N transport in alcohol vapors and in water vapor. Work done in collaboration with: Marija Pualv{c}, Antonije \DJ or'dj evil{c}, Jelena Marjanovi{c}, Gordana Malovi{c} and Zoran Lj. Petrovi{c}

*MESTD of Serbia, projects ON171037 and III41011; and SASA project F133

Bulletin of the American Physical Society**72nd Annual Gaseous Electronics Conference**

Monday–Friday, October 28–November 1 2019; College Station, Texas

Session DT3: Modeling and Simulation I

10:00 AM–12:15 PM, Tuesday, October 29, 2019

Room: Century III

Chair: Xiaopu Li

Abstract: DT3.00004 : Modeling of RF breakdown in different atmospheres*

10:45 AM–11:00 AM

[Preview Abstract](#)[← Abstract →](#)**Authors:**Zoran Petrovic
(Institute of Physics, University of Belgrade, Serbia)Marija Puač
(Institute of Physics, University of Belgrade, Serbia)Antonije Dorđević
(School of Electrical Engineering, University of Belgrade, Serbia)

Physical background of radio-frequency (RF) breakdown can be analyzed by observing evolution of electron swarm between two electrodes. That leads to Monte Carlo method as a superior technique for RF-breakdown investigation. After analysis of voltage breakdown curve in argon [1], we are now focusing on RF breakdown in different planetary atmospheres. Starting point is gas mixture that represents air, consisting of 80[%] N_2 and 20[%] O_2 . Peculiar feature of this mixture is appearance of the second minimum at lower pressures in voltage breakdown curve. This minimum is direct consequence of the secondary electron emission at electrodes by ion bombardment. By observing spatial plots of electrons concentration, mean energy and rate of ionization, we have analyzed how changes in pressure/voltage at fixed value of voltage/pressure determine the shape of the voltage breakdown curve. On the other hand, investigation of RF breakdown in atmosphere of Mars can address whether devices for power electronics and telecommunications may have problems due to an induced breakdown. As the pressure at Mars surface is low, it is close to the minimum of the breakdown curve and RF breakdown may be induced by relatively low voltages. [1] Pualv[ć] et al, Plasma Sources Sci. and Technol. 27 (2018) 075013.

*Projects SASA 133 and 155

New phenomenology of gas breakdown in DC and RF fields

Zoran Lj Petrović^{1,3,4}, Jelena Sivoš¹, Marija Savić¹, Nikola Škoro¹, Marija Radmilović Rađenović¹, Gordana Malović¹, Saša Gocić² and Dragana Marić¹

¹Institute of Physics, University of Belgrade, POB 68, 11080 Zemun, Serbia

²Faculty of Natural Sciences, University of Niš, 33 Višegradska, 18000 Niš, Serbia

E-mail: Zoran@ipb.ac.rs

Abstract. This paper follows a review lecture on the new developments in the field of gas breakdown and low current discharges, usually covered by a form of Townsend's theory and phenomenology. It gives an overview of a new approach to identifying which feedback agents provide breakdown, how to model gas discharge conditions and reconcile the results with binary experiments and how to employ that knowledge in modelling gas discharges. The next step is an illustration on how to record volt-ampere characteristics and use them on one hand to obtain the breakdown voltage and, on the other, to identify the regime of operation and model the secondary electron yields. The second aspect of this section concerns understanding the different regimes, their anatomy, how those are generated and how free running oscillations occur. While temporal development is the most useful and interesting part of the new developments, the difficulty of presenting the data in a written form precludes an easy publication and discussion. Thus, we shall only mention some of the results that stem from these measurements. Most micro discharges operate in DC albeit with complex geometries. Thus, parallel plate micro discharge measurements were needed to establish that Townsend's theory, with all its recent extensions, is still valid until some very small gaps. We have shown, for example, how a long-path breakdown puts in jeopardy many experimental observations and why a flat left-hand side of the Paschen curve often does not represent good physics. We will also summarize a kinetic representation of the RF breakdown revealing a somewhat more complex picture than the standard model. Finally, we will address briefly the breakdown in radially inhomogeneous conditions and how that affects the measured properties of the discharge. This review has the goal of summarizing (rather than developing details of) the current status of the low-current DC discharges formation and operation as a discipline which, in spite of its very long history, is developing rapidly.

1. Introduction: Townsend's theory and low-current DC discharges - 100 years ago and now

With the development of basic phenomenology and theory of gas breakdown, Townsend's theory was forged some 100 years ago [1-3]. In this paper we shall give a review of how in the past 20 years the basic Townsend's theory and phenomenology have been revived, extended, revitalized and put in perspective of modelling higher current technological discharges and plasmas. This was primarily done by the groups of Art Phelps and the Gaseous Electronics Laboratory in Belgrade.

³ Author affiliation: also at Serbian Academy of Sciences and Arts, Belgrade, Serbia.

⁴ To whom any correspondence should be addressed.



Recent advances in diagnostics and modelling of complex plasma systems opened an opportunity to revisit the breakdown in gases both in DC and RF fields and also for micro gaps. We shall first discuss the experimental techniques to determine the breakdown voltage. Typical errors, such as neglecting the long-path breakdown on the left-hand side of the Paschen minimum, conditioning of the electrode and measuring properties within an unstable (oscillating) regime, will be covered briefly. In addition, we shall describe a proper methodology to establish volt-ampere (V - I) characteristics and how to use those with the goal of determining the breakdown voltage and the secondary electron yields.

Time-resolved imaging [4] provides us with information on the development of the anatomy of the discharge and its different modes. Using the spatial profile one may decide which of the mechanisms dominate the discharge. The Townsend regime is the low-current diffuse discharge with exponential growth towards the anode [5]. It is necessary to observe such a profile to ascertain that the discharge operates in the Townsend regime where Townsend's theory may be used to establish the condition for breakdown and effective secondary electron yield. The temporal development of the normal glow or abnormal glow following the breakdown reveals transient multi-regime operation that requires a new paradigm.

When considering volt-ampere characteristics, one may first observe the negative differential resistance in the Townsend regime which may be explained by a combination of space-charge effects and an energy-dependent secondary electrons yield. Thus, V - I characteristics should be used in addition to the Paschen curve to determine the secondary electrons yields. With the newly found field of discharges in and above liquids, we have also analyzed breakdown in water vapor and ethanol [6,7].

RF and microwave breakdowns have a different phenomenology as the secondary ions production of electrons at the cathode may not be necessary. Yet the RF breakdown is prone to phenomena not often observed in DC breakdowns, like S shaped (double valued) Paschen-like curves, frequency/gas number density scaling and additional mechanisms like multipactors. The principal experimental problem with the RF breakdown is the magnitude of the displacement current that thwarts the measurement of the conduction current making it difficult to ascertain the initiation of the discharge.

2. Gas breakdown, feedback mechanism, secondary electron yields and how to use them

Traditionally, the gas breakdown is characterized by Paschen curves. In figure 1 we show one such example of Paschen curves for the topical water vapor and ethanol vapor [6,7].

While most people will argue (including the present authors) that the Paschen law itself is developed with limiting assumptions

$$V_b = \frac{Bpd}{\ln(Apd) - \ln\left[\ln\left(1 + \frac{1}{\gamma}\right)\right]}, \quad (1)$$

the breakdown equation from the Townsend's law is in principle exact if the assumptions of the primary feedback through ions are correct:

$$\gamma(E/N)\left(e^{\alpha(E/N)d} - 1\right) = 1. \quad (2)$$

Different forms of analytical laws have been employed for the DC breakdown in order to provide some insight [8,9], but one needs to be aware of the approximate nature of some of the basic formulae. Still, the same limitations that enter the analytical form of Paschen law may enter the implementation

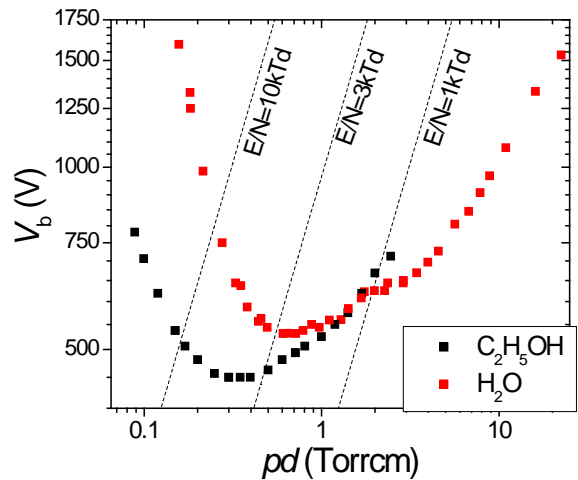


Figure 1. Paschen curves for water [6] and ethanol vapor [7].

of equation (2). Over the years, a large amount of data on γ have been accumulated, yet seldom those have been compared and systematically collected. Even more importantly, comparisons to binary collision (beam-surface) experiments [10] have been almost avoided in the literature presumably due to poor agreement (both qualitative and quantitative). One example where both systematic collection of data and comparisons to binary experiments have been made is the paper of Phelps and Petrović [3].

In figure 2 we show a comparison of the secondary electron yields obtained from Paschen curves in argon for a range of experiments [3]. These should be compared with a constant yield of 0.08 obtained by beam experiments with an atomically clean surface [10] or to the dot-dash line obtained for the same conditions of the cathode as found in discharge experiments. Discharge results are one order of magnitude too high at higher E/N , one order of magnitude lower at moderate E/N and two orders of magnitude higher at the lowest E/N . Phelps and Petrović managed to reconcile the binary collision data and the discharge results by including the following:

- ionization coefficient fitted in a wide range of E/N ;
- a region close to the cathode where electrons gain energy and become in equilibrium with the local field, the simplest way of representing this being using a delay distance d_0 ;
- ion-induced yields at the cathode, modified to represent surfaces that are not atomically clean;
- back-diffusion, i.e. the return of newly emitted electrons back to the cathode;
- secondary electron production by metastables;
- secondary electron production by fast neutrals;
- secondary electron production by resonant radiation – the photo effect;
- trapping of resonant radiation;
- secondary electron production by fast neutrals;
- secondary production due to molecular emission.

The solid and dashed lines in figure 2 indicate the model predictions based on binary collision data (for two limits of possible contributions by molecular radiation). These two lines encompass most of the available experimental data. The good agreement with the experiments shows that all pertinent processes have been included. It also shows that the process of secondary yields modelling may be quite complex and quite challenging due to the need for a wide range of data.

The fact that Townsend's theory could associate all the yields with the flux of ions is because all fluxes are proportional to the electron flux and the system is linear in the breakdown-Townsend discharge phase. On the other hand, one cannot expect linearity to hold for higher current modes, such as glow discharges. For those, one is left with fitting the experimental data. Thus, we compared the fitting procedure with one based on the breakdown data from Phelps and Petrović [3]. We found [11] that fitting of the glow discharge is well represented by the procedure recommended for the breakdown data [3], except when pd is quite low and fast neutral effects become dominant. Yet, for RF discharges, for example, or for some more complex geometries, one needs to provide a clear guidance as to how the secondary electron yield may be modelled. Also, we need a considerable effort to provide the data for a number of relevant gases, as argon is the only gas covered so far by the detailed analysis.

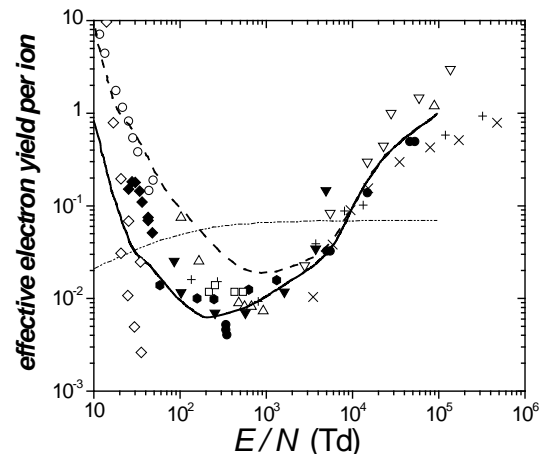


Figure 2. Effective secondary electron yield γ for argon obtained from breakdown data [3]. The different types of points indicate different experiments - see [3]. The dot-dash curve shows binary collision experiment data.

3. Volt-ampere characteristics and spatial emission profiles

There are two ways to determine the breakdown voltage. The first option is very accurate albeit very difficult – one can extrapolate pre-breakdown currents. The second one, favored by our group, is to establish a self-sustained discharge in the low-current diffuse, i.e. Townsend, discharge and then extrapolate the measurements to zero current. All other techniques suffer from arbitrariness, either induced by the long statistical time lags or by a direct transition to the glow regime. The Townsend's regime is recognized by an exponential growth peaking at the anode and a normally broad diffusion-determined profile over the entire surface [5,12], as can be seen in figure 3.

In conducting such measurements, we (re)established that in the Townsend regime one has a negative differential resistance. As the effective resistance of the discharge is negative, sometimes, coupled with the external circuit, the overall loop resistance may become negative and oscillations may occur [13,14]. As it turns out, the space charge due to ions increases the field in front of the cathode, which increases the electron production allowing a lower field elsewhere and thus the overall voltage is reduced [14,15]. Thus, the dependence of γ on the mean energy is the reason for the negative differential resistivity, brought about by space charge induced electric field and represented as a current dependence of γ . As the discharge approaches constriction, non-linearities become important [16] and a sudden transition eventually takes place. It has also been shown that if γ were constant, the slope of the V - I characteristics in Townsend's regime could become positive [16]. Thus one may conclude that for the full representation of the secondary electron yield one needs to fit not only the Paschen curve but also the V - I characteristics. The realm of oscillations often precludes us from achieving stable operation in Townsend's regime but it is also a source of information on important processes. Thus, fitting of the induced damped or free running oscillations may reveal identity of the dominant ionic species, multiplication and may be related to basic transport properties of relevant particles.

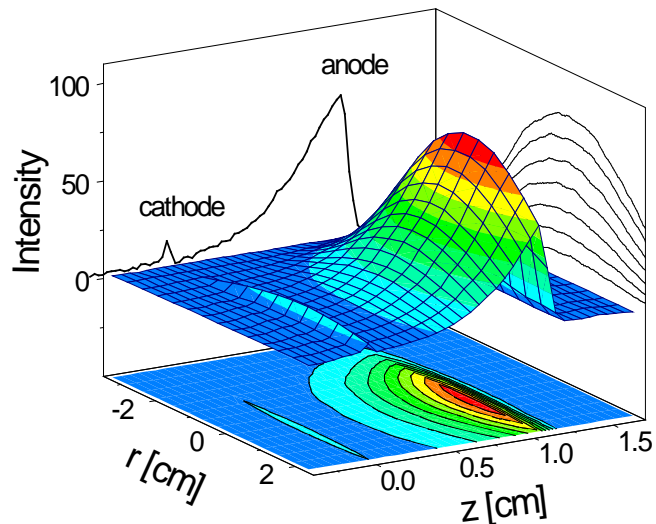


Figure 3. Spatial profile of the Townsend's regime low-current diffuse discharge [12].

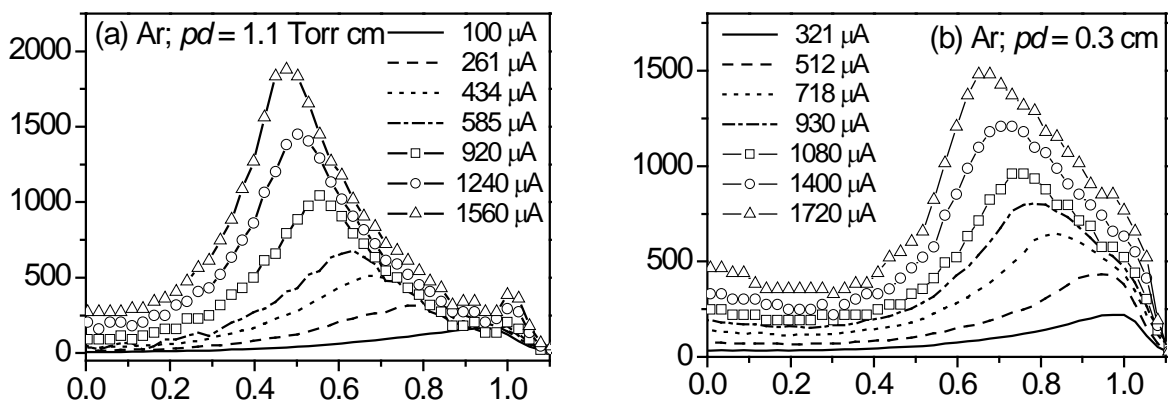


Figure 4. Axial profiles of higher current discharge regimes in argon, at (a) $pd = 1.1$ Torr cm (close to the Paschen minimum); (b) $pd = 0.3$ Torr cm (in the left-hand branch of the Paschen curve).

Another important aspect that stems from figure 3 is that spatial profiles not only give us information on the regime of operation (see figure 4 – the peak in front of the anode is for Townsend's low current discharges, the peak in the bulk corresponds to the glow discharge) but also (if put on an absolute scale) a basis to establish absolute cross sections and even profile of the field. It also shows whether and to what extent is equilibrium (with the field) developed or whether fast neutral excitation is important as recognized by the peak right in front of the cathode.

4. Scaling of the basic properties of micro discharges

Micro discharges were basically developed to take advantage of the non-equilibrium plasma that is formed around the Paschen minimum, but at a much higher pressure. Atmospheric pressure would require a 10 μm gap. On the other hand, to achieve a stable operation at high pressures one needs to use complex geometries as it proved very difficult to operate parallel plate micro discharges. Yet, many authors have assumed parallel plate geometries with narrow strips crossing at small distances and assumed that the breakdown occurs at the shortest distances. This has led to a number of papers where the left hand side of the Paschen curve showed no or little variation that could be erroneously interpreted as the onset of field emission (that was predicted to occur only for $d < 10 \mu\text{m}$ [9]). We have made an effort to perform measurements in well defined and contained parallel plate discharges, to test the applicability of Townsend's phenomenology at small gaps [17].

Before proceeding to any modelling, we needed to test the laws of scaling, which for low pressure collision dominated discharges are E/N , pd and jd^2 (and also ω/N and B/N for time varying fields and for magnetic fields). The critical scaling is due to the current density j . Rarely are the V - I characteristics represented through j (as it should be) and even then it is not stated that j is actually determined by dividing the current by the entire area of the electrodes. In reality, however, constriction dominates in the glow regime. Even in the Townsend's and in the abnormal glow regimes the radial profile is quite different and so is the effective area. Taking advantage of transparent yet conducting materials for electrodes and also of ICCD cameras, we were able to record V - I characteristics and scale them to the real current density even in cases of complex constricted modes. First, we established that in the normal size discharges, when the current density is properly determined, it remains constant throughout the glow regime (so it is represented by a single point in V - I characteristics [18]).

Secondly, we have been able to show that for discharges bordering on micro discharges (0.5 and 1 mm gaps) the jd^2 scaling works and finally we have extrapolated those findings (by using pD scaling where D is the diameter of the constricted region) to smaller gaps where we could not easily record the current profiles [17]. It was found, as can be seen in figure 5, that a Townsend type of scaling holds at those gaps until perhaps some smaller geometries where field emission really comes into play [19]. We have even shown that the spatial profiles scale well so that the ionization coefficient could be determined rather accurately from the axial emission profile of micro discharges [20].

It was also shown that the Paschen curves obtained for micro discharges (and sometimes even for the standard size discharges) that do not show a change of voltage on the left hand side beyond the minimum are due to an incorrectly assumed shortest distance for the gap when long path breakdown was allowed [21]. Reducing the chances for the long path breakdown brings back the Paschen curve to agreement with that obtained for standard dimensions/pressures.

The fact that we proved scaling and also were able to obtain accurate readings of ionization coefficients proves that it is possible to apply Townsend's phenomenology and even to some degree theory to micro discharges. The jd^2 scaling allows Townsend regime to operate at considerably higher current densities.

5. Time resolved measurements

A preliminary publication of our results on time dependent recordings of the development of the breakdown and DC discharge regimes was given in [9,22], while the majority of the data remain unpublished. The results may be summarized as follows. During the initial stage, the discharge passes through the Townsend regime and, as the current increases, glow and abnormal glow regimes are visited. During the minimum of oscillations, the discharge almost immediately returns to the

Townsend regime and then changes occur again and again following oscillations in current. Studies such as this one performed for a parallel plate geometry are needed to provide the background for understanding developments in more complex geometries [23] and different scales.

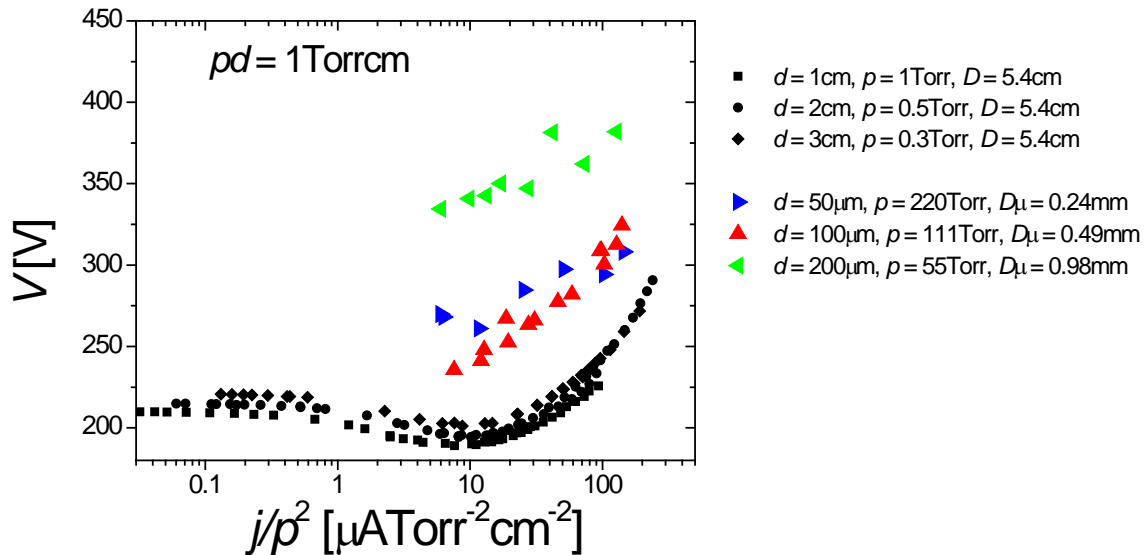


Figure 5. V - I characteristics for standard size and micro discharges obtained by using the jd^2 scaling and pD scaling for the size of the constricted regions. One should not pay attention to the actual vertical scale, normally it is taken care of by subtracting the breakdown voltages in each case, but in the case of micro discharges we could not make accurate measurements as it was not possible to achieve stable operation in the Townsend regime. The vertical scale variations are due to different conditions on the electrodes surface [17].

6. Discharges with inhomogeneous cathodes

The usual assumption in the low current limit is that the discharge is uniform over the entire surface and the radial profile is the solution to the diffusion equation. Only in the higher current (glow) regime a constriction develops and only when the field ceases to be constant along the axis. This has been questioned recently for micro discharges when it was found that the scaling laws are maintained only when an assumption of localized modes is made, the modes that have a dimension proportional to the diffusion length for the given pressure [17]. The problem is hindered further by the high pressure that reduces the diffusion length and by the fact that the ratio of gap to radius becomes very small in practical experiments [17].

We have, however, observed localized discharges in Townsend regime for standard size discharges (1 cm) and moderately low pressures [24]. In figure 6 we show one such example in nitrogen where the discharge is limited in the radial direction by the region of deposited material due to numerous pulses in the high current mode. It is clear that the deposited region has a lower secondary electron yield γ and thus the discharge cannot be self-sustained over that area for the given voltage. In order to overcome this region of reduced γ , the volt-ampere characteristics have to be quite different as compared to the one with pristine cathode. Even a positive differential resistance is observed [24].

The characteristics of such a discharge may be a prototype for the breakdown in pulsed DC discharges where numerous discharges change the properties of the cathode considerably. In addition, one may construct cathodes of different materials and design desired characteristics. For example, cathodes coated by a semiconductor [25, 26] have been often used for achieving some properties that are not easily accessible by conducting electrodes. The high resistance of the semiconductor which is in the innermost circuit assures a broader range of stable operation [14]. Combining conducting and semiconductor materials may help reduce the breakdown potential while achieving a V - I characteristic that is less prone to oscillations.

7. RF breakdown

When rate of change of the field is such that ions cannot complete their trajectories, then it is possible to operate in conditions when electrons may be the only particles sustaining the discharge. The feedback is provided by returning electrons in the second half of the period and thus a full circle is achieved. It has been assumed in old textbooks and papers [27] and in more recent papers [28, 29] that an optimum breakdown condition is achieved when the average electron can cross the gap in one half period. In fact, the breakdown condition has been used to obtain experimental values of the drift velocities for RF fields and convert them to DC values by assuming that in RF fields the drift velocity is a sinus function peaking with the DC drift velocity and having no delay [29]. We modelled the RF breakdown using a detailed Monte Carlo

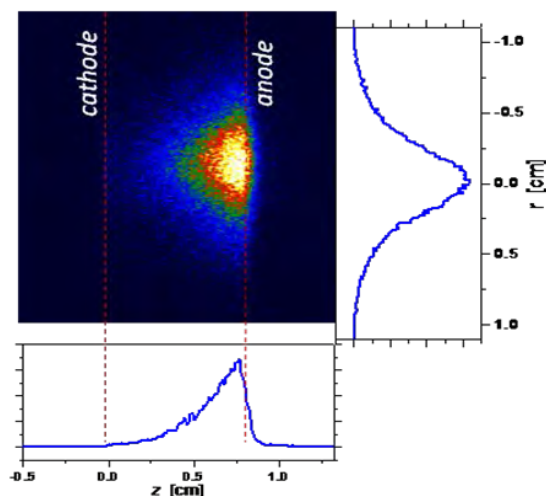


Figure 6. Townsend regime discharge in N_2 with Cu cathode and for $d = 0.8$ cm, $D = 2$ cm, $p = 2$ Torr and $V_b = 310$ V. The axial profile shows exponential growth peaking at the anode while the radial profile is very narrow covering only a small part of the diameter (D).

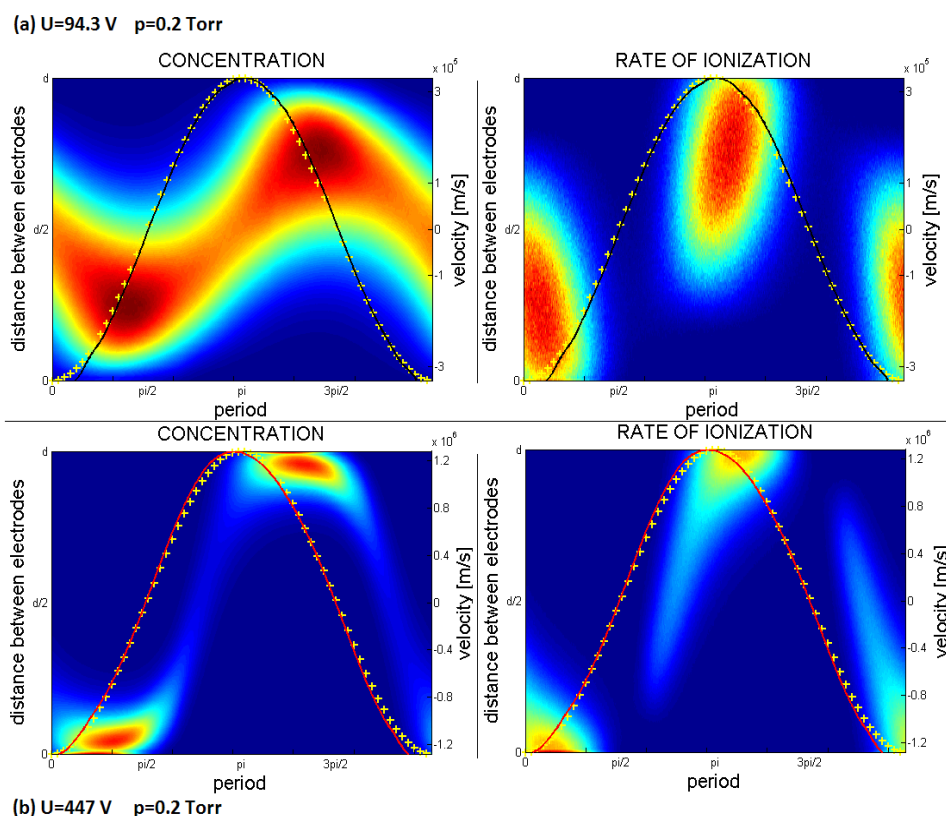


Figure 7. Development of density and ionization rate for the breakdown of RF swarms. Solid curves represent mean velocity (different colours are for better contrast), while the dotted sinusoidal lines represent inversed AC field. Both curves are for 0.2 Torr; the top curves are for the minimum breakdown voltage (93 V) while the bottom curves are for the maximum breakdown voltage (447 V) [30].

representation of all the collisions and field dependence on time. Figure 7 shows the temporal development of the concentration of electrons and of the ionization rate [30]. As the quasi-Paschen curve for the RF breakdown has double values for breakdown voltage at the same pd (for a range of pd) we show results at the lower and at the higher breakdown point. Outside these borders the discharge cannot be ignited. At the lower point, the breakdown condition is achieved by merely matching the production without much of the electrodes overlapping with the swarm. At the higher end, however, the swarm overlaps considerably with the electrodes thus representing significant losses to the electrodes. At the same time, the peaking ionization must compensate for all the losses.

We found that, while the standard explanation of the RF breakdown is very good, still some fine tuning needs to be done by a full kinetic representation (such as a Monte Carlo simulation) to be able to describe all the intricacies. In addition, one needs to extend our model by the contribution of ions and fast neutrals as well as photons. These will modify the Paschen like curve and hopefully make it more realistic but for a wide range of conditions one may find that electrons dominate in sustaining the plasma. We also have to include the secondary electrons formed by the electron impact on electrodes. This effect will lead to the so-called multipacting modes.

One should also note that numerous attempts to use analytical and semi analytical models based on simplified expressions for the basic properties have migrated from DC discharges to the RF breakdown. These results provide insight into pertinent processes [31-34] but require some form of fitting to provide quantitative agreements.

8. Conclusions

The oldest chapter in the book on plasma physics, the breakdown and low current discharges, has been changed tremendously in the past twenty years. The main agent facilitating the feedback needed to achieve DC breakdown, the ions colliding with surfaces, have been changed to include photons, fast neutrals, metastables as well as ions. By including all these processes, as well as back-diffusion [3,35] one was able to predict effective yields and Paschen curves based on the binary collision data [3].

The field of low pressure DC discharges proved to be a fertile ground for both fundamental studies and for obtaining and testing the applicability of the fundamental data that would eventually be used for modelling of more complex systems. Extensions to micro discharges and RF breakdown have been made, together with first attempts to model RF plasmas with secondary electron yields [36] as obtained in a more detailed and recent analysis.

With the new drive for benchmarking plasma modelling systems [37], we believe that the best strategy would be to start from the swarm benchmarks and then use the negative differential resistance of a DC Townsend discharge as a benchmark for space charge effects and also use some additional breakdown properties. This would provide clear and simple experimental observables that may be modelled exactly and independently and provide the next step for more complex plasma benchmarks.

Acknowledgement

This paper has been completed under the overall support of projects 171037 and III41011 of the Ministry of Education and Science of Serbia, and project 155 of the Serbian Academy of Sciences and Arts. Numerous discussion, shared research and data and ideas from the late Art V. Phelps are gratefully acknowledged.

References

- [1] Townsend J S 1910 *The Theory of Ionization of Gases by Collision* (Constable, London)
- [2] Townsend J S 1915 *Electricity in Gases* (Oxford: Clarendon) 313
- [3] Phelps A V and Petrović Z Lj 1999 *Plasma Sources Sci. Technol.* **8** R21
- [4] Marić D, Malović G and Petrović Z Lj 2009 *Plasma Sources Sci. Technol.* **18** 034009
- [5] Petrović Z.Lj. and Phelps A.V. 2009 *Phys. Rev.E* **80** 016408
- [6] Škoro N, Marić D, Malović G, Graham W G and Petrović Z Lj 2011 *Phys. Rev. E* **84** 055401R
- [7] Petrović Z Lj, Sivoš J, Škoro N, Malović G and Marić D 2013 *Bul. Am. Phys. Soc. Ser. II* **58/8**

HW1 35

- [8] Kihara T 1952 *Rev. Modern Phys.* **24** 45
- [9] Radmilovic-Radjenović M and Lee J K 2005 *Phys. Plasmas* **12** 063501
- [10] Hagstrum H D 1954 *Phys. Rev.* **96** 336
- [11] Marić D, Hartmann P, Malović G, Donko Z and Petrović Z Lj 2003 *J. Phys. D: Appl. Phys.* **36** 2639
- [12] Petrović Z Lj, Donko Z, Marić D, Malović G and Živanov S 2002 *IEEE Trans. Plasma Sci.* **30** 136-7
- [13] Petrović Z Lj and Phelps A V 1993 *Phys. Rev. E* **47** 2806
- [14] Phelps A V, Petrović Z Lj and Jelenković B M 1993 *Phys. Rev. E* **47** 2825
- [15] Živanov S, Živković J, Stefanović I, Vrhovac S and Petrović Z Lj 2000 *Eur. Phys. J. AP* **11** 59
- [16] Nikolić M, Đorđević A, Stefanović I, Vrhovac S and Petrović Z Lj 2003 *IEEE Trans. Plasma Sci. PS* **31** 717
- [17] Petrović Z Lj, Škoro N, Marić D, Mahony C M O, Maguire P D, Radmilović-Radenović M and Malović G 2008 *J. Phys. D: Appl. Phys.* **41** 194002
- [18] Škoro N, Marić D and Petrović Z Lj 2008 *IEEE Trans. Plasma Sci.* **36** 994
- [19] Radmilović-Radjenović M, Matejčik Š, Klas M and Radjenović B 20013 *J. Phys. D:-Appl. Phys.* **46** 015302
- [20] Kuschel T, Stefanović I, Malović G, Marić D and Petrović Z Lj 2013 *Plasma Sources Sci. Technol.* **22** 045001
- [21] Marić D, Škoro N, Maguire P D, Mahony C M O, Malović G and Petrović Z Lj 2012 *Plasma Sources Sci. Technol.* **21** 035016
- [22] Marić D, Malović G and Petrović Z Lj 2007 *J. Phys.: Conf. Series* **86** 012009
- [23] Wagenaars E, Bowden M D and Kroesen G M W 2005 *IEEE Trans. Plasma Sci.* **33** 254
- [24] Gocić S R, Škoro N, Marić D and Petrović Z Lj 2010 *20th ESCAMPIG* (Novi Sad Serbia July 2010) P3.17
- [25] Kurt H, Çetin S, and Salamov B G 2011 *IEEE Trans. Plasma Sci.* **39** 1086
- [26] Portsel L M, Lodygin A N and Astrov Yu A 2009 *J. Phys. D: Appl. Phys.* **42** 235208
- [27] Gill E B and von Engel A 1949 *Proc. R. Soc. A* **197** 107
- [28] Lisovskiy V A and Yegorenkov V D 1994 *J. Phys. D: Appl. Phys.* **27** 2340
- [29] Lisovskiy V, Booth J-P, Landry K, Douai D, Cassagne V and Yegorenkov V 2006 *J. Phys. D: Appl. Phys.* **39** 660
- [30] Savić M, Radmilović-Radjenović M, Šuvakov M, Marjanović S, Marić D and Petrović Z Lj 2011 *IEEE Trans. Plasma Sci.* **39** 2556
- [31] Sato M and Shoji M 1997 *Jpn. J. Appl. Phys.* **36** 5729
- [32] Iliev I, Gocheva-Ilieva S and Sabotinov N 2004 *Proc. SPIE* **5449** 131
- [33] Iliev I, Gocheva-Ilieva S and Sabotinov N 2009 *J. Optoelectr. Adv. Mater.* **11** 1392
- [34] Smith H B, Charles C and Boswell R W 2003 *Phys. Plasmas* **10** 875
- [35] Radmilović M and Petrović Z Lj 2000 *Eur. J. Appl. Phys.* **11** 35
- [36] Radmilović-Radjenović M and Petrović Z Lj 2009 *Eur. Phys. J. D* **54** 445
- [37] Turner M M, Derzsi A, Donkó Z, Eremin D, Kelly S J, Lafleur T and Mussenbroc T 2013 *Phys. Plasmas* **20** 013507

Monte Carlo modeling of radio-frequency breakdown in argon

Marija Puač^{1,2,4} , Dragana Marić² , Marija Radmilović-Radjenović²,
Milovan Švakov² and Zoran Lj Petrović^{2,3}

¹ School of Electrical Engineering, University of Belgrade, 11120 Belgrade, Serbia

² Institute of Physics, University of Belgrade, Pregrevica 118, 11080 Zemun, Serbia

³ Serbian Academy of Sciences and Arts, Knez Mihailova 35, 11001 Belgrade, Serbia

E-mail: smarija@ipb.ac.rs

Received 29 March 2018, revised 29 May 2018

Accepted for publication 12 June 2018

Published 13 July 2018



CrossMark

Abstract

This paper contains results of the detailed simulation study of the breakdown in low-pressure radio-frequency (RF) argon discharges. Calculations were performed by using a Monte Carlo code including electrons only, with the assumption that the influence of heavy particles was negligible. The obtained results are in a good qualitative agreement with the available experimental data and clearly show the multivalued nature of the left-hand branches of the breakdown voltage curves. The physical processes defining the breakdown conditions were analyzed based on the spatial profiles of electron density, local mean energy and the number of elastic and ionization collisions. Under the conditions where two breakdown values existed one could identify two regimes and two different balances between the electron losses and production. Using the dependence of the breakdown voltage on the product of the pressure and the interelectrode distance, and the product of the frequency and the interelectrode distance, similarity laws for RF breakdown have been reexamined.

Keywords: plasma modeling, Monte Carlo simulation, radio-frequency breakdown, similarity law

1. Introduction

Capacitively coupled radio-frequency (RF) discharges are attracting increasing attention due to their wide applications in many technological processes [1] such as plasma etching for semiconductor materials, thin film deposition, plasma cleaning [2] and increasingly popular biomedical applications [3–5]. One of the crucial issues is understanding the pertinent processes that drive the breakdown and transition to RF plasma and how those could be modeled. In that respect a wealth of information can be obtained from the breakdown voltage curves. Gas breakdown represents the first step in plasma generation. A specific characteristic of RF plasmas is that the self-sustained discharge may be maintained merely through ionization by electrons. There the feedback process is the return of electrons when the field changes direction, as a replacement of the ion drifts towards the cathode, which is the feedback in DC discharges [6–9].

Although gas breakdown has been studied for more than 100 years, many aspects are poorly understood. A simplified explanation dating back to an early version of the textbook by von Engel [8] (and perhaps dating back even further) is that only the group of electrons that completes the transition in one half period from one electrode to the other has a chance of being multiplied. Basically, the drift velocity that is integrated and averaged over the half period has to be equal to the gap between two electrodes [6, 7]. Most certainly the points that need clarification are the mechanism of the double-valued breakdown curve, the validity of the proposed mechanism of the relationship between drift in one half period and the gap, and also the role of non-locality on the development of the breakdown. All of these processes are properly accounted for in the simulation presented here.

In the first half of the 20th century there has been a major development of techniques to solve the time dependent Boltzmann equation [10–16] continued by Wilhelm and Winkler in the '70s and Makabe in the '80s [17, 18]. First exact solutions for the time dependent transport were obtained by using Monte

⁴ Author to whom any correspondence should be addressed.

Carlo (MC) simulations [19] and numerical solutions to the time dependent Boltzmann equation [20, 21]. Numerous approximate experimental and theoretical papers have been published on the breakdown in RF using simplified semi-analytic forms [22–26]. At the same time fluid, hybrid and particle-in-cell (PIC) models of RF plasmas include early stages of the growth of ionization [18, 27, 28]. In recent years, computer modeling and simulation has emerged as an effective tool that complements laboratory experiments and analytic models. PIC/MC simulations have been used extensively to study fundamental processes in capacitively coupled RF discharges [29–32].

In this paper calculations were performed for argon discharges by using an MC code under the condition of a low degree of ionization so that the transport of particles could take place in the externally defined uniform field. In doing so we tried to use the advantage of the well tested MC codes that may provide very accurate time dependent transport data [33, 34]. At the same time the development of the plasma through weakly ionized phases was studied in order to test the applicability of the transport coefficients and fluid models in representing such a breakdown. Thus, we have used a fully tested and benchmarked code for electrons (that also has the facility to include heavy particles, ions and neutrals) with a full range of sampling and treatment of the cross-section data. The logic is that during the breakdown the swarm physics exactly describes the charged particle ensemble and only a much higher density particle needs to include the space-charge effects. As it has been mentioned earlier, that electrons alone may maintain discharge through ionization and described the main features of the breakdown curves, we start with electrons as the only agents precipitating the breakdown. Only after we start comparing with the experiment do we add other effects (ion induced secondaries, metastable induced secondaries, fast neutrals and their effect, photon induced secondaries and finally electron induced secondary-multipactors). But those are not in the scope of this paper. This paper represents one of the first steps in obtaining a more complete description of the low-pressure RF argon discharge, which provides us with an insight into the basic physics of the breakdown (preliminary results are presented in [35]).

2. Methods

For this study an MC code, which was developed and tested (tested both for DC and RF benchmarks [33, 34, 36]) is used. Since MC technique have been explained elsewhere [37, 38], only a brief description of the code will be given here. We developed an MC code that traced electrons only. Heavy particles and the effect of photons were also added, but those results are not included in this paper. The code was tested for electron (and ion) transport and was shown to give accurate electron energy distribution functions (EEDFs) and transport coefficients in model gases and in argon [33, 37].

The calculations were carried out for argon discharges generated between infinite plane-parallel electrodes at a frequency of 13.56 MHz (unless specified otherwise). Argon was chosen for many reasons: first of all, it is an atomic gas with a simple energy transition spectrum and it is easy to operate with.

At the same time, its cross-section data and other necessary input data are available and well tested, thus are reliable. One can refer to argon as a ‘benchmark’ gas in discharge studies. We included a set of cross-sections that were shown to provide excellent agreement with the measured transport data and which included: elastic scattering of electrons, excitation to the effective triplet state levels, excitation to the effective singlet state levels and ionization. The two excitation cross-sections had been well tested for argon swarms [39, 40]. This paper includes a complete set of the electron–argon interactions included in the modeling representing all the processes that we needed to produce the basic breakdown curves and explain their features.

At the beginning, the electrons were released from the middle of the gap between the two electrodes with no initial energy. Any further electron motion and different interactions depended on the applied alternating current (AC) field, random number generator and the solutions of the kinetic and balance equations. At this point, the surface effects of the electrodes were not included. When an electron reached the boundary, it was assumed to be removed and had no influence on the discharge kinetics. We had a facility to add reflection or other surface processes easily based on the available experimental data.

In our simulations the breakdown voltage curves were recorded in accordance with the procedure described in [6, 41, 42]. On the right-hand side of the breakdown voltage curve, the breakdown voltage was determined by fixing a pressure and increasing the applied voltage. For the left-hand side of the curve, the voltage was fixed while the pressure was varied. In the MC simulations these two procedures were equally simple while the case of experiments with variations of pressure may be more complex.

Figure 1 shows the changes in the number of electrons over time for: (a) the fixed maximum voltage of $V = 160$ V and at three different pressures ($p_1 = 0.134$ Torr, $p_2 = 0.135$ Torr and $p_3 = 0.136$ Torr) and (b) the fixed pressure of 0.2 Torr and five different voltages (60, 94, 270, 447 and 700 V). As can be seen from figure 1(a), at the pressure $p_1 = 0.134$ Torr there was no electron amplification in the required quantity that could compensate the electron losses at the electrode, so the total number of electrons decreased over time and the slope is negative. At the pressure $p_2 = 0.135$ Torr, however, there was a notable increase in the total number of electrons over time, which can be interpreted as an increased number of ionizations due to the higher density (as compared to p_1) of the background atoms and consequently a larger number of collisions. The breakdown occurred somewhere between $p_1 = 0.134$ Torr and $p_2 = 0.135$ Torr. The pressure resolution was 0.001 Torr. A more accurate pressure can be obtained by interpolation between the nearest two values of pressure, in this case p_1 and p_2 .

Figure 1(b) is presented to depict how the number of electrons changed over time with large variations in the voltage. The pressure (0.2 Torr) and voltages that were chosen correspond to the vertical line in figure 2(a). When the pressure was fixed (see figure 1(b)), there were two values where the mean number of electrons was barely maintained, which means that those are the boundaries of the breakdown (94 and 447 V). In-between the two breakdown values one has excessive growth in the density (in a real circuit this would push the operating point to either of the

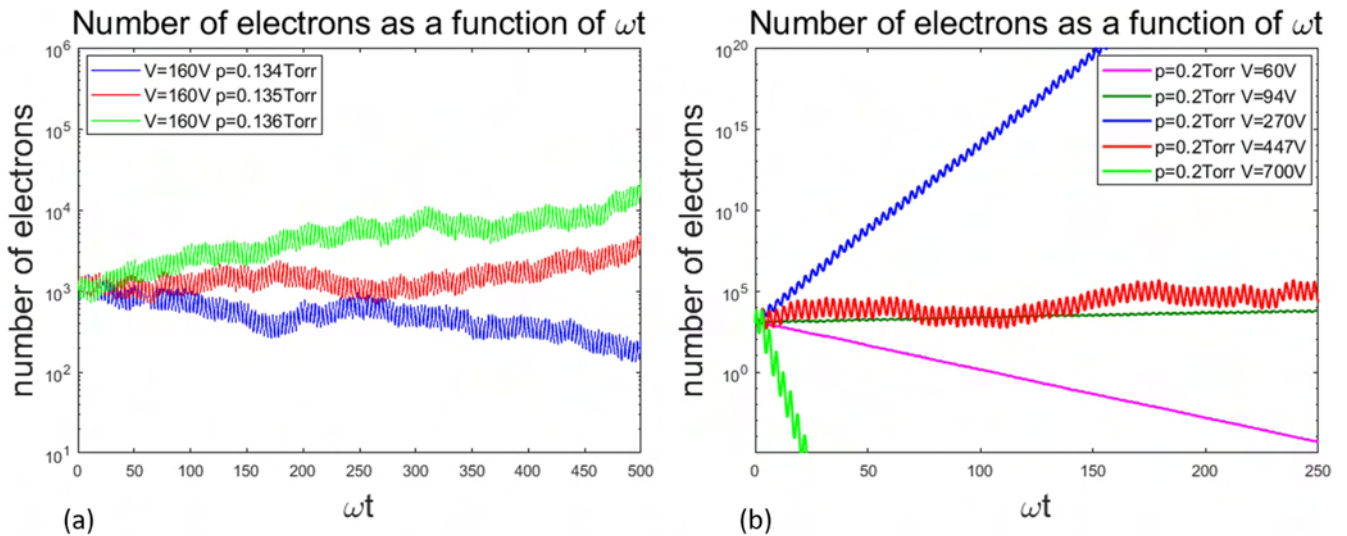


Figure 1. The time dependence of the simulated number of electrons for: (a) the fixed voltage of 160 V and various pressures and (b) constant pressure of 0.2 Torr and various voltages.

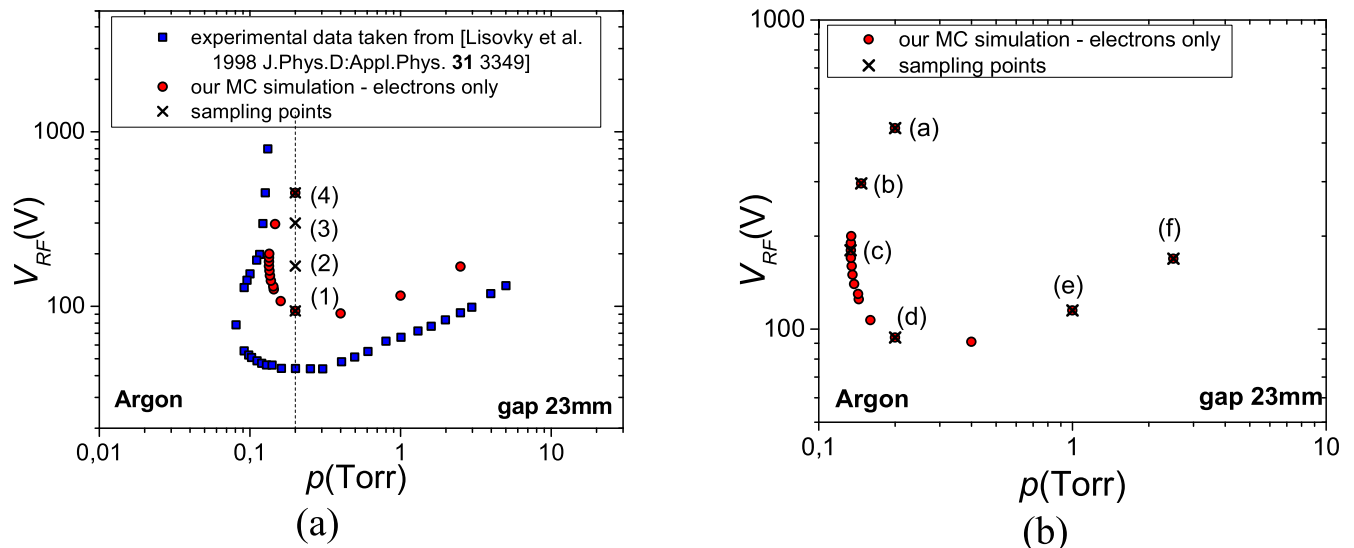


Figure 2. The breakdown voltage curves for argon RF discharges at 13.56 MHz and the gap size of 23 mm. The Monte Carlo Simulation (MCS) includes electrons only. (a) Comparison of the breakdown voltage curve obtained by MCS (red circles) and experimental available data [6] (blue squares). Vertical line for $p = 0.2$ Torr and different voltages indicates sampling points presented in figures 3 and 4. (b) MCS obtained curve indicating sampling points of spatial profiles presented in figure 5. Sampling points are marked by numbers and letters.

two breakdown voltages). Results within that range are on a positive slope, whereas results outside that range showed decay advancing towards termination (e.g. data for 60 and 700 V). Outside the breakdown region (above 447 V and below 94 V) the density of the electrons rapidly diminished (60 and 700 V).

In both figures 1(a) and (b), there are periodic oscillations of the electron number. In figure 1(a), with a fixed voltage, these oscillations are the same in the sense of period and amplitude. In figure 1(b) the period of the oscillations is the same while the amplitudes are different depending on the applied voltage. With changes in voltage the effective rates that define the speed of relaxation may change and affect the undulations of the properties such as the number of electrons. This is because the high voltage electrons reached the ionization energies more easily and in larger numbers so the

number of electrons changed more rapidly within one period of time. The losses at the electrodes may have balanced the increased production, they increased because more of the electrons were being pushed to the electrodes by a strong AC field. As the voltage decreased less energy was transferred from the field to the electrons and the number of ionizations reduced (the increasing number of electrons within one period was smaller). For a lower voltage both the loss and production were smaller as the electrons did not reach the electrodes (oscillations were barely noticeable for a voltage of 60 V). One can conclude that the period of oscillation of the electron number was determined by the frequency of the external AC field while the amplitude of the oscillation of the electron number depended on the amplitude of the applied AC field (energy transfer from the field to the electrons).

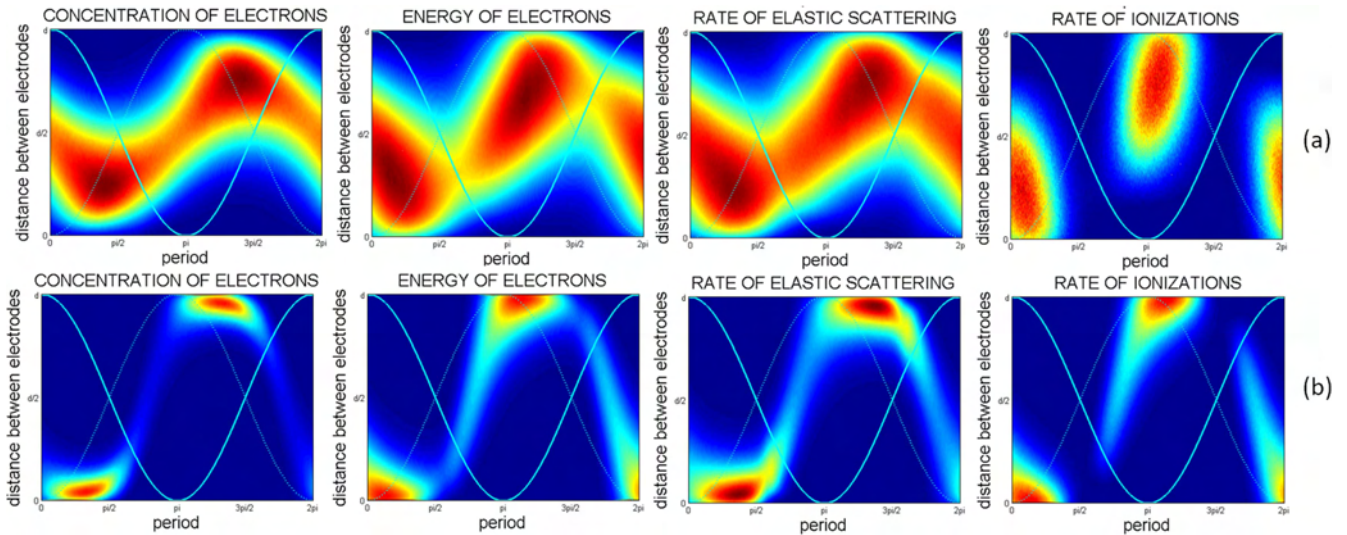


Figure 3. Spatial distributions of: electron concentration, mean energy and rates of elastic scattering and ionization for the pressure of 0.2 Torr and two breakdown points: (a) $V = 94$ V and (b) $V = 447$ V (points are marked in figure 2(a), (a) corresponds to (1) and (b) corresponds to (4)). The light blue line represents the AC field, while the dashed light blue line corresponds to the field dependence inverted to represent the force affecting the electrons. Interelectrode gap is 23 mm and frequency is 13.56 MHz. Number of electrons in the simulation was selected to have a similar statistical quality of the results with the smallest rate (i.e. ionization). Thus the color scales are not representing any quantitative data that may be compared for different conditions only the indication of the profile of the ensemble.

3. Results and discussion

3.1. Spatial profiles of electron density and ionization rate as a representation of the potential for achieving breakdown

The dependence of the RF breakdown voltage on the pressure is presented in figure 2. The results of our MC simulations (red circles) are compared with the experimental data taken from [6] (blue squares) in figure 2(a). As can be seen on the left-hand side of the simulated curve, for a fixed pressure there are two values for the breakdown voltage. The discharge may start between these two values, while above and below it quenches rapidly (as indicated in figure 1). This observation is in agreement with the previously published experimental data [6], at least qualitatively. The crosses correspond to the sampling points on a vertical line $p = 0.2$ Torr. Two points are on the breakdown curve (94 and 447 V) and two points are in-between (170 and 300 V). In principle, in a simulation operation above the breakdown conditions the growth of electrons is allowed. In experiments, however, the operating point will move towards either of the two breakdown curves. The development of the spatial profiles (see figures 3, 4) along the vertical line provides an insight into the pertinent physical processes. On the other hand in figure 2(b) the sampling points marked by letters are on the breakdown curve. The spatial profiles associated with these points and shown in figure 5 indicate a difference in the physical processes with a variation of p (pd).

The spatio-temporal development of the profiles of: electron density, mean energy, elastic collisions and ionization are shown in figure 3. The calculations were performed for a frequency of 13.56 MHz, a gap size of 23 mm, a pressure of 0.2 Torr and two breakdown points: (a) 94 V and (b) 447 V (as indicated in figure 2(a)). As the voltage increased,

the low voltage breakdown point was reached, but most of the electrons did not reach the electrodes. The profile of the electron cloud is broad, not really sinusoidal, but generally follows a sinusoidal shape. There were maxima in density, elastic scattering and in mean energy when the cloud was closest to the electrodes. The peaks were delayed by a large phase delay to the voltage waveform. In fact, the peak started moving towards the center of the gap only at the phase when the field changed direction and not for the maximum of the field. This can be easily understood because for ionization only two regions close to the maximum of the applied voltage (field) were abundant in the collisions while still following a similar temporal and spatial dependence.

At the higher breakdown point the spatial profiles were much narrower and there was a strong overlap with the electrode. While the electron density peaks were slightly away from the electrode the highest energy/the most likely to ionize the electrons' peak was right at the edge of the electrode.

It is important to note that our MC code obtained a double-valued voltage on the breakdown curve by treating electrons only. For some gases [43] even 'S' shaped curves with three points may be observed. The explanation of this phenomenon is as follows: for the lower voltage one needs to compensate losses at electrodes by increasing ionization, and any increase in voltage leads to a higher ionization. If we move to higher voltages, ionization is increased but so are the losses at the instantaneous anode. This is a consequence of pushing electrons closer to the electrodes with an increasing AC field. The losses may be represented by imagining the remaining electron ensemble spatial distributions that extend over the electrode edge into its bulk and this distribution increases with the applied voltage. At a certain point this part of the ensemble that passes past the electrode will increase so

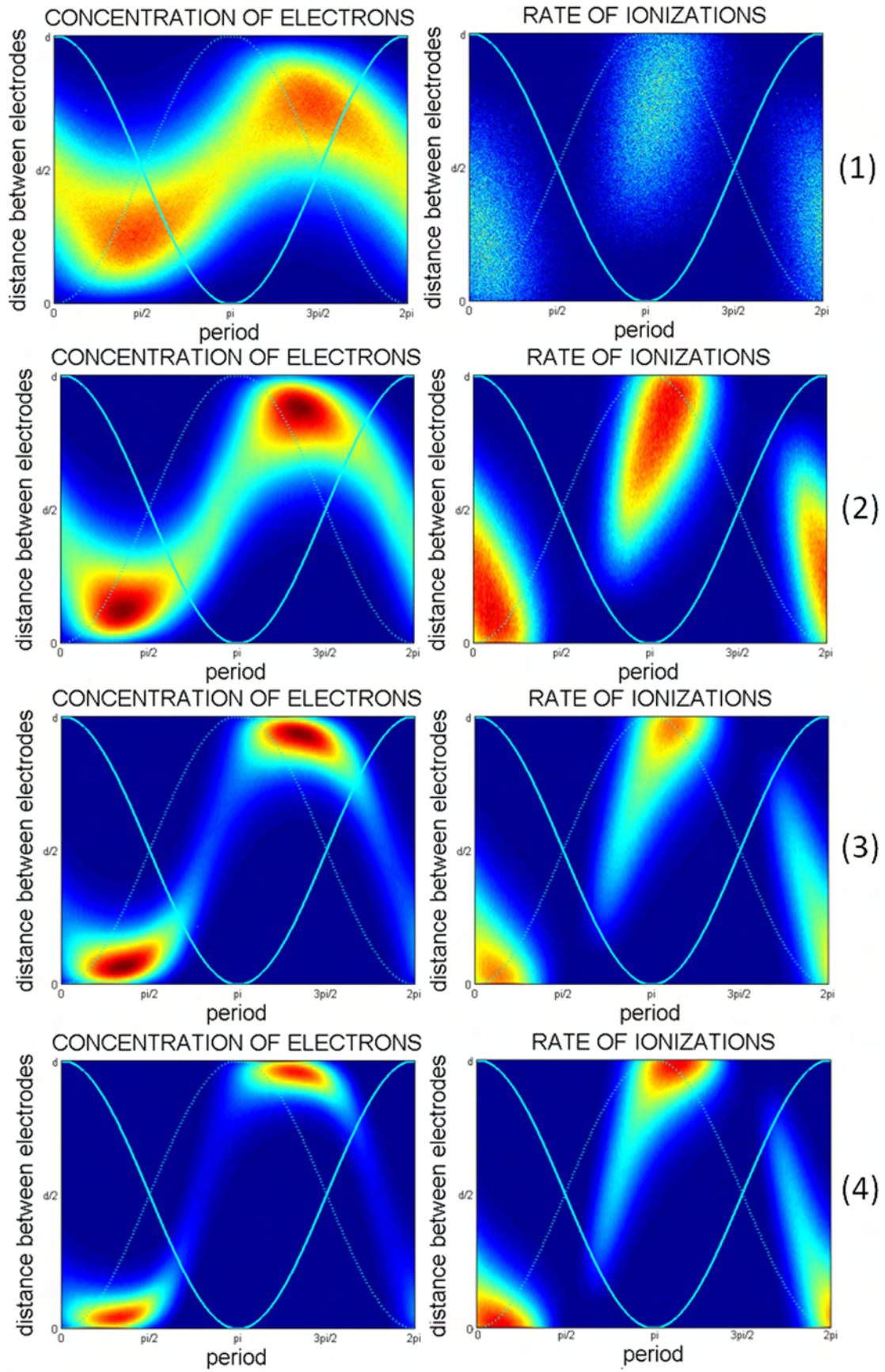


Figure 4. Spatial profiles of the electron concentration and ionization rates for the pressure of 0.2 Torr and voltages of (1) 94 V, (2) 170 V, (3) 300 V and (4) 447 V. Points are marked in figure 2(a). Interelectrode gap is 23 mm and frequency is 13.56 MHz. All figures are obtained with the same initial number of electrons so the relative magnitudes of the same coefficient are indicated by the colors scale.

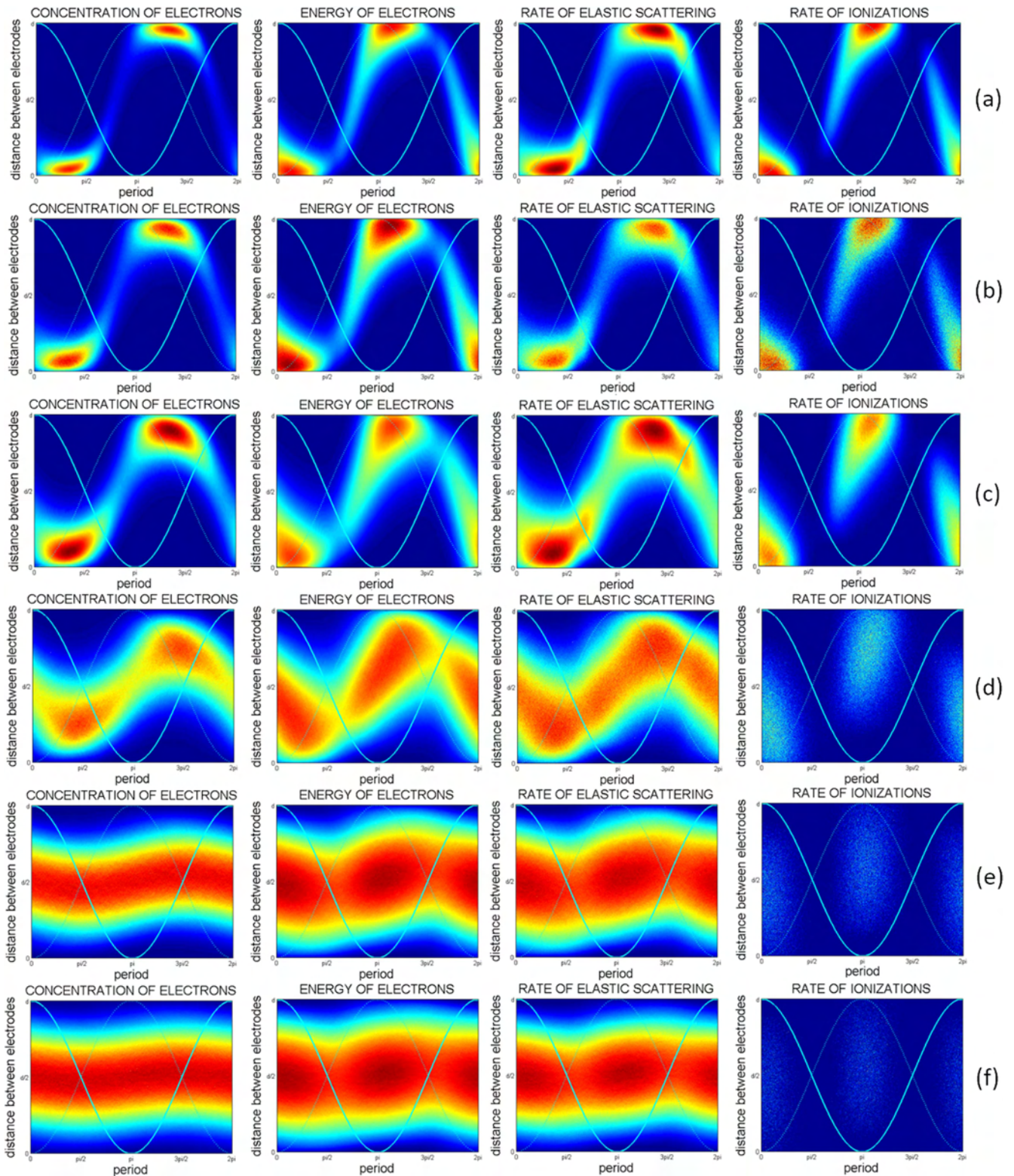


Figure 5. Spatial distributions of concentration of electrons, electron energy and rates of elastic scattering and ionization: (a) 447 V 0.2 Torr, (b) 296 V 0.147 Torr, (c) 180 V 0.1335 Torr, (d) 94 V 0.2 Torr, (e) 115 V 1 Torr and (f) 169 V 2.5 Torr. Points are marked in figure 2(b). Interelectrode gap is 23 mm and frequency is 13.56 MHz. All figures are obtained with the same initial number of electrons so the relative magnitudes of the same coefficient are indicated by the colors scale.

much that ionization in the gas (in front of the electrode) cannot compensate the losses and the discharge will switch itself off. In figure 3 this is represented by the spatial profile of the electron concentration and mean energy, which indicates the potential for ionization.

The profile of the increasing ionization rate of the group closest to the anode is shown in figure 4 along the fixed $p = 0.2$ Torr for four points marked in figure 2(a). With an increasing voltage more and more of the ionization-capable electrons would be lost at the surface. At the lower applied voltage (94 V) though, the swarm oscillates between two electrodes without reaching them and the majority of ionization-capable electrons have no difficulty ionizing.

3.2. Variation of the spatial profiles with pd along the breakdown curve

Having presented results that indicate the changes in the spatial profiles of all the discharge parameters along a vertical line ($p = \text{const.}$), figure 5 exhibits the spatial profiles along the Paschen-like breakdown potential curve. Stating that the curve is Paschen-like does not imply in any way that the Paschen mechanism is relevant here in its entirety. The points on the V - p plane that have been selected to show the spatial profiles of the various properties of the electron swarm ensemble are marked on the breakdown curve shown in figure 2(b).

Plots (a) and (d) in figure 5 are repeated from the previous figures. The first represents the higher point on the breakdown curve, the second the lower point on the breakdown curve for $p = 0.2$ Torr. Plots (b) and (c) on the left are the rapidly rising branch of the breakdown curve. It is clear that under those conditions the magnitude of the field manages to bring all of the electrons close (within one mean free path) to the electrodes during one half period. Those points have all the characteristics of the operation well above the lower breakdown points and close to the upper branch. The principal issue here is whether the losses at the electrode may be balanced by the production of electrons in its proximity, the production that is made more and more difficult by the reduced number of collisions in a similar fashion to the left-hand branch of the DC–Paschen curve. As a result of this balancing between losses and gains the peak of the mean energy and the number of ionizing collisions clearly occur right before reaching the electrode and after the maximum in the field. At the same time the peak in density occurs a little later as a consequence of the ensuing burst of ionization. The number of elastic collisions follows the profile of the density better, while, as stated, the number of ionizations follows the profile of the mean energy.

The spatial profiles in figure 5(c) also become somewhat closer to the lower branch profiles of figure 5(d), where the majority of ionizations occur in the bulk of the discharge, and the whole ensemble merely brushes against the electrodes. The balance between losses and gains, as displayed in figure 5(d), seems optimal as there are minimal losses while the number of collisions provides ample opportunities to compensate for them. As the pressure increases (for a fixed d) the number of collisions increases further and thus it is more difficult to achieve higher energies so the breakdown voltage

increases but slowly. More importantly, the density profile of the electrons loses sharp peaks and becomes more sinusoidal in the center of the gap with vanishing density due to losses close to the walls. The mean energy is still modulated following the field dependence albeit with a delay. A similar modulation is observed in the elastic collisions mainly due to the energy dependence of the cross-section. It is important to note that collisions occur on both halves of the gap, as the density profile, while modulated, does not show complete migration of electrons towards the instantaneous anode and away from the cathode. As a result of the ensemble overlapping from one to the other electrode, the highest energy electrons responsible for ionization will be generated throughout the gap and under those conditions, ionization, however weak, spreads on both halves almost equally (figures 5(e), (f)). The difference between ionization profiles in figures 3(a) and 5(d) is that in the former one we have enhanced the number of events by the accumulation of events through releasing more electrons for the same set of conditions to make the simulation conditions the same for all figures in the cluster of figure 5.

Furthermore, we employed an MC code to provide a more detailed picture of the physical processes by observing the energy distribution function that has to be related to the processes occurring in the region of active ionization (i.e. near the electrode). As can be seen in figure 6, the overlap of the distribution function with the relevant cross-sections (both excitation of metastable and ionization) is of essential importance for the maintenance of the discharge. For high voltages (figure 6(a)) there is a significant overlap of the EEDF and cross-section for ionization. A great deal of high energy electrons that can ionize were being absorbed by the electrodes and lost. Under these conditions ($V = 447$ V and $p = 0.2$ Torr) there was a fine balance between the losses and production of electrons. A significant increase in the EEDF right in front of the electrode at higher voltages (i.e. lower pressures) is also observed. The increase means energy (and the mean free path) for lower pressures was the result of a reduced number of collisions as the electrons crossed the gap so ionization was to become more efficient. As for high pressures (figure 6(b)) only the tail of the EEDF at the electrodes is overlapping with the cross-section for ionization. There is no significant loss of ionization-capable electrons and discharge is easier to maintain which can be observed as smaller increase of voltage in right branch of breakdown voltage curve as compared to the left branch.

3.3. Scaling of RF breakdown profiles: breakdown voltage depending on the gap length and frequency

RF breakdown has a different nature compared to DC breakdown. Therefore, pd scaling that is applicable in DC breakdown voltage curves needs to be extended to include frequency dependence. Figure 7 shows the breakdown voltage curves for various: (a) gaps and (b) frequencies. The curves have a similar shape with a large variation of parameters. For a fixed frequency one cannot maintain the scaling, as in addition to pd scaling there is also fd (interelectrode distance times frequency) scaling

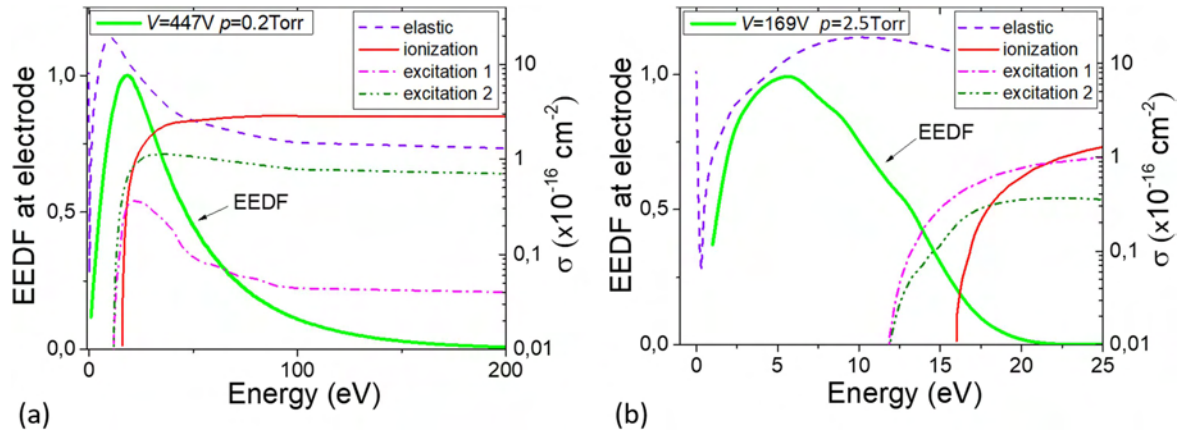


Figure 6. Electron energy distribution function at the electrodes separated by 23 mm at the frequency of 13.56 MHz for: (a) $V = 447$ V, $p = 0.2$ Torr and (b) $V = 169$ V, $p = 2.5$ Torr. Right-hand side y-axes shows set of cross-sections for argon.

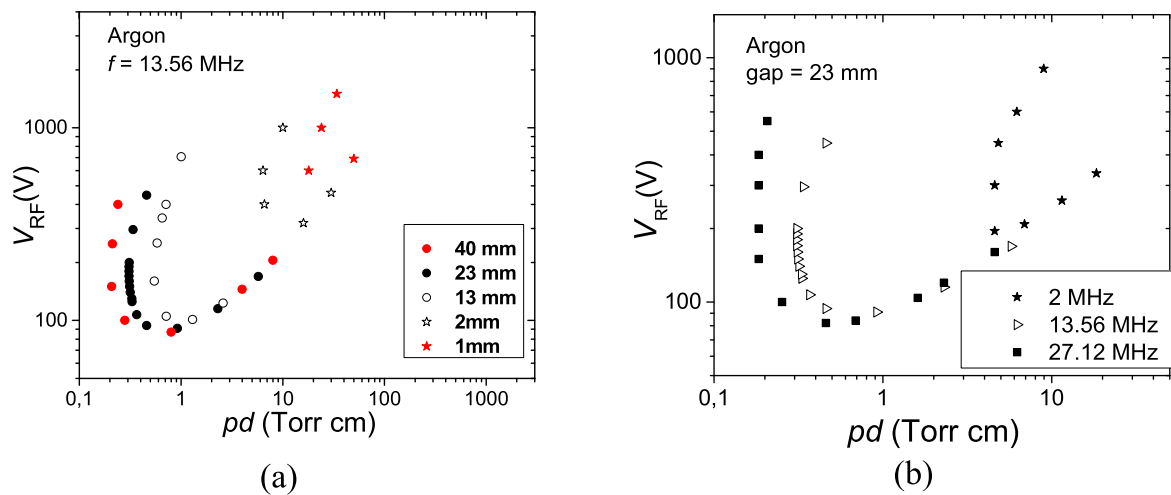


Figure 7. (a) Simulated breakdown voltage curves for: (a) a fixed frequency of 13.56 MHz and various gaps sizes and (b) a fixed gap of 23 mm and various frequencies.

that needs to be satisfied [44–46]. The same is valid for a fixed gap. Scaling with proper variation of both the frequency and the gap is shown in figure 8.

Both the frequency and gap are varied while keeping the fd constant and observing the pd dependence. We can see a very good overlap that is excellent at higher values of pd while at lower values of pd and higher breakdown voltages there is more of a difference, presumably due to the nonlinearities brought about by the overlap of the electron cloud with the electrode. While presenting breakdown curve scaling is important and indeed points out the validity of the scaling. The critical test of the scaling would be the observation of the spatial profiles depicted in figure 9 for pd around 0.34 Torr cm and a number of frequencies with the corresponding gaps. It is clear that for a narrow range of fd and pd all the spatial profiles coincide. That is the physical foundation of the scaling laws, which basically scales the number of collisions per length and time.

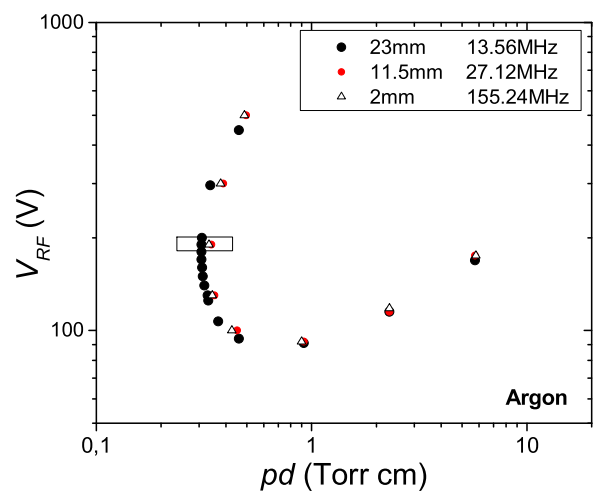


Figure 8. Scaling according to pd and fd scaling laws of RF voltage breakdown curves. Box indicates region with points for which the spatial profiles are plotted in figure 9.

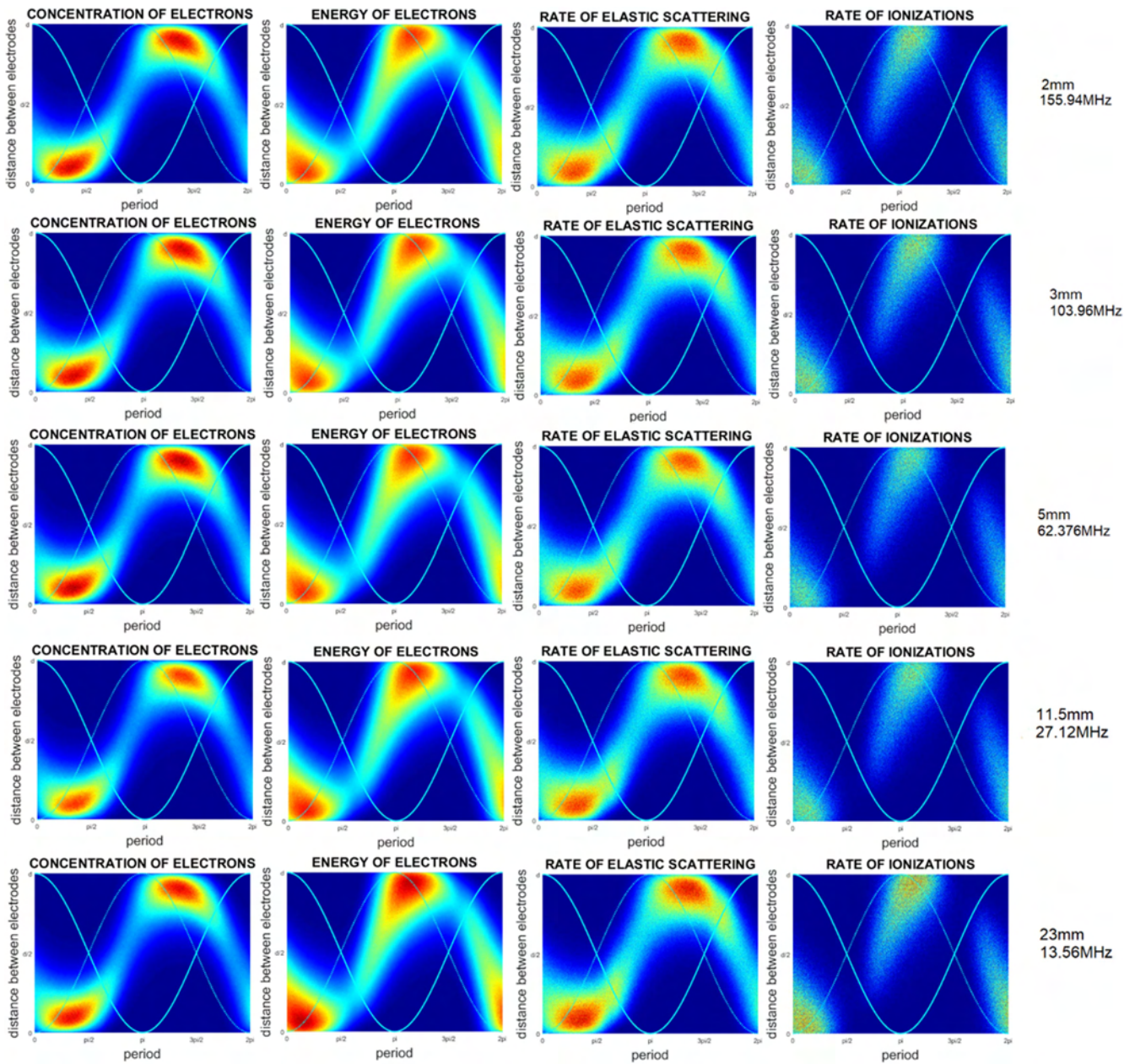


Figure 9. Spatial distributions for a number of points that have the same product of frequency and distance between electrodes ($fd = \text{constant}$) and also for a fixed $pd = 0.34$ Torr cm. All figures are obtained with the same initial number of electrons so the relative magnitudes of the same coefficient are indicated by the colors scale.

4. Conclusion

In this paper the physical background of low-pressure RF argon discharges is studied. It is found that the simplified phenomenology of transfers from one electrode to the other is often not met especially at higher pressures where electrons may produce sufficient ionization while crossing shorter distances. At lower pressures, conditions to reach the electrodes are acquired at the cost of an increased breakdown voltage. Under those conditions the balance between new electrons being produced and the increase in mean energy determines the breakdown. Thus it is possible to have two breakdown points (and the region of the double-valued breakdown curve coincides with the region where electrons reach electrodes in

one half period) for one pd value. The higher point is where the balance is encountered due to the losses of high energy electrons hitting the anode and being absorbed by it.

Another issue of scaling is illustrated well with the obtained results. The breakdown follows the standard pd scaling very well but it has to adjust itself to the fd scaling as well. The fd scaling has been discussed within the terms of breakdown physics by Lisovsky *et al* [45] and it addressed [44]. However both scalings have been established in the earlier electron transport (swarm) studies [14–16, 46] basically as a condition to maintain the number of collisions per certain distance or in certain time. The spatial profiles of the electron properties shown in figure 9 give an indication of how scaling involves identical spatial distributions and other properties thus supporting the predicted scaling.

Results, presented and discussed here, confirm that the modeling of RF breakdown by using a detailed MC code provides an excellent and relatively easy entrance into the pertinent physical processes. In the later stages plasma properties become important and one has to follow the space-charge development, which makes the situation much more complex. Yet the onset of the breakdown is purely a swarm phenomenon and the beginning of the development of the plasma may be clearly envisioned and explained even quantitatively by a swarm model.

Acknowledgments

This paper was completely finalized at the Institute of Physics University of Belgrade under basic funding from projects OI 171037 and III 41011 of the Serbian Ministry of Education, Science and Technological development of Serbia. ZLjP is grateful to the Serbian Academy of Sciences and Arts and its project F155 for its partial support. Authors are grateful to Dr Srđan Marjanović for help in several stages of the development of the code.

ORCID iDs

Marija Puač  <https://orcid.org/0000-0002-6011-0434>

Dragana Marić  <https://orcid.org/0000-0002-1728-5458>

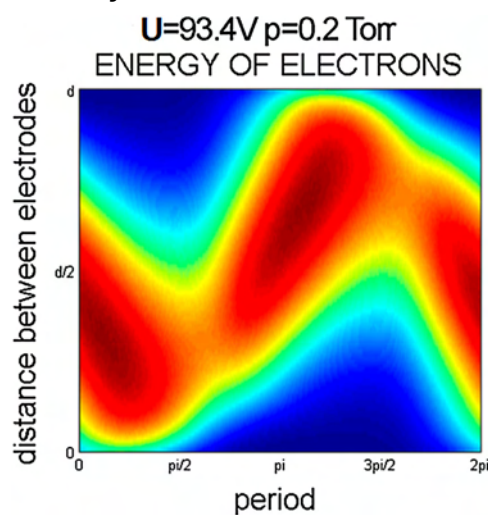
References

- [1] Adamovich I et al 2017 *J. Phys. D: Appl. Phys.* **50** 323001
- [2] Makabe T and Petrović Z Lj 2006 *Plasma Electronics: Applications in Microelectronic Device Fabrication* (London: Taylor and Francis)
- [3] Puač N, Škoro N, Spasić K, Živković S, Milutinović M, Malović G and Petrović Z Lj 2017 *Plasma Process Polym.* **15** e1700082
- [4] Lazović S et al 2010 *New J. Phys.* **12** 083037
- [5] Puač N, Gherardi M and Shiratani M 2018 *Plasma Process Polym.* **15** e1700174
- [6] Lisovskiy V A and Yegorenkov V D 1998 *J. Phys. D: Appl. Phys.* **31** 3349
- [7] Gill E B W and von Engel A 1949 *Proc. R. Soc. A* **197** 107
- [8] von Engel A 1965 *Ionized Gases* (Oxford: Clarendon Press)
- [9] Phelps A V and Petrović Z Lj 1999 *Plasma Sources Sci. Technol.* **8** R21
- [10] Allis W P 1956 Motions of ions and electrons *Electron-Emission Gas Discharges I Encyclopedia of Physics* ed S Flugge vol 21 (Berlin: Springer) pp 383–444
- [11] Allis W P and Brown C 1952 *Phys. Rev.* **87** 419
- [12] MacDonald A D 1966 *Microwave Breakdown in Gases* (New York: Wiley)
- [13] Morse P M, Allis W P and Lamar E S 1935 *Phys. Rev.* **48** 412
- [14] Margenau H and Hartman L M 1948 *Phys. Rev.* **73** 309
- [15] Holstein T 1946 *Phys. Rev.* **70** 367
- [16] Ginzburg V L and Gurevich A V 1960 *Sov. Phys. Usp.* **70** 393
- [17] Wilhelm J and Winkler R 1969 *Ann. Der Physik* **23** 28
- [18] Goto N and Makabe T 1990 *J. Phys. D* **23** 686
- [19] Bzenic S, Petrović Z Lj, Raspopovic Z and Makabe T 1999 *Jpn. J. Appl. Phys.* **38** 6077
- [20] Dujko S, White R D and Petrović Z Lj 2011 *IEEE Trans. Plasma Sciences* **39** 2560
- [21] White R D, Ness K F and Robson R E 2002 *Appl. Surf. Sci.* **192** 26
- [22] Kihara T 1952 *Rev. Mod. Phys.* **24** 45
- [23] Raizer Y P 1991 *Gas Discharge Physics* (Berlin: Springer)
- [24] Makabe T, Nakano N and Yamaguchi Y 1992 *Phys. Rev. A* **45** 2520
- [25] Klas M, Moravsky L, Matejček Š, Radjenović B and Radmilović-Radjenović M 2015 *J. Phys. D: Appl. Phys.* **48** 405204
- [26] Klas M, Matejček Š, Moravsky L, Radjenović B and Radmilović-Radjenović M 2017 *EPL* **120** 25002
- [27] Lee I, Graves D B and Lieberman 2008 *Plasma Sources Sci. Technol.* **17** 015018
- [28] Kushner M J 2009 *J. Phys. D: Appl. Phys.* **42** 194013
- [29] Donko Z 2011 *Plasma Sources Sci. Technol.* **20** 024001
- [30] Verboncoeur J P 2005 *Plasma Phys. Control. Fusion* **47** A231
- [31] Birdsall C K and Langdon A B 1985 *Plasma Physics via Computer Simulation* (New York: McGraw-Hill)
- [32] Birdsall C K 1991 *IEEE Trans. Plasma Sci.* **19** 65
- [33] Raspopovic Z M, Sakadzic S, Bzenic S A and Petrović Z Lj 1999 *IEEE Trans. Plasma Sci.* **27** 1241
- [34] Petrović Z Lj, Raspopovic Z M, Dujko S and Makabe T 2002 *Appl. Surf. Sci.* **192** 1–25
- [35] Savić M, Radmilovic-Radjenovic M, Šuvakov M, Marjanović S, Marić D and Petrović Z Lj 2011 *IEEE Trans. Plasma Sci.* **39** 2556
- [36] Šuvakov M, Ristivojević Z, Lj P Z, Dujko S, Raspopović Z M, Dyatko N A and Napartovich A P 2005 *IEEE Trans. Plasma Sci.* **33** 532
- [37] Ristivojevic Z and Petrović Z Lj 2012 *Plasma Sources Sci. Technol.* **21** 035001
- [38] Petrović Z Lj, Bzenic S, Jovanovic J and Đurovic S 1995 *J. Phys. D: Appl. Phys.* **28** 2287
- [39] Petrović Z Lj, Šuvakov M, Nikitović Ž, Dujko S, Šašić O, Jovanović J, Malović G and Stojanović V 2007 *Plasma Sources Sci. Technol.* **16** S1–12
- [40] Phelps A V https://fr.lxcat.net/data/set_specA.php
- [41] Korolov I, Derzsi A and Donko Z 2014 *J. Phys. D: Appl. Phys.* **47** 475202
- [42] Korolov I and Donko Z 2015 *Phys. of Plasmas* **22** 093501
- [43] Lisovskiy V, Booth J-P, Landry K, Douai D, Cassagne V and Yegorenkov V 2006 *J. Phys. D: Appl. Phys.* **39** 660
- [44] Francis G 1956 Gas discharges II *Encyclopedia of Physics* ed By ed S Flugge **XXII** (Berlin: Springer)
- [45] Lisovskiy V, Booth J-P, Landry K, Douai D, Cassagne V and Yegorenkov V 2008 *Europhys. Lett.* **82** 15001
- [46] Margenau H 1948 *Phys. Rev.* **73** 326

Using Swarm Models as an Exact Representation of Ionized Gases

Zoran Lj. Petrović,* Dragana Marić, Marija Savić, Srdan Marjanović, Saša Dujko, Gordana Malović

In this review, several examples of ionized gases are presented where swarm models may be employed to provide full description. Those situations include low space charge pre-breakdown, Townsend region breakdown where space charge effects may be calculated from the swarm model and used as the first order perturbation to describe oscillations and transient signal and afterglows. In addition, implications are considered for microdischarges, discharges in and close to liquids, gas-filled particle traps, thermalization of particles in living tissue, and many more. In all those situations, swarm models provide full description of the discharge, while for most other collision dominated non-equilibrium plasmas swarm physics (transport-related phenomena) provides a part of the foundation of modeling.



1. Introduction

Swarm data and the basic transport equations have been the foundation of the modeling of low temperature (i.e., non-equilibrium) plasmas.^[1–4] In doing so, it is often assumed that the transport data obtained under such conditions fit well the fluid or other equations used to model plasmas. Without going into discussion of whether that is the case or not, we need to stress that the use of swarm data or of the swarm derived cross-section sets^[5–7] is a prerequisite in achieving proper energy, momentum, and number balances in plasma models and in having properly calculated non-equilibrium distribution functions. Even

though in RF fields and in the presence of strong variations of the distribution function, the use of swarm parameters may become complex due to non-locality^[8–10] these data have been used successfully and with little evidence of inadequacy. That is presumably due to a robust nature of plasma models (physics) dictated primarily by the space charge adjustment that provides a field distribution necessary to maintain the existence of the plasma itself.

In this paper, we shall, however, focus on the ionized gases where the swarm models are an exact representation of the system, as exact as the available data allow it and as exact as small perturbations of the external field do not constitute a major source of the relevant particles. Usually it is assumed that by cornering yourself into the low current limit and favoring situations where ionized gas does not use its ability to self adjust the field profile, will lead to very few, if any (with exception of swarm experiments of course), examples where such physical models is adequate. That, luckily, is not true and we have a number of examples where swarm models provide sufficient and even complete description. This paper attempts to provide a review of such examples and also to

Prof. Z. Lj. Petrović, Dr. D. Marić, M. Savić, S. Marjanović,
Dr. S. Dujko, Dr. G. Malović
Institute of Physics Belgrade, University of Belgrade, POB 68 11080
Zemun, Belgrade, Serbia
E-mail: zoran@ipb.ac.rs
Prof. Z. Lj. Petrović
Serbian Academy of Sciences and Arts, Knez Mihajlova 35, 11000
Belgrade, Serbia

provide an insight on how swarm models may be used as plasma models. This work is naturally primarily focused on the results of our group.

1.1. What Are Swarms?

Swarms have been defined as ensembles of charged (although the paradigm may be extended beyond charge) ensembles of particles freely moving through the background gas, gaining energy from the external electric field, being under the influence of the external magnetic field, and dissipating energy and momentum in collisions with the gas molecules. It is assumed that all collisions are with the pristine, unperturbed gas and also that space charge effects and Coulomb coupling are both negligible. In other words, it is the zero ionization limit of plasmas where collisions reign supreme and where the field is “known,” i.e., defined by the external voltage. The behavior of charged particles is defined by collisions and also by the energy gain and the field configuration. Thus, this is the end where atomic and molecular physics, integrated into the transport theory, and overall kinetic calculations dominate.

An additional condition is also often introduced that boundaries (such as metallic walls, sometimes grounded, sometimes at some potential) are not felt throughout most of the volume of the discharge. That, however, is not absolutely necessary, it is merely there to provide the basis for the so called hydrodynamic expansion that allows us to separate the distribution function into a velocity space distribution (f) multiplied by the real space particle density profile ($n(\mathbf{r}, t)$) by using spatial gradients of the density:

$$f(\mathbf{r}, v, t) = \sum_{k=0}^{\infty} f^{(k)}(v) \otimes (-\nabla)^k n(\mathbf{r}, t) \quad (1)$$

and spherical harmonics:

$$f(v) = \sum_{l=0}^{\infty} f_{lm}(v) P_l^m(\cos \theta) e^{-im\varphi}, \quad (2)$$

where $P_l^m(\cos \theta)$ are Legendre polynomials and θ and φ are polar angles.

Very important aspect of this expansion, that allows us a much easier numerical solution to the Boltzmann equation, is the fact that if it is satisfied we effectively assume the distribution function to be uniform throughout the entire volume of the discharge. The standard swarm experiments, and swarm physics have always been strongly associated with well-defined experiments, that are able to achieve such conditions throughout most of the volume of the discharge. To do so, a combination of the use of high pressure and control of the current density is required. In any case, substituting Equation (1) and (2) into Boltzmann

equation:

$$\frac{\partial f}{\partial t} + \mathbf{c} \cdot \frac{\partial f}{\partial \mathbf{r}} + \frac{q}{m} (\mathbf{E} + \mathbf{c} \times \mathbf{B}) \cdot \frac{\partial f}{\partial \mathbf{c}} = -J(f, F_0) \quad (3)$$

where $J(f, F_0)$ is the collision operator, provides the means to define and calculate the transport (swarm) coefficients.

On the other hand, most low temperature plasmas operate under conditions where hydrodynamic approximation may not be appropriate. Those include low pressure discharges, where mean free path may be comparable to the size of the vessel, sheaths, and electrode regions and also high gradient areas, like those found in the front of the streamers, thermalization from the initial distribution, or the very high E/N conditions, when charged particles may achieve a runaway. Thus we shall apply swarm models in both sets of circumstances allowing for non-hydrodynamic conditions when required.

1.2. Swarm Models

A swarm model would be a model based on a Boltzmann equation (BE),^[11–14] Monte Carlo simulation (MCS),^[15–18] or some of the simplified equations such as the Momentum transfer theory (MTT).^[19–21] More than actual modeling, one may use transport data to directly calculate properties in hydrodynamic region. If, however, it is not hydrodynamic then the ionized gas should perhaps be modeled by MCS.

An important feature of swarm models is that those are often approximate, like MTT in general, or BE if only two terms are maintained (in expansion given by Equation (2)) or some model collisional operator is employed. Verifying exact nature of the model is thus an important issue and for that purpose, swarm benchmarks are often employed.^[15,18,22–25] We will not spend more time on this issue as it has been well covered by a number of papers.^[26]

We will, however, define conditions where swarm models are expected to be appropriate and then proceed to illustrate some, such as:

- Low space charge density ionized gas in general like the charges in the atmospheric gas.
- Pre-breakdown avalanches requiring external field but not quite making it to the self-sustained regime.
- Breakdown where the initial phase and the transition to the self-sustained regime are in swarm regime while the final stage may be a fully developed plasma, and thus the conditions for the breakdown are defined by the swarm regime.
- Gaseous dielectrics are also defined by the operation in the swarm regime as their use is to prevent development of the plasma in the first place.
- Gas-filled traps such as Penning Malmberg Surko trap for positrons.

- Detectors of elementary particles starting from Willson's chamber and Geiger counter, through drift and avalanche chambers and finally including the most frequently used resistive plate chambers (RPC) detectors.
- Low current diffuse discharge (Townsend discharge) that operates in the low space charge limit, although even when space charge starts making the entrance it is usually as a perturbation to the swarm model.^[27–29]
- Afterglows, after the collapse of the ambipolar field.
- Thermalization of elementary particles emitted from radioactive sources or of cosmic rays and of their secondary products, and many more.

2. Pre-Breakdown, Free Electrons in Ionized Gases

Pre-breakdown, or transport of charged particles in field free conditions or in fields too weak to achieve self-sustained operation have been studied for many years. For obvious reasons, the primary target of such studies has always been modeling of swarm experiments that have been designed to provide high accuracy without uncertainties in interpretation so that the measured transport coefficients may be used to normalize the sets of cross-sections. It is important to say that modeling may be done in the real space and thus provide the connection between observables and actual transport coefficients under the study. Modeling may also be in the velocity space where calculating data is easier and then one comes to the point when it is possible that due to differences between the real space (bulk) and velocity space (flux) transport coefficients one needs to actually model non-conservative aspects of the complete transport in the experiment in order to fit the measured observables and the resulting transport data.^[8,9] In a basic swarm model in weakly ionized gas, would be the use of an equation:

$$j = e n v_{dr} \quad (4)$$

where j is the current density, v_{dr} the electron drift velocity, and n is the charged particle density together with the swarm data for the drift velocity. The spatial and temporal profiles of swarms are usually described in hydrodynamic approximation by using the so called continuity equation^[30]:

$$-\frac{\partial n}{\partial t} + (v_i - v_{att})n - v_{dr} \frac{\partial n}{\partial z} + D_T \left(\frac{\partial^2 n}{\partial x^2} + \frac{\partial^2 n}{\partial y^2} \right) + D_L \left(\frac{\partial^2 n}{\partial z^2} \right) = 0 \quad (5)$$

where D is the diffusion coefficient (which may be either transverse (T) or longitudinal (L)) and non-conservative rate coefficients are ν (ionization – i and attachment – att).

Equations such as 4 and 5 have been used successfully to model a number of experiments^[30–32] provided that hydrodynamic approximation holds. Best examples of the validity of this approach and the use of continuity equation may be observed in photon emission profiles of time of flight experiments of Blevin and Fletcher.^[31,33] In some way, these profiles are akin to the detected profiles of avalanches by Raether^[34] in gaseous elementary particle detectors (see also ref.^[35] and discussion of detectors later on in the paper).

When, however, assumptions going into the hydrodynamic approximation are not valid,^[9] then a door is opened for kinetic effects such as diffusion or attachment heating or cooling,^[36–40] transient negative mobility,^[41–43] negative absolute mobility,^[43–47] anomalous time varying diffusion,^[48,49] negative transient diffusion,^[50] Holst Oosterhuis (Frank Hertz) luminous layers,^[51–53] negative differential conductivity (NDC),^[20,54] and many more. A group of kinetic phenomena may occur even when hydrodynamic conditions are not met and transport is not local.

As an example of how we may use swarm physics to get an insight about the functioning of a device, we may use a display of NDC to discuss its role in gas-filled (diffuse discharge) switches. In Figure 1, we show drift velocity of electrons in pure CF_4 where the most prominent feature is a peak around 20 Td. The region beyond the peak where drift velocity counter intuitively decreases is the NDC.

One class of devices, the so called diffuse discharge switches, were developed to control inductive storage of energy. Apparently, the power density in inductive discharges is two orders of magnitude greater than the power density of capacitive storage, which proved to be essential for applications in space. Unlike capacitive storage switch, the switch for inductive storage requires a high conductivity at low E/N and low conductivity at high. Thus it has been possible just to use the calculated drift

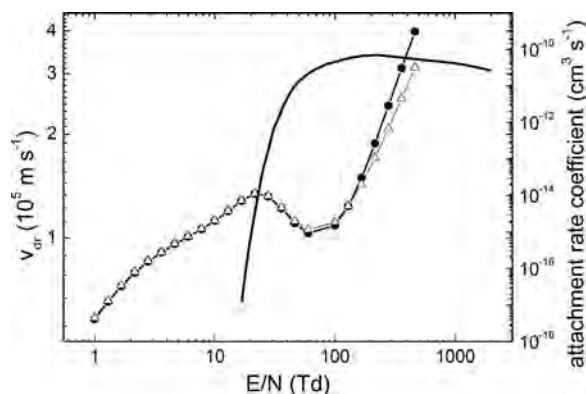


Figure 1. Drift velocity v_{dr} (points triangles flux, solid circles bulk) and attachment rate (line) for electrons in pure CF_4 .^[55] The drift velocity shows NDC from 20 to 60 Td while the attachment rate peaks at around 120 Td.

velocity versus E/N to select the best candidates for practical devices.^[56,57]

2.1. DC Breakdown

In studies of the breakdown, the self-sustained discharge is achieved when production exceeds the losses. For electro-positive gases, losses are difficult to calculate and depend strongly on the geometry of the discharge. In case of electronegative gases attachment dominates the losses and as it is a gas phase process, it is easily established in general terms. Thus, one could claim that the breakdown E/N (which defines the breakdown voltage for a specific geometry) is that where ionization rate becomes greater than the attachment rate; or when the effective multiplication coefficient ($\nu_i - \nu_{att}$) (or represented in spatial Townsend rate coefficients ($\alpha - \eta$)) becomes zero. Actually it has to be larger than zero to compensate other geometry

dependent losses, but zero point is a good indicator of the dielectric strength of the gas (mixture). In Figure 2, we also show effective multiplication rate coefficient for tetrafluoroethane mixtures with argon.^[58,59]

One can see in Figure 2 that for a low content of the electronegative gas (5%), the breakdown E/N is smaller, around 25 Td. For 50%, it is more than 70 Td and for pure tetrafluoroethane it is more than 110 Td. Thus, having in mind a cross-section set for a good gaseous dielectric, it is required that there is an attachment process (dissociative presumably) peaking at high energies just below the threshold for ionization in order to postpone to higher E/N the predominance of production over losses. Good dielectrics, however, also have an attachment (scavenging process) that would peak at the lowest energies and thus remove low energy electrons before they have a chance of accelerating to higher energies. SF_6 is such a gas with several non-dissociative and dissociative attachment processes covering continuously energies from zero to just

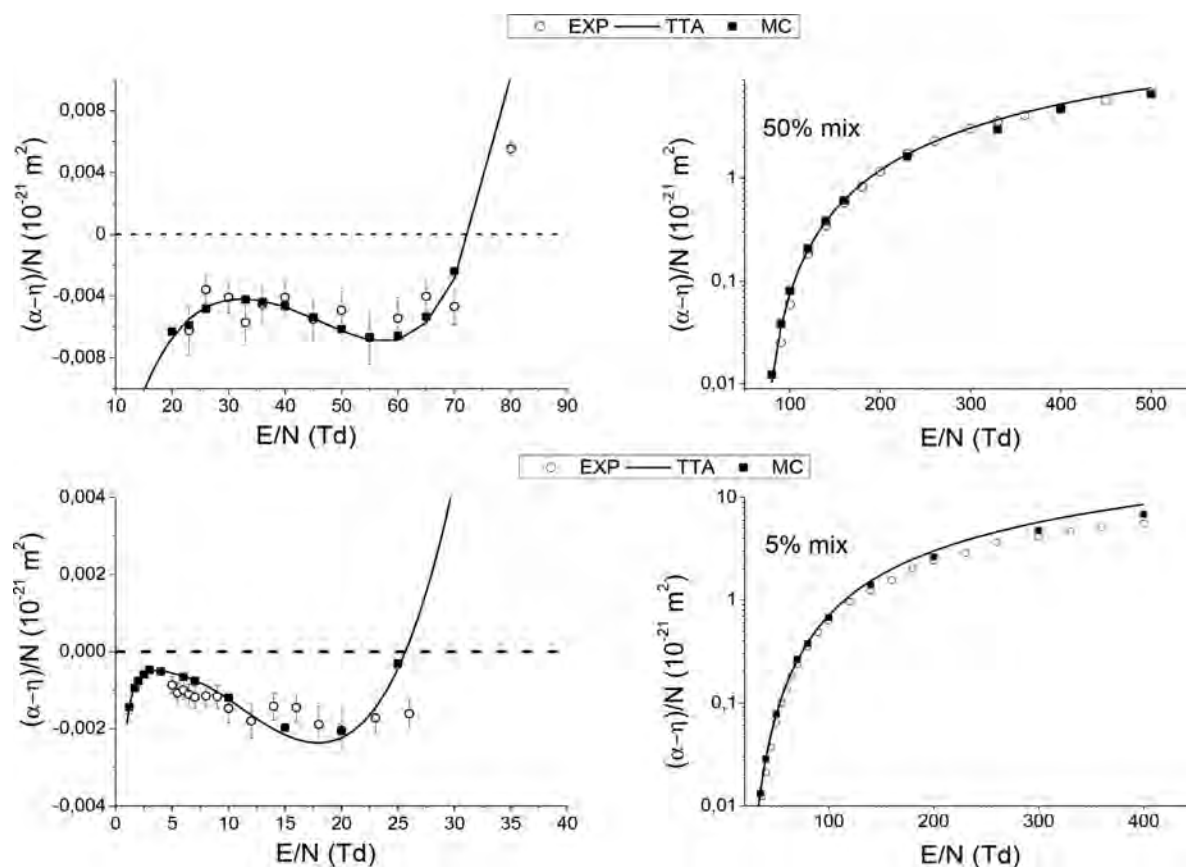


Figure 2. Effective multiplication rate for the mixture of tetrafluoroethane (5 and 50%) and argon. As we had to show the ionization rate (denoted by α) in a logarithmic plot, the negative part due to the attachment rate (denoted by η) is shown separately on a linear scale.^[58,59] MC denotes results of a Monte Carlo simulation, while TTA is an abbreviation for the two term approximation theory. Both sets of calculated results are compared to experiment. The cross-sections were obtained by employing a standard swarm procedure to the available experimental transport data.^[58,59] The principal thing that should be observed here is that for gases with large attachment, the breakdown E/N may be easily established from the calculated ionization and attachment rates as a crossover point. For many application, such analysis is sufficient for making engineering decisions.

below the ionization. Other issues in developing a good dielectric would certainly include plasma chemistry that ensues after a possible breakdown. It is preferable that the original molecule is re-formed to ascertain the longevity of the dielectric, and should the gas from the dielectric be released to the atmosphere, toxicity of products of a discharge may become an issue. Except for the plasma chemistry calculations of the dissociative effects, all other aspects of gaseous dielectrics may be modeled by a swarm model or related zero dimensional chemical kinetics models.

Similar issues need to be resolved in gas discharge switches except that the conducting phase involves high conductivity plasma that may (or may not) require a full plasma model. Yet the breakdown itself, a critical feature of the switch, is established easily through swarm modeling. Returning to the diffuse discharge opening switch, the basic principle involving NDC in gaseous mixture may be improved upon by adding a gas with a high threshold attachment that would reduce further the conductivity at the high (off phase) E/N , but in this case without the low energy attachment (as that would be a hindrance). CF_4 would be excellent for this purpose (as shown in Figure 1).

The issue of breakdown in general terms is also related purely to swarm modeling and it has been covered in some detail by Phelps and Petrović.^[60] The standard Townsend model of breakdown consists of an electron-induced avalanche and ion feedback producing new electrons at the cathode by secondary emission. It turned out^[60] that actually photo emission at low E/N , fast neutrals at high, and metastables at all E/N contribute significantly to the breakdown, sometimes even dominating. Adding to this the loss processes not accounted for in the Townsend model, such as back-diffusion, we may actually have an effective secondary electron yield obtained from the breakdown curves (according to the Paschen's theory) one order of magnitude lower or up to two orders of magnitude higher than the secondary electron yield measured in a binary beam experiment.^[60] Townsend's theory worked basically because in the SWARM regime, all fluxes are proportional (linearly) and thus the effective production could be associated with the flux of only one particle. However, in real plasmas with non-linearities and especially temporal developments the basic Townsend theory may not be adequate and thus analysis akin to that of Phelps and Petrović (that is still a swarm-type modeling) may be in order.

2.2. RF Breakdown

Basic data for radio-frequency plasma applications can be acquired from simulations and experimental results, and from recorded breakdown voltage curves. DC breakdown

voltages versus pd (p -pressure, d -gap between two parallel electrodes) are known as Paschen curves. For RF breakdown, pd scaling may be expected to work again but the curves, although similar in shape, are not determined by the Paschen law. Nevertheless, these curves are often called Paschen curves in the literature while it is better to call them RF breakdown curves or sometimes even Paschen-like RF breakdown curves.

One should never attempt to determine secondary electron yields from RF breakdown curves in a direct manner, at least for the following reason. A necessary condition for a self-sustained discharge is to have feedback between the electron growth toward instantaneous anode and their initialization at the cathode. In DC breakdown, it is the drift of ions toward the cathode coupled with a secondary electron production that provides the feedback. In RF fields, however, electrons go in both directions, depending on the phase, so a discharge may be supported purely by electrons. We have performed calculations with only electrons and also with added heavy particles, ions, and fast neutrals.

Initially, electrons were released from the middle of the gap. Cross-section sets have been compiled and tested (argon, oxygen – Itikawa^[61]; synthetic air – Phelps^[62]). In our previous paper, we have examined radio-frequency breakdown in argon under conditions when ion-induced secondary emission is negligible (electron-dominated regime).^[63] In this paper, we move further by including ions and their contribution to secondary electrons emitted from electrodes surfaces. Breakdown points are determined by slowly increasing the voltage to approach the breakdown from below the curve (right hand side and lower branch of the curve) and by increasing pressure to approach higher breakdown voltage branch (left hand side). Breakdown point is established as the one where the number of electrons begins to increase over extended time of many periods (detailed discussion is given in ref.^[63]).

At first, we examine MC simulation that includes only electrons with distance between electrodes of 1 cm. Figure 3 shows RF breakdown curves for synthetic air. Furthermore, we adjust two parameters to try to fit the experimental data, the first being the reflection coefficient for electrons on the surface of electrodes (R) and also the secondary electron yield γ (gamma) due to ion bombardment. One can observe deformation of Paschen-like curve pushing breakdown point toward lower voltages when reflection coefficient is increased arbitrarily. However the "second minimum," as Korolov et al.^[65] obtained in their experiment (also shown in Figure 3), is only achieved through an addition of the effect of secondary electron emission due to ions. Multipacting effects are observed only at much lower pressures and higher voltages. A good agreement with Korolov et al. was achieved by an assumption that secondary electron yield for ions is 0.002.

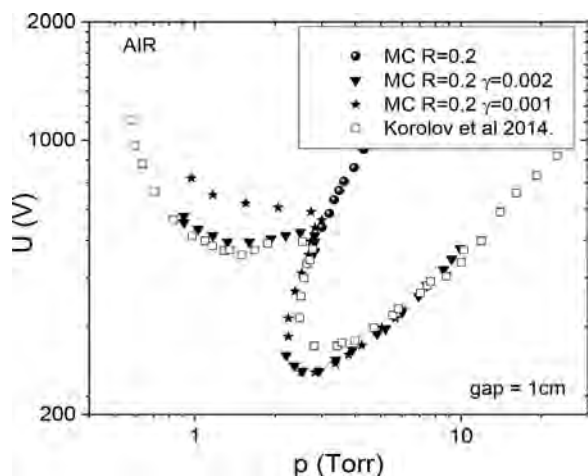


Figure 3. Paschen-like RF breakdown curves in synthetic air.^[64] Gap is 1 cm, frequency 13.56 MHz. Open points are the available experimental results in the literature.^[65] At first, only reflection of electrons (R) was adjusted but it failed to reproduce the shape of the experimental data. Furthermore, a secondary electron yield due to ion bombardment (γ) was added and a good fit of the left side branches has been achieved for $\gamma = 0.2\%$. It must be noted that Korolev et al. managed to fit their experimental points equally well by using a particle in the cell (PIC) code. While technically their code is a plasma code and thus more complex and perhaps less detailed than our Monte Carlo code. Their code has all the ingredients of a swarm model but it was not certain to what degree in their modeling the plasma-related features were necessary to fit and explain the experiments.

In Figure 4, we show space time resolved development of electron swarm properties in an RF breakdown in argon. Results are presented for both conditions where a self-sustained mode (lower (a) and higher (b) peak voltages) is operational (i.e., this is done in the region of the breakdown curves where for a fixed pd there are two values of the curve). For argon, we have used data from ref.^[60] At the lower branch of the breakdown curve, majority of electrons does not make a translation from one electrode to another as assumed in simple models^[66,67] and the discharge is maintained by a small group of higher energy particles some of which reach the electrodes. At higher branch, most electrons make the excursion along the entire gap. Remaining and newly produced electrons stay by the electrode until direction of the field changes and thus some phase shift between the positions and the field waveforms are observed together with a skewness for some properties. In both situations, the critical issue is in achieving high energies and consequently ionization to compensate the losses at the surface.

3. Low Current Discharges

In the low current limit of DC discharges, the space charge effects are either negligible or small enough to be treated as a perturbation to the external field.^[27,28,68,69] In particular, the diffuse low current regime known as

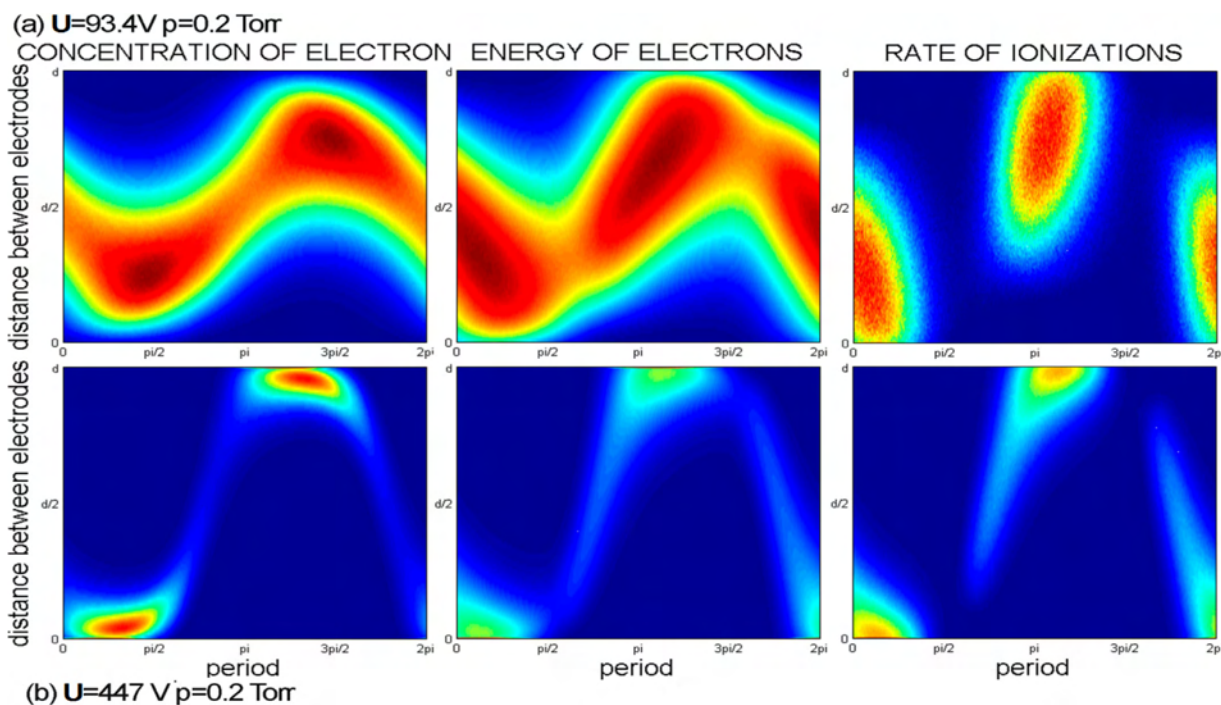


Figure 4. Spatial profiles of electron density, energy, and electron-induced ionization under conditions of an RF breakdown.^[63]

Townsend regime of DC discharges is often taken as a representation of swarm conditions^[70,71] (steady state Townsend experiment^[32,72]).

3.1. Townsend Regime/DC Discharges

If one records axial and radial profiles of emission along the Volt–Ampere (V – A) characteristics (Figure 5) of the low current DC discharges, it is clear that for the lowest of currents the profile is diffusion defined and centered^[73] while electron density exponentially increases all the way to the anode. That is the sign of the space charge free conditions and the swarm-based models will suffice or in other terms the regime is the so called Townsend discharge. The profiles in the two other regimes (Figure 5 – normal and abnormal glow) reveal a strong effect of the space charge, one in the radial the other in the axial direction. Nevertheless, even under those circumstances, charged particles may not be strongly coupled and for the purposes of theoretical description may behave like swarms, within the limitations of the modified local electric field, thus allowing the swarm physics and transport theory to be the foundation for the description of plasma.

In spite of being supposedly free of space charge effects and any strong coupling, the V – A characteristics shows

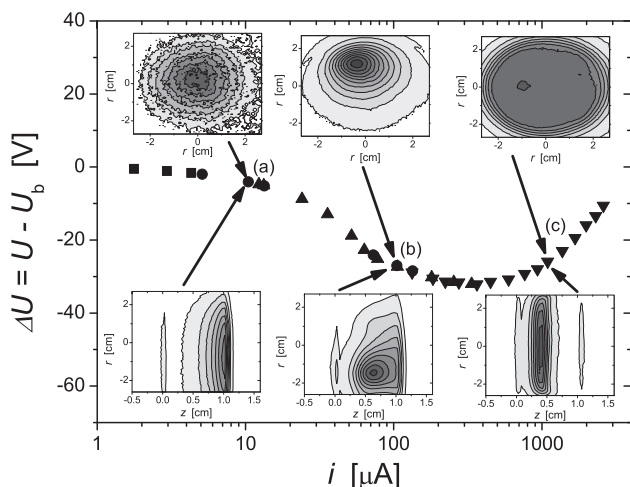


Figure 5. Spatial profiles of emission in low current DC discharges, covering the three regimes with three characteristic profiles: (a) Townsend regime or diffuse low current discharge-falling well under the realm of swarm models; (b) glow discharge-constricted low current discharge; and (c) abnormal glow-diffuse high current discharge^[73] (© IOP Publishing. Reproduced with permission. All rights reserved – doi: 10.1088/0963-0252/18/3/034009). Anode is at 1.1 cm and cathode at 0 cm and some small amount of scattered light indicates the positions of electrodes.

negative slope even in the low current limit (according to the basic Townsend theory, it should be constant) and as a result of the overall V – A characteristics and external circuit the discharge may slip into oscillations of different kinds.^[73,74]

The model developed to explain these oscillations due to the negative slope (and thus to extend Townsend's theory) is an example of swarm-based models where space charge effect is calculated based on swarm calculations and added as a perturbation. The basic assumption is that the field right next to the cathode is affected by the space charge and is affecting the energy of ions. The feedback coefficient – the secondary electron yield – cannot be assumed to be constant, as it has been well established that it is dependent on the energy of ions hitting the surface.^[60] During oscillations, the voltage and the field will change and affect secondary electron yield (the development from Equation (6) to (11) follows the theory in Phelps et al.^[27]):

$$\gamma - \gamma_p + k_U U + k_I I, \quad (6)$$

The term k_U describes the linear component of the voltage dependence. However, the critical assumption in the model is the term proportional to the current. It is actually representation of the space charge which is proportional to the current which then provides additional effect due to the slightly skewed electric field right next to the cathode. It is possible to use the density profiles of electrons and ions (ions being much slower have a much higher density and predominantly define the field perturbation) obtained by swarm physics considerations (drift and free diffusion). Using a Poisson equation we get:

$$E_{Sz}(z) - E_S^C = \frac{1}{\epsilon_0} \frac{j_z}{W_{+z}} \frac{1}{[\alpha_0 z - \exp(\alpha_0(z-d)) + \exp(-\alpha_0 d)]}, \quad (7)$$

where n_+ and n_e are concentrations of ions and electrons, j_z electrical current density in z -direction, W_{+z} drift velocity of ions, e elementary charge of electrons. The corresponding voltage drop is thus equal to:

$$\begin{aligned} \delta U_S &= - \int_0^d (E_{Sz}(z) - E_S^C) dz \\ &= - \frac{1}{\epsilon_0} \frac{j_z}{W_{+z}} f(\alpha_0, d), \end{aligned} \quad (8)$$

where f is:

$$f(\alpha_0, d) = d^2 \left[\frac{1}{2} + \frac{\exp(-\alpha_0 d)}{\alpha_0 d} - \frac{(1 - \exp(-\alpha_0 d))}{(\alpha_0 d)^2} \right], \quad (9)$$

with round the loop multiplication being

$$g(t) = \gamma[\exp(\alpha(t)d) - 1] = 1. \quad (10)$$

The effective normalized discharge resistance is

$$R_N = \frac{A}{d^2} R_D = \frac{A}{d^2} \frac{\delta U}{I} = - \frac{\hat{\gamma}}{\epsilon_0 W_{+z} \hat{g}} \frac{f(\alpha d)}{d^2}, \quad (11)$$

where A is the area of the electrode and \hat{g} is the logarithmic derivative of the multiplication factor g ($\hat{g} = \hat{\gamma} + \gamma \alpha d \exp(\alpha d) \hat{\alpha}$).

Experimental tests have confirmed the theory both in the field distribution and in the scaling of the effective resistance.^[75] R_N depends on variation with the field (and current) of the secondary electron yield but the theory also provides a foundation for the standard scaling of discharge parameters E/N , pd (Nd), and even jd^2 . This bit of theory is added here as an example of how swarm-type considerations are weaved into the plasma theory as its fundamental aspect and also how swarm data enter such calculations as the basic input on atomic and molecular collisions.

3.2. High E/N -Runaway Swarms

If one extends the range of measurements to the left hand branch of the Paschen curve, two things become obvious. The first is that the voltage drop between the Townsend regime and the glow discharge diminishes (see Figure 2 in ref.^[76]) and sometimes it is even a continuous transition. The reason is simply in the large mean free paths and then the effect of the space charge become less obvious (spread over a larger area). Another effect is observed if energy distribution function (EDF) is sampled, whereby the EDF has a strong peak at maximum available energy thus indicating a runaway.^[77] This is a situation where the initial conditions (energy distribution) is maintained (augmented by the energy drop in during the travel through the discharge) and thus properties vary from one point to the next. The low energy tail of secondary electrons also develops, which varies according to the position. Thus a hydrodynamic model is not appropriate, but a MCS may produce excellent results. It may also allow for exact inclusion of the boundary conditions, such as energy-dependent yields due to ions and electrons, energy-dependent angular distribution of secondary or reflected particles, energy-dependent energy loss, and energy-dependent electron reflection. The procedure allows for exact, experimental data to be included for any other possible boundary effect related to electrons, ions, neutrals, reactive species, metastables, and photons. At high E/N that corresponds to the left hand side of the Paschen curve, electrons are not very efficient in ionization (requiring a rapid increase in the voltage necessary for the breakdown

as pd is reduced) and even then the multiplication coefficients are only slightly higher than 1.

Due to the low pressure, mean free paths become large for both electrons and ions and they gain much larger energy than in standard discharges. This is particularly critical for ions, allowing them to extend much beyond the standard low energies (below 1 eV) all the way up to the maximum available energy. This opens the door for charge transfer collisions producing fast neutrals. It turns out that fast neutrals are at those conditions more efficient in excitation than either electrons or ions and this all leads to a peak of emission close to the cathode, that is the signature of fast neutral excitation.^[78,79] Under those circumstances, momentum transfer in heavy particle collisions leads to a transfer of kinetic energy producing Doppler profiles with excessively high energy wings.^[79–81] As a result, one could predict a possible application for fast neutral etching that would reduce the charging problems^[82,83] in treating dielectrics in nanoelectronics and allow even higher aspect ratios of nanostructures with an increased spatial resolution.

While being mostly non-hydrodynamic, the high E/N discharges are best described by swarm physics. They also open the need for similar models of ions and fast neutrals.

3.3. Microdischarges, Atmospheric Pressure Discharges, Discharges in Liquids

By the virtue of the jd^2 scaling (that has been tested), the Townsend regime may be extended to higher currents at very small gaps. While being counterintuitive, this is a well established fact at least as long as the standard gas discharge physics operates (i.e., below the onset of field emission).^[84] Extension of the Townsend regime into higher currents allows for applications of microdischarges that take advantage of the flexibility and ability to directly adjust and achieve a high efficiency of excitation and dissociation (by merely changing the E/N) while still having a high enough total output of photons and/or chemically active species^[85] for possible applications.

Microdischarges are one way to produce non-equilibrium plasma at high pressures. They simply operate close to the Paschen minimum and thus allow for much higher pressure for the given reduction in the discharge gap. In the atmosphere, the kinetics of charges is defined by swarm physics, yet if a field is added, the increase of charge density is quite large and a quick transition to highly conductive thermal plasma ensues. Atmospheric pressure discharges often have a high charge density, but in general, the whole atmosphere is an ionized gas that may be described by the physics of swarms. Of the plasmas, the corona discharge consists of streamers and diffuse discharge, which falls under the swarms jurisdiction.^[86] Calculation of transport of

electrons, ions, and other particles may proceed mainly by using free electron and ion diffusion, but one needs to take into account clusters formed by water vapor molecules and other issues.

One of the lines of the fastest development and new applications are the discharges in water (liquids in general), at the interface between liquid and gas phase, and in gas phase of vapors.^[87,88] In liquids one needs to re-establish both cross-sections, transport theory, and transport coefficients. More data are needed for low pressure transport (in gas or vapor).^[89,90] In addition, we need to establish techniques to determine and apply data at high pressures and in liquid, i.e., and multiple collision conditions,^[91] and under the influence of hydration and breakdown^[92] of clusters. In addition, even the low pressure collision and transport data for the most important ions in water vapor are missing.^[93] The liquid-related discharges^[94] provide a number of challenges and in many circumstances swarm modeling (albeit adjusted to the needs of very high densities) is required. A comprehensive review on discharges associated with liquids may be found in a forthcoming article, containing most importantly list of open issues.^[92]

3.4. Afterglow

Upon switching off of the discharge, the space charge may remain for a while as long as the charged particle densities are sufficient to produce a modified field profile. At some moment, the ambipolar field will collapse and free diffusion will ensue that is modeled by swarm physics. In that period, electrons are supposed to continuously lose energy and diminish in numbers. Under some circumstances (depending on the gas, impurities, initial energy, and distribution function and electron and ion densities), an increase of the mean energy occurs during the afterglow leading to a transient peak in the decay of the mean electron energy. Sometimes that peak may be even greater than the initial mean energy, again depending on the gas and on the initial conditions. This phenomenon has often been explained by evoking atomic and molecular physics, including processes such as Penning ionization, Rydberg states, superelastic collisions and recombination.^[95,96]

However, a very important process is often overlooked. It is the above-mentioned diffusion heating or cooling^[37] (also there is a possibility of an attachment cooling or heating^[40]). While the aforementioned processes depend on the initial densities of excited states, this process is universal as it depends only on the ground state momentum transfer cross-section. The presence of the Ramsauer–Townsend minimum in some gases allows very large mean free paths and escape of electrons to the wall of the vessel, thus increasing losses (speeding up thermalization as this could be regarded as evaporative cooling).

Results of a MCS are shown in Figure 6 where we present the development of the mean energy in a limited size discharge vessels and also for an infinite plasma in argon. In an infinite case, thermalization is slow while in the parallel plate geometry decay is much faster (Figure 6a). We also show the decay of the number density of electrons (Figure 6b). In Figure 7, we show energy distribution functions in the parallel plate and in infinite cases. In the latter case, the high energy tail disappears quickly, while the rest of the distribution is close to the Maxwell Boltzmann (MB) distribution with the same energy. This graph also shows as a very general conclusion that, even when the bulk of the distribution function is a Maxwellian, the extrapolation to the high energy tail by a Maxwellian may lead to errors of many orders of magnitude. The reason is that the high energy loss processes such as ionization

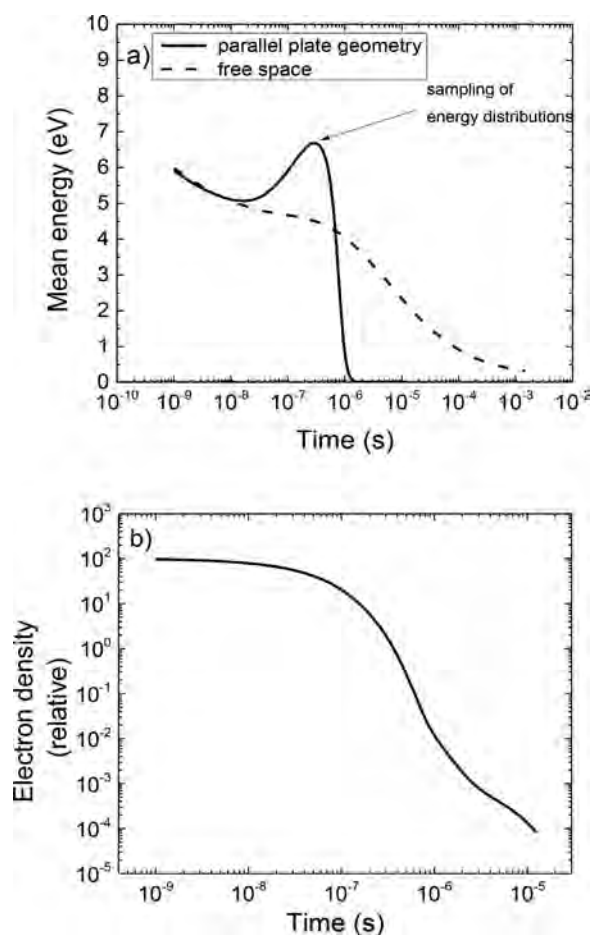


Figure 6. Thermalization (a) and decay of the number (b) of electrons in Ar from the initial MB distribution at 7 eV (argon at 1 Torr and a gap of 1 cm) in plane-parallel geometry and in free space. Arrow marks the point in time where the energy distributions that are shown in Figure 7 are sampled. Two Maxwell Boltzmann distributions are shown for comparison, each at a mean energy equal to that in the decayed measured distribution (6.5 and 4.4 eV).

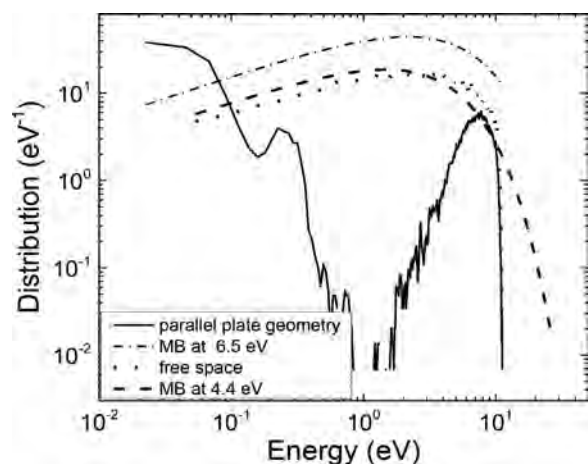


Figure 7. Energy distribution functions at the point marked in Figure 6 for the parallel plate geometry (solid) and infinite geometry (dashed). Two Maxwell Boltzmann distributions for the mean energies corresponding to the two distributions are shown.

deplete the high energy tail of the EDF especially in the low pressure discharges. The bulk of the distribution, and therefore the mean energy, slowly head toward the room temperature thermal equilibrium energy.

For the parallel plate system, due to the long mean free paths as compared to the size of the discharge (even for 1 Torr of argon and 1 cm dimension), a hole is rapidly burned in the Ramsauer–Townsend energy range. At higher energies, the distribution is similar to that of the corresponding Maxwellian, albeit with the high energy tails removed by high energy loss collisions. With the peak of the mean energy greater than the initial energy, the diffusion cooling should be taken into account by including a complete calculation of thermalization (with all the cross-sections and atomic and molecular processes). Diffusion cooling will invariably take place depending on the cross-section shapes; in case of resonant attachment a similar heating/cooling situation may arise and these processes may affect strongly non-local (non-hydrodynamic) systems such as plasma sheaths, Langmuir probe at low pressures^[97] and distribution function at the beginning of thermalization or close to the walls.

4. Data Bases for Pristine Gases and Gases with a Large Density of Excited States and Radicals

It is often discussed that the main basis of the plasma modeling is in a set of fluid equations supplied by the swarm data. It is truly important to set up the data bases with a well-prescribed procedures for evaluation in order to be able to appraise different calculations with seemingly

same gas mixtures. In addition, coherence between the cross-sections and transport data should be achieved and maintained. The fluid models that use swarm coefficients must be compared to the kinetic and hybrid codes that are based on the cross-sections. Consistency between the two sets should be achieved and it is the task of the atomic, molecular collision physics and necessarily also the swarm physics. A number of data bases has been developed for the purpose of providing low temperature plasma physics with data starting with the JILA data Center (Joint Institute for Laboratory Astrophysics of the Colorado University at Boulder and National Institute for Science and Technology),^[98] the data base of Art Phelps at JILA,^[62] NIST Data reviews,^[99] the data base of Prof. Hayashi,^[99] our data base,^[100] and many more. The most focused and certainly the largest in number of participants and quantity of data is the currently active LxCAT data base.^[101,102] One needs to include the data for ions^[100,103] including the most comprehensive data base of Prof. L. Viehland as included in LxCAT^[101] and fast neutrals.^[104] If the system is a candidate for being described by swarm models sometime it suffices just to observe the available data for some of the transport coefficients to at least appreciate qualitatively the feasibility of the particular system. However, if some kinetic phenomena and in particular non-hydrodynamic kinetic phenomena are involved a full-fledged kinetic simulation is necessary. In that case, however, in order to have proper balances of number, momentum, and energy a swarm normalized cross-sections are necessary to obtain the quantitative comparisons with experiments.

A separate issue is the modeling of plasmas when the background gas may not be regarded as pristine (unperturbed). This issue may be introduced to plasma modeling by making a self-consistent (coupled) calculations of the excited state populations and then of the energy distribution functions and effective rates and other coefficients. While the very presence of the excited states breaks the principal definition of swarms as developed for swarm experiments^[105] this, self-consistent modeling extends the applicability of swarm physics to the realm of higher currents/densities of electrons and elevated temperatures. Under these circumstances, a whole new realm of transport data opens, that involves the cross-sections for excited states (stepwise excitation, stepwise ionization, etc.). Not surprisingly first important applications involved modeling of CO₂ lasers,^[106] but also hydrogen discharges^[107,108] and nitrogen containing discharges.^[109,110] Perhaps the widest and the simplest similar modeling is that involving properties of discharges in rare gases with a large abundance of metastables in particular in argon.^[111–113] Interest in CO₂ has been reactivated recently due to the activity in energy conversion and storage.^[114] In a similar fashion, swarm models may be applied to discharges where fragments of the molecules that may have certain

properties abound. For example, the issue of attachment in CF_4 when a significant part of the molecules has been dissociated has been considered in ref.^[115] In this section, we did not attempt to make a comprehensive review, we only show few examples and we apologize to those whose work was not included in the list. There are many better sources for detailed bibliography and many much more comprehensive reviews. We only wanted to stress the importance of data when swarm modeling is attempted and also that this approach may be used in the realm of strongly perturbed gases by a large degree of excitation or dissociation thus extending the domain of applicability of swarm physics but requesting a wide range of new data.

5. Conclusion

In addition to all the examples covered here, we have recently made swarm-type modeling in a number of cases involving ionized gases but outside the realm of standard low temperature plasmas. These applications will be the subject of a separate publication^[116]:

- 1) Studies of swarms of positrons may be modeled in the same manner as electrons (without the comfort of production in collisions through ionization, although ionization produces a lot of secondary electrons).^[117] With real swarm experiments lacking, the models cannot be used to get quantitative scaling of the cross-sections, but the results provide an insight into processes and new kinetic phenomena, such as Positronium (Ps) formation fueled negative differential conductivity of the bulk component of the drift velocity.^[118]
- 2) In the absence of swarm data measurements, one may define averaged properties that may be used in the same fashion as the swarm data, for example thermalization times (or full thermalization development), ranges of particles, density of deposited energy, and more.^[119]
- 3) Trajectories of particles have been used to describe the properties, although each individual particle does not have enough distinction to give a full insight on the pertinent processes. Still, overall image, obtained by a large set of particles or individual trajectories that are selected, provide sufficient information to make important conclusions.^[120,121]
- 4) Thermalization of positronium in gases.^[122,123]
- 5) Modeling of PET like environment and modeling of chemistry induced by the initial positrons in living tissue/liquid.^[91]
- 6) Modeling of gas-filled positron (and electron) traps, such as Penning Malmberg Surko traps^[124,125] or other gas-filled traps.
- 7) Avalanches and current pulses in gas-filled RPC frequently used detectors in elementary particle

detection and the corresponding properties of the gases used in the mixture.^[126]

- 8) Streamer breakdown conditions.^[127,128]
- 9) Modeling of ionization fronts in streamers.^[129,130]

The list does not end here and in all those cases swarm studies provide models or an insight into the most salient properties of the discharge. At the same time, one should pay more attention to understanding plasma modeling (from the global to the complex hybrid and PIC codes), the role of plasma models in crossed electric and magnetic fields (e.g., for propulsion studies) and the description of some atmospheric and astrophysical systems (elves, blue jays, clouds of electrons and positrons formed in the vicinity of neutron stars, etc.).

Swarm physics is one of the building blocks of the physics of non-equilibrium plasmas. Another important building block is the swarm data which originate from swarm studies. In addition to being sufficient for some systems, learning how to deal with those will improve our knowledge on applying swarm-based transport equations and data in plasma models. In the meantime, each of the problems mentioned here is interesting, even fun to pursue and a worthwhile contribution.

Acknowledgements: This work is partly supported by Ministry of Education, Science and Technology of Republic Serbia projects ON171037 and III410011. Z. Lj. P. is also grateful to the SASA project F155. Authors are grateful to J. de Urquijo, O. Šašić, and S. Dupljanin for collaboration in obtaining results shown in Figure 2 and to M. Radmilović Radenović for collaboration in obtaining some of the results shown in Figure 4.

Received: July 3, 2016; Revised: August 12, 2016; Accepted: August 25, 2016; DOI: 10.1002/ppap.201600124

Keywords: breakdown; plasma modeling; swarm; Townsend discharge

- [1] M. A. Lieberman, A. J. Lichtenberg, "Principles of Plasma Discharges and Material Processing", Wiley, Hoboken, NJ, USA 2005.
- [2] T. Makabe, Z. Petrović, "Plasma Electronics: Applications in Microelectronic Device Fabrication", Taylor and Francis, CRC Press, New York 2006.
- [3] M. J. Kushner, *J. Phys. D: Appl. Phys.* **2009**, *42*, 194013.
- [4] S. Samukawa, M. Hori, S. Rauf, K. Tachibana, P. Bruggeman, G. Kroesen, J. Ch. Whitehead, A. B. Murphy, A. F. Gutsol, S. Starikovskaia, U. Kortshagen, J. P. Boeuf, T. J. Sommerer, M. J. Kushner, U. Czarnetzki, N. Mason, *J. Phys. D: Appl. Phys.* **2012**, *45*, 253001.

- [5] S. Pancheshnyi, S. Biagi, M. C. Bordage, G. J. M. Hagelaar, W. L. Morgan, A. V. Phelps, L. C. Pitchford, *Chem. Phys.* **2012**, *398*, 148. UBCdatabase, www.lxcat.net, June 30, 2016.
- [6] R. W. Crompton, *Adv. At. Mol. Opt. Phys.* **1994**, *33*, 97.
- [7] A. V. Phelps, *Rev. Mod. Phys.* **1968**, *40*, 399.
- [8] Z. Lj. Petrović, M. Šuvakov, Ž. Nikitović, S. Dujko, O. Šašić, J. Jovanović, G. Malović, V. Stojanović, *Plasma Sources Sci. Technol.* **2007**, *16*, S1.
- [9] Z. Lj. Petrović, S. Dujko, D. Marić, G. Malović, Ž. Nikitović, O. Šašić, J. Jovanović, V. Stojanović, M. Radmilović-Radenović, *J. Phys. D: Appl. Phys.* **2009**, *42*, 194002.
- [10] R. E. Robson, R. D. White, Z. Lj. Petrović, *Rev. Modern Phys.* **2005**, *77*, 41303.
- [11] K. Kumar, H. R. Skullerud, R. E. Robson, *Aust. J. Phys.* **1980**, *33*, 343.
- [12] S. Dujko, R. D. White, Z. Lj. Petrović, *J. Phys. D: Appl. Phys.* **2008**, *41*, 245205.
- [13] R. D. White, R. E. Robson, *Phys. Rev. E* **2011**, *84*, 031125.
- [14] R. E. Robson, "Introductory Transport Theory for Charged Particles in Gases", World Scientific Publishing Company, Singapore 2006.
- [15] I. D. Reid, *Aust. J. Phys.* **1979**, *32*, 231.
- [16] V. D. Stojanović, Z. Lj. Petrović, *J. Phys. D* **1998**, *31*, 834.
- [17] Z. M. Raspopović, S. Sakadžić, S. Bzenić, Z. Lj. Petrović, *IEEE Trans. Plasma Sci.* **1999**, *27*, 1241.
- [18] Z. Ristivojević, Z. Lj. Petrović, *Plasma Sources Sci. Technol.* **2012**, *21*, 035001.
- [19] R. E. Robson, *Aust. J. Phys.* **1984**, *37*, 35.
- [20] S. B. Vrhovac, Z. Lj. Petrović, *Phys. Rev. E* **1996**, *53*, 4012.
- [21] R. D. White, R. E. Robson, P. Nicoletopoulos, S. Dujko, *Eur. Phys. J. D* **2012**, *66*, 117.
- [22] L. C. Pitchford, A. V. Phelps, *Phys. Rev. A* **1982**, *25*, 540.
- [23] P. Segur, M. Bordage, J. Balaguer, M. Yousfi, *J. Comp. Phys.* **1983**, *50*, 116.
- [24] R. D. White, M. J. Brennan, K. F. Ness, *J. Phys. D: Appl. Phys.* **1997**, *30*, 810.
- [25] S. Dujko, Z. M. Raspopović, Z. Lj. Petrović, *J. Phys. D: Appl. Phys.* **2005**, *38*, 2952.
- [26] R. D. White, R. E. Robson, B. Schmidt, M. A. Morrison, *J. Phys. D: Appl. Phys.* **2003**, *36*, 3125.
- [27] A. V. Phelps, Z. Lj. Petrović, B. M. Jelenković, *Phys. Rev. E* **1993**, *47*, 2825.
- [28] Z. Lj. Petrović, I. Stefanović, S. Vrhovac, J. Živković, *J. Phys. IV France* **1997**, *C4*, 3412.
- [29] S. Živanov, J. Živković, I. Stefanović, S. Vrhovac, Z. Lj. Petrović, *Eur. Phys. J. AP* **2000**, *11*, 59.
- [30] L. G. H. Huxley, R. W. Crompton, "Diffusion and Drift of Electrons in Gases", Wiley-Interscience, New York 1974.
- [31] H. A. Blevin, J. Fletcher, S. R. Hunter, *J. Phys. D* **1976**, *9*, 471.
- [32] Z. Lj. Petrović, *PhD Thesis*, Australian National University (Canberra), February 1985.
- [33] H. A. Blevin, J. Fletcher, *Aust. J. Phys.* **1984**, *37*, 593.
- [34] H. Raether, *Electron avalanches and breakdown in gases (Butterworths advanced physics series)*, Butterworths, 1964.
- [35] S. Dujko, D. Bošnjaković, R. D. White, Z. Lj. Petrović, *Plasma Sources Sci. Technol.* **2015**, *24*, 054006.
- [36] T. Rhymes, R. W. Crompton, *Aust. J. Phys.* **1975**, *28*, 675.
- [37] R. E. Robson, *Phys. Rev. A* **1976**, *13*, 1536.
- [38] H. I. Leemon, K. Kumar, *Aust. J. Phys.* **1975**, *28*, 25.
- [39] K. Koura, *J. Chem. Phys.* **1982**, *76*, 390.
- [40] D. R. A. McMahon, R. W. Crompton, *J. Chem. Phys.* **1983**, *78*, 603.
- [41] B. Shizgal, D. R. A. Mc Mahon, *Phys. Rev. A* **1985**, *31*, 1894.
- [42] J. M. Warman, U. Sowada, M. P. De Haas, *Phys. Rev. A* **1985**, *31*, 1974.
- [43] Z. Donko, N. Dyatko, *Eur. Phys. J. D* **2016**, *70*, 135.
- [44] N. A. Dyatko, A. P. Napartovich, S. Sakadžić, Z. Lj. Petrović, Z. Raspopović, *J. Phys. D* **2000**, *33*, 375.
- [45] R. E. Robson, Z. Lj. Petrović, Z. M. Raspopović, D. Loffhagen, *J. Chem. Phys.* **2003**, *119*, 11249.
- [46] M. Šuvakov, Z. Ristivojević, Z. Lj. Petrović, S. Dujko, Z. M. Raspopović, N. A. Dyatko, A. P. Napartovich, *IEEE Trans. Plasma Sci.* **2005**, *33*, 532.
- [47] S. Dujko, Z. M. Raspopović, T. Makabe, Z. Lj. Petrović, *IEEE Trans. Plasma Sci.* **2003**, *31*, 711.
- [48] R. D. White, R. E. Robson, K. F. Ness, *Aust. J. Phys.* **1995**, *48*, 925.
- [49] K. Maeda, T. Makabe, N. Nakano, S. Bzenić, Z. Lj. Petrović, *Phys. Rev. E* **1997**, *55*, 5901.
- [50] R. D. White, S. Dujko, K. F. Ness, R. E. Robson, Z. Raspopović, Z. Lj. Petrović, *J. Phys. D: Appl. Phys.* **2008**, *41*, 025206.
- [51] M. Hayashi, *J. Phys. D* **1982**, *15*, 1411.
- [52] R. E. Robson, B. Li, R. D. White, *J. Phys. B: At. Mol. Opt. Phys.* **2000**, *33*, 507.
- [53] S. Dujko, Z. M. Raspopović, R. D. White, T. Makabe, Z. Lj. Petrović, *Eur. Phys. J. D* **2014**, *68*, 166.
- [54] Z. Lj. Petrović, R. W. Crompton, G. N. Haddad, *Aust. J. Phys.* **1984**, *37*, 23.
- [55] M. Kurihara, Z. Lj. Petrović, T. Makabe, *J. Phys. D* **2000**, *33*, 2146.
- [56] L. G. Christophorou, S. R. Hunter, "Electron Molecule Interactions", Academic Press, New York 1984.
- [57] K. H. Schoenbach, G. Schaefer, E. E. Kunhardt, M. Kristianson, L. L. Hatfield, A. H. Guenther, *IEEE Trans. Plasma Sci.* **1982**, *PS-10*, 246.
- [58] O. Šašić, S. Dupljanin, J. de Urquijo, Z. Lj. Petrović, *J. Phys. D: Appl. Phys.* **2013**, *46*, 325201.
- [59] O. Šašić, S. Dupljanin, S. Dujko, D. Bošnjaković, A. Banković, J. de Urquijo, Z. Lj. Petrović, **2017**, unpublished.
- [60] A. V. Phelps, Z. Lj. Petrović, *Plasma Sources Sci. Tech.* **1999**, *8*, R21.
- [61] Y. Itikawa, *J. Phys. Chem. Ref. Data* **2009**, *38*, 1.
- [62] A. V. Phelps, http://jila.colorado.edu/~avp/collision_data/electronneutral/ELECTRON.TXT, 2016.
- [63] M. Savić, M. Radmilović-Radjenović, M. Šuvakov, S. Marjanović, Z. Lj. Petrović, *IEEE Trans. Plasma Sci.* **2011**, *39*, 2556.
- [64] M. Savić, J. Sivoš, D. Marić, G. Malović, Z. Lj. Petrović, **2017**, unpublished.
- [65] I. Korolov, A. Derzsi, Z. Donko, *J. Phys. D: Appl. Phys.* **2014**, *47*, 475202.
- [66] A. von Engel, "Ionized Gases", Clarendon Press, Oxford 1955.
- [67] V. A. Lisovskiy, V. D. Yegorenkov, *J. Phys. D: Appl. Phys.* **1998**, *31*, 3349.
- [68] V. I. Kolobov, A. Fiala, *Phys. Rev. E* **1994**, *50*, 3018.
- [69] R. R. Arslanbekov, V. I. Kolobov, *J. Phys. D: Appl. Phys.* **2003**, *36*, 2986.
- [70] K. Tachibana, A. V. Phelps, *J. Chem. Phys.* **1981**, *75*, 3315.
- [71] S. A. Lawton, A. V. Phelps, *J. Chem. Phys.* **1978**, *69*, 1055.
- [72] Y. Sakai, H. Tagashira, S. Sakamoto, *J. Phys. D* **1977**, *10*, 1035.
- [73] D. Marić, G. Malović, Z. Lj. Petrović, *Plasma Sources Sci. Technol.* **2009**, *18*, 034009.
- [74] Z. Lj. Petrović, A. V. Phelps, *Phys. Rev. E* **1993**, *47*, 2806.
- [75] I. Stefanović, Z. Lj. Petrović, *Jpn. J. Appl. Phys.* **1997**, *36*, 4728.
- [76] D. Marić, M. Savić, J. Sivoš, N. Škoro, M. Radmilović-Radjenović, G. Malović, Z. Lj. Petrović, *Eur. Phys. J. D* **2014**, *68*, 155.

- [77] S. B. Vrhovac, V. D. Stojanović, B. M. Jelenković, Z. Lj. Petrović, *J. Appl. Phys.* **2001**, *90*, 5871.
- [78] D. A. Scott, A. V. Phelps, *Phys. Rev. A* **1991**, *43*, 3043.
- [79] Z. Lj. Petrović, A. V. Phelps, *Phys. Rev. E* **2009**, *80*, 016408.
- [80] E. Li Ayers, W. Benesch, *Phys. Rev. A* **1988**, *37*, 194.
- [81] A. V. Phelps, B. Jelenkovic, L. C. Pitchford, *Phys. Rev. A* **1987**, *36*, 5327.
- [82] Z. Lj. Petrović, V. D. Stojanović, *J. Vac. Sci. Technol. A* **1998**, *16*, 329.
- [83] S. Samukawa, K. Sakamoto, K. Ichiki, *J. Vac. Sci. Technol.* **2002**, *A20*, 1.
- [84] Z. Lj. Petrović, N. Škoro, D. Marić, C. M. O. Mahony, P. D. Maguire, M. Radmilović-Radenović, G. Malović, *J. Phys. D: Appl. Phys.* **2008**, *41*, 194002.
- [85] J. G. Eden, S.-J. Park, *Plasma Phys. Control. Fusion* **2005**, *47*, B83.
- [86] N. Hasan, D. S. A. Farouk, *Plasma Sources Sci. Technol.* **2014**, *23*, 035013.
- [87] N. Škoro, D. Marić, G. Malović, W. G. Graham, Z. Lj. Petrović, *Phys. Rev. E* **2011**, *84*, 055401(R).
- [88] J. Sivoš, N. Škoro, D. Marić, G. Malović, Z. Lj. Petrović, *J. Phys. D: Appl. Phys.* **2015**, *48*, 424011.
- [89] R. D. White, M. J. Brunger, N. A. Garland, R. E. Robson, K. F. Ness, G. Garcia, J. de Urquijo, S. Dujko, Z. Lj. Petrović, *Eur. Phys. J. D* **2014**, *68*, 125.
- [90] F. Blanco, A. M. Roldán, K. Krupa, R. P. McEachran, R. D. White, S. Marjanović, Z. Lj. Petrović, M. J. Brunger, J. R. Machacek, S. J. Buckman, J. P. Sullivan, L. Chiari, P. Limão-Vieira, G. Garcia, *J. Phys. B: At. Mol. Opt. Phys.* **2016**, *49*, 145001.
- [91] R. E. Robson, M. J. Brunger, S. J. Buckman, G. Garcia, Z. Lj. Petrović, R. D. White, *Sci. Rep.* **2015**, *5*, 12674.
- [92] P. Bruggeman, M. Kushner, B. Locke, H. Gardeniers, B. Graham, D. Graves, R. Hofman-Caris, D. Maric, J. Reid, E. Ceriani, D. Fernandez Rivas, J. Foster, S. Garrick, Y. Gorbanev, S. Hamaguchi, F. Iza, H. Jablonowski, E. Klimova, F. Krcma, J. Kolb, P. Lukes, Z. Machala, I. Marinov, D. Mariotti, S. Mededovic Thagard, D. Minakata, E. Neyts, J. Pawlat, Z. Petrovic, R. Pflieger, S. Reuter, D. Schram, S. Schroeter, M. Shiraiwa, B. Tarabova, P. Tsai, J. Verlet, T. von Woedtke, K. Wilson, K. Yasui, G. Zvereva, *Plasma Sources Sci. Technol.* **2016**.
- [93] V. Stojanović, Z. Raspopović, D. Marić, Z. Lj. Petrović, *Eur. Phys. J. D* **2015**, *69*, 63.
- [94] P. Bruggeman, C. Leys, *J. Phys. D: Appl. Phys.* **2009**, *42*, 053001.
- [95] A. B. Blagoev, Tc. K. Popov, *Phys. Lett. A* **1979**, *70*, 416.
- [96] Y. Celik, T. V. Tsankov, M. Aramaki, S. Yoshimura, D. Luggenhölscher, U. Czarnetzki, *Phys. Rev. E* **2012**, *85*, 046407.
- [97] V. Godyak, B. Alexandrovich, *Plasma Sources Sci. Technol.* **2015**, *24*, 052001.
- [98] L. J. Kieffer, *A Compilation of Electron Collision Cross. Section Data for Modeling Gas Discharge Lasers*, JILA Report #13 **1973**.
- [99] M. Hayashi, "Electron Collision Cross Sections Determined from Beam and Swarm Data by Boltzmann Analysis", in *Nonequilibrium Processes in Partially Ionized Gases*, Plenum Press, New York **1990**, or LXcat database: <http://fr.lxcat.net>
- [100] Institute of Physics University of Belgrade, Center for non-equilibrium processes database: <http://mail.ipb.ac.rs/~cep/ipb-cnp/ionsweb/database.htm> **2016**.
- [101] LXCAT database: http://fr.lxcat.net/data/set_type.php **2016**.
- [102] L. C. Pitchford, L. L. Alves, K. Bartschat, S. F. Biagi, M. C. Bordage, A. V. Phelps, C. M. Ferreira, G. J. M. Hagelaar, W. L. Morgan, S. Pancheshnyi, V. Puech, A. Stauffer, O. Zatsarinny *J. Phys. D: Appl. Phys.* **2013**, *46*, 334001.
- [103] Z. Lj. Petrović, Z. M. Raspopović, V. D. Stojanović, J. V. Jovanović, G. Malović, T. Makabe, J. de Urquijo, *Appl. Surf. Sci.* **2007**, *253*, 6619.
- [104] A. V. Phelps, *J. Phys. Chem. Ref. Data* **1991**, *20*, 557.
- [105] L. G. Huxley, R. W. Crompton, "The Drift and Diffusion of Electrons in Gases", Wiley Interscience, New York **1974**.
- [106] J. J. Lowke, A. V. Phelps, B. W. Irwin *J. Appl. Phys.* **1973**, *44*, 4664.
- [107] C. Gorse, M. Capitelli, J. Bretagne, M. Bacal, *Chem. Phys.* **1985**, *93*, 1.
- [108] R. Celiberto, R. K. Janev, A. Laricchiuta, M. Capitelli, J. M. Wadehra, D. E. Atems, *Atomic Data Nucl. Data* **2001**, *77*, 161.
- [109] P. A. Sá, V. Guerra, J. Loureiro, N. Sadeghi, *J. Phys. D: Appl. Phys.* **2004**, *37*, 221.
- [110] G. M. Petrov, J. P. Matte, I. Pérès, J. Margot, T. Sadi, J. Hubert, K. C. Tran, L. L. Alves, J. Loureiro, C. M. Ferreira, V. Guerra, G. Goussset, *Plasma Chem. Plasma Process.* **2000**, *20*, 183.
- [111] F. Tochikubo, Z. Lj. Petrović, S. Kakuta, N. Nakano, T. Makabe, *Jpn. J. Appl. Phys.* **1994**, *33*, 4271.
- [112] S. Wang, A. E. Wendt, J. B. Boffard, C. C. Lin, S. Radovanov, H. Persing, *J. Vac. Sci. Technol. A* **2013**, *31*, 021303.
- [113] D. P. Lymberopoulos, D. J. Economou, *J. Appl. Phys.* **1993**, *73*, 3668.
- [114] L. D. Pietanza, G. Colonna, V. Laporta, R. Celiberto, G. D'Ammando, A. Laricchiuta, M. Capitelli, *J. Phys. Chem. A* **2016**, *120*, 2614.
- [115] Ž. D. Nikitović, V. D. Stojanović, J. Paul Booth, Z. Lj. Petrović, *Plasma Sources Sci. Technol.* **2009**, *18*, 035008.
- [116] Z. Lj. Petrović, I. Simonovic, S. Marjanović, D. Bošnjaković, D. Maric, G. Malovic, S. Dujko, *Plasma Phys. Control. Fusion* **2016**, submitted.
- [117] A. Banković, S. Dujko, S. Marjanović, R. D. White, Z. Lj. Petrović, *Eur. Phys. J. D* **2014**, *68*, 127.
- [118] A. Banković, S. Dujko, R. D. White, J. P. Marler, S. J. Buckman, S. Marjanović, G. Malović, G. Garcia, Z. Lj. Petrović, *New J. Phys.* **2012**, *14*, 035003.
- [119] Z. Lj. Petrović, S. Marjanović, S. Dujko, A. Banković, G. Malović, S. Buckman, G. Garcia, R. White, M. Brunger, *Appl. Radiat. Isotopes* **2014**, *83*, 148.
- [120] S. Marjanović, A. Banković, R. D. White, S. J. Buckman, G. Garcia, G. Malović, S. Dujko, Z. Lj. Petrović, *Plasma Sources Sci. Technol.* **2015**, *24*, 025016.
- [121] G. Garcia, Z. Lj. Petrović, R. White, S. Buckman, *IEEE Trans. Plasma Sci.* **2011**, *39*, 2962.
- [122] S. Marjanović, M. Šuvakov, J. J. Engbrecht, Z. Lj. Petrović, *Nucl. Instrum. Methods Phys. Res. B* **2012**, *279*, 80.
- [123] M. R. Natisin, J. R. Danielson, C. M. Surko, *J. Phys. B: At. Mol. Opt. Phys. B* **2014**, *47*, 225209.
- [124] J. R. Danielson, D. H. E. Dubin, R. G. Greaves, C. M. Surko, *Rev. Mod. Phys.* **2015**, *87*, 247.
- [125] S. Marjanović, M. Šuvakov, A. Banković, M. Savić, G. Malović, S. J. Buckman, Z. Lj. Petrović, *IEEE Trans. Plasma Sci.* **2011**, *39*, 2614.
- [126] D. Bošnjaković, Z. Lj. Petrović, S. Dujko, *J. Instrum.* **2014**, *9*, P09012.
- [127] J. Teunissen, U. Ebert, *Plasma Sources Sci. Technol.* **2016**, *25*, 044005.
- [128] S. Nijdam, J. Teunissen, E. Takahashi, U. Ebert, *Plasma Sources Sci. Technol.* **2016**, *25*, 044001.
- [129] A. H. Markosyan, J. Teunissen, S. Dujko, U. Ebert, *Plasma Sources Sci. Technol.* **2015**, *24*, 065002.
- [130] S. Dujko, A. H. Markosyan, R. D. White, U. Ebert, *J. Phys. D: Appl. Phys.* **2013**, *46*, 475202.

Gas breakdown and secondary electron yields^{*}

Dragana Marić^a, Marija Savić, Jelena Sivoš, Nikola Škoro, Marija Radmilović-Radjenović, Gordana Malović, and Zoran Lj. Petrović

Institute of Physics Belgrade, University of Belgrade, Pregrevica 118, 11080 Belgrade, Serbia

Received 31 January 2014 / Received in final form 8 April 2014

Published online 23 June 2014 – © EDP Sciences, Società Italiana di Fisica, Springer-Verlag 2014

Abstract. In this paper we present a systematic study of the gas breakdown potentials. An analysis of the key elementary processes in low-current low-pressure discharges is given, with an aim to illustrate how such discharges are used to determine swarm parameters and how such data may be applied to modeling discharges. Breakdown data obtained in simple parallel-plate geometry are presented for a number of atomic and molecular gases. Ionization coefficients, secondary electron yields and their influence on breakdown are analyzed, with special attention devoted to non-hydrodynamic conditions near cathode.

1 Introduction

It is often said that atomic and molecular collisions define the physics of non-equilibrium (so-called low-temperature) plasma. However, in plasma modeling, where space charge and field profile effects intervene with atomic and molecular collisions, often it is claimed that the collisional cross sections, rate coefficients and swarm transport data do not need to be very accurate as the processes are so complicated that high accuracy is not required. Gas breakdown, on the other hand, is the point where inaccuracies of the atomic collision and swarm data are amplified and at the same time the conditions for the breakdown often define the operating conditions for the plasma. To illustrate this we may give an example that ionization rate enters the breakdown condition in exponent and also that rate is often exponentially dependent on the gas density normalized electric field E/N . The mean energy and the shape of the distribution function that define the rate (together with the cross section for ionization) are on the other hand strongly dependent on all relevant inelastic processes. Breakdown under DC fields and slowly varying AC fields also depends on surface collisions of ions and atoms. Thus, breakdown condition is a very sensitive projection of atomic and molecular collision and swarm transport physics onto the realm of plasma physics.

Gas breakdown has been studied over 100 years and yet many open issues still remain. In DC discharges, the breakdown is usually described by the standard Townsend's theory [1]. Within the past 20 years, with development of experimental and modeling techniques, it

became clear that the standard (basic Townsend's theory as depicted in the textbooks) theory of breakdown and low-current discharges (the so-called Townsend's regime) requires improvement. Phelps and coworkers [2–5] initiated a comprehensive revision of the theory in all its aspects.

This revision in the lowest current limit (breakdown) included taking into account the contribution of all feedback mechanisms and space-charge effects in breakdown and low-current discharges [5]. These authors only covered one gas (argon) with detailed analysis. This is why we felt that a survey of the existing well documented breakdown data would be of value as the basis for further study on the data and elucidation of the issues in use of secondary electron yields in plasma modeling. All of the presented results were obtained in our laboratory and an utmost care has been invested to avoid the usual problems in determining the breakdown data (often depicted as Paschen curves). Those include variable surface conditions, jumping straight into the glow discharge mode, recording the operating conditions for the glow discharge and also the uncertainties that arise from the long statistical delays in initiation of gas discharges.

For many years swarm experiments have represented the primary source of data for gas discharge modeling, which, on the other hand, was based on the transport theory for swarms. With only very few exceptions, the models are based on the hydrodynamic (in equilibrium with the electric field and spatially uniform) transport data. This is however not applicable in most breakdown experiments as the early stages of the breakdown occur before equilibration of the electron swarm. Thus we present also an analysis of electron excitation cross sections and studies of spatial profiles of emission to separate excitation by electrons and fast neutrals [6]. Our results also allow us to determine the width of the non-hydrodynamic region close to the cathode and the effective multiplication as

^{*} Contribution to the Topical Issue "Electron and Positron Induced Processes", edited by Michael Brunger, Radu Campeanu, Masamitsu Hoshino, Oddur Ingólfsson, Paulo Limão-Vieira, Nigel Mason, Yasuyuki Nagashima and Hajime Tanuma.

^a e-mail: draganam@ipb.ac.rs

well as the approximate determination of the field distribution in dark Townsend discharges. These data all need to be applied to determine the secondary electron yields and in modeling of plasmas.

Over the past two decades determination of the secondary electron yields [6,7] has had renewed interests, for two reasons. First, a systematic survey [5] has been made of all the processes that participate to secondary electron production and it was shown that the basic assumption of Townsend's theory that ions produce the secondary electrons is correct only in a very narrow range of conditions, while photons and gas phase ionization by neutrals contribute to the secondary electron production in a much wider range of E/N . Most importantly, it became possible to model the observed secondary electron yields in the breakdown by using binary collision (beam to surface) data.

It was shown that it is not possible to use directly the binary collision (beam-surface) data for the analysis of gas discharges and low temperature plasmas as those would have specific distributions of all the relevant fluxes that otherwise might be connected through nonlinear relations. The analysis performed for the breakdown (where all fluxes are in linear relation to the initial flux of electrons) proved to be quite robust and still fit most of the data for the glow discharges [8,9]. Nevertheless, it is possible that for some gases or some plasmas, nonlinearities may prevail and the required model may depart from the breakdown model.

In this paper we present the data on breakdown voltages (shown as Paschen curves) for a large number of gases, we show some examples on how these data are coupled with Volt-Ampere (V - A) characteristics, and we proceed to determine secondary electron yields for rare gases (assuming ions to be the primary agent producing secondary electrons) with the inclusion of the effects of equilibration and proper determination of the ionization growth coefficient.

2 Breakdown voltages and Paschen curves

Breakdown is usually represented by a Paschen curve i.e. dependence of the breakdown V_b voltage on the pd (pressure $p \times$ gap d). Parameter pd is a scaling parameter proportional to the number of collisions over a unit distance. In this respect, a typical sharp increase of the breakdown voltage at low pd -s can be explained by the need to compensate for a small number of collisions. On the other hand, at high pd -s, due to a large number of collisions, breakdown voltage is increased in order to enhance energy gain between collisions, when mean free path is getting shorter and the energy gained between two collisions becomes smaller. In the range of the Paschen minimum, production of charges by ionization and secondary electron emission and losses by attachment, diffusion and drift are well balanced.

In Figure 1 Paschen curves for several atomic and molecular gases are presented. Measurements with H_2 , SF_6 , CF_4 , H_2O and C_2H_5OH vapours are taken with the

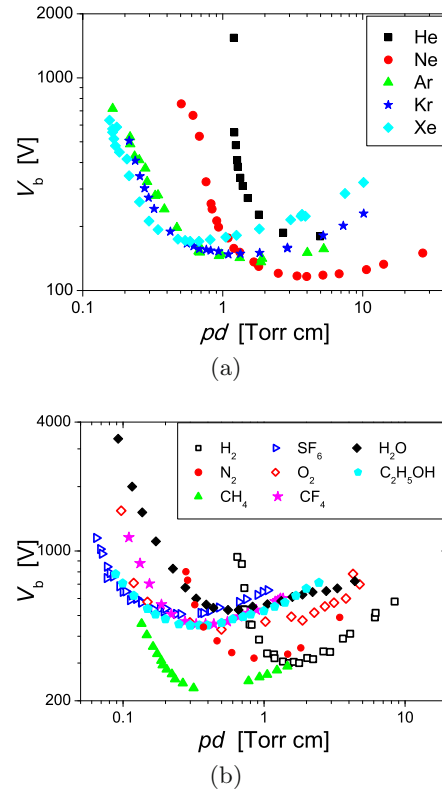


Fig. 1. Paschen curves for (a) atomic gases: Ar, He, Ne, Xe, Kr [6] and (b) molecular gases H_2 , SF_6 , O_2 , CH_4 , N_2 [12], CF_4 [10], and H_2O [11] and C_2H_5OH vapours. Measurements with H_2 , SF_6 , CF_4 , H_2O and C_2H_5OH vapours were obtained with copper cathode, for other gases stainless steel cathode was used.

copper cathode, with 1 cm electrode gap and 5.4 cm diameter [10,11]. For all other gases, stainless steel cathode was used in measurements in 2.9 cm gap and 8 cm electrode diameter [6,12]. Some of the data had preliminary presentation in the second edition of the textbook by Lieberman and Lichtenberg [13].

For most of the gases Paschen minimum is situated at pd of the order of 1 Torr cm and breakdown voltages are of the order of several hundred volts. In the case of electronegative gases, it is usually shifted towards smaller pd -s and higher voltages. This can be understood from the point of view of the balance of production and losses of charged particles. In electronegative gases, at low E/N i.e. high pd , attachment becomes important. As a loss mechanism for electrons, it will increase the breakdown voltage and shift the Paschen minimum to lower pressures as an even higher E/N is required to provide sufficient ionization.

There are several issues that one has to be aware of in breakdown measurements. Breakdown voltage depends on the gas mixture through identities of ions and on the cathode material. Even more important than the cathode material is the state of the cathode surface – roughness or possible oxide layers and other impurities deposited on its surface either by exposing the cathode to the laboratory environment or during the discharge operation. Sometimes

the state of the cathode surface has larger influence on the Paschen curve than the material of the cathode itself. For this reason, in our experiments cathode surfaces are treated in low-current ($\sim 30 \mu\text{A}$) hydrogen discharge prior to the breakdown measurements. This procedure proved to give stable conditions during measurements and reproducible results over large periods of time. Even when basic breakdown voltage varies due to surface conditions, the Paschen curve (and also the V - A characteristics) maintain their shape and so normalization onto the breakdown voltage is a good way to analyze the data [5,14].

Another issue that has to be taken into account in experiments is the regime in which the discharge ignites. Breakdown voltage should not be confused with the operating voltage. The point where the discharge operates is at the crossing of the circuit load-line and the Volt-Ampere characteristics. Quite often, especially with a small series resistance and sufficiently large overvoltages, this is in the regime of a glow discharge, where voltage can be significantly smaller than the breakdown voltage. Actual breakdown voltage, in the sense that is represented by the Paschen law, can only be found by extrapolating Volt-Ampere characteristics to zero current in the dark Townsend discharge mode. An alternative technique is to study the pre-breakdown currents [15,16]. Sometimes it is even necessary to record the spatial profile of the discharge in order to confirm the exponential increase of emission from the cathode all the way to the anode, which is typical for low-current Townsend discharge.

It is important to emphasize that, besides the Paschen curves, Volt-Ampere characteristics are essential in understanding the process of breakdown. These data are needed to establish the electric field/energy dependence of the secondary electron yields and as a consequence the slope of the V - A characteristics in the Townsend regime is defined. The slope of the characteristics is typically negative in the low-current region and it reveals the ion energy dependence of the secondary electron yield and field distortion due to the initial growth of space charge [2,3,17]. In practice, for a full description of the discharge a 3D plot should be constructed [18], such as the one shown in Figure 2, with discharge voltage (V), pressure \times electrode gap product (pd) and discharge current (i) presented at the axes.

Low-current limit represents Paschen curve and in this case it is projected onto $1 \mu\text{A}$ as further changes of voltage at even lower currents would be negligible. Measurements are taken in a parallel-plate electrode system, with 1 cm gap, 5.4 cm electrode diameter and copper cathode. Considerable difference between the glow regime and Townsend regime voltages is clearly seen from the characteristics.

3 Model of the gas breakdown and secondary electron yields

Secondary electron emission is one of the key mechanisms of DC breakdown and operation of discharges. Still, there

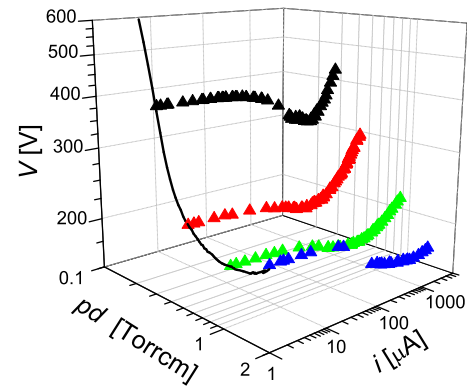


Fig. 2. Experimental V - A - pd characteristics for argon.

is a great confusion in literature in respect to the meaning of the data entering the breakdown condition. In fact, the secondary electron yield data obtained from the gas breakdown have always failed to match the direct measurements in the binary beam-surface experiments. As Phelps and Petrović [5] confirmed in the case of argon, the basic phenomenology of Townsend's theory required extension. Almost constant secondary yield of around 8% for argon ions that has been obtained by ion beams on surfaces cannot be applied to model even the basic low pressure breakdown. While one could justify a greater secondary yield due to additional processes, in the main section of mean energies the yield is actually ten times smaller than that from beam measurements. Phelps and Petrović developed a comprehensive model for argon that included all possible feedback mechanisms – secondary emission by ions, metastables, fast neutrals and photons. They also included back-diffusion of electrons and discussed conditions at the surface where standard gas discharge experiments cannot reach the conditions defined for atomically clean surfaces in ultra-high vacuum. Their study showed that one has to take into account energy dependent yields for each of the species from binary experiments in order to be in accordance with results of direct breakdown measurements. Here, we shall follow the standard procedure to determine secondary yields from the breakdown data and we shall also try to correct some of the problems and provide the data required for such corrections.

Under the conditions of the breakdown and low-current Townsend discharges, the effective secondary emission yield (γ) is related to the ionization coefficient (α) in accordance with the Townsends self-sustaining condition:

$$\gamma = \frac{1}{e^{(\alpha/N) \times Nd} - 1} \quad (1)$$

where N represents the gas number density and d is the gap between the electrodes. $\gamma(E/N)$ may be deduced from Paschen curves by using $\alpha/N(E/N)$ data from the literature [19] as was done in [6]. One may also use an analytic form of $\alpha/N(E/N)$, e.g. Marić et al. [20], as it was shown in [21]. This procedure is the standard one. Perhaps the most important problem in the procedure is that

the non-hydrodynamic region close to the cathode (d_0) affects the total multiplication, and therefore the secondary electron yield obtained from the Paschen curve. The second problem is that the ionization rate taken from the literature may give quite different multiplication as compared with the actual experiment. Even small errors in ionization coefficient result in large discrepancies of the secondary electron yield.

4 Determination of the equilibration distance

It is well-known that hydrodynamic conditions are characterized by transport coefficients that are constant in space and time [22]. However, in low-current electrical discharges at low pressures electrons do not reach the equilibrium state immediately after leaving the cathode. Only at a certain distance from the cathode electrons establish equilibrium with the gas and parameters of electron transport become spatially independent [23,24]. In a simplified approach the width of the non-hydrodynamic region may be used to separate discharge into two regions: one that can be referred to as the non-equilibrium region, with no ionization and the other where ionization behaves as if electrons are in hydrodynamic equilibrium. The problem is then how to determine the delay distance from independent measurements, by using semi-empirical formula such as the one suggested by Phelps and Petrović [5] or by kinetic calculations.

It was shown that inclusion of the effect of equilibration causes a large difference in secondary electron yield data [5], but most authors in the available literature obtain the secondary electron yields from the breakdown data without paying attention to this correction. The role of the equilibration length in determination of the secondary electron yield was studied by Folkard and Haydon [24]. A more detailed discussion of the application of the delay distance and correct determination of the effective electron yield have already been published for the case of argon [6] and for nitrogen [21].

The appropriate form of multiplication factor under Townsend's breakdown conditions is [5]:

$$\gamma = \frac{1}{e^{\alpha(d-d_0)} - 1} \quad (2)$$

where d is the gap between electrodes, and d_0 is the delay distance which has to be passed before electrons reach hydrodynamic equilibrium allowing avalanching characterized by the equilibrium ionization coefficient α . As there is a great need to determine accurate yield coefficients for plasma modeling, there is also a need to establish procedures to determine the equilibration distance.

In our experiments it is possible to obtain equilibration distances from spatial scans of emission. The width of the non-hydrodynamic region d_0 may be used to separate the discharge into two regions. Figure 3 shows two examples of spatial profiles of emission which illustrate the procedure for determination of the equilibration distance and ionization coefficients. In the case of xenon, the non-hydrodynamic width is exhibited as a flat region close to

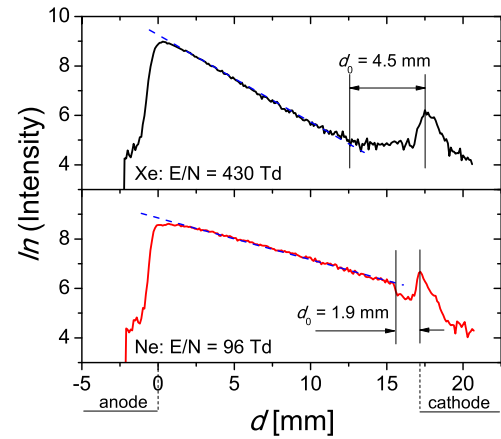


Fig. 3. Examples of the spatial emission profiles in xenon (upper plot) and neon (lower plot), with non-hydrodynamic regions indicated.

the cathode followed by exponential growth of emission. In the case of neon, there is even a sudden jump of emission just after the equilibration distance. It is still not clear what is the origin of emission in the region next to the cathode [25], as one would expect that there is no emission in non-equilibrium region. Growth of emission in hydrodynamic region is determined by a single exponential that is in excellent agreement with the equilibrium ionization coefficient [26]. While this is not the most accurate method to determine ionization coefficients, it is useful in some situations when the data are lacking and also to indicate the realistic conditions in a particular system which may be affected strongly by the contamination of the gas. Finally, this is the only direct way to obtain total multiplication as required by the breakdown theory.

When the spatial scans of emission are not available in the experiment that is being analyzed but were available for other experiments, the delay distance d_0 can also be determined by using semi-empirical formulas such as that given in [5] through the expression for the effective value of the electrode potential difference before the exponential growth of the current:

$$V_0 = 16 \sqrt{1 + \left(\frac{E/N}{1000} \right)^2} \quad (3)$$

Probably the best method to produce delay distances is by using Monte Carlo simulations. In this paper we apply a Monte Carlo code that has been well documented in previous publications (details can be found in [27,28]), so only a brief description will be given here. The code is based on generalized null-collision technique [29]. In the code we follow electrons released at the cathode until they reach the anode. The set of cross sections that is used involves inelastic (excitation) processes, ionization and elastic scattering. Each of these processes has associated differential cross sections that are necessary only to establish the angle of scattering. The probability of scattering is determined on the basis of the total cross section. From the simulation of the spatial profile of excitation, one may observe a region

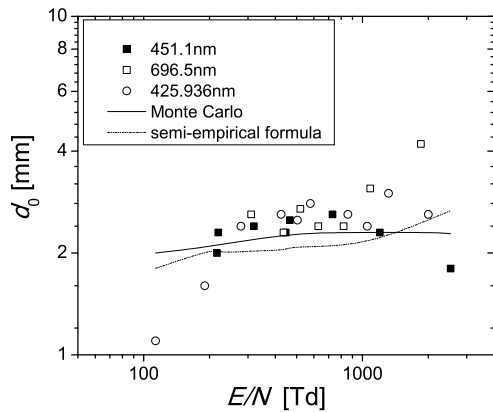


Fig. 4. The dependence of the delay distance d_0 on the reduced field E/N for argon. The delay distances were obtained by three different techniques. Calculations were performed assuming isotropic angular distribution of electrons, the gap between the electrodes of 1.72 cm.

next to the cathode where excitation is zero, followed by an exponential growth of emission and finally a growth with the hydrodynamic ionization coefficient. The hydrodynamic region is extrapolated to the zero value and that point determines the distance as applied in equation (2).

In Figure 4 we compare results for the equilibration distance as a function of the reduced field E/N in argon obtained by experiment (symbols), Monte Carlo simulation (solid line) and semi-empirical formula (dashed line). The results obtained by using three different techniques show good agreement, except for the lowest and highest values of the reduced field. It is necessary to consider here the accuracy of experimental determination of the distance d_0 at those values of E/N . At low values of E/N multiplication is very high and it is not so sensitive on the accuracy of determination of d_0 which is small anyway. On the contrary, at high E/N i.e. low pressures, overall multiplication is small, so inclusion of d_0 does not make significant difference. We may say that the agreement between the experimental data, semi-empirical formula and Monte Carlo simulations is excellent for the purpose of determining the secondary yield coefficients. Still, in experiment, due to reflection from the cathode and scatter of light, the results can be significantly scattered, as it is shown in Figure 4, so for the purpose of determination of secondary electron yields, we use results of Monte Carlo simulations when possible.

While Figure 4 shows results for equilibration distance along the Paschen curve, further on, we explore d_0 behavior for the general non-self-sustained conditions. Pressure dependence of d_0 at a fixed E/N is shown in Figure 5a and the E/N dependence at a fixed pressure in Figure 5b. In both cases, we present the results obtained using our Monte Carlo simulation code (curve) and semi-empirical formula (symbols). For a fixed reduced field, the delay continuously decreases as the gas number density (pressure) increases. On the other hand, the E/N dependence of the equilibration distance for a fixed gas number density (pressure) shows that the equilibration distance becomes

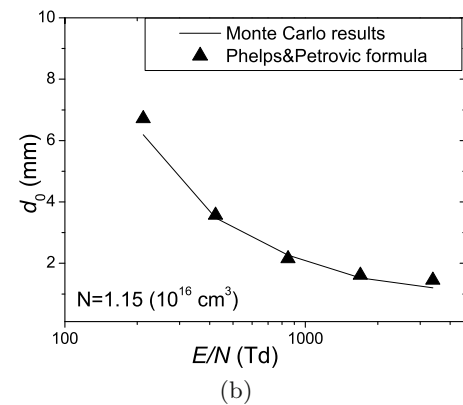
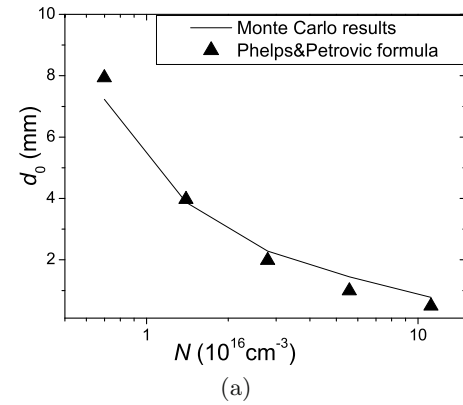


Fig. 5. The dependence of the delay distance on: (a) the gas number density for a fixed reduced field for argon; (b) the reduced field for a fixed gas number density for argon.

smaller as the reduced field increases (for a fixed gas number density). In both cases, the results obtained by semi-empirical formula and the Monte Carlo simulations are in satisfactory agreement. The experimental measurements are in fact less reliable than the simulation due to limited spatial resolution and possible scattering of light. Thus we really seek a general agreement and put our confidence in simulations. On the contrary, the measured exponential growth, if defined well and if not overlapping with the contribution of fast neutrals, provides better representation of multiplication in the actual experiment. Agreement between results proves that scaling for the equilibration employed in the development of the semi-empirical formula is appropriate.

In Figure 6 we show calculated equilibration distances for different gasses. We have performed analysis mainly for the rare gases and in a limited sense as compared to Phelps and Petrović [5]. Partly, the reason is that experimental determination of the delay distance in molecular gases is very difficult due to several sources of emission and complex quenching. In those gases we recommend Monte Carlo simulation of the whole system both the delay gap and the exponential growth. In Figure 6 it can be seen that the equilibration distance increases with the atomic mass; however it does not change much for a specific gas in the range of E/N -s investigated here.

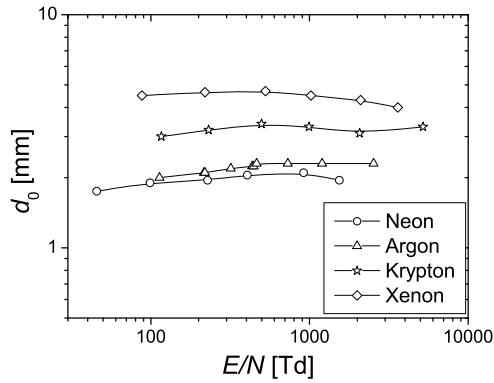


Fig. 6. Equilibration distances for different gases.

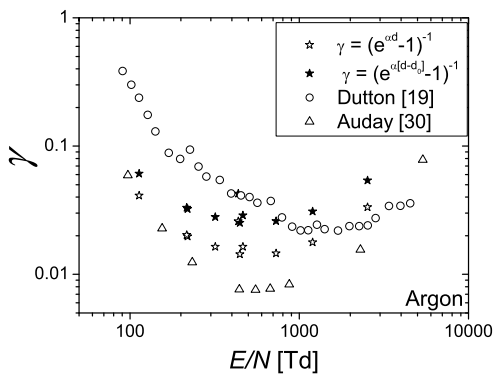


Fig. 7. Comparison of secondary electron yields for argon obtained with different data for ionization coefficients. The first three sets of data were obtained using our Paschen curve, the first two (stars) with our multiplication coefficient without and with the inclusion of the delay distance d_0 in the analysis. The third set (circles) was obtained by using the ionization coefficients from [19] to determine the multiplication. The same ionization coefficients were used in the fourth set [30] but the basis for the results was their measurements of the Paschen curve.

5 Determination of the secondary electron yields and the role of ionization rate

As discussed in previous subsection, the non-hydrodynamic region near the cathode does not necessarily have a significant influence at very low and very high E/N . However, not taking into account the existence of non-equilibrium region can significantly change results for secondary electron yields in medium range of reduced electric fields. In Figure 7 we compare the secondary electron yields in argon obtained by taking into account and not taking into account the equilibration length d_0 (solid and open stars respectively). $\alpha/N(E/N)$ data obtained directly from the experiment are used here to determine γ . As expected, taking equilibration length into account has the largest effect close to the minimum and in the right branch as compared to the left branch. Yet, towards both ends the differences induced by including d_0 diminish. The largest difference between the secondary yields with and without d_0 is a factor of

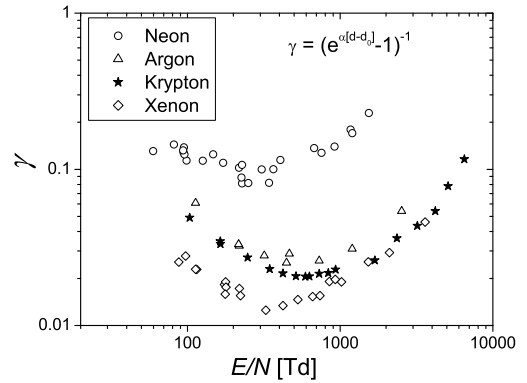


Fig. 8. Secondary electron yields for several different gases, with the same cathode surface (stainless steel).

two and it coincides with the minimum of the Paschen curve.

Taking the ionization rate from the literature may give a quite different multiplication as compared with the actual experiment and even small errors in the ionization coefficient result in large discrepancies of the secondary electron yield. In Figure 7 we also show secondary electron yields obtained from our Paschen curves by using ionization coefficients from the review [19] which are mostly based on experiments of Kruthiof (circles). These results are up to a factor of 10 different from our data mostly at high E/N .

We also show results of Auday et al. [30] who have analyzed their Paschen curve with the ionization rates from Dutton (triangles). Although those two sets of Paschen curves are apparently quite similar, the differences of yields are considerable, as large as a factor of 10.

For the low values of E/N , γ in our experiment rises more strongly than those obtained by using values of α/N from the literature. This can be explained by the fact that secondary emission of electrons can be due to any combination of numerous mechanisms of varying importance depending on the value of E/N . In the case of small values of E/N , dominant mechanism is the photoelectron emission.

Finally, a similar analysis for the secondary electron yields has been carried out for several other gases. In Figure 8 we show only final results obtained by using the most complete (correct) procedure. As expected the yield increases presumably proportional to potentials of the ion and the metastable states.

6 Conclusions

Measurements of properties of low-current discharges which include Paschen curves, Volt-Ampere characteristics and spatial profiles of emission proved to be a fertile basis for modeling of plasmas and discharges. In this paper we gave a short overview of the results of our breakdown studies covering five rare gases and eight molecular gases. We pointed out the most important issues in deducing secondary electron yields from the breakdown and swarm

experiments, compared results obtained by employing different procedures and we presented results for secondary yields for several rare gases obtained by a proper procedure. One should bear in mind that in this analysis the effective coefficients are attached to ion fluxes and a more thorough analysis along the same lines as done by Phelps and Petrović [5] should be performed for all gases together with an analysis of the applicability of the data in higher current discharges.

In conclusion, we may say that the treatment of electron non-equilibrium motion near the cathode includes determination of the delay in reaching the hydrodynamic rates of electron excitation and ionization. The results obtained when the equilibration distance is accounted for allow us to conclude that not taking into account the non-equilibrium region and correct values of ionization coefficients one may make quite large errors in obtaining secondary yields for the relevant particles in the discharge. These differences between the γ coefficients may result in some of the discrepancies between the swarm and the binary collision technique data for γ coefficients, which remains yet to be analyzed.

Monte Carlo simulation provides complete representation of non-equilibrium effect and influence of the electrodes and it is exact representation of breakdown itself, so it should be employed for modeling. A satisfactory agreement between the experimental data and the results obtained using Monte Carlo simulation code and semi-empirical formula proves that our treatment of the electron non-equilibrium behavior close to the cathode is accurate. It also became possible to make more direct comparisons between the secondary electron yields obtained from Paschen's law and from experiments consisting of a beam of ions hitting the surface under high vacuum conditions and separate detailed analyses should be made for all gases that are of interest.

This work was supported by MESTD ON171037 and III41011 projects.

References

1. J.S. Townsend, *The Theory of Ionization of Gases by Collision* (Constable, London, 1910)
2. Z.Lj. Petrović, A.V. Phelps, Phys. Rev. E **47**, 2806 (1993)
3. A.V. Phelps, Z.Lj. Petrović, B.M. Jelenković, Phys. Rev. E **47**, 2825 (1993)
4. Z.Lj. Petrović, A.V. Phelps, Phys. Rev. E **56**, 5920 (1997)
5. A.V. Phelps, Z.Lj. Petrović, Plasma Sources Sci. Technol. **8**, R21 (1999)
6. G. Malović, A. Strinić, S. Živanov, D. Marić, Z.Lj. Petrović, Plasma Sources Sci. Technol. **12**, S1 (2003)
7. L.C. Pitchford, C. Pedoussat, Z. Donko, Plasma Sources Sci. Technol. **8**, B1 (1999)
8. D. Marić, K. Kutasi, G. Malović, Z. Donkó, Z.Lj. Petrović, Eur. Phys. J. D **21**, 73 (2002)
9. D. Marić, P. Hartmann, G. Malović, Z. Donko, Z.Lj. Petrović, J. Phys. D **36**, 2639 (2003)
10. N. Škoro, J. Phys.: Conf. Ser. **399**, 012017 (2012)
11. N. Škoro, D. Marić, G. Malović, W.G. Graham, Z.Lj. Petrović, Phys. Rev. E **84**, 055401(R) (2011)
12. V. Stojanović, J. Božin, Z.Lj. Petrović, B.M. Jelenković, Phys. Rev. A **42**, 4983 (1990)
13. M.A. Lieberman, A.J. Lichtenberg, *Principles of plasma discharges and materials processing*, 2nd edn. (John Wiley & Sons Inc., Hoboken, 2005)
14. I. Stefanović, J. Berndt, D. Marić, V. Šamara, M. Radmilović-Radjenović, Z.Lj. Petrović, E. Kovačević, J. Winter, Phys. Rev. E **74**, 026406 (2006)
15. R.W. Crompton, J. Dutton, S.C. Haydon, Nature **176**, 1079 (1955)
16. A.N. Prasad, J.D. Craggs, Proc. Phys. Soc. **76**, 223 (1960)
17. M. Nikolić, A. Djordjević, I. Stefanović, S. Vrhovac, Z.Lj. Petrović, IEEE Trans. Plasma Sci. **31**, 717 (2003)
18. V.I. Kolobov, A. Fiala, Phys. Rev. E **50**, 3018 (1994)
19. J. Dutton, J. Phys. Chem. Ref. Data **4**, 727 (1975)
20. D. Marić, M. Radmilović-Radjenović, Z.Lj. Petrović, Eur. Phys. J. D **35**, 313 (2005)
21. V.Lj. Marković, S.R. Gocić, S.N. Stamenković, Z.Lj. Petrović, Eur. Phys. J. Appl. Phys. **30**, 51 (2005)
22. Z.Lj. Petrović, S. Dujko, D. Marić, G. Malović, Ž. Nikitović, O. Šašić, J. Jovanović, V. Stojanović, M. Radmilović-Radjenović, J. Phys. D **42**, 194002 (2009)
23. J. Fletcher, J. Phys. D **18**, 221 (1985)
24. M.A. Folkard, S.C. Haydon, J. Phys. B **6**, 214 (1973)
25. A.V. Phelps, B.M. Jelenković, Phys. Rev. A **38**, 2975 (1988)
26. Z.M. Jelenak, Z.B. Velikić, Z.Lj. Petrović, B.M. Jelenković, Phys. Rev. E **47**, 3566 (1993)
27. V.D. Stojanović, Z.Lj. Petrović, J. Phys. D **31**, 834 (1998)
28. M. Radmilović, Z.Lj. Petrović, Eur. Phys. J. Appl. Phys. **11**, 35 (2000)
29. H.R. Skullerud, J. Phys. D **1**, 1567 (1968)
30. G. Auday, P. Guillot, J. Galy, H. Brunet, J. Appl. Phys. **83**, 5917 (1998)

On Explanation of the Double-Valued Paschen-Like Curve for RF Breakdown in Argon

Marija Savić, Marija Radmilović-Radjenović, Milovan Šuvakov, Srdjan Marjanović, Dragana Marić, and Zoran Lj. Petrović

Abstract—This paper represents an investigation of the dependence of the breakdown voltage on the gas pressure in radio-frequency argon discharges under conditions when ion-induced secondary electron production is negligible. Calculations were performed by using a Monte Carlo collision code including electrons only. Our simulation results clearly show a region, occurring at low pressure, where multiple values of the breakdown voltage exist at a given pressure, in agreement with previous experimental observations. The two different regimes of operation, each satisfying the breakdown condition, may be best analyzed in contour plots of electron density, ionization rate, and mean energy.

Index Terms—Breakdown, Monte Carlo (MC) simulations, radio frequency (RF) discharges.

GAS breakdown is the first step in the generation of plasma and therefore is one of the most fundamental processes [1]. In studies of the breakdown characteristics of gas discharges, the usual observable that is modeled is the Paschen curve. This breakdown voltage curve represents a balance between the number of electrons lost by diffusion and drift in the interelectrode gap and the number of secondary electrons generated at the cathode.

In the case of radio frequency (RF) discharges, it is actually possible to achieve self-sustained operation with electrons only, as the field changes direction. The Paschen-like breakdown voltage dependence is similar in shape to that of the dc discharges. The breakdown voltage generally forms a curve with unique values for each pd . Under certain circumstances, the left-hand branch of the curve exhibits a multivalued nature, i.e., a single pd corresponds to two different breakdown voltages [2]. In other words, on lowering the pressure, the breakdown voltage first decreases, passing through a minimum on the breakdown curve, before increasing to approach a turning point on the breakdown curve [2]. Lisovski and Yegorenkov [2] assert that, at this turning point, the electrons will drift exactly one-half of the gap in a one-half period of the field and are therefore all going to be swept to the electrodes. At a pressure lower than the turning point, it becomes impossible to achieve breakdown for any value of the applied voltage (ignoring multipactor effect) period.

Manuscript received November 30, 2010; revised May 30, 2011; accepted May 30, 2011. Date of publication July 22, 2011; date of current version November 9, 2011. This work was supported by the MNTRS Project 171037.

The authors are with the Institute of Physics, University of Belgrade, 11080 Belgrade, Serbia (e-mail: smarija@ipb.ac.rs; marija@ipb.ac.rs; suki@ipb.ac.rs; msrdjan@ipb.ac.rs; draganam@ipb.ac.rs; zoran@ipb.ac.rs).

Color versions of one or more of the figures in this paper are available online at <http://ieeexplore.ieee.org>.

Digital Object Identifier 10.1109/TPS.2011.2159244

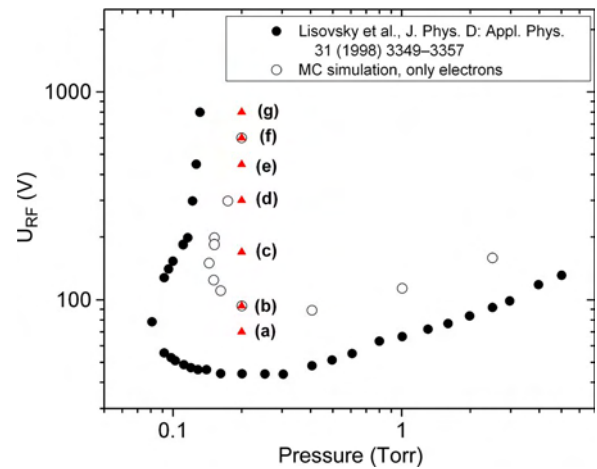


Fig. 1. Breakdown voltage versus the gas pressure in argon RF discharges at 13.56 MHz and the gap size of 2.3 cm. The (solid circles) experimental data taken from [2] are compared with (open circles) our MC simulation results taking into account electrons only. Calculations were performed for the pressure of 0.2 torr and five different voltages (red symbols).

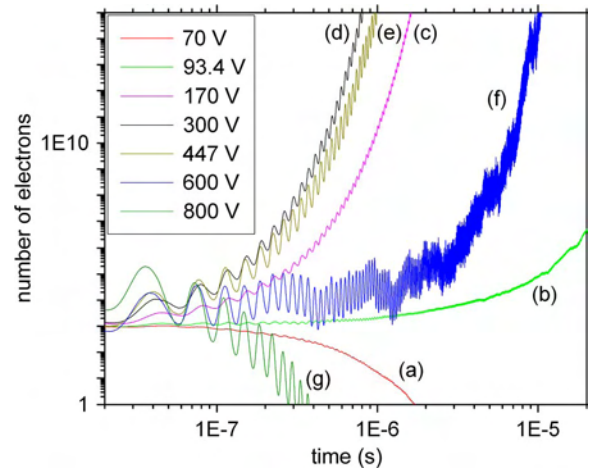


Fig. 2. Time dependence of the number of electrons for the conditions shown by red symbols in Fig. 1.

The purpose of this paper is to model the RF breakdown in an electron-dominated regime (with negligible effects of ions and multipacting) and try to understand the basic phenomenology by employing kinetic representation.

A Monte Carlo (MC) code used for the studies of RF breakdown is developed and tested in our group. The code follows the transport of electrons across the gap between electrodes. The cross-sectional set consisting of momentum transfer, two excitation, and ionization cross sections has been well tested

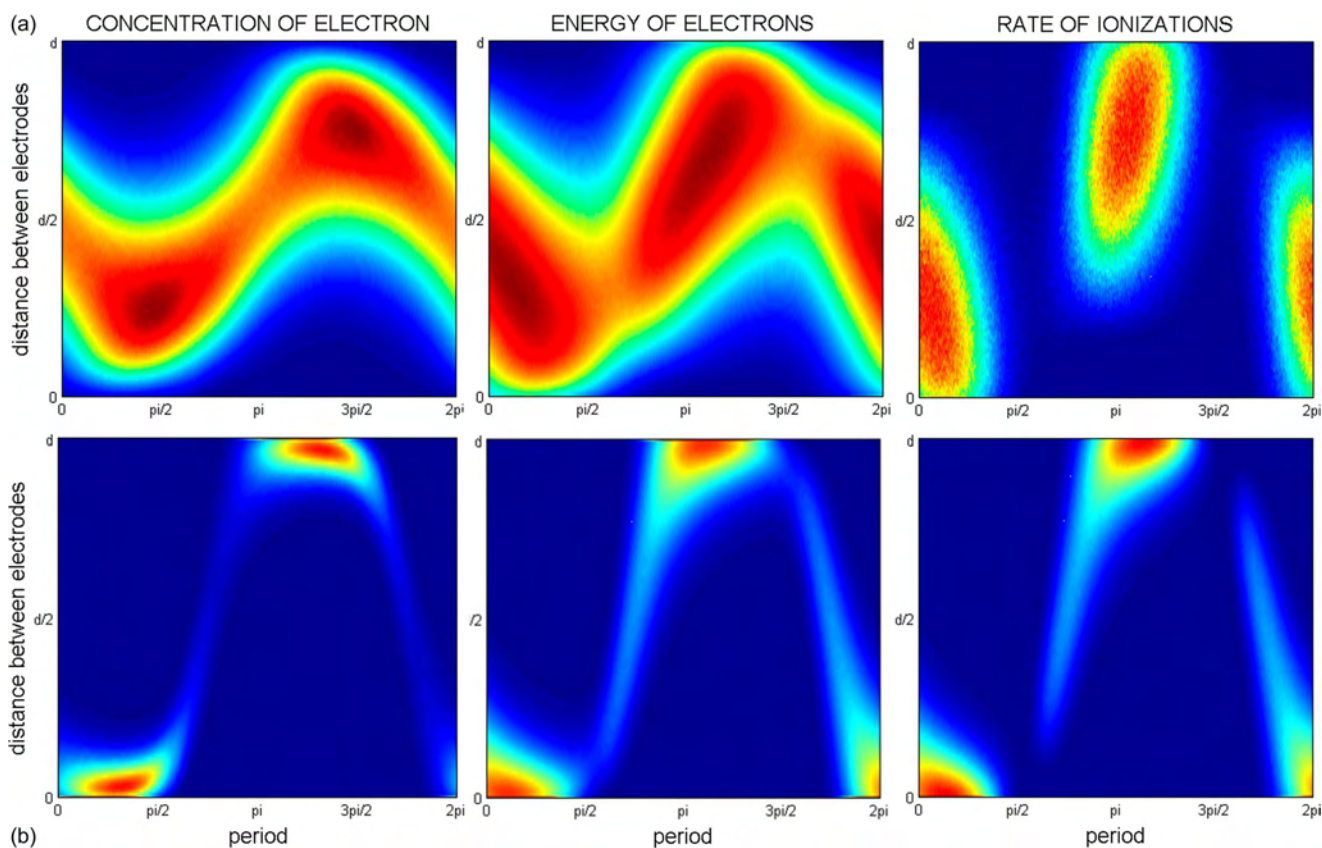


Fig. 3. Changes of various characteristics (the electron concentration, the electron energy, rates of elastic scattering and ionizations, respectively) during one period along the vertical $pd = \text{const}$ line. Calculations were carried out in argon at 13.56 MHz, 0.2 torr, and voltages of (a) 93.4 V and (b) 600 V both satisfying the breakdown criterion as seen in Fig. 2.

for argon swarms [3]. We start the simulation with 100 000 electrons and follow the development. In the case of fast ionization or losses, we rescale the numbers but weight the number density.

Breakdown is essentially determined in the same way as that in experiment, i.e., by slowly increasing the voltage to approach from below the curve and by increasing the pressure to approach higher voltage values in the double-value region. We set out to establish the differences between two points satisfying breakdown for the same pd . The voltage or pressure steps close to the breakdown are very slow, and the uncertainty of the breakdown voltage is on the order of 0.1 V. Simulations are performed for the experimental conditions in [2].

In Fig. 1, we show the simulated Paschen curve; in shape, we get agreement with the experiment, but apparently, our turning point occurs at higher pressure. Slight differences may be explained by the fact that we neglected ion motion and secondary electron production, as well as electron reflection and secondary electron production by energetic electrons. Also, some possible experimental uncertainties could lead to the differences. In any case, the two-value behavior of the Paschen curve is confirmed, and agreement with experiment in that respect is reasonable. In Fig. 2, we show the curves representing the time dependence of electron density, and curves (b) and (f) are the first curves with the positive growth in their own conditions (93.4 and 600 V). In between these points, growth is extreme, and outside, the curve electron density decays.

The spatial profiles (see Fig. 3) of the swarm properties are shown for two stable breakdown points (b and f), and the profiles are quite different. For the lower voltage, one needs to achieve sufficient ionization to compensate for the losses, and therefore, any increase in voltage leads to a higher ionization. In both cases, most of the electrons are produced in proximity of the electrodes. For the higher breakdown voltage, one can see that most of electrons are pushed to the electrode by the strong field, and therefore, losses have increased sufficiently to compensate excessive production by ionization. Any further increase of voltage will make losses greater than production by ionization. It also becomes critical to observe where ionization occurs and the degree of multiplication that is allowed to develop before electrons are lost.

Kinetic representation of RF breakdown not only reveals details of phenomenology but also provides tools to convert experimental breakdown data into relevant coefficients.

REFERENCES

- [1] A. V. Phelps and Z. L. Petrović, "Cold-cathode discharges and breakdown in argon: Surface and gas phase production of secondary electrons," *Plasma Sourc. Sci. Technol.*, vol. 8, no. 3, pp. R21–R44, Aug. 1999.
- [2] A. V. Lisovskiy and V. D. Yegorenkov, "RF breakdown of low-pressure gas and a novel method for determination of electron-drift velocities in gases," *J. Phys. D, Appl. Phys.*, vol. 31, no. 23, pp. 3349–3357, Dec. 1998.
- [3] Z. L. Petrović, M. Šuvakov, Ž. Nikitović, S. Dujko, O. Šašić, J. Jovanović, G. Malović, and V. Stojanović, "Kinetic phenomena in charged particle transport in gases, swarm parameters and cross section data," *Plasma Sources Sci. Technol.*, vol. 16, no. 1, pp. S1–S12, Feb. 2007.

Numerical Modeling of Thermalization of Positrons in Gas-Filled Surko Traps

Srdjan Marjanović, Milovan Šuvakov, Ana Banković, Marija Savić, Gordana Malović, Stephen J. Buckman, and Zoran Lj. Petrović

Abstract—In this paper, we present the results of our Monte Carlo-based numerical simulation of a Penning–Malmberg–Surko positron trap. The results of simulations show the effect that various processes (such as positronium (Ps) formation, annihilation, losses on walls, etc.) have on trapping efficiency. The thermalization profile is shown, along with the evolution of the energy distribution that morphs from a particle beam to a broad swarm-type distribution.

Index Terms—Buffer gas trap, numerical simulation, particle beams, positrons.

BUFFER GAS traps are a general prerequisite for the study of cold positrons and their interaction with matter. Penning–Malmberg–Surko traps [1] and their variations [2] have shown excellent performance and are widely accepted as an ideal tool for atomic and molecular collision physics and material science diagnostics. The gas most commonly used for trapping is N_2 because its electronic excitation cross sections are comparable to or larger than those for positronium formation in the near-threshold region. A small portion of CF_4 is used in the last stage of the trap in order to speed up the thermalization at lower energies through vibrational scattering.

Our model consists of three cylindrical stages with varying radii to achieve different pressures. Positrons are moving through them, accelerating, and decelerating along the axis as they fall in, and climb out of, potential wells. An axial magnetic field is applied for beam confinement.

The Monte Carlo method, tested on numerous electron benchmarks, is used for simulating the collisions with the buffer gas. The potential of the electrodes was set so that each stage of the trap (I, II, and III) had the well depths of 10, 11, and 12 eV and pressures of 10^{-3} , 10^{-4} , and 10^{-6} torr, respectively. The buffer gas is N_2 with 10% of CF_4 in the third stage. These traps have strong axial magnetic field and cylindrical symmetry

Manuscript received November 30, 2010; revised May 26, 2011; accepted May 28, 2011. Date of publication July 5, 2011; date of current version November 9, 2011. This work was supported by the MNTR, Serbia, under Contracts ON171037 and III41011.

S. Marjanović, M. Šuvakov, A. Banković, M. Savić, G. Malović, and Z. Lj. Petrović are with the Institute of Physics, University of Belgrade, 11080 Belgrade, Serbia (e-mail: msrdjan@ipb.ac.rs; suki@ipb.ac.rs; anchuga@ipb.ac.rs; smarija@ipb.ac.rs; malovic@ipb.ac.rs; zoran@ipb.ac.rs).

S. J. Buckman is with CAMS, ANU, Canberra, A.C.T. 0200, Australia (e-mail: stephen.buckman@anu.edu.au).

Color versions of one or more of the figures in this paper are available online at <http://ieeexplore.ieee.org>.

Digital Object Identifier 10.1109/TPS.2011.2159129

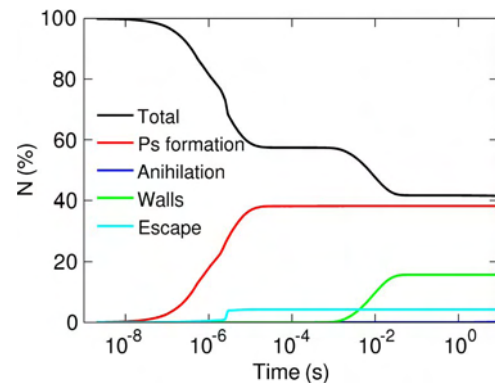


Fig. 1. Number of particles in the trap and loss processes. The process of annihilation is negligible on this timescale.

with three stages at different potentials and gas pressures [1], [2] which were selected to be similar with the setup in [1]. Cross sections for $e^+ - N_2$ may be found in [3]. We normally release between 10 000 and 100 000 particles, and the simulations last several hours.

The positrons enter the first stage with an energy width of 1 eV and are accelerated to an energy of 10 eV in the first potential well. Particles that make the trip through the well, bounce off the potential wall, return, and still have energy over 10 eV are lost and are represented in Fig. 1 as *escaped*. The most important loss process, as shown in Fig. 1, is *positronium formation*. *Escape* and *losses to walls* can be diminished by changing the geometry of the trap and the combination of gas pressures and magnetic field. As the positrons suffer more and more collisions, their mean energy drops down (see Fig. 2).

In order to understand the performance of the trap, one needs to visualize the positron energy distribution development (see Fig. 2) which starts as a 10-eV beam. As particles enter stages II and III, they gain energy, but meanwhile, around 8 eV is lost due to electronic excitation of the N_2 molecule. This leads to the splitting of the original beam into several beams (see Fig. 2) that combine together as they cool down and become a particle swarm with a broad energy distribution and a mean energy that eventually becomes close to thermal (see Fig. 2), and the distribution becomes a Maxwell–Boltzmann distribution.

The initial width of the beam is 1 mm, and it expands up to 6 mm. The particles on the front, leading the expansion, are those that scatter and transfer most of their energy to the transverse plane. These results are shown in Fig. 3 where a 3-D plot gives the magnitude of the perpendicular energy as

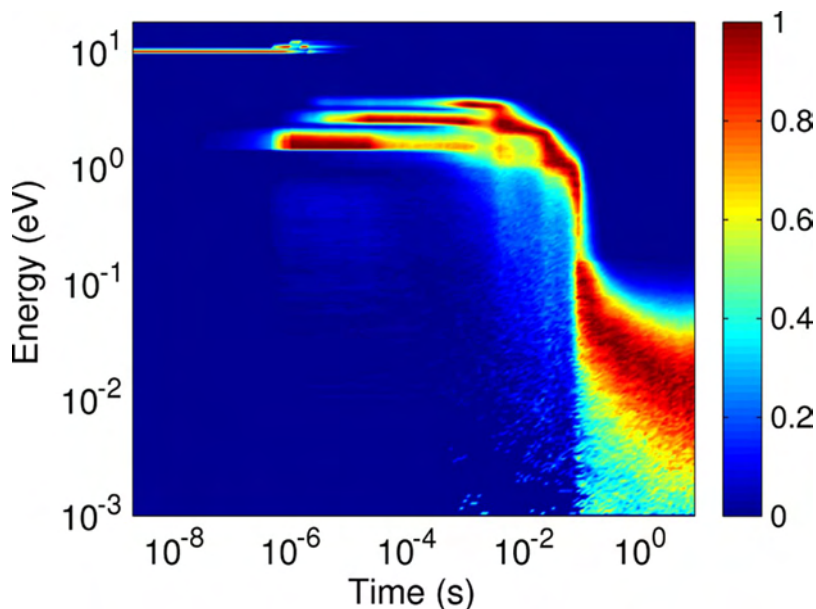


Fig. 2. Evolution of the positron kinetic energy distribution over time. Distributions are normalized for better presentation over a wide dynamic range.

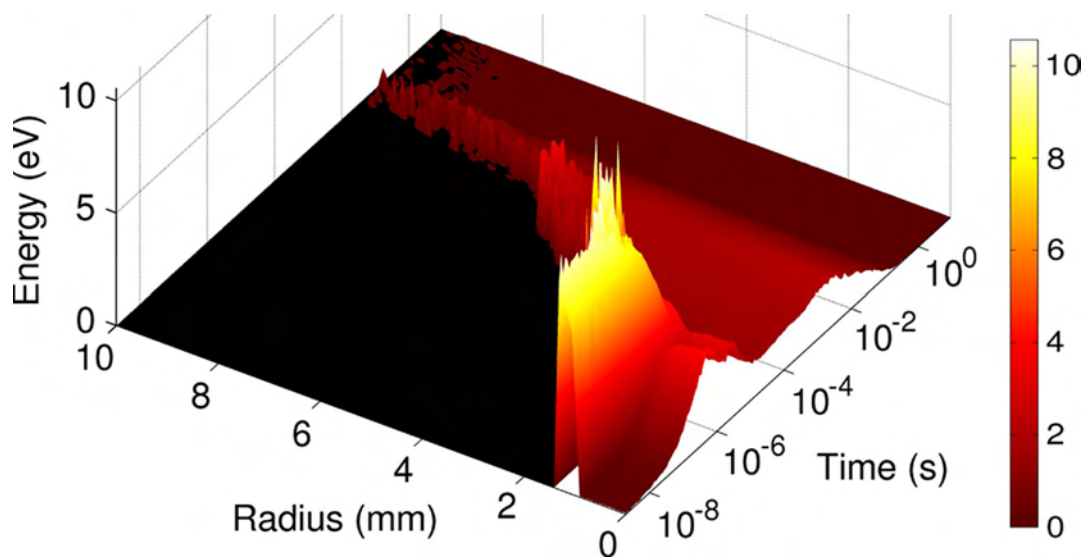


Fig. 3. Radial distribution of the transversal kinetic energy, impacting the rate of the widening of the beam and the amount of loss to the walls.

a function of spatial position. The leakage to the side walls is generated mainly by the particles with high perpendicular scattering in the last stage, in spite of the fact that higher perpendicular energies may be found in the initial stages when the beam still has mostly the original radius. The losses are mainly due to the very long time that positrons spend in the last stage due to the need to employ rotational excitation and elastic scattering to achieve the last stages of thermalization below 100 meV.

Modeling of the Surko trap by the electron-swarm-related Monte Carlo code works well because of the similar nature of the electron-molecule and positron-molecule scattering. The functioning of the trap may be best visualized with temporally resolved results for positron positions, energy distributions

of the particles, and losses. Thus, the code becomes a tool that may provide means to optimize the trap further. This may be accomplished, to a large degree, by observing visual information.

REFERENCES

- [1] C. M. Surko and R. G. Greaves, "Emerging science and technology of antimatter plasmas and trap-based beams," *Phys. Plasmas*, vol. 11, no. 5, pp. 2333–2348, May 2004.
- [2] J. P. Sullivan, A. Jones, P. Caradonna, C. Makochekanwa, and S. J. Buckman, "A positron trap and beam apparatus for atomic and molecular scattering experiments," *Rev. Sci. Instrum.*, vol. 79, no. 11, p. 113 105, Nov. 2008.
- [3] A. Banković, J. P. Marler, M. Šuvakov, G. Malović, and Z. L. Petrović, "Transport coefficients for positron swarms in nitrogen," *Nucl. Instrum. Methods Phys. Res. B*, vol. 266, no. 3, pp. 462–465, Feb. 2008.

Microwave Field Strength Computing for the Resonator Designs and Filters

M. RADMILOVIĆ-RADJENović*, B. RADJENović AND M. SAVIĆ
Institute of Physics, University of Belgrade, Pregrevica 118, 11080 Zemun, Serbia

(Received March 29, 2013)

Recent development of microwave pulse generators, which are now capable of delivering very short and very intensive pulses requires properly generalized classical breakdown theory. On the other hand, the trend to design microwave devices as small and compact as possible, leads to a concern about the concomitant breakdown strength of the construction, involving more complicated geometries, such as in microwave resonators and filters. In this paper, several aspects of microwave field strength in commercially available resonator designs and filters are presented and analyzed. The numerical predictions based on the Slater theorem are compared with the analytical results and predictions of the fluid approach, demonstrating very good agreement.

DOI: [10.12693/APhysPolA.129.289](https://doi.org/10.12693/APhysPolA.129.289)

PACS/topics: 52.80.-s, 52.90.+z

1. Introduction

Microwave breakdown in gases under various physical and technical conditions is well-known and intensively studied problem from early days of gaseous electronics [1–3]. More recent, interest in microwave-induced breakdown is shifted to studies of microwave breakdown at atmospheric pressures due to its relevance both for industrial applications [4–6] and for a deeper understanding of fundamental plasma behavior [7–9]. The microwave breakdown strength of the gas is useful information for high power filter and antenna engineering [10], for determination of the conductivity and dielectric constant of a plasma [11], for modification the ionosphere for long range radio propagation [12], etc. The microwave breakdown phenomenon provides both problems and opportunities reflected in the applications of the microwave breakdown theory. The application can be divided into two main categories: the so-called no-breakdown devices — where breakdown should be avoided for proper operation of the device and breakdown devices — where breakdown is an intrinsic feature of operation.

In numerous microwave devices, the geometrical configuration contributes to local strongly enhanced microwave fields. Such regions are potentially dangerous from the point-of-view of breakdown since the field here may be much stronger than the globally predicted breakdown field. On the other hand, a locally overcritical field does not necessarily imply global breakdown. In that case, the influence of local field enhancement on the global breakdown condition has to be included.

This paper contains result of our studies of the microwave induced dielectric breakdown of gases in a uniform electric field. Cavity resonators have often been used [13, 14], but field distributions are inhomogeneous,

resulting in a spatially dependent ionization rate and breakdown which is strongly influenced by the diffusion of charged particles out of the high electric field region.

2. Models

Several different models of the microwave breakdown criteria exist, with varying degree of accuracy in the description. Fluid models provide description with enough details that can be used in large classes of research becoming very important for technical applications [15]. On the other hand, the kinetic approach has potential to offer a very detailed description of the mechanism and represents the basis on which other models rely. The great details in descriptions, however, make the kinetic approach very complex and more useful in pure physical research with simplified geometry.

2.1. The Slater theorem for computing the electric field in the gap

The electric field inside a microwave resonator can be determined analytically based on an analytic solution to the Maxwell equations. The electric and magnetic fields inside a resonator have a complicated spatial variation, which nevertheless satisfies the Helmholtz wave equation under the constraints of the conductive boundary conditions. Analytic solutions of the electric and the magnetic fields exist only for a few simple cavity geometries. It is not usually possible to analytically find the magnitude of the fields inside most resonators, let alone their geometric distribution. The field strength can be determined numerically using full-wave electromagnetic field simulation [14].

The perturbation theory of Slater is used here to obtain the local electric field. Only a small fraction of the empty space inside an electromagnetic resonator is filled with the dielectric material with relative permittivity ϵ_r , and relative permeability μ_r . The interaction between the magnetic permeability of the material and the magnetic field of the resonator will cause the reactance to increase

*corresponding author; e-mail: marija@ipb.ac.rs

and thus raise the resonant frequency by the inductive loading. Likewise, the interaction between the electric permittivity of the material and the electric field of the resonator will cause the reactance to decrease and thus lower the resonant frequency by the capacitive loading. This frequency shift, $f_0 - f$ can be expressed via the Slater theorem [14]:

$$\omega^2 = (2\pi f)^2 = \omega_0^2 \left[1 + \frac{\int_{\text{dielectric}} (\mu_0 \mu_r H^2 - \varepsilon_0 \varepsilon_r E^2) dV}{\int_{\text{cavity}} (\frac{1}{2} \mu_0 H^2 + \frac{1}{2} \varepsilon_0 E^2) dV} \right], \quad (1)$$

where H and E represent the magnetic and electric fields, respectively, while $\omega_0 = 2\pi f_0$ is the original, unperturbed angular frequency. The top integral is evaluated over the dielectric perturbation, and gives the energy stored in the perturbation. The bottom integral is evaluated over the entire empty cavity and is equal to the peak energy stored per cycle in the resonator — U_0 .

2.2. An analytical-experimental approach

There is also a simple complementary approach obtained by combination of an analytical and experimental investigations suggested in [13]. Actually, the method is based on experimental data of the breakdown voltages at low pressures and their extrapolation over a wide range of pressures. The expression for the breakdown voltage is written in the form [13]:

$$E_b = 3.75p \left[1 + \left(\frac{2\pi f}{\nu_c} \right)^2 \right]^{1/2} \left(\frac{D}{pL_D^2} + 6.4 \times 10^4 \right)^{3/16}, \quad (2)$$

where E_b represents the real rms electric field and the characteristic length L_D determines the curvature of the breakdown voltage curve.

2.3. Fluid approach

In the case of microwave electric fields, the continuity equation describes the time evolution of the electron density n_e which is

$$\frac{\partial n_e}{\partial t} = \nabla \cdot (D_e \nabla n_e) + \nu n_e, \quad (3)$$

where D_e is the electron diffusion coefficient and ν is the net production rate of electrons per electron. The microwave breakdown can be determined as a balance between the ionization rate and the loss rate of electrons by diffusion mathematically formulated by relation [15]:

$$\nu_i = \frac{D_e}{\Lambda^2}, \quad (4)$$

with the characteristic diffusion length Λ depending on the geometry of the discharge vessel, i.e. radius R and height L in accordance with the expression

$$\frac{1}{\Lambda^2} = \left(\frac{2.4}{R} \right)^2 + \left(\frac{\pi}{L} \right)^2, \quad (5)$$

where the diffusion to the end plates is given by the first on the right, while the second term describes the diffusion to the cylindrical walls.

In general, the electron diffusion is anisotropic, but at very high frequencies the transverse and longitudinal diffusions become almost isotropic with the values nearly equal to the transverse one D_τ at $\omega \rightarrow 0$. Therefore, in Eq. (3), the electron diffusion coefficient D_e can be replaced by the transverse diffusion coefficient D_τ that corresponds to the dc field. Combining Eq. (3) with $\nu_i = \alpha \mu E$:

$$\frac{\varepsilon}{\Lambda^2} = \frac{\alpha E_r}{\sqrt{1 + \left(\frac{\omega}{\nu_c} \right)^2}}, \quad (6)$$

where $\varepsilon = D_\tau/\mu$ represents the characteristic energy, while μ is the electron mobility. When an ac electric field $E_r \cos \omega t$ is applied in a weakly ionized gas, a dominant collision processes are electron-neutral collisions characterized by the collision frequency ν_c . The frequency effect can be comprehended by introducing the effective field strength

$$E_{\text{eff}} = \frac{\nu_c}{\sqrt{\nu_c^2 + \omega^2}} E_r. \quad (7)$$

Finally, substituting expression for the first Townsend coefficient $\alpha = Ap \exp(Bp/E_{\text{dc}})$ [15] and replacing E_{dc} by E_{eff} given by Eq. (6), we obtain expression for the electric field E_r as a function of the pressure p :

$$E_r = \frac{\varepsilon \sqrt{\omega^2 + \nu_c^2} \exp\left(Bp \sqrt{\omega^2 + \nu_c^2} / (\nu_c E_r) \right)}{\nu_c \Lambda^2 Ap}, \quad (8)$$

where ω represents angular frequency of the applied field.

3. Results

Atmospheric plasma source based on a microstrip splitting resonator (MSSR) is depicted in Fig. 1 with a schematic view given in Fig. 2. We have modelled the

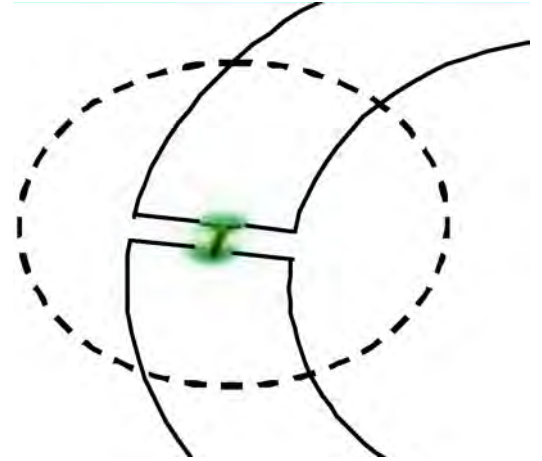


Fig. 1. Microstrip split-ring resonator.

electric field inside a microwave resonator numerically based on evaluation integrals in the Slater theorem. Coupling between electric and magnetic fields inside an electromagnetic resonator is demonstrated in Fig. 3. For the microwave threshold field of the gas which fills the resonator volume, however, the magnetic field is very low

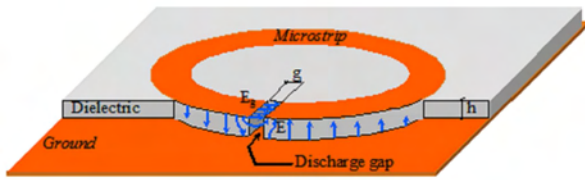


Fig. 2. Schematic view of microstrip split-ring resonator.

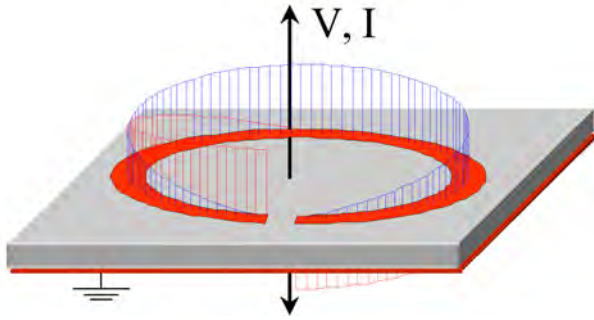


Fig. 3. Schematic view of split-ring resonator.

and can be neglected. Electric field can be treated as uniform over the volume of the dielectric. Calculated values of the magnitude of the electric field are shown in Fig. 4.

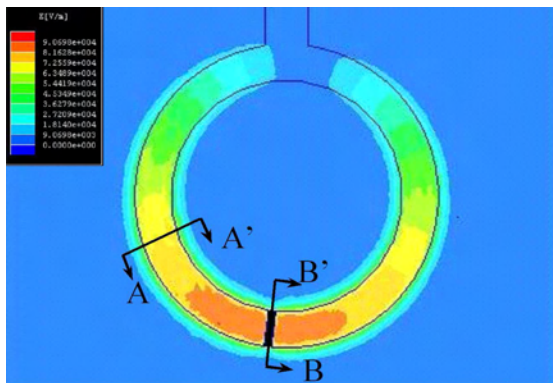


Fig. 4. Magnitude of the electric field.

The breakdown field strength as a function of pressure in nitrogen at microwave frequency of 1.85 GHz is shown in Fig. 5. Our numerical results are presented by solid line, while dot and dash lines correspond to the predictions obtained by using Eqs. (2) and (8), respectively. Theoretical predictions based on both analytical and fluid approaches provide relatively good results at lower pressures. Our numerical results, however, are in a good agreement with the data taken from [14] at all pressure values.

A good agreement between our numerical results (solid line) and results published in [14] (solid symbols) is also achieved for the pressure dependence of the breakdown field strength in nitrogen at 2.76 GHz at the temperature

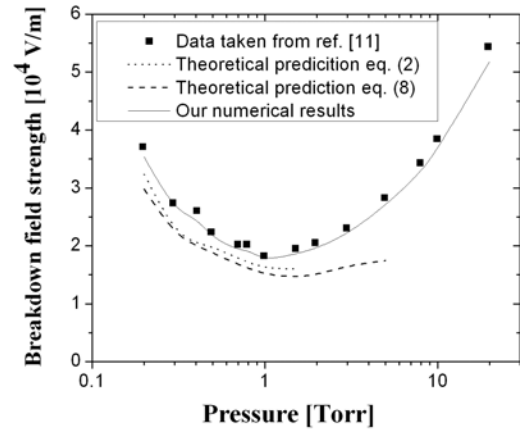


Fig. 5. The breakdown field strength versus the pressure in nitrogen at frequency of 1.85 GHz.

of 230 K (as can be seen from Fig. 6). Finally, how the pressure at the minimum breakdown voltage curve depends on frequency is illustrated in Fig. 7. As expected, there is a linear dependence indicating that the pressure at the minimum increases as the frequency is increased.

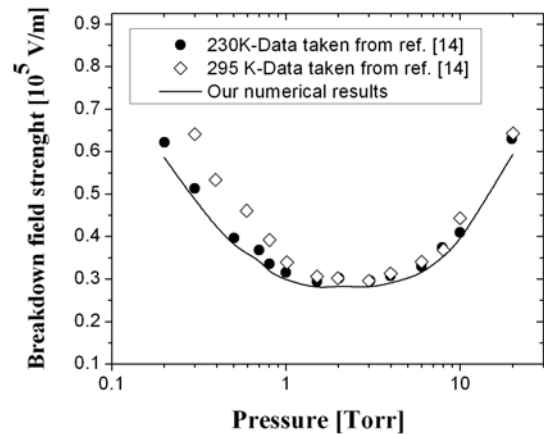


Fig. 6. The pressure dependence of the breakdown field strength in nitrogen at frequency of 2.76 GHz.

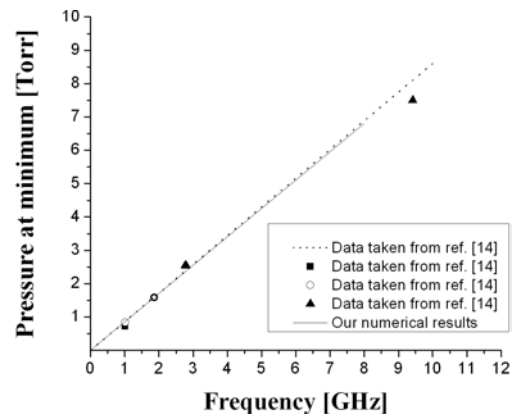


Fig. 7. The pressure at the minimum as a function of frequency in nitrogen.

4. Conclusion

Nowadays, there is a growing interest in microplasma sources due to their economics, portability, less operation costs, and small sizes. The utility derived from macroscale plasmas combined with current microfabrication techniques has allowed for the development of microscale devices which use microdischarges for operation. Having in mind that relatively complicated geometrical configurations in microwave devices enhance the strong local microwave fields and such fields may be much stronger than the globally predicted breakdown field. This paper is devoted to our numerical studies of the microwave field strength computing in commercially available resonator designs and filters. Numerical method is based on Slater's theorem. Our numerical results satisfactorily agree with the available data [14] indicating their applicability for a wide range of parameters.

The results presented here, except for resonator and filters, can be also useful in localized diagnostics of ICs during their manufacture, in choosing appropriate conditions for electro mechanical micro systems which may eventually lead to nanomachining, in localized treatment of materials and assembly of nanostructures and in micro and nanobiological processing and diagnostics.

Acknowledgments

The work has also been carried out under by Ministry of Education and Science Republic of Serbia O171037 and III41011 projects.

References

- [1] M.J. Druyvestayn, F.M. Penning, *Rev. Mod. Phys.* **12**, 87 (1940).
- [2] D.Q. Posin, *Phys. Rev.* **73**, 496 (1948).
- [3] S. Krasik, D. Alpert, A.O. McCoubrey, *Phys. Rev.* **76**, 722 (1949).
- [4] F.C. Fehsenfeld, K.M. Evenson, H.P. Broida, *Rev. Sci. Instrum.* **36**, 294 (1965).
- [5] M. Radmilović-Radjenović, B. Radjenović, *Central Europ. J. Phys.* **9**, 265 (2011).
- [6] B. Radjenović, M. Milanović, M. Radmilović-Radjenović, *Phys. Scr. T* **149**, 014026 (2012).
- [7] W.P. Allis, S.C. Brown, *Phys. Rev.* **87**, 419 (1952).
- [8] H.J. Oskam, *J. Appl. Phys.* **27**, 848 (1956).
- [9] A.D. MacDonald, D.U. Gaskell, H.N. Gitterman, *Phys. Rev.* **130**, 1841 (1963).
- [10] F. Werner, D. Korzec, J. Engemann, *Plasma Sources Sci. Technol.* **3**, 473 (1994).
- [11] T. Fleisch, Y. Kabouzi, J. Pollack, E. Castañón-Martínez, H. Nowakowska, M. Moisan, *Plasma Sourc. Sci. Technol.* **16**, 173 (2007).
- [12] D. Anderson, U. Jordan, M. Lisak, T. Olsson, M. Ahlander, *IEEE Trans. Microwave Theory Techn.* **47**, 2547 (1999).
- [13] S.K. Remillard, A. Hardaway, B. Jork, J. Gilliland, J. Gibbs, *Progr. Electromagn. Res. B* **15**, 175 (2009).
- [14] M. Radmilovic-Radjenovic, J.K. Lee, F. Iza and G.Y. Park, *J. Phys. D: Appl. Phys* **38**, 950 (2005).
- [15] R. Tomala, U. Jordan, D. Anderson, M. Lisak, *Contr. Plasma Phys.* **46**, 287 (2006).

The Role of the Field Emission Effect in the Breakdown Mechanism of Direct-Current Helium Discharges in Micrometer Gaps

Š. Matejčík¹, M. Klas¹, B. Radjenović², M. Durian¹, M. Savić², and M. Radmilović-Radjenović^{2*}

¹ Department of Experimental Physics, Comenius University, Mlynski dolina F2, 84248 Bratislava, Slovakia

² Institute of Physics, University of Belgrade, Pregrevica 118, 11080 Zemun, Serbia

Received 24 May 2013, revised 11 June 2013, accepted 11 June 2013

Published online XXX 2013

Key words Field emission, microdischarges, breakdown mechanism.

This paper presents results of experimental studies of the direct current breakdown voltage curves and volt-ampere characteristics of discharges generated in a system consisting of two plane-parallel electrodes tungsten and molybdenum electrodes at separations from 100 μm to 1 μm . The measurements were performed in the pressure range from 22.5 Torr to 738 Torr. The results are presented in the form of Paschen curves. Based on the measured breakdown voltage curves, the effective yields have been estimated in the case of different cathode materials. Differences between them are attributed to the influence of the work function of the cathode material on the current-voltage characteristics due to field emission effect in small gaps and high pressures. At low-pressures, however, vaporation of impurities from electrodes material becomes significant. The present paper delivers new data on DC breakdown under these experimental conditions and conditions on the validity of the Paschen law in helium and provides better insight into the role of the field emission and the electrode materials on the breakdown voltage.

© 2013 WILEY-VCH Verlag GmbH & Co. KGaA, Weinheim

1 Introduction

Studies of low-temperature helium plasmas that exist in various astrophysical and laboratory environments are relevant in numerous scientifically and technologically important areas. High pressure non-equilibrium microdischarge plasmas have applications including excimer radiation sources, sensors, plasma display panels, ozonizers, immersion ion implantation, military and civilian aerospace applications, biomedical and environmental applications [1]– [5]. On the other hand, plasma diagnostics procedures are indispensable for better understanding of microdischarge physics and optimizing device performance. One possibility to achieve high-pressure discharges which are still non-equilibrium is to operate at very small gaps (of the order of a few micrometers) [6]– [8].

In the past few decades, a considerable number of studies on microdischarges have been made [9]– [12]. Fundamental knowledge of the electric breakdown in helium, however, has not kept pace with these increasing interests, mostly due to the complexity of the phenomena related to the plasma breakdown process. At large separations, the breakdown voltage follows the well known Paschen law and dependence on the pd product (pressure times the electrode separation) [13]. At small gap sizes when a high electric field is generated, however, departures from the Paschen law have been reported indicating that ion-enhanced field emission strongly affects the left hand branch of the Paschen curve [14, 15]. The importance of the role of field emission and vapor arc have been demonstrated for gaps smaller than 10 μm , leading to the description of the "modified" Paschen curve. The general conclusion is that the breakdown voltage decreases rapidly for smaller gaps due to field emission [7, 8, 12, 14].

In spite of a large number of publications devoted to the measurements of breakdown voltages at micro separation there exist only few studies in the literature for separation smaller than 300 μm and in homogeneous electric field [11, 16]. For this reason we built a new system to measure the DC breakdown from 100 μm to 1 μm separations between plane-parallel tungsten and molybdenum electrodes in homogeneous electric field. Tungsten and

* author. E-mail: marija@ipb.ac.rs

molybdenum materials are used for many years in the field of lighting materials. They have many unique and advantageous properties at an elevated temperature and they are widely used for electric and electronic equipments, electronic devices, medical devices, lighting devices and so on.

In this paper measurements of the breakdown voltage curves for DC discharges in helium over a full range of pd values are presented. Measurements have been performed for several values of the gas pressure by varying the micrometer gap sizes. The principal problems in obtaining accurate measurements of the electrical breakdown potential are addressed by the electrode preparation and simultaneous measurements of the current-voltage characteristics. Experimental results are supported by the theoretical predictions based on the Fowler-Nordheim theory. The roles of the field emission effect as well as the material and the conditions of the cathode materials are analyzed and discussed.

2 Experimental

The discharge system contains two planar electrodes placed in the high vacuum chamber as shown in Fig. 1 [15, 16]. The vacuum chamber itself consists of three parts: positioner for centering the electrode position in three directions (with accuracy about $1\ \mu\text{m}$) and tilting the upper electrode which is located in the upper part. In the middle part there is a glass crux with four fused silica windows. In the bottom part there is also positioning system for tilting electrode as well as improved system for very ultra fine tilting. In this experiment, two different geometries of electrodes were used. Tungsten electrodes were highly polished and their sides were covered by dielectric glass cap in order to prevent discharge to ignite at longer paths. These electrodes allow to study the breakdown voltages in whole range of pd of Paschen curve. Whereas the molybdenum electrodes with Bruce profile were used to compare measured breakdown voltages on the right side of Paschen curve with tungsten electrodes as well as the influence of long path discharge on the left side of Paschen curves. For both electrodes the same procedures for measurement were applied. One of the electrodes was fixed while the other was moved continuously with micrometer scale linear feed-through. The $0\ \mu\text{m}$ separation of the electrodes was established by checking the electrical contact between the electrodes and then the movable electrode was pulled away by the means of the micrometer screw at the upper electrode. Both tungsten electrodes were equipped with dielectric caps (immune to vacuum, dielectric breakdown strength $=13.8\text{kV}/\text{mm}$) to prevent the ignition of the discharge at longer path at low pressures. The electrode surface has been polished by the finest diamond paste ($0.25\ \mu\text{m}$ grain size) in order to achieve the average roughness of the electrode better than $0.25\ \mu\text{m}$ and measured by using SEM.

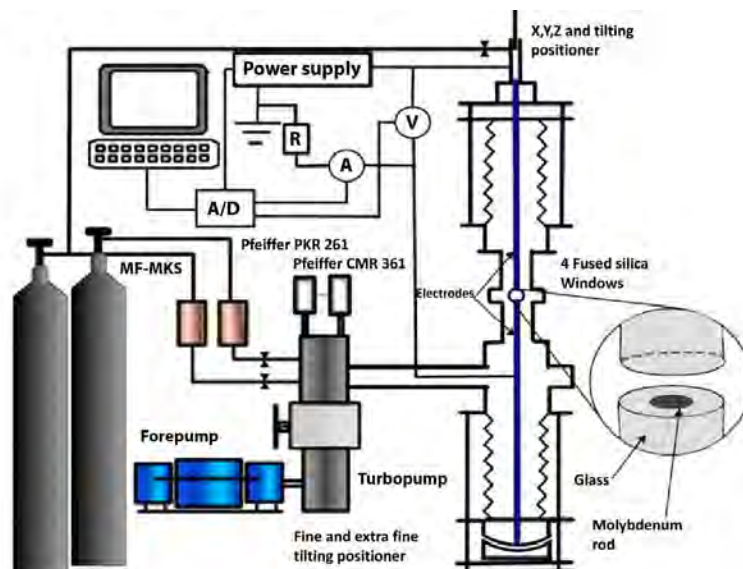


Fig. 1 Schematic view of the experimental apparatus built for the measurements of the breakdown voltage and volt-ampere characteristics in direct-current discharges in micrometer gaps.

Determination of the breakdown voltages were based on recording the current-voltage characteristics by using a digital oscilloscope and the AD card (National Instruments NI USB-6211). The potential across the discharge tube was increased with rate 0.3 V/s to 20 V/s (depends on the pressure). Faster ramp voltage can be used in the left side of Paschen curve where free electrons are emitted easily from the electrode surface by field emission. The AD card used for the current-voltage measurements has sampling frequency 10 kHz and averages 10 samples. The discharge current was limited to 2 mA for protection of the electrodes. The value of resistor R_1 was in most cases 300 k Ω , in the case of resistor R_2 , where the current was measured the value was 520 Ω .

3 Theoretical background

Field emission can be described as the extraction of electrons from the surface by the application of very high electric fields. The current density of the emitted electrons is related to the applied electric field by the Fowler-Nordheim (F-N) theory [17]:

$$j_{FE} = \frac{A^2 \beta^2 E^2}{\phi t^2(y)} \exp\left(-\frac{B \phi^{3/2} v(y)}{\beta E}\right) \quad (1)$$

where ϕ is the work function of the metal, β is the field enhancement factor, while A and B are constants given by:

$$A = 6.2 \times 10^{-6} \text{ A/eV}$$

$$B = 6.85 \times 10^7 \text{ V/cm/eV}^{3/2}.$$

The terms $v(y)$ and $t^2(y)$ represent corrections that were included later in the F-N theory [18]:

$$v(y) \approx 0.95 - y^2$$

$$t^2(y) \approx 1.1,$$

with $y \approx 3.79 \times 10^{-4} \sqrt{\beta E} / \phi$. The enhancement factor β strongly depends on the geometrical effects at the surface such as roughness which in turn depend on the technique used to fabricate the devices. Fowler and Nordheim [17] originally have been calculated the current for a cold flat surface, although the current weakly depends on temperature, but it is strongly dependent on emitter shape. To take shape into account, there is a geometric field enhancement parameter $\beta = E/E_{app}$ which is defined as the ratio of the local emitter field over the applied field. In principle, this factor has a direct physical meaning only for metallic protrusions. If the shape of the protrusion is reasonably simple, the parameter β value can be calculated quite accurately. Experimentally, the numerical value of β can be determined from the F-N plot. At the same time, such plot may allow us to determine if the current flow is due to field-emitted electrons (see, for example, [19]). In general, the F-N equation (1), which are derived from quantum-mechanical considerations, implies that a perfect surface has a β value of unity. However, curve fitting of experimental results requires higher values of β [19]. This is attributed to field gradient enhancements resulting from microscopic surface.

4 Results and discussions

The behavior of gases under low pressures and uniform and non-uniform fields, in particular the breakdown characteristics, are covered in details in work by Craggs and Meek [13]. Under low pressures, the gaseous breakdown mechanism is dominated mostly by the electrodes and not affected much by the gases involved. Fig. 2 contains the current-voltage characteristics measured for tungsten electrodes in vacuum at very low pressure of 1.5×10^{-5} Torr. For the 1 μm gap size and voltages greater than 150 V, there is a clear increase in current that grows larger as breakdown is approached. The current starts at around 0.5 μA (resolution of AD card) and increases rapidly. If the electric field generated in micro gaps is sufficiently strong, some of the conduction electrons in the metal lattice are literally pulled into the gap and accelerating toward the electrode. Even if the mean free path is longer than the gap size and electrons could not gain sufficient energy to ionize atoms, a breakdown occurs. With increasing electrode gap, increase of the current appears at higher voltages. From these measurements, determined values of the breakdown voltages for 1 μm , 2.5 μm , 5 μm and 10 μm are 220 V (220 kV/mm) 600 V (240 kV/mm), 1000 V (20 kV/mm) and 1600 V (160 kV/mm). For the 1 μm gap size the voltage is estimated within the accuracy of around 20%, while for the 10 μm within 10 – 15%.

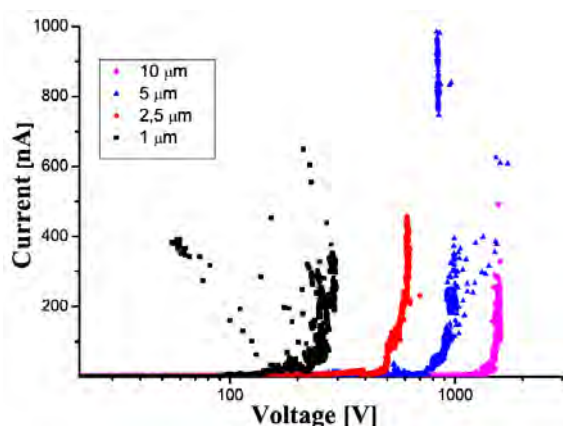


Fig. 2 Breakdown in vacuum for tungsten electrodes separated by $1\ \mu\text{m}$ (black symbols), $2.5\ \mu\text{m}$ (red symbols), $5\ \mu\text{m}$ (blue symbols) and $10\ \mu\text{m}$ (pink symbols). The measurements were performed at very low pressure of 1.5×10^{-5} Torr.

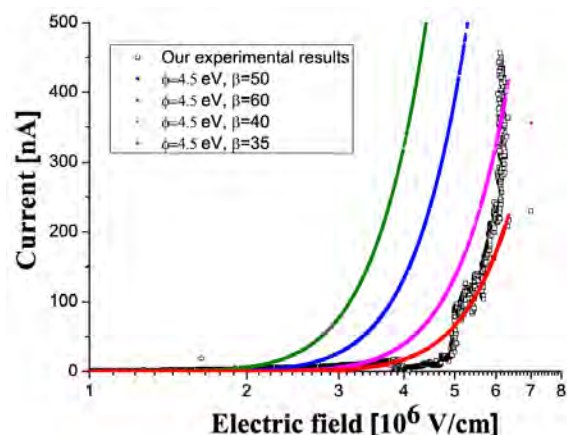


Fig. 3 Comparison of measured current-voltage characteristics for the $2.5\ \mu\text{m}$ gap size (black symbols) with corresponding F-N theory curves in accordance with the equation (1) for various values of β .

The influence of the enhancement factor on the current-voltage characteristic is illustrated in Fig. 3. Black symbols represent our experimental results for the tungsten electrodes ($\phi = 4.5\ \text{eV}$) separated by the $2.5\ \mu\text{m}$. Calculations were performed in accordance with the F-N equation (1) for the enhancement factor of 35 (red symbols), 40 (pink symbols), 50 (blue symbols) and 60 (green symbols). Since the experimental results agree well with the calculations results obtained with $\beta = 40$, we assume such value for the enhancement factor.

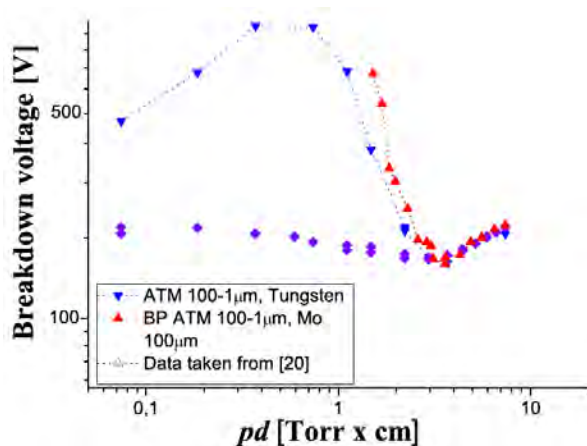


Fig. 4 The breakdown voltage versus pd product. Our measurements for tungsten electrodes (blue symbols) and molybdenum electrodes (violet symbols) are compared with the data for copper electrodes (open symbols) and tungsten electrodes (red symbols) taken from [20].

The helium breakdown voltage curves for various gap sizes from $1\ \mu\text{m}$ to $100\ \mu\text{m}$ are shown in Fig. 4. Two sets of measurements have been performed: i) with tungsten electrodes with dielectric cap (blue symbols) and ii) with electrodes made of molybdenum with Bruce profile (violet symbols). The results are compared with the Paschen curve obtained at constant electrode separation of $100\ \mu\text{m}$ for tungsten electrodes (red symbols) and $10\ \text{mm}$ (open symbols) gap sizes taken from [20]. On the left branch of the breakdown voltage curve, results for the molybdenum electrodes at constant atmospheric pressure and variable electrode distance are much lower and have a different shape than those for tungsten and copper electrodes ref. [20]. However, these results are in agreement with expectations of long path discharge breakdown allowed by construction of electrodes. Thus on the left side of Paschen curve breakdown voltage are more or less equal or slightly higher than minimum breakdown voltage for Helium gas. In contrast to molybdenum electrodes, the results taken for tungsten electrodes do not show long path breakdown at the left side of the Paschen curve due to dielectric cap. For the pd values greater than $3\ \text{Torr} \times \text{cm}$, all results have similar trends indicating that the electrode materials play no significant role

on the right hand branch of the breakdown curve. Our data for tungsten electrodes (blue symbols) satisfactorily agree with data from other electrode materials for the pd values of $1.5 \text{ Torr} \times \text{cm}$ and higher. Below this value the effects associated with the high values of the electric field cause departure from the standard Paschen law. In other words, combination of small electrode distance and high reduced electric field leads to decrease of breakdown voltages.

Based on the breakdown voltage curves from Figure 4, the effective yields have been estimated and shown in Figure 5a. It is well known that the effective yield in microgaps depends on the cathode material in accordance with the expression:

$$\gamma_{eff} = Ke^{-D/E}, \quad (2)$$

where E is the electric field near the cathode and K and B are material and gas dependent constants. Although the molybdenum and tungsten have very similar work function (4.2 eV and 4.5 eV, respectively), their current-voltage characteristics determined from expression (2) are different as shown in Figure 5b which could explain the large discrepancies between the yields observed in Figure 5a, especially at large ratios E/p . On the other hand, different purity of helium also affects the results. Although, we used the same purity of helium, differences can be caused by the evaporation of impurities from electrodes material at low pressures.

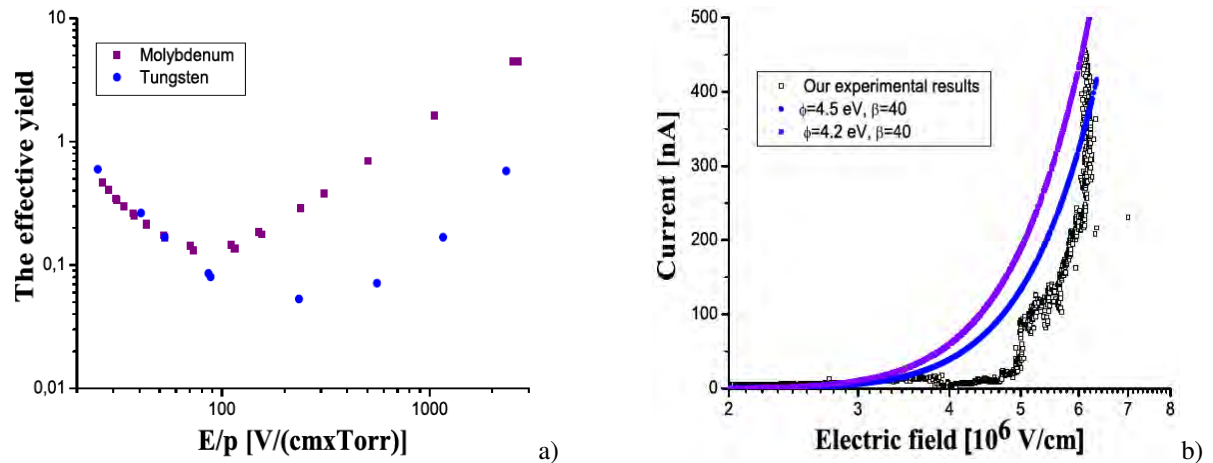


Fig. 5 The dependence of the effective yield on the E/p ratio estimated from the breakdown voltage curves and b) current versus the electric field, for two different cathode materials: tungsten (blue symbols) and molybdenum (violet symbols).

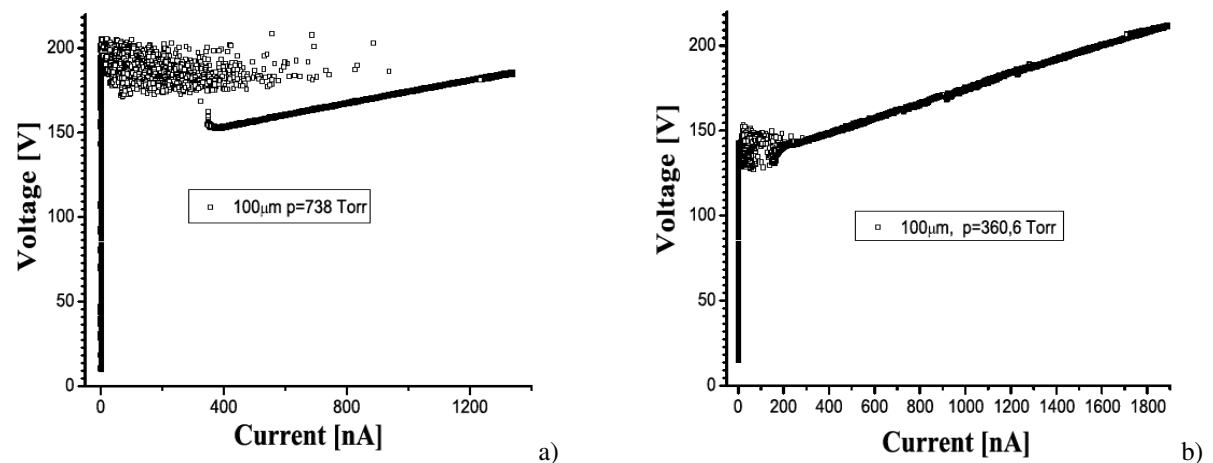


Fig. 6 Volt-Ampere characteristics for the $100 \mu\text{m}$ gap size at the pd of: a) $7.4 \text{ Torr} \times \text{cm}$ and b) $3.6 \text{ Torr} \times \text{cm}$.

The breakdown voltage curve for $100\ \mu\text{m}$ gap shows no apparent departure from Paschen law and thus we consider it as a normal discharge. This is confirmed by the Volt-ampere characteristics recorded at two different pd values of: $7.4\ \text{Torr} \times \text{cm}$ (Figure 6a) and $3.6\ \text{Torr} \times \text{cm}$ (Figure 6b). The measurements carried out at different pressures have similar tendencies and correspond to the normal discharge characteristics. On the other hand, at $5\ \mu\text{m}$ electrode separation and the atmospheric pressure the breakdown curve shows departure from Paschen law and thus discharge generated at this electrode separation represents a different type of discharge due to important role of processes associated with high electric field. The Volt-ampere characteristic for this discharge (see Figure 7) clearly demonstrates, that the current is practically limited by the field emission of the electrons from the electrode.

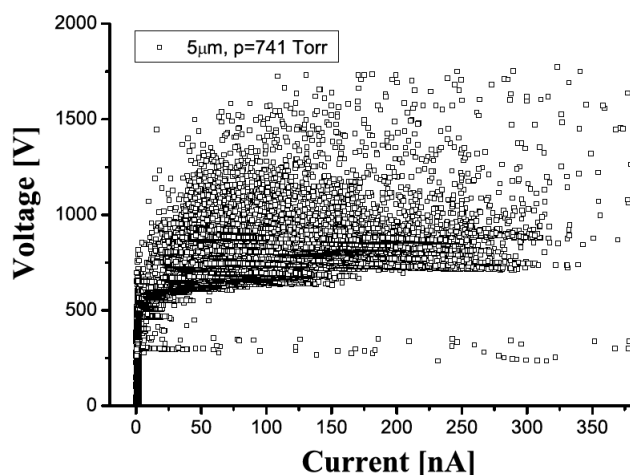


Fig. 7 Volt-Ampere characteristics for the $5\ \mu\text{m}$ gap spacing and the pd value of $0.37\ \text{Torr} \times \text{cm}$.

5 Conclusions

In this paper novel experimental results for the DC breakdown voltage curves in helium for the gap sizes ranging from $1\ \mu\text{m}$ to $100\ \mu\text{m}$ were presented and discussed. Results for the tungsten electrodes are in a good agreement with the previously published data [20]. Results for the molybdenum electrodes (Bruce profile geometry) are systematically lower than results for tungsten and copper electrodes, especially at lower pd values (left hand branch of the breakdown curve). The results show that the right hand branch, seems to be almost independent of the electrode material.

Based on the measured breakdown voltage curves, the effective yields as a function on the E/p ratio have been determined. The obtained values clearly illustrated dependence of the yield on the cathode material. Although some materials have a similar work functions, their current-voltage characteristics that correspond to the F-N equation (1) are different. It was also found out that differences between yields for various materials are due to evaporation of impurities from electrodes material at lower pressures.

Besides the electrode materials, the electrode geometry and the electrode separations have important influence on the Paschen curve. With increasing electrode separation, the breakdown voltage increases since the contribution of field emission progressively decreases. Violation of the standard scaling law was observed when the strength of the electric field is high enough to induce the field emission of electrons. Field emission combined with other mechanisms is known to limit usable voltages to values well below those predicted by avalanche breakdown.

Acknowledgements The work has been carried out under Ministry of Education and Science Republic of Serbia O171037 and III41011 projects. This work has also been supported by the VEGA grant agency; project VEGA 1/0514/12, the Slovak Research and Development Agency Projects APVV-0733-11 and DO7RP-0025-11, and the Slovak Research and Development Agency under Contract SK-SRB-0026-11. The authors are very grateful to Dr Nikola Škoro and Dr Vladimir Stojanović at the Institute of Physics for very useful comments and suggestions.

References

- [1] T. Ito, T. Izaki and K. Terashima, *Thin Solid Films* **386**, 300 (2001).
- [2] T. Makabe and Z.Lj. Petrović, *Plasma Electronics: Applications in Microelectronic Device Fabrication* (Taylor & Francis, New York, 2006).
- [3] U. Kogelschatz, *Contribution to Plasma Physics* **47**, 80 (2007).
- [4] S. Adili and C.M. Franck, *IEEE Transaction Dielectrics and Insulation* **19**, 1833 (2012).
- [5] C.M. Du, J. Wang, L. Zhang, H.X. Li, H. Liu, and Y. Xiong, *New Journal of Physics* **14**, 013010 (2012).
- [6] R.S. Dhariwal, *IEE Proceedings - Science, Measurement and Technology* **147**, 261 (2000).
- [7] M. Radmilović-Radjenović, J.K. Lee, F. Iza, and G.Y. Park, *J. Phys. D: Appl. Phys.* **38**, 950 (2005).
- [8] E. Munoz-Serrano, G. Hagelaar, Th. Callegari, J. Boeuf, and L.C. Pitchford, *Plasma Physics and Controlled Fusion* **48**, B391 (2006).
- [9] W.S. Boyle and P. Kisliuk, *Physics Review* **97**, 55 (1955).
- [10] P. Rumbach and D.B. Go, *Journal of Applied Physics* **112**, 103302 (2012).
- [11] Z.Lj. Petrović, N. Škoro, D. Marić, C.M.O. Mahony, P.D. Maguire, M. Radmilović-Radjenović and G. Malović, *J. Phys. D: Appl. Phys.* **41**, 194002 (2008).
- [12] E. Hourdakis, B.J. Simonds, and N.M. Zimmerman, *Review of Scientific Instruments* **77**, 034702 (2006).
- [13] J.M. Meek and J.D. Craggs, *Electrical breakdown of gases* (Oxford University Press, Oxford, 1953).
- [14] M. Radmilović-Radjenović and B. Radjenović, *Contrib. Plasma Phys.* **47**, 165 (2007).
- [15] M. Klas, Š. Matejčik, B. Radjenović, and M. Radmilović-Radjenović, *Physics Letters A* **376**, 1048 (2012).
- [16] M. Radmilović-Radjenović, Š. Matejčik, M. Klas, and B. Radjenović, *J. Phys. D: Appl. Phys.* **46**, 015302 (2013).
- [17] K. Yuasa, A. Shimoi, I. Ohba, and C. Oshima, *Surf. Sci.* **520**, 18 (2002).
- [18] R.E. Burgess and H. Kroemer, *Phys. Review* **90**, 515 (1953).
- [19] M. Radmilović-Radjenović and B. Radjenović, *IEEE Trans. Plasma Science* **35**, 1223 (2007).
- [20] P. Hartmann, Z. Donkó, G. Bánó, L. Szalai, and K. Rózsa, *Plasma Sourc. Sci. Technol.* **9**, 183 (2000).

The surface charging effects in three-dimensional simulation of the profiles of plasma-etched nanostructures

M. Radmilović-Radjenović^{*,†}, B. Radjenović and M. Savić

Institute of Physics, University of Belgrade, Pregrevica 118, 11080 Belgrade, Serbia

SUMMARY

Particles and fields represent two major modeling paradigms in pure and applied science at all. Particles typically exist in a spatial domain and they may interact with other particles or with field quantities defined on that domain. A field, on the other hand, defines a set of values on a region of space. In this paper, a methodology and some of the results for three-dimensional (3D) simulations that includes both field and particle abstractions are presented. In our studies, charging damage to a semiconductor structure during plasma etching is simulated by using 3D level set profile evolution simulator. The surface potential profiles and electric field for the entire feature were generated by solving the Laplace equation using finite elements method. Calculations were performed in the case of simplified model of Ar⁺/CF₄ non-equilibrium plasma etching of SiO₂. Copyright © 2010 John Wiley & Sons, Ltd.

Received 15 February 2010; Revised 2 August 2010; Accepted 7 November 2010

KEY WORDS: plasma etching; profile charging; finite elements method; level set method

1. INTRODUCTION

Since its introduction in the 1970s, plasma etching has become an integral part of semiconductor integrated circuit (IC) processing, treatment of materials (such as implantation) and especially for achieving massively parallel production of well-organized and designed nanostructures [1–3]. Plasma etching requires a high etching rate, anisotropy, uniformity across the wafer, and process reproducibility [4,5]. Precise monitoring of the etched profile in microelectronic devices during plasma etching process is one of the most important tasks of front-end and back-end microelectronic devices manufacturing technologies. Charging effects during plasma etching of high-aspect ratio structures can cause gate oxide degradation during gate etching and profile deformation issues such as notching or bowing [6–8]. The origin of this phenomenon is due to the difference in directionality between ions and electrons when they cross the plasma sheath and interact with three-dimensional (3D) structures. The potential for using modeling and simulation to benefit industrial users of plasma processes and equipment has never been greater [9,10]. Plasmas are used in about 30% of all semiconductor manufacturing processing steps, and about the same fraction of processing equipment is plasma-based in a typical microelectronics fabrication facility. In the last several years, computational costs continue to decrease steadily and considerable progress has been achieved in establishing the major modeling strategies that are necessary to achieve practical industrial objectives. Nevertheless, low-temperature plasma processing science is a relatively young field, and has not therefore received the in-depth,

^{*}Correspondence to: M. Radmilović-Radjenović, Institute of Physics, University of Belgrade, Pregrevica 118, 11080 Belgrade, Serbia.

[†]E-mail: marija@ipb.ac.rs

sustained attention that is required to have a significant, timely impact in industry. This situation is perhaps most evident in the area of the database for physical and chemical processes in plasma materials processing [11]. The profile surface evolution during plasma etching, deposition, and lithography development is a significant challenge for numerical methods for interface tracking itself. Level set methods for evolving interfaces [12,13] are specially designed for profiles, which can develop sharp corners, change topology, and undergo orders of magnitude changes in speed. Additionally, etching submicron features in insulating material such as SiO₂ or materials masked with insulators, e.g. photoresist-masked polysilicon, is accompanied by feature charging effects caused by the differences in electron and ion angular distributions. The plasma charging reported by Yoshida [14] has been studied in recent decades [15,16]. The phenomenon can be described as follows: because of the acceleration in the sheath, the angular distribution is more directional than that of electrons. The difference causes the electron shading effect at the etched feature, thus generating positive potential at the deep trench bottom. This charging effect leads to many serious plasma process induced damage problems such as bowing, trenching, reactive ion etching lag, and notching. The reduction in the device size and multilayer structures requires a high-aspect ratio in the SiO₂ etching. As the aspect ratio increases, the charging effect becomes more observable as reported by Makabe *et al.* [17,18]. The negative charge that might develop on the sidewalls can bend the trajectories of the ions passing close to them. This bending effect may contribute to microtrenching. In addition, etching rate reduction with time and notching of polysilicon sidewalls during the overetching step have been attributed in part to feature charging effects. The main goal of this paper is to include charging effects in our 3D level set etching profile simulator. For that purpose, some basic aspects of the etching profile simulation procedure, the profile surface movement via level set method, particle fluxes calculations using Monte-Carlo method and the electric field (generated by the profile charge) calculations on the basis of the finite elements method will be described. Finally, the obtained simulation results illustrating charging effect will be presented and discussed.

2. SIMULATION TECHNIQUE

2.1. Sparse field level set method

In the level set method considered surface at a certain time t is represented by the so-called level set function $\phi(t, x)$. The initial surface is given by $\{x | \phi(0, x) = 0\}$. The evolution of the surface in time is caused by the surface processes in the case of the etching. The velocity of the point on the surface normal to the surface denoted by $R(t, x)$ is called velocity function. The velocity function generally depends on the time and space variables and we assume that it is defined on the whole simulation domain. At a later time $t > 0$, the surface is as well as the zero level set of the function $\phi(t, x)$. Namely, it can be defined as a set of points $\{x | \phi(t, x) = 0\}$. This leads to the level set equation in Hamilton–Jacobi form:

$$\frac{\partial \phi}{\partial t} + H(\nabla \phi(t, x)) = 0, \quad (1)$$

in the unknown function $\phi(t, x)$, where Hamiltonian function is given by $H = R(t, x)|\nabla \phi(t, x)|$ and where $\phi(0, x) = 0$ determines the initial surface. Several approaches for solving level set equations have been developed. Among them, the most important are narrow band level set method, widely used in etching process modeling tools, and recently developed sparse-filed method [19]. The sparse field method uses an approximation to the level set function that makes it feasible to recompute the neighborhood of the zero level set at each time step. As a result, the number of computations increases with the size of the surface, rather than with the resolution of the grid.

It is well known that Hamiltonian function H is convex if the following condition is fulfilled

$$\frac{\partial^2 H}{\partial \phi_{x_i} \partial \phi_{x_j}} \geq 0, \quad (2)$$

where φ_{x_i} is a partial derivative of $\varphi(t, \mathbf{x})$ with respect to x_i . During plasma etching and deposition processes, the etching (deposition) rate, which defines the surface velocity function $R(t, \mathbf{x})$, depends on the geometric characteristics of the profile surface itself, or more precisely, on the angle of the incidence of the incoming particles. In our studies, we shall consider an etching beam coming down in the vertical direction, conditions that are characteristic for ion milling technology, but angular dependence of the etching rates appears, more or less, in all etching processes. In these cases, the most useful finite difference scheme that can be applied is the Lax–Friedrichs scheme, one that relies on the central difference approximation to the numerical flux function, and preserves monotonicity through a second-order linear smoothing term. It is shown [20] that it is possible to use the Lax–Friedrichs scheme in conjunction with the sparse field method, and to preserve sharp interfaces and corners by optimizing the amount of smoothing in it. This is of special importance in the simulations of the etching processes in which spatially localized effects appear, such as notching and microtrenching.

2.2. Particle fluxes calculations

Particles are usually used in one of the two ways in computer scientific applications: In the first way, the particles known as ‘tracers’ are tracking in order to gather statistics that describe the conditions of a complex physical system. The second way is based on performing direct numerical simulation of systems that contain discrete point-like entities such as ions or molecules. In both cases, there are one or more sets of particles, while each set contains some data associated with it that describes its members’ characteristics, such as charge, mass, or momentum. The state of the physical system is determined by these data.

Simulation of the etch process in details requires knowledge of the etching rates at all the points of the profile surface during the etching process. These rates are directly related to fluxes of the etching species on the profile surface, which are themselves determined by the plasma parameters in the etching device. Electrons do not contribute directly to the material removal, but they are the source, together with positive ions, of the profile charging that has many negative consequences on the final outcome of the process especially in the case of insulating material etching, SiO_2 for example. As can be observed from Figure 1 that shows the electron energy distribution functions (EEDF) and the energy distribution function for Ar^+ ions (IEDF), a large number of electrons have low energies while the energy of ions is spread to higher energies. On the other hand, the angular distribution function for electrons (EADF) is different from the angular distribution function for Ar^+ ions (IADF) indicating that ions are directed toward small angles. These distribution functions obtained by particle-in-cell (PIC) calculations using XPDC1 code [21–23] are used as the boundary conditions for the calculations of ion fluxes incident on the profile surface.

The etching process in medium/high density fluorocarbon plasmas is believed to consist of concurrent etching (of the SiO_2 substrate in our case) and deposition (of a fluorocarbon polymer layer) phenomena [24]. In this paper, the deposition process is neglected and ion-enhanced etching and physical sputtering and pure chemical etching of SiO_2 are considered. It is also assumed that the electrons are absorbed at the hitting points, while the neutrals can be absorbed or diffusively reflected, once or many times depending on its sticking coefficient. The positive ions can be absorbed, or specularly reflected, depending on their energy and incident angle. It is assumed that charged particles pass on their charge when they hit the surface, and that this charge does not move after that, what is reasonable for insulating materials. At the boundaries above the profile surface, periodic conditions are assumed. The surface neutrals coverage (i.e. the fraction of surface covered by free radicals) θ_n satisfies the balance equation:

$$\frac{d\theta_n}{dt} = J_n S_n (1 - \theta_n) - k_{ni} J_{ion} Y_{ni}^{\text{eff}} \theta_n - k_{ev} J_{ev} \theta_n, \quad (3)$$

where J_n and J_{ion} are neutral and ion fluxes, S_n is the neutral sticking coefficient, k_{ni} and k_{ev} are etchant stoichiometry factors, and Y_{ni}^{eff} is the effective etching yield for ion-enhanced chemical etching. Here, by the term ‘effective’, we denote a quantity related to the integral flux, not to an individual particle. J_{ev} is evaporation flux that corresponds to pure chemical etching. It is related

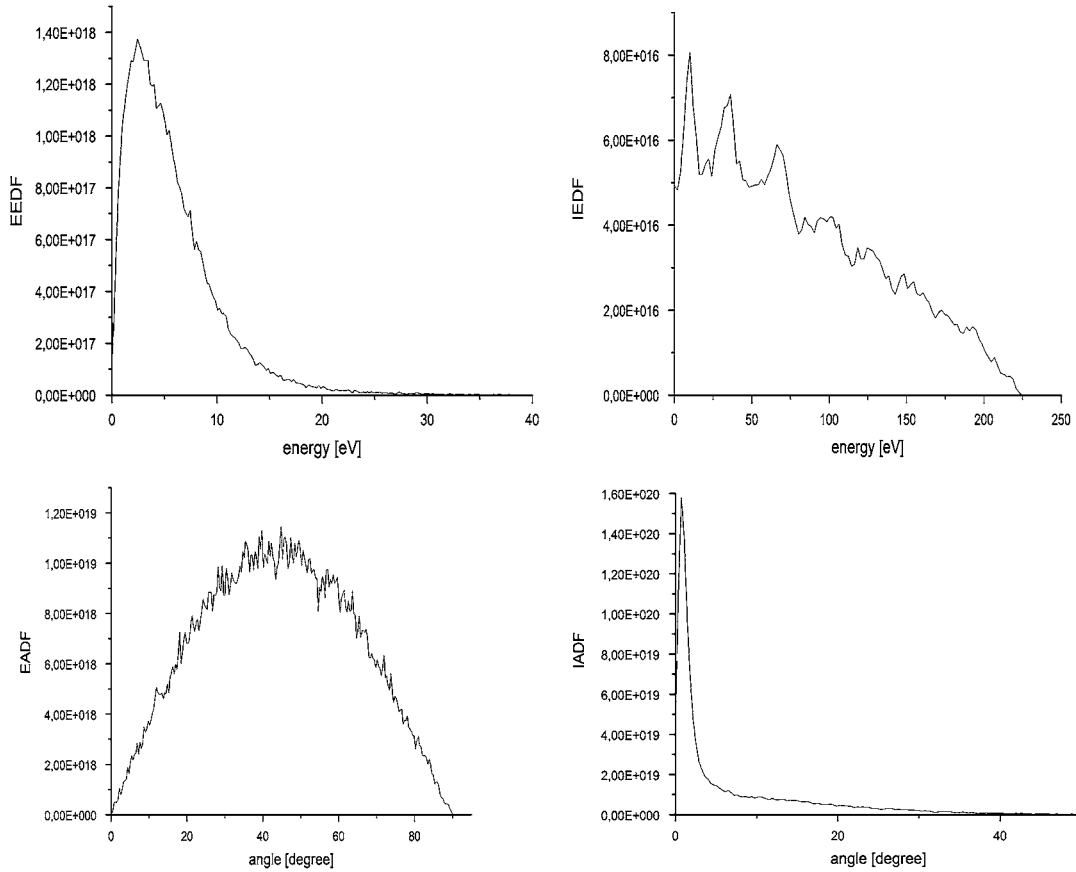


Figure 1. Energy distribution functions of electrons and Ar^+ ions (EEDF and IEDF, respectively) and angular distribution functions of electrons and Ar^+ ions (EADF and IADF, respectively) obtained by PIC/MCC simulations.

to the neutrals flux by the Arrhenius law:

$$J_{\text{ev}} = K_{\text{SiO}_2} e^{-\frac{E_{\text{SiO}_2}}{k_b T}} J_n. \quad (4)$$

Balance condition $d\theta_n/dt = 0$ gives the equilibrium surface coverage:

$$\theta_n = \frac{J_n S_n}{J_n S_n \theta_n + k_{\text{ni}} J_{\text{ion}} Y_{\text{ni}}^{\text{eff}} + k_{\text{ev}} J_{\text{ev}}}. \quad (5)$$

So, now we can write equation defining the etching rate ER in the form

$$\text{ER} = \frac{1}{\rho_{\text{SiO}_2}} [J_{\text{ion}} Y_{\text{ni}}^{\text{eff}} \theta_n + J_{\text{ion}} Y_{\text{ni}}^{\text{eff}} (1 - \theta_n) + J_{\text{ev}} \theta_n], \quad (6)$$

where ρ_{SiO_2} is SiO_2 density and $Y_{\text{ni}}^{\text{eff}}$ is the effective physical spattering etching yield. The etching rate ER defines the velocity function $V(t, \mathbf{x})$ at the profile surface. In actual calculation, the feature profile surface is represented by a set of connected triangles, and the above formula should be applied to the every single particular triangle. So, instead of effective etching yields we should define etching yields for every particular ion:

$$Y_{\text{ni}}(E_i, \alpha_i) = A_{\text{ni}} (\sqrt{E_i} - \sqrt{E_{\text{in}}^{\text{th}}}) \cos \alpha_i, \quad (7)$$

and

$$Y_{sp}(E_i, \alpha_i) = A_{sp}(\sqrt{E_i} - \sqrt{E_{sp}^{th}})\cos \alpha_i(1 + B_{sp}\sin^2 \alpha_i), \quad (8)$$

where E_i is the ion energy and α_i is the angle between the surface normal and the ion incident direction at the point of incidence. Numerical values of the constants appearing in relations (3), (4), (6), (7), and (8) are taken from the Reference [18]. The triangular representation of the profile surface requires that instead of integral particle fluxes J_n and J_{ion} , corresponding summations over every particle incident on the particular triangle

$$J_n = \frac{R_n}{A\Delta t_{etch}} N_n, \quad (9)$$

$$J_{ion} Y_{ni}^{eff} = \frac{R_{ion}}{A\Delta t_{etch}} \sum_i Y_{ni}(E_i, \alpha_i), \quad (10)$$

and

$$j_{ion} Y_{sp}^{eff} = \frac{R_{ion}}{A\Delta t_{etch}} \sum_i Y_{spi}(E_i, \alpha_i), \quad (11)$$

should be used. Here, N_n denotes the number of neutrals absorbed on the particular triangle, R_n (R_{ion}) is the ratio of actual number of neutrals (ions) passing the upper computational domain boundary during the etching time interval and number of neutrals (ions) used in Monte Carlo calculations, A is the particular triangle area, and Δt_{etch} is the etching time interval. The ions can be absorbed, or specularly reflected, depending on their energy and incident angle. The probability of specular reflection P_d is given by [25]:

$$P_d = 1 - C_1 \sqrt{E_i} \left(\frac{\pi}{2} - \alpha_i \right). \quad (12)$$

Neutrals (F radicals) density is supposed to be 10^{19} m^{-3} . The simulation time is 100 s, and it is divided in 100 equal etching intervals (Monte Carlo steps).

2.3. Electric fields calculations

In general, electromagnetic field equations were identified with the ‘Maxwell equations’, i.e. with partial differential equations, which are extremely rich in symmetries and (hence) conservation laws. In the continuum, many conservation laws follow directly from invariances of the Lagrangian (Noether symmetries) such as energy or momentum conservation, while others have an inherent topological aspect, such as magnetic charge. When Maxwell’s equations are discretized on a mesh, a number of symmetries of the continuum theory are modified or broken. However, some conservation laws may be preserved on a discrete setting. This is because they often relate a quantity on certain region of space to an associated quantity on the boundary of the region. Because the boundary is a topological invariant, such conservation laws should not depend on the metric of the space. A natural mathematical language that explores this aspect is the calculus of exterior differential forms and associated algebraic topological structures [26]. In this approach, the scalar electrostatic potential is a 0-form, the electric and magnetic fields are 1-forms, the electric and magnetic fluxes are 2-forms, and the scalar charge density is a 3-form. The basic operators are the exterior (or wedge) product, the exterior derivative, and the Hodge star. Precise rules (i.e. a calculus) prescribe how these forms and operators can be combined. In this modern geometrical approach to electromagnetics, the fundamental conservation laws are not obscured by the details of coordinate system-dependent notation. By working within the discrete differential forms framework, we are guaranteed that resulting spatial discretization schemes are fully mimetic. Finite difference method cannot be used when the geometry of the problem is irregular, as it is usual for the etching profiles. Hence, it is naturally to use finite elements method. The calculations of the electric fields in this paper are performed by integrating a general finite element solver GetDP [27] in our simulation framework. GetDP is a thorough implementation of discrete differential forms calculus, and uses mixed finite elements

to discretize de Rham-type complexes in one, two, and three dimensions. Meshing of the computational domain is carried out by TetGen tetrahedral mesh generator [28]. TetGen generates the boundary constrained high-quality (Delaunay) meshes, suitable for numerical simulation using finite element and finite volume methods. As a part of the post-processing procedure, the electric fields, obtained on the unstructured meshes, are recalculated on the Cartesian rectangular domains containing the regions of the particles movement. In this manner, the electric field on the particles could be calculated by simple trilinear interpolation.

3. RESULTS AND DISCUSSION

Our simulation results involve the profile charging calculations for the fixed profile surface. All the calculations are performed on $128 \times 128 \times 384$ rectangular grid. The initial profile surface is a rectangle deep with dimensions $0.1 \times 0.15 \times 0.1 \mu\text{m}$. Above the profile surface is the empty space (trench region). The incident particles are generated randomly at the top of the simulation region. In the case of the ion-enhanced chemical etching, the dependence of the surface velocity on the incident angle is simple: $V = V_0 \cos \theta$ and the evolution of the etching profile is displayed in Figure 2. Although, this is the simplest form of angular dependence, but it describes the ion-enhanced chemical etching process correctly [19]. In this case, we expect that the horizontal surfaces move downward, while the vertical ones stay still. This figure shows that it with optimal amount of smoothing gives minimal rounding of sharp corners, while preserving the numerical stability of the calculations. In order to illustrate the obtained results more clearly, Figure 3 shows the surface mesh of the tetrahedral mesh corresponding to the last profile in Figure 2. This mesh defines the profile surface for the subsequent particle flux and electric field calculations.

The fluxes of different particles are shown in Figure 4. Collisions in the simulation domain are neglected because mean-free path of ions and electrons is much longer than the simulation domain size. Also, the probability that more than two particles exist in the simulation space at the same time is very low because the life time of ions or electrons in the simulation region is much shorter than the incident time interval. The neutral and the electron fluxes distributions are similar: they are concentrated on the top of the wafer and upper portion of the sidewalls, while the ions, due its directionality, are accumulated at the bottom of the profile. Solving the Laplace equation with such a charge distribution as boundary condition leads to the potential distribution on the profile shown in Figure 5. The maximal value of the potential at the bottom



Figure 2. The time evolution of the profile during ion-enhanced chemical etching.

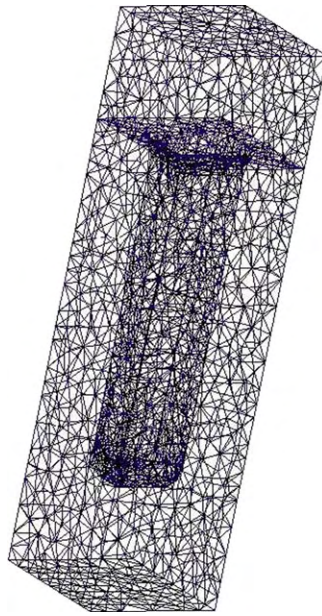


Figure 3. The surface mesh generated by Tetgen related to the last profile.

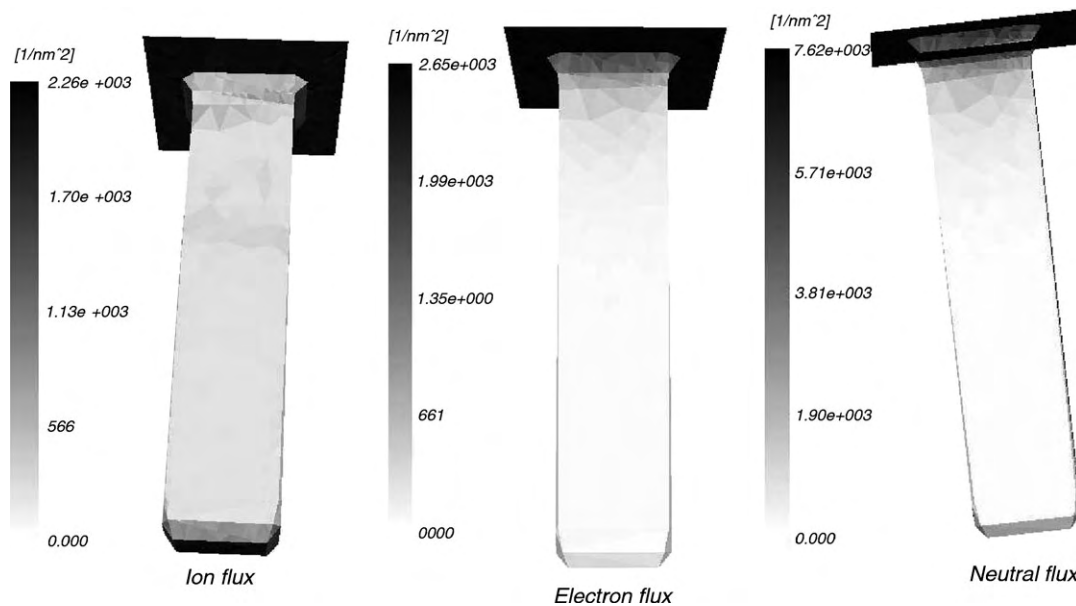


Figure 4. Fluxes of neutrals, electrons, and ions at the profile surface.

of the profile is somewhat bigger than the average ion energy, while the top surface is slightly negatively biased. Since the electrons leave the plasma with relatively high energies, they have very anisotropic distribution as they slow down in the sheath, so they are deposited mainly at the sidewalls and cannot reach the bottom. The deposited electrons at the entrance to the nano trench or nano hole actually also contribute to prevent other electrons from reaching the bottom of the structure and neutralizing the charge. Negative ions from the plasma have low energies so they cannot cross the sheath which was designed to slow down the much more energetic electrons. Similar, Figure 6 illustrates the potential cut. The aspect ratio of a feature typically refers to the ratio of the depth of the feature to its smallest horizontal cross-sectional dimension. It was shown that for the aspect ratios greater than 7 the potential at the bottom of the structure becomes equal to the potential corresponding to the ion energy. On the other hand, the potential

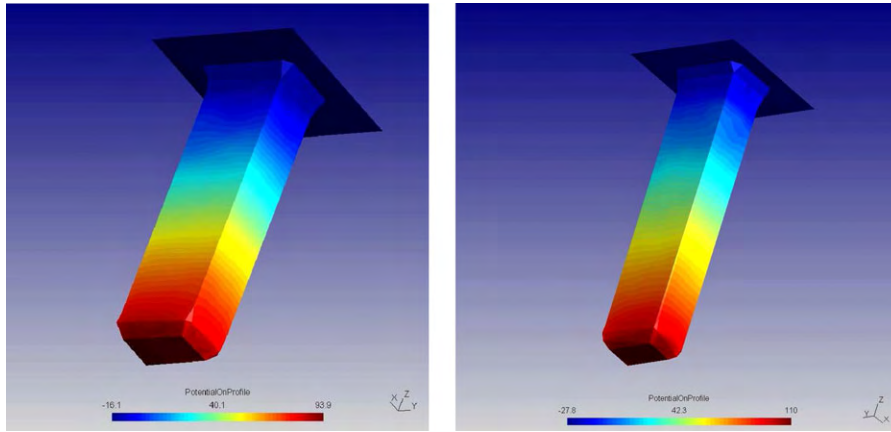


Figure 5. Potential distribution on the profile surface for two different values of the aspect ratio: (a) AR = 4.5 and (b) AR = 6.

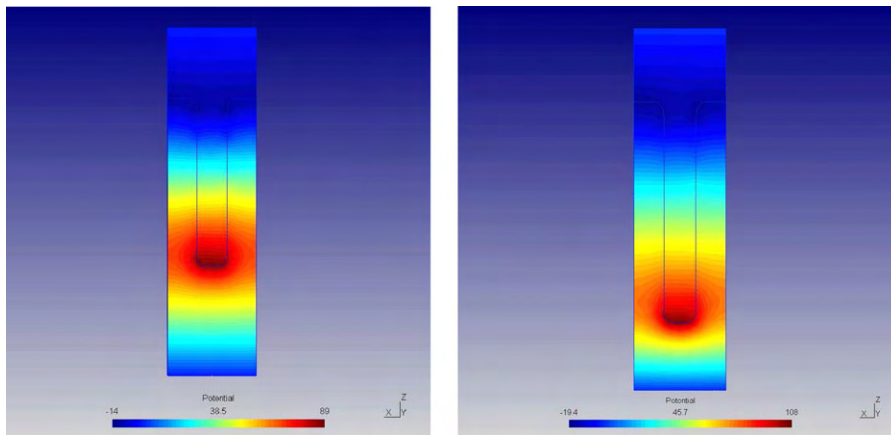


Figure 6. Potential cut in the case of: (a) AR = 4.5 and (b) AR = 6.

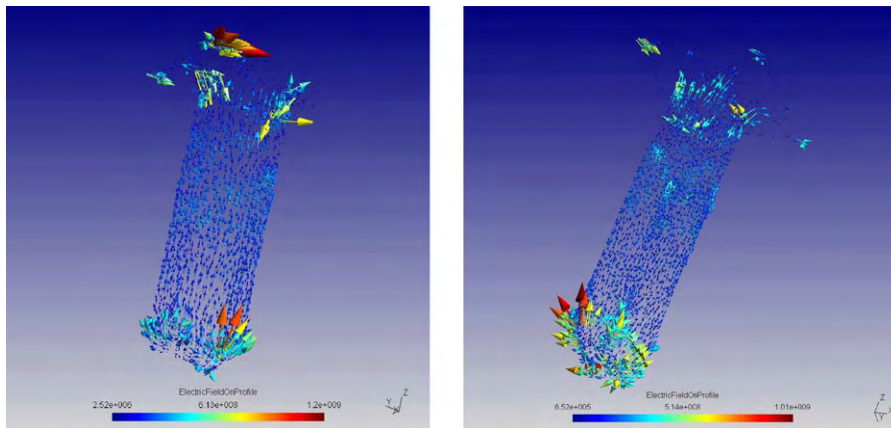


Figure 7. Electric field on the profile surface (expressed in V/m) for: (a) AR = 4.5 and (b) AR = 6.

at the sidewalls of the structure closer to the top is small as it is defined by the energy of electrons reaching the sidewalls.

The influence of the aspect ratio on the electric field vectors on the profile surface is depicted in Figure 7. It is obvious that the field stimulate notch creation by directing the ions toward sidewalls, as it is explained in Reference [8]. At the very top, the field accelerate the ions

downward, but it quickly changes direction at the lower positions of the profile. The zero field border height is determined by the etching plasma parameters.

4. CONCLUSIONS

As one of the crucial aspect of the modern technologies, plasma processing plays a significant role in fabrication of integrated circuits (IC) and consequently in electronics and consumer goods in general. Damage to ICs during manufacturing as a result of charging of the dielectrics during finalization of interconnects is both reducing the profitability and reducing the ability to reach large sizes of microchips and make complex system integration on a single chip. Therefore, realistic three-dimensional etching profile simulations are needed, although still lacking. It is understandable that realistic calculations should involve complex surface reactions set, the effects of the profile charging, polymer deposition, as well as better statistic (greater number of particles) in the Monte Carlo step of the calculations, which is usually limited by the available computational resources. Emphasis should be placed on etching rates, uniformity, anisotropy, selectivity, and critical dimension control. In this paper, we have presented 3D simulation results for the profile evolution during ion-enhanced etch process as well as potential on profile and the electric fields for different aspect ratio values. The electron shading effect and the resultant charging damage to the structure begin to be significant in etched features having an aspect ratio greater than about 2. The electron shading effect gets worse as the aspect ratio increases, since the electron accumulation near the opening and top sidewalls of the feature makes it increasingly difficult for anything but the positively charged high-energy species to get past that entrance and any distance down into the deepening etched features that arrive at the wafer surface.

ACKNOWLEDGEMENTS

The present work has been supported by project 141025 financed by the Ministry of Science and Environmental Protection.

REFERENCES

1. Rogers BR, Cale TS. Plasma processes in microelectronic device manufacturing. *Vacuum* 2002; **65**:267–279.
2. Lieberman MA, Lichtenberg AJ. *Principles of Plasma Discharge and Materials Processing*. Wiley: New York, 1994.
3. Makabe T, Petrovic ZLJ. *Plasma Electronics: Applications in Microelectronic Device Fabrication*. Taylor and Francis, CRC Press: New York, 2006.
4. Armstrong NP, Maleham J. A two-stage solution to the anisotropic polysilicon etching problem. *Vacuum* 1983; **33**:291–294.
5. Kassing R, Rangelow IW. Etching processes for High Aspect Ratio Micro Systems Technology (HARMST). *Microsystem Technologies* 1996; **3**:20–27.
6. Hashimoto K. Charge damage caused by electron shading effect. *Japanese Journal of Applied Physics* 1994; **33**:6013–6018.
7. Cismaru C, Shohet JL, McVittie JP. Synchrotron radiation-induced surface-conductivity of SiO₂ for modification of plasma charging. *Applied Physics Letters* 2000; **76**:2191–2193.
8. Radjenović B, Radmilović-Radjenović M, Petrović ZLJ. Dynamic of the profile charging during SiO₂ etching in plasma for high aspect ratios trenches. *IEEE Transactions on Plasma Science* 2008; **36**:874–875.
9. Zhang D, Kushner MJ. Surface kinetics and plasma equipment model for Si etching by fluorocarbon plasmas. *Journal of Applied Physics* 2000; **87**:1060.
10. Radjenovic B, Radmilović-Radjenović M. Level set simulations of 3D etching profile evolution in the anisotropic wet etching of silicon. *Thin Solid Films* 2009; **517**:4233.
11. Petrović ZLJ, Dujko S, Marić D, Malović G, Nikitović Ž, Šašić O, Jovanović J, Stojanović V, Radmilović-Radjenović M. Measurement and interpretation of swarm parameters and their application in plasma modeling. *Journal of Physics D: Applied Physics* 2009; **42**:194002 (33pp).
12. Sethian J. *Level Set Methods and Fast Arching Methods: Evolving Interfaces in Computational Geometry, Fluid Mechanics, Computer Vision and Materials Sciences*. Cambridge University Press: Cambridge, UK, 1998.
13. Osher S, Fedkiw R. *Level Set Method and Dynamic Implicit Surfaces*. Springer: Berlin, 2002.
14. Yoshida Y, Watanabe T. Gate breakdown phenomena during reactive ion etching process. *Proceedings of the Symposium on Dry Process*, Tokyo, 1983; 4.
15. Radjenović B, Radmilović-Radjenović M, Petrović ZLJ. Influence of charging on SiO₂ etching profile evolution etched by fluorocarbon plasmas. *Material Science Forum* 2007; **555**:53–58.

16. Palov AP, Mankelevich YuA, Rakhimova TV, Shamiryan D. Charging and the secondary electron–electron emission on a trench surface: broadening and shift of ion energy spectrum at plasma trench etching. *Journal of Physics D: Applied Physics* 2010; **43**:075203.
17. Matsui J, Maeshige K, Makabe T. Effect of aspect ratio on topographic dependent charging in oxide etching. *Journal of Physics D: Applied Physics* 2001; **34**:2950–2955.
18. Makabe T, Maeshige K. Vertically integrated computer-aided design for device processing. *Applied Surface Science* 2002; 176–200.
19. Whitaker R. A level-set approach to 3D reconstruction from range data. *The International Journal of Computer Vision* 1998; **29**:203–231.
20. Radjenović B, Lee JK, Radmilović-Radjenović M. Sparse field level set method for non-convex Hamiltonians in 3D plasma etching profile simulations. *Computer Physics Communications* 2006; **174**:127–132.
21. Birdsall CK. Particle-in-cell charged-particle simulations, plus Monte Carlo collisions with neutral atoms. *IEEE Transactions on Plasma Science* 1991; **19**:65–85.
22. Verboncoeur JP, Alves MV, Vahedi V, Birdsall CK. Simultaneous potential and circuit solution for 1d bounded plasma particle simulation codes. *Journal of Computational Physics* 1993; **104**:321–328.
23. Kim HC, Iza F, Yang SS, Radmilović-Radjenović M, Lee JK. Particle and fluid simulations of low-temperature plasma discharge: benchmarks and kinetic effects. *Journal of Physics D: Applied Physics* 2005; **38**:R283–R301.
24. La Magna A, Garozzo G. Factors affecting profile evolution in plasma etching of SiO₂—modeling and experimental verification. *Journal of Electrochemical Society* 2003; **150**:F178–F185.
25. Hwang GS, Anderson C, Gordon M, Moore T, Minton T, Giapis K. Gas-surface dynamics and profile evolution during etching of silicon. *Physical Review Letters* 1996; **77**:3049–3052.
26. Geuzaine C. High order hybrid finite element schemes for Maxwell's equations taking thin structures and global quantities into account. *Ph.D. Thesis*, Universite de Liege, 2001.
27. GetDP. Available from: <http://www.geuz.org/getdp>.
28. TetGen. Available from: <http://tetgen.berlios.de>.

AUTHORS' BIOGRAPHIES



Dr Marija Radmilovic-Radjenovic obtained her MSc and PhD degrees at the Faculty of Physics, University of Belgrade. Dr Radmilovic-Radjenovic has been employed at the Institute of Physics, University of Belgrade as research professor. She is the leader of the subproject: Physical bases for application of non-equilibrium plasmas in nanotechnology and the treatment of materials. She was a general secretary of the organizing committee of the 5th EU-Japan Workshop on Plasma Processing. She has published more than 50 papers in refereed journals and her interests include plasma etching, nanotechnology, micro discharges, rf plasma modeling and gas breakdown studies. She has been cited more than 200 times in leading international journals.



Dr Branislav Radjenović obtained his BEng, MSc and PhD degrees at the Faculty of Electrical Engineering, University of Belgrade (1990). Dr Radjenović has been employed at the Institute of Physics, University of Belgrade as research professor. Dr Radjenović was also elected as associate professor in 2002 at the Military and Technical Academy in Belgrade. He has published more than 40 papers in refereed journals and his interests include plasma etching profile simulation and development of the simulation package for 3D profile evolution based on the level set method.



Marija Savić is a PhD student who obtained her BEng and MSc degrees at the Faculty of Electrical Engineering. Marija Savić has been employed at the Institute of Physics, University of Belgrade as research assistant. She has published 3 papers in refereed journals and her interests include rf plasma modeling and gas breakdown studies.

UTICAJ SEKUNDARNE EMISIJE ELEKTRONA NA KARAKTERISTIKE RADIO-FREKVENTNIH PLAZMI

U ovom radu proučavan je uticaj sekundarne emisije elektrona na karakteristike radio-frekventnih (rf) plazmi. Korišćenjem jednodimenzionalnog PIC/MCC (Particle in Cell with Implemented Monte Carlo Collisions) koda modelovan je kapacitivno spregnuti plazma reaktor, napajan pomoću dva rf generatora na različitim frekvencijama. Sekundarna emisija elektrona je jedan od ključnih procesa, kako sam po sebi tako i zbog uticaja na karakteristike pražnjenja. Sekundarna emisija elektrona sa površina modelovana je pomoću izraza koji su predložili Phelps i Petrović (Plasma Sources Sci. Technol. 8 (1999) R21–R44) za tretirane i netretirane metalne površine. Pokazano je da su karakteristike plazme u velikoj meri zavisne od uslova na površinama elektroda.

Nauka o materijalima nalazi se u žiži savremenog naučno-tehnološkog progressa. U širokom dijapazonu naučnih i inženjerskih disciplina za sintezu novih materijala, nalazi se i upotreba neravnotežne plazme, kao jedan od ključnih postupaka u razvoju široke klase novih materijala. Naročito značajna u razvoju mikro i nano elektronske industrije, upotreba neravnotežnih plazmi predstavlja nezamenljiv tehnološki proces za nagrizanje dielektričnih interkonekt slojeva visokog odnosa dubine i širine [1–3]. Uzimajući u obzir da ovi koraci predstavljaju oko 80% aktivnosti u proizvodnji integrisanih kola, neravnotežnim plazmama se posvećuje velika pažnja u istraživanjima koja, u skorije vreme, obuhvataju sve veći broj novih tehnika. Zahvaljujući razvoju brzih računara, računarske simulacije su postale veoma popularna i pouzdana istraživačka tehnika, koja trenutno ima veliki udeo u istraživanju nanotehnologije [4–8].

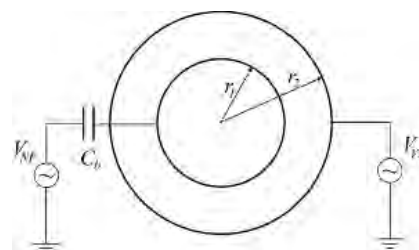
U ovom radu, naročitu pažnju smo posvetili modelovanju procesa sekundarne emisije elektrona kod kapacitivno spregnutog reaktora cilindrične geometrije, korišćenjem jedno-dimenzionalnog PIC/MCC (eng. *Particle in Cell with Implemented Monte Carlo Collisions*) koda [9–11].

Premda je uloga sekundarnih elektrona u procesima električnog proboja u gasovima kod niskostrujnih stacionarnih pražnjenja tematika koja datira još sa početka XX veka, svi njeni aspekti još uvek nisu u potpunosti izučeni. U skorije vreme, uticaj sekundarne emisije elektrona na karakteristike plazmi se ponovo nalazi u žiži interesovanja, pre svega zbog njihove uloge u fundamentalnim istraživanjima i zbog niza industrijskih aplikacija [12–16].

Do sada, modelovanje plazma reaktora je podrazumevalo uključivanje i procesa sekundarne emisije elektrona pretpostavljajući da je prinos sekundarnih elektrona konstantan, što je u velikoj meri prouzrokovalo

značajna odstupanja rezultata modelovanja od eksperimentalno dobijenih podataka. U ovom radu, modelovanje je ostvareno koristeći realne modele za prinos sekundarnih elektrona u argonu, koristeći izraze preuzete iz rada Phelps-a i Petrovića [12].

Simulirani asimetrični dvo-frekventni kapacitivno spregnuti reaktor (slika 1), predstavlja vrstu reaktora koji se najčešće koriste u praksi zbog niza pogodnosti. Povoljna karakteristika dvo-frekventnih reaktora se sastoji u mogućnosti da se proizvodnja plazme i energija jona kontrolišu različitim generatorima. Pod uslovom da je sprega između generatora mala, možemo postići selektivnu kontrolu procesa u plazmi. Za praksu je značajna kontrola jona koji udaraju površinu unutrašnje elektrode, odnosno kontrola onih jona koji se koriste u obradi materijala.



Slika 1. Shematski prikaz asimetričnog kapacitivno spregnutog reaktora sa dve frekvencije.

Figure 1. Schematic representation of the asymmetric dual-frequency capacitively coupled reactor.

U literaturi se može naći detaljno objašnjenje kako dolazi do formiranja napona na unutrašnjoj elektrodi usled ambipolarne difuzije čestica iz plazme. Ovde ćemo reći samo da se prednapon, ili jednosmerna komponenta naizmjeničnog napona, na unutrašnjoj elektrodi formira tako da se izjednače gubici jona i elektrona iz plazme. Prednapon unutrašnje elektrode utiče na srednju vrednost električnog polja u prielektrodnoj oblasti. Zbog brzo-promenljivog električnog polja u plazmi, koje ima srednju vrednost različitu od nule, joni kao znatno inertnije čestice od elektrona kreću se prateći srednju vrednost polja u vremenu. Srednja vrednost električnog polja u prielektrodnoj oblasti je odgovorna za ubrzanje

Autor za prepisku: A. Bojarov, Institut za fiziku, Centar za neravnotežne procese, Pregrevica 118, 11080 Zemun, Srbija.

E-pošta: bojarov@mail.ipb.ac.rs

Rad primljen: 10. avgust 2010.

Rad prihvaćen: 28. oktobar 2010.

jona, a samim tim utiče i na energiju jona koji bombarduju unutrašnju elektrodu i emituju sekundarne elektrone.

U simulacijama, interesovao nas je, pre svega, uticaj sekundarne emisije na karakteristike plazme. Karakteristike od posebnog interesa su koncentracija plazme, fluks i raspodela energije jona koji dospevaju do elektroda (eng. *Ion Energy Distribution Function*, IEDF), s obzirom da koeficijent sekundarne emisije elektrona zavisi od energije jona koji udaraju u neku od elektroda.

Za metalne elektrode uzeli smo koeficijente sekundarne emisije prema izrazima Phelps-a i Petrovića za nekoliko slučajeva različito tretiranih elektroda. U osnovi su nam dve glavne postavke reaktora: a) kada je unutrašnja elektroda čista i spoljašnja neočišćena (skraćeno čista–neočišćena reaktor) i b) kada je unutrašnja neočišćena i spoljašnja čista elektroda (skraćeno neočišćena–čista reaktor). Pored ove dve postavke, simulirali smo i kombinaciju elektroda kada nema sekundarne emisije na unutrašnjoj, dok je na spoljašnjoj elektrodi koeficijent sekundarne emisije $\gamma = 0,2$ (skraćeno 0-0.2 reaktor) i kada na obe elektrode nema sekundarne emisije (skraćeno 0-0 reaktor).

Pražnjenje u gasu spada u domen plazme niskog pritiska, neutralni gas je na pritisku od 20 Pa. Unutrašnji poluprečnik reaktora je 0,03 m, dok je spoljašnji poluprečnik 0,0519 m. Generator više frekvencije je na 28 MHz, amplitude 2000 V i vezan je za spoljašnju (veću) elektrodu, dok je generator niže frekvencije na 2 MHz, amplitude 500 V i vezan je za unutrašnju (manju) elektrodu. Kapacitivnost kondenzatora je direktno povezana sa geometrijom reaktora i vrednost od 100 pF je usklađena sa brojem naelektrisanih čestica koji pune kondenzator, odnosno sa padom potencijala u prielektrodnoj oblasti.

Sekundarna emisija elektrona sa elektroda

Jedna od najznačajnijih pojava koja je ponovo postala aktuelna u poslednje vreme je sekundarna emisija elektrona sa elektroda, koja je posledica udara različitih čestica o površinu elektrode. Za održavanje pražnjenja u gasovima neophodna je proizvodnja sekundarnih elektrona koji treba da zamene elektrone izgubljene na površinama elektroda i na zidovima reaktora. Uslov za sam čin proboja je da sekundarna lavina postane jednaka primarnoj, odnosno da se ukupna proizvodnja elektrona u kružnom toku primarne lavine, povratne sprege i sekundarne lavine izjednači sa gubicima elektrona na anodi. Pod pojmom sekundarne lavine podrazumevamo sve lavine koje nastaju iza prve i to, što posebno ističemo, usled udara jona o površine elektroda.

Procese sekundarne emisije elektrona sa površine izazvane različitim vrstama čestica, opisujemo prinosom sekundarnih elektrona γ koji, u znatnoj meri, zavisi od stanja površine i upadne energije čestica. Kada se joni i atomi sudare sa čistom površinom može se desiti neko-

liko vrsta procesa, ali je najvažniji izbacivanje elektrona sa površine. Ovaj proces direktno utiče na tok električnih pražnjenja obezbeđujući i mehanizam povratne sprege neophodne da se održava pražnjenje u gasovima. Sekundarnu emisiju elektrona uzrokuju četiri osnovna procesa:

- fotoelektronska emisija,
- emisija kao posledica sudara metastabila sa površinom,
- potencijalna emisija u sudarima jona sa površinom i
- kinetička emisija u sudarima jona i atoma sa površinom.

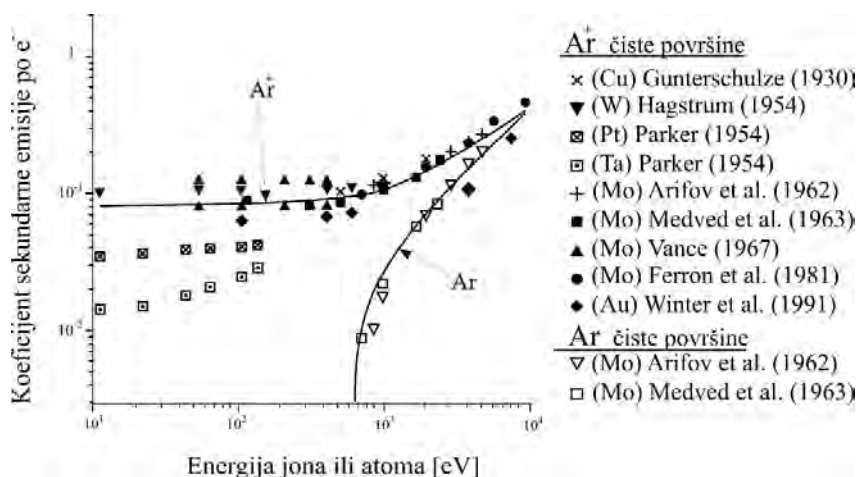
Sva četiri navedena procesa su moguća kod pražnjenja u argonu i međusobno su povezana. Ostali važni procesi na površinama uključuju: sudarno gašenje metastabila (što je povezano sa drugim procesom) i procese refleksije elektrona, jona i neutrala sa površina.

Najpre ćemo dati kratak pregled postojećih rezultata za prinos sekundarnih elektrona izazvanih delovanjem jona na tzv. čiste i neočišćene površine elektroda. Pod pojmom čiste elektrode podrazumeva se elektroda koja je tretirana zagrevanjem njene površine na temperaturi od oko 2000 K u uslovima dobrog vakuuma, dok se sama merenja koeficijenta sekundarne emisije elektrona vrše na sobnoj temperaturi u veoma visokom vakuumu. Ponekad se proces čišćenja katode ostvaruje i skidanjem njenog površinskog sloja jonskim spaterovanjem.

Neočišćene površine elektroda predstavljaju površine obrađene u radionici standardnim mehaničkim i hemijskim tehnikama koje, potom, bivaju izložene atmosferskom gasu što može rezultirati oksidacijom ili nekim drugim kontaminirajućem procesom u procesu pumpanja do relativno niskog vakuuma, kao što je depozicija para iz pumpe. Stabilni oksidni slojevi se na ovaj način ne mogu očistiti, čak ni u slučaju plemenitih metala kao što je zlato.

Na slici 2 prikazani su eksperimentalni rezultati za prinos sekundarnih elektrona za snopove Ar^+ jona i Ar atoma koji padaju na različite čiste metalne površine u zavisnosti od njihove upadne energije. Slika je preuzeta iz rada Phelps-a i Petrovića [12] i obuhvata sve pronađene podatke za energije ispod 1 keV.

Za većinu katodnih površina koeficijent sekundarne emisije elektrona po jonu gotovo da ne zavisi od upadne energije jona u opsegu jonskih energija ispod 500 eV. Ova nezavisnost od energije se pripisuje Augere-ovom procesu koji se naziva potencijalno izbacivanje elektrona. Oblast zavisnosti koeficijenta sekundarne emisije od upadne energije jona na energijama od nekoliko keV pripisuje se kinetičkom izbacivanju, premda priroda ovog procesa još uvek nije sasvim razjašnjena. Granica na kojoj nastaje kinetičko izbacivanje je određena procesima multielektronske emisije elektrona



Slika 2. Energijska zavisnost prinosa sekundarnih elektrona kada snopovi Ar⁺ jona i Ar atoma padaju na različite čiste katodne površine. Puni simboli predstavljaju rezultate različitih autora za Ar⁺ jone, dok otvoreni simboli odgovaraju rezultatima za Ar jone. Figure 2. Energy dependence of the secondary electron yield for Ar⁺ ions and Ar atoms hitting clean surfaces of different materials. Full symbols represent results from various authors for Ar⁺ ions and open symbols correspond to Ar atoms.

sa površine katode. Možemo smatrati da je za većinu metala koeficijent sekundarne emisije elektrona po jonu približno jednak 0,1 za energije ispod 1 keV.

Na slici 3 prikazani su eksperimentalni rezultati za γ_i koeficijente u slučaju Ar⁺ jona, kao i za γ_a koeficijente u slučaju Ar atoma koji padaju na metalne površine izložene u različitom stepenu kiseoniku, vodi, okolnom gasu ili koje su na nespecificiran način kontaminirane. Podaci sa slike pokazuju da su na nižim energijama (<150 eV) vrednosti koeficijenta γ_i za Ar veoma rasute (više od jednog reda veličine). Većina ovih podataka za Ar ukazuje na slabu energijsku zavisnost koeficijenta od jonske energije.

U našim PIC/MCC proračunima koristili smo izraze preuzete iz rada Phelps i Petrović [12] za prinos

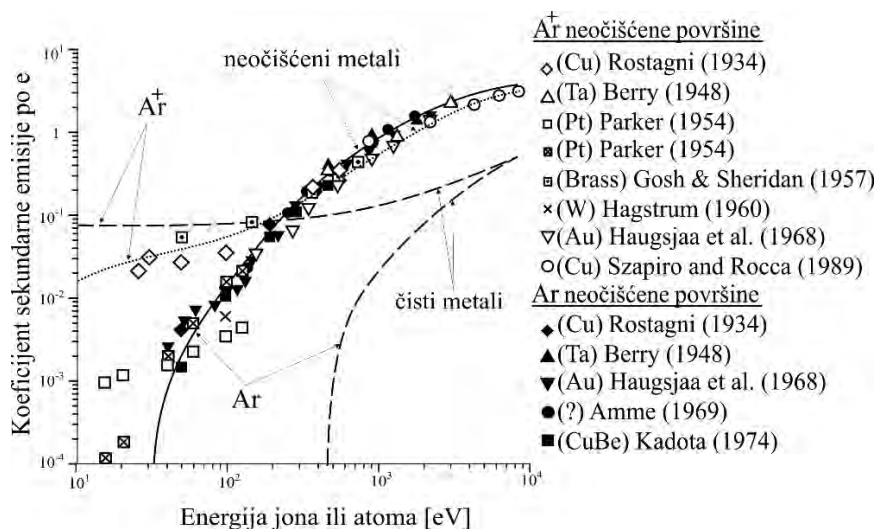
sekundarnih elektrona koje su predstavljene na slici 3. Analitički izrazi za zavisnost koeficijenta sekundarne emisije, γ_i , od energije jona, ϵ_i , su:

– Za čiste površine, Phelps i Petrović [12]:

$$\gamma_i^c = 0,07 + \frac{1 \times 10^{-5} (\epsilon_i - 500)^{1,2}}{1 + \left(\frac{\epsilon_i}{7000}\right)^{0,7}} \quad (1)$$

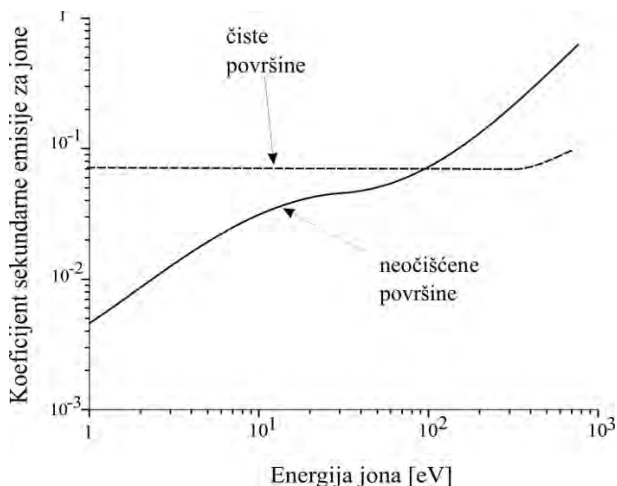
– Za neočišćene površine, Phelps i Petrović [12]:

$$\gamma_i^d = \frac{0,006\epsilon_i}{1 + \left(\frac{\epsilon_i}{10}\right)^{1,5}} + \frac{1,05 \times 10^{-4} (\epsilon_i - 80)}{1 + \left(\frac{\epsilon_i}{8000}\right)^{1,5}} \quad (2)$$



Slika 3. Energijska zavisnost prinosa sekundarnih elektrona kada snopovi Ar⁺ jona i Ar atoma padaju na različite neočišćene katodne površine. Puni simboli predstavljaju rezultate različitih autora za Ar⁺ jone, dok otvoreni simboli korespondiraju rezultatima za Ar jone. Figure 3. Energy dependence of the secondary electron yield for Ar⁺ ions and Ar atoms hitting dirty surfaces of different materials. Full symbols represent results from various authors for Ar⁺ ions and open symbols correspond to Ar atoms.

Prinos drugog sabirka u svakom od izraza (1) i (2) jednak je nuli za energije incidentnih jona ispod 500 eV i 80 eV, za čiste i neočišćene površine redom. Na slici 4 date su krive koje odgovaraju izrazima za koeficijent sekundarne emisije.



Slika 4. Koeficijent sekundarne emisije elektrona u zavisnosti od energije čestice za snopove Ar^+ jona koji padaju na različito tretirane površine. Obe krive su nacrtane koristeći izraze (1) i (2).

Figure 4. Coefficient of secondary electron emission induced by Ar^+ ions hitting differently treated surfaces. Curves represent graphs of the relations (1) and (2).

Opravdanost rezultata simulacije

Pre pretstavljanja samih rezultata simulacije, dajemo kratak kvantitativni uvid u same parametre simulacije kako bi utvrdili da ne postoje velika odstupanja koja bi eventualno mogao da unese sam PIC/MCC kod. Osnovni zahtev koji treba da zadovolji PIC tehnika jeste dobra prostorna rezolucija pojedinih ćelija, kako bi se razlučile sve karakteristične dužine koje se javljaju u gasnim pražnjenjima. Jedna od najmanjih karakterističnih dužina je svakako Debay-eva dužina termalnih elektrona u središnjem delu pražnjenja (balku), koja je u rf gasnim pražnjenjima reda $\lambda_D \approx 10^{-4}$ m. Prostor pražnjenja izdelažen je na 2000 ćelija, odnosno ćelijama dužine $\Delta x = 1,095 \times 10^{-5}$ m, što omogućava dobro razlaganje dužine λ_D . Ovim se minimizuje odstupanje izazvano aproksimacijom konačnih elemenata s obzirom da je zadovoljen uslov:

$$\frac{\Delta x}{\lambda_D} \approx 0,11 < 1 \quad (3)$$

Takođe, vrlo važan parametar simulacije je vremenski korak, Δt , za koji je uzeto da je 1/5000 periode generatora od 28 MHz, odnosno $\Delta t = 7,142857 \times 10^{-12}$ s. Time je postignuto razlučivanje brzine čestica do:

$$\Delta x / \Delta t \approx 1,533 \times 10^{11} \text{ m/s} \quad (4)$$

što u potpunosti pokriva, čak i za više redova veličine, opseg energija svih čestica koje se javljaju u simulaciji.

Potrebno je da vremenski korak razluči i maksimalnu kolizionu frekvenciju na osnovu korišćenih preseka sudara [17]. Uzima se u obzir najgori slučaj, odnosno maksimalna vrednost totalnog preseka sudara, iz domena od važnosti, za jone $\sigma_{i_{\max}} \approx 1,80 \times 10^{-18} \text{ m}^2$ i elektrone $\sigma_{e_{\max}} \approx 1,25 \times 10^{-19} \text{ m}^2$, zatim energije jona na kojima je presek maksimalan (uzimamo što veće vrednosti) za jone $E_{i_{\max}} \approx 1000 \text{ eV}$ i za elektrone $E_{e_{\max}} \approx 100 \text{ eV}$. Pritisak neutralnog gasa argona je 20 Pa na temperaturi od 300 K. Izraz za kolizionu frekvenciju je:

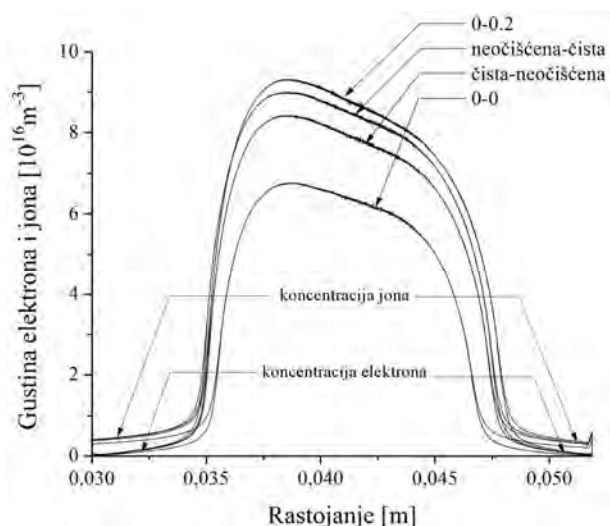
$$f = n_n \sigma \sqrt{\frac{2E}{m}} \quad (5)$$

gde se gustina neutralnog (pozadinskog) gasa, n_n , dobija iz zakona o gustini idealnog gasa, m je masa elektrona ili jona, σ i E su gore definisani totalni presek i energija čestice, redom. Ovim je frekvencija sudara za jone i elektrone $f_i \approx 1,91 \times 10^7 \text{ Hz}$ i $f_e \approx 3,58 \times 10^9 \text{ Hz}$, što opravdava korišćenje Monte Carlo tehnike sudara za dati vremenski korak, s obzirom da je frekvencija sudara u najgorem slučaju nekoliko redova veličine niža od vrednosti $1/\Delta t$.

Koncentracija plazme

Jedna od osnovnih karakteristika svakog pražnjenja jeste koncentracija naelektrisanih čestica u gasu, odnosno njihova raspodela u prostoru pražnjenja. Središnji deo pražnjenja sadrži većinu naelektrisanih čestica koje su kvazineutralnoj ravnoteži, odnosno koncentracije jona i elektrona su skoro identične, kao što se može videti sa slike 5. Prielektrodne oblasti sadrže vrlo mali broj naelektrisanih čestica, međutim, zbog toga što postoji neravnoteža u koncentraciji jona i elektrona (slika 5), one utiču gradijentom polja na ubrzanje jona ka elektrodama i time direktno utiču i na procese na površinama. Profil plazme dostiže svoj ustaljeni oblik nakon samo nekoliko mikrosekundi, a zatim se koncentracija čestica samo povećava, bez velikih odstupanja od uspostavljenog profila.

Na slici 5, na kojoj su date usrednjene vrednosti koncentracija čestica u vremenu, može se primetiti uticaj koji sekundarna emisija ima na apsolutnu koncentraciju elektrona i jona u plazmi. Najuočljivija je razlika između krive dobijene za sistem bez sekundarne emisije (0-0) i krivih za sistem sa sekundarnom emisijom. Osnovan zaključak je da se za precizan opis profila plazme mora u model pražnjenja uključiti sekundarna emisija elektrona od strane jona. Međutim, kao što se može zaključiti sa slike 5, odnosno iz razlike krivih za $\gamma = 0,2$ i $\gamma = \gamma(\varepsilon)$ ($\gamma(\varepsilon)$ odgovara slučajevima čista-neočišćena i neočišćena-čista), nije dovoljno samo da postoji koeficijent sekundarne emisije za jone, već on mora da bude konzistentan sa realnim fizičkim procesima.



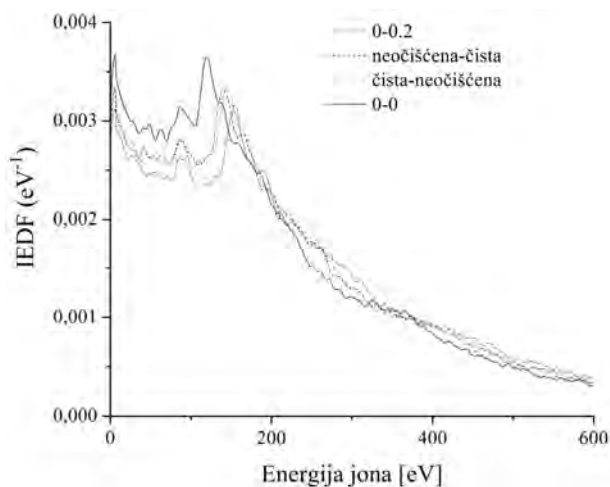
Slika 5. Koncentracija jona i elektrona za četiri konstrukcije reaktora sa različito tretiranim elektrodama, nakon proteklih 5 μ s simulacionog vremena.

Figure 5. Ion and electron concentrations for four reactor constructions with differently treated electrodes, after 5 μ s of simulated time.

Raspodela energije jona na elektrodama

Sledeća važna karakteristika plazme, naročito za praksu, jeste raspodela energije jona (IEDF) na unutrašnjoj elektrodi. Uzimajući u obzir da se dvo-frekventni kapacitivno spregnuti reaktori najčešće koriste zapravo zbog energetskih jona koji padaju na unutrašnjoj elektrodi, vrlo je važno precizno poznavanje raspodele energije jona u blizini elektroda.

Na slici 6 prikazane su krive raspodele za četiri ispitivana slučaja, gde se vidi razlika za različite koeficijente sekundarne emisije. Zavisnost IEDF-a od sekundarne emisije je složena, zbog toga što veza između ova dva parametra ima oblik povratne sprege. Pored ovoga,



Slika 6. Raspodela jona po energijama koji padaju na unutrašnju elektrodu.

Figure 6. Ion energy distributions on the inner electrode.

koncentracija plazme koja je takođe zavisna od sekundarne emisije, utiče na profil IEDF na unutrašnju elektrodu.

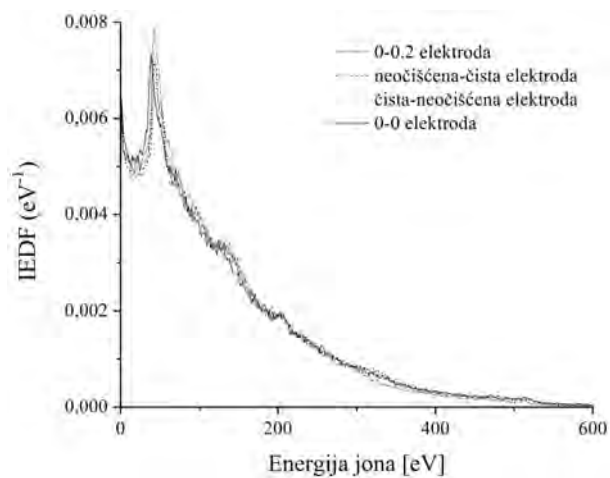
Sa slike 7 vidi se da je uticaj sekundarne emisije na raspodelu energije jona koji dospevaju na spoljašnju elektrodu, relativno mali. Relativno velike razlike u koeficijentu za spoljašnju elektrodu (od 0 do 0,2) ne unose bitne promene u raspodeli energije jona, što znači da će pri istim uslovima više elektrona nastati iz površine sa većim koeficijentom sekundarne emisije.

Dosadašnji rezultati nas mogu dovesti do zaključka da zbog razlike u gustini plazme i IEDF-a na unutrašnju elektrodu (slika 6) sekundarna emisija sa elektroda ima veliki uticaj na raspodelu energije jona na unutrašnju elektrodu, što je vrlo važan parametar kada se govori o primeni rf plazme u obradi materijala.

Potencijal plazme

Potencijal plazme ima ulogu da zadrži elektrone u plazmi i da izazove da što veći broj jona napusti plazmu. S obzirom na to, potencijal plazme je uvek na većoj vrednosti od potencijala elektroda. U toku vremena potencijal plazme se menja, prateći uglavnom oscilacije nisko-frekventnog izvora, pri ovome dolazi i do promene pada potencijala u prielektrodnoj oblasti. Na slici 8 primećuje se da za realne postavke reaktora (čiste i neočišćene elektrode) nema razlike u prostornom potencijalu plazme. Drugim rečima, joni u reaktorima konfiguracije čista-neočišćena i neočišćena-čista elektroda padaju na unutrašnju i spoljašnju elektrodu pod istim uslovima. Naravno, ovo još više dovodi u prvi plan uticaj sekundarne emisije, jer i pri istim uslovima u plazmi promena koeficijenta sekundarne emisije dovodi do drastičnih promena karakteristike plazme (slike 5 i 6).

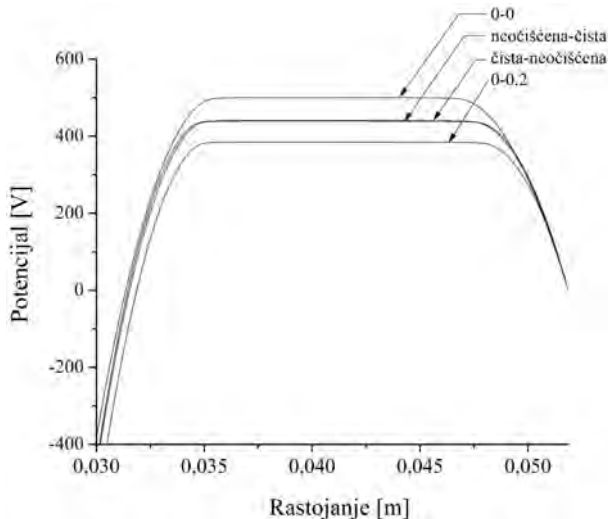
Napomena je da ovi zaključci važe u slučaju realnog modelovanja sekundarne emisije prema izrazima Phelps-a i Petrovića, gde koeficijent sekundarne emisije



Slika 7. Raspodela jona po energijama koji dospevaju na spoljašnju elektrodu.

Figure 7. Ion energy distributions on the outer electrode.

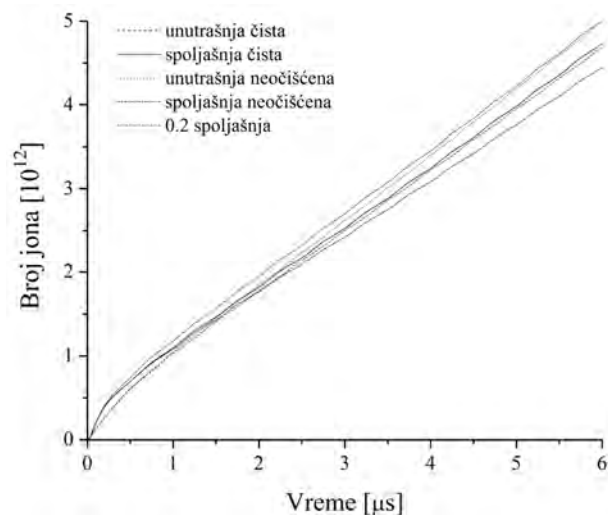
zavisi od energije jona. Sa slike 8 može se zaključiti da nerealni modeli sekundarne emisije drastično menjaju sliku procesa u pražnjenju, što se vidi iz razlike prostornog potencijala za elektrode sa konstantnom sekundarnom emisijom.



Slika 8. Prostorni potencijal u plazmi usrednjen po vremenu.
Figure 8. Time averaged plasma potential.

Efektivni γ koeficijenti

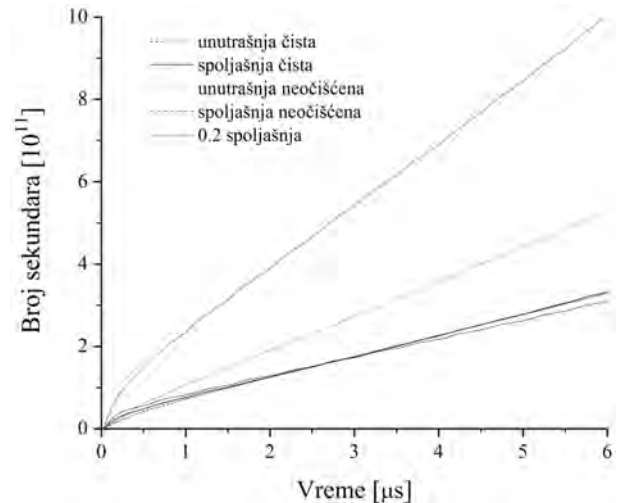
U ovom odeljku, cilj je da se pokaže kako može da se predstavi koeficijent sekundarne emisije njegovom efektivnom vrednošću, na osnovu simulacionih rezultata za fluks jona (slika 9) i fluks sekundarnih elektrona (slika 10).



Slika 9. Broj jona koji je pao na nekoj od elektroda u toku vremena.
Figure 9. Number of ions that have fallen on the electrodes.

Po definiciji, koeficijent sekundarne emisije predstavlja verovatnoća da jon proizvede sekundarni elektron. Drugim rečima, odnos između broja sekundarnih

elektrona koji nastaje na elektrodi i broja jona koji nastane na njoj jednak je koeficijentu sekundarne emisije. Koristeći ovu činjenicu, možemo na osnovu flukseva jona i sekundarnih elektrona da izračunamo efektivni γ koeficijent, odnosno vrednost konstantnog γ koeficijenta koji bi u toku vremena dao isti broj sekundarnih jona kao i sekundarna emisija zavisna od energije.



Slika 10. Broj sekundarnih elektrona emitovanih sa nekoj od elektroda u toku vremena.
Figure 10. Number of secondary electrons that have been emitted from the electrodes.

Na osnovu koeficijenata pravih, odnosno flukseva jona i sekundarnih elektrona (slike 9 i 10), možemo napisati izraz iz kojeg se može naći efektivna vrednost sekundarne emisije:

$$\gamma_{\text{eff}} = \frac{\alpha_s}{\alpha_i} \quad (6)$$

gde su α_s fluks sekundarnih elektrona sa površine, α_i fluks jona na površini i γ_{eff} efektivni koeficijent sekundarne emisije. Za različite slučajeve imamo:

$$\text{- spoljašnja 0,2: } \gamma_{\text{eff}} = \frac{1,111 \times 10^6}{5,556 \times 10^6} \approx 0,2$$

$$\text{- spoljašnja neočišćena: } \gamma_{\text{eff}} = \frac{3,310 \times 10^5}{4,882 \times 10^6} \approx 0,0678$$

$$\text{- unutrašnja neočišćena: } \gamma_{\text{eff}} = \frac{6,077 \times 10^5}{5,700 \times 10^6} = 0,1066$$

$$\text{- spoljašnja čista: } \gamma_{\text{eff}} = \frac{3,692 \times 10^5}{3,250 \times 10^6} \approx 0,1136$$

$$\text{- unutrašnja čista: } \gamma_{\text{eff}} = \frac{3,731 \times 10^5}{5,306 \times 10^6} \approx 0,0703$$

Iz dobijenih rezultata možemo izvesti zaključak koja je površina elektroda najefikasnija u proizvodnji sekundarnih elektrona, pored konstantne 0,2 površine,

koju smo uzeli kao primer. Najveći koeficijent sekundarne emisije imaju unutrašnja neočišćena i spoljašnja čista elektroda, što znači da će ova konstrukcija reaktora biti najefikasnija u proizvodnju sekundarnih elektrona, kao što smo već i utvrdili (slika 5).

Važno je napomenuti da date efektivne sekundarne emisije važe samo za dati reaktor, sa parametrima koje smo naveli na početku. Za svaku drugu simulacionu postavku, menjaće se i efektivne sekundarne emisije. Odatle se može videti značaj ove simulacije, kao i računarskih simulacija uopšte, s obzirom da smo uspeli da dobijemo vrednosti efektivne sekundarne emisije na osnovu preciznih fizičkih modela koji se mogu koristiti u praksi.

ZAKLJUČAK

Istraživali smo uticaj sekundarne emisije elektrona različito tretiranih površina na karakteristike dvo-frekventnih kapacitivno spregnutih pražnjenja. Osnovni motiv ovog istraživanja je velika praktična primena dvo-frekventnih plazmi u industriji, kao i potreba preciznog opisivanja sekundarne emisije sa površina, uzimajući u obzir da se upravo u praksi ovaj tip plazmi najčešće koriste za plazma-nagrizanje dielektrika.

Rezultate do kojih smo došli govore nam da za precizan opis plazme moramo da uzmemo u obzir sekundarnu emisiju elektrona koja zavisi od energije jona koji vrše jonizaciju. Precizan model sekundarne emisije su dali Phelps i Petrović, na osnovu kojeg smo u ovom radu modelovali interakciju jona sa površinama elektroda na kojima dolazi do sekundarne emisije. Pokazali smo na osnovu rezultata simulacije da gustina plazme zavisi od sekundarne emisije i to tako što se njena vrednost u centru pražnjenja drastično povećava sa porastom γ koeficijentata. Raspodela energija jona na unutrašnjoj elektrodi je, takođe, pokazala zavisnost od koeficijenta sekundarne emisije, dok smo sa druge strane pokazali da to ne važi za raspodelu energije jona na spoljašnjoj elektrodi. Zaključili smo da potencijal plazme zavisi od sekundarne emisije sa obe elektrode, tako što je za realne površine pokazivao male razlike ukazujući na to da postoje procesi koji dovode do kompenzacije efekata sekundarne emisije za različite konfiguracije reaktora.

Svakako, najvažnije je to što smo uspeli da pomoću simulacije dobijemo efektivne koeficijente sekundarne

emisije, koji se mogu koristiti u praksi za jednostavnije opisivanje simuliranih plazma-reaktora, pri tom zadržavajući precizni model sekundarne emisije. Značaj dobijenih rezultata opravdava korišćenje simulacionih modela za dobijanje podataka, koji su korisni u praksi i koji smanjuju vremenske i materijalne troškove eksperimentalnih postupaka.

LITERATURA

- [1] J.M.A. Liberman, A.J. Lichtenberg, Plasma Discharges and Materials Processing, Wiley, New York, 1994.
- [2] T. Makabe, Z.Lj. Petrović, Plasma Electronics: Applications in Microelectronic Device Fabrication, Taylor & Francis, New York, 2006.
- [3] Z.Lj. Petrović, B. Radjenović, M. Radmilović-Radjenović, Proceedings of 26th International Conference on Microelectronics, MIEL, Niš, Serbia, 2008, p. 19.
- [4] M. Radmilović-Radjenović, J.K. Lee, Phys. Plasmas **12** (2005) 063501–063508.
- [5] A. Bojarov, M. Radmilović-Radjenović Z.Lj. Petrović, 24th Summer School and International SPIG, Contributed Papers, p. 387.
- [6] M. Radmilović-Radjenović, B. Radjenović, Plasma Sources Sci. Technol. **15** (2006) 1–7.
- [7] A. Bojarov, M. Radmilović-Radjenović, Z.Lj. Petrović, Hem. Ind. **63** (2009) 233–238.
- [8] M. Radmilović-Radjenović B. Radjenović, Contrib. Plasm. Phys. **47** (2007) 165–172.
- [9] V. Vahedi M. Surendra, Comput. Phys. Commun. **87** (1995) 179–168.
- [10] C.K. Birdsall, IEEE Trans. Plasm. Sci. **19** (1991) 65–85.
- [11] J.P. Verboncoeur, Plasma Phys. Control. Fusion **47** (2005) A231–A260.
- [12] A.V. Phelps, Z.Lj. Petrović, Plasma Sources Sci. Technol. **8** (1999) 445–449.
- [13] J.K. Lee, N.Yu. Babaeva, H.C. Kim, O.V. Manuilenko, J.W. Shon, IEEE Trans. Plasma Sci. **32** (2004) 47–53.
- [14] M. Radmilović-Radjenović, Z.Lj. Petrović, Europ. J. Phys. D **54** (2009) 445–449.
- [15] M. Radmilović-Radjenović, Z.Lj. Petrović, B. Radjenović, J. Phys. Conf. Ser. **71** (2007) 012007, p. 19.
- [16] M. Radmilović-Radjenović, Z. Lj. Petrović, G.N. Malović, D. Marić, B. Radjenović, C. J. Phys. **56** (2006) B996–B1001.
- [17] A.V. Phelps, J. Phys. Chem. Ref. Data **20** (3) (1991) p. 557.

SUMMARY**INFLUENCE OF THE SECONDARY ELECTRON EMISSION ON THE CHARACTERISTICS OF RADIO FREQUENCY PLASMAS**

Aleksandar Bojarov, Marija Radmilović-Radjenović, Marija Savić

Institute of Physics, Belgrade, Serbia

(Scientific paper)

In this paper the influence of secondary emission on the characteristics of rf plasmas has been studied. An asymmetrical dual-frequency capacitively coupled plasma reactor has been modeled with one dimensional PIC/MCC (Particle in Cell with Implemented Monte Carlo Collisions) code. The main feature of the modeling code represents the realistic model of the ion-induced secondary electron emission. Secondary emission of electrons is one of the important processes that effects the characteristics of rf plasmas. For modeling the secondary yield per ion, we have used equations proposed by Phelps and Petrović (Plasma Sources Sci. Technol. **8** (1999) R21–R44) for differently treated metal surfaces. In the model, the energy dependence of the yields per ion for differently treated metal surfaces has been implemented. Results are compared for yields for the so called “dirty” and “clean” surfaces, and the spatial profiles of charged particles and ion energy distributions were observed. The simulation results indicate that the plasma characteristics are greatly affected by the ion-induced secondary emission, changing the overall parameters of dual-frequency capacitively coupled plasma reactors especially in applications as etching devices. Conclusion is that an exact model of the secondary electron emission should be included, as to ensure better agreement between simulation and experiment.

Ključne reči: Radio-frekventna pražnjenja • Računarske simulacije pražnjenja u gasovima • Sekundarna emisija

Key words: Radio frequency discharges • Computer simulations of gas discharges • Secondary emission of electrons

MARIJA B. SAVIĆ
MARIJA
RADMILOVIĆ-RAĐENOVIĆ

Institut za fiziku, Beograd, Srbija

NAUČNI RAD

UDK 537.565:621.3.032.21

DOI: 10.2298/HEMIND091221022S

MODELOVANJE PROBOJA U GASOVIMA NA NISKIM PRITISCIMA MONTE KARLO TEHNIKOM*

Osnovna pretpostavka Townsend-ove teorije da joni prouzrokuju emisiju sekundarnih elektrona sa katode važi u veoma uskom opsegu vrednosti redukovanog električnog polja E/N . U skladu sa revidiranim Townsend-ovom teorijom koju su koncipirali Phelps i Petrović, sekundarni elektroni nastaju usled udara jona, brzih neutrala, metastabila i fotona o katodu, ili jonizacijom atoma gasa brzim neutralima. U ovom radu smo pokušali da izgradimo model koji će omogućiti određivanje vrednosti za prinos sekundarnih elektrona za različite tipove čestica, korišćenjem Monte Karlo tehnike. Dobijeni rezultati su u saglasnosti sa analitičkim rezultatima Phelps-a i Petrovića (Plasma Sources Sci. Technol. 8 (1999) R1).

Pod terminom gasno pražnjenje podrazumevamo proticanje struje kroz gas. Gas, sam po sebi, predstavlja neprovodnu sredinu. Međutim, ukoliko u gasu postoje naelektrisane čestice, pod uticajem dovoljno jakog električnog polja, može doći do slabe provodnosti, ili čak do proboja u gasu. Gas se tada ponaša kao provodnik, koji omogućava proticanje električne struje uz malu otpornost.

Uticaj lavina sekundarnih elektrona u procesima električnog proboja u gasovima, kod niskostrujnih stacionarnih pražnjenja, dobro je izučen u velikom broju radova i udžbenika [1–3]. Uslov za sam čin proboja podrazumeva da sekundarna lavina elektrona postane jednaka primarnoj. Preciznije rečeno, proboj nastaje kada se ukupna proizvodnja elektrona u kružnom toku primarne lavine, povratne sprege i sekundarne lavine izjednači sa gubicima elektrona na anodi. Mi ćemo pod pojmom sekundarne lavine podrazumevati sve elektrone koji nastaju nakon primarne. Elektronska emisija sa površine katode indukovana pozitivnim jonima, brzim atomima, fotonima i metastabilnim atomima, sudarna jonizacija brzim jonima i atomima proizvedenim u ranijim lavinama, sudarna jonizacija elektronima koji su reflektovani sa anode i fotojonizacija gasa fotonima nastalim u ranijim lavinama predstavljaju osnovne procese nastajanja sekundarnih elektrona [4].

Osnovu modela koji su razvili Phelps i Petrović [4] čini uključivanje dodatnih mogućih izvora sekundarne emisije elektrona, kao i emisije nastale usled dejstva fotona, metastabila na katodu. Sekundarna emisija elektrona može nastati i usled jonizacije izazvane dejstvom neutrala u gasnoj fazi i dejstvom elektrona reflektovanih sa anode. Pored toga, razmatran je i efekat povratne difuzije elektrona na katodu. Samim tim, ovaj jedinstveni model, osim što predstavlja reviziju Townsend-ove teo-

rije, pruža detaljan opis procesa koji dovode do sekundarne emisije elektrona.

Jedna od egzaktnih tehnika koja se može koristiti za proučavanje sekundarne emisije elektrona sa elektrode je, svakako, Monte Karlo tehnika [5]. Za dobijanje rezultata, predstavljenih u ovom radu, korišćen je kompjuterski kod baziran na Monte Karlo metodu, razvijen u Institutu za fiziku [6]. Simulacije su izvršene, najpre za pražnjenje u argonu, koristeći dobro definisan set efektivnih preseka detaljnije opisanih u radu [5].

MODEL PHELPS–PETROVIĆ

Predstavljeni model je analitički aproksimativni model pomoću koga se mogu izvršiti proračuni stacionarnih flukseva različitih vrsta čestica: elektrona, Ar^+ , brzih Ar atoma, metastabila i rezonantnih fotona u prostorno uniformnom električnom polju.

Analizom do sada objavljenih rezultata, Phelps i Petrović su pokazali da prinos sekundarnih elektrona značajno zavisi od stanja površine katode. U tom smislu, razlikujemo površine koje su na neki način tretirane (recimo za materijale sa visokom tačkom ključanja zagrejane na 2000 K u vakuumu, dok se eksperimenti vrše na sobnoj temperaturi) i njih nazivamo čistim površinama. Osim njih, postoje i netretirane ili neočišćene površine, kod kojih je izvršen neki postupak čišćenja, ali ne zagrevanjem do visokih temperatura kao kod čistih površina.

Ovaj model nam omogućava da odredimo vrednosti prinosa sekundarnih elektrona sa katode indukovane jonima, brzim atomima, metastabilima ili fotonima, u zavisnosti od uslova na metalnoj površini, kao i od vrednosti redukovanog električnog polja. Parcijalni doprinos pojedinih čestica (fotona, jona, metastabila i atoma) sekundarnoj emisiji elektrona [4], prikazan je na slikama 1 i 2.

U ovom radu smo koristili izraze koje su predložili Phelps i Petrović [4], za koeficijente sekundarne emisije elektrona sa katode pri udaru atoma, jona i fotona o površinu katode za čiste (*eng. clean*), odnosno neočišćene (*eng. dirty*) površine, jednačine (1)–(6):

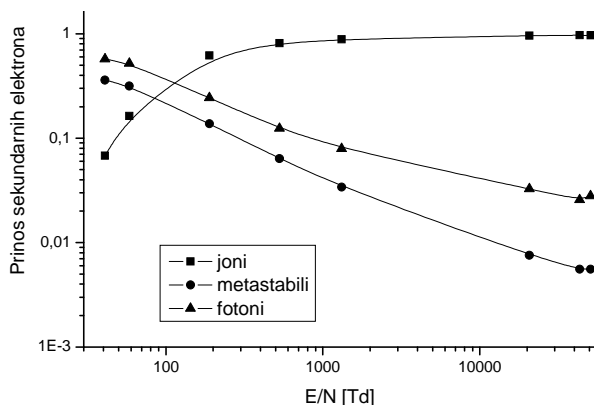
*Rad saopšten na skupu „Osma konferencija mladih istraživača“, Beograd, 21–23. decembar 2009.

Autor za prepisku: M.B. Savić, Institut za fiziku, Pregrevica 118, 11080 Beograd, Srbija.

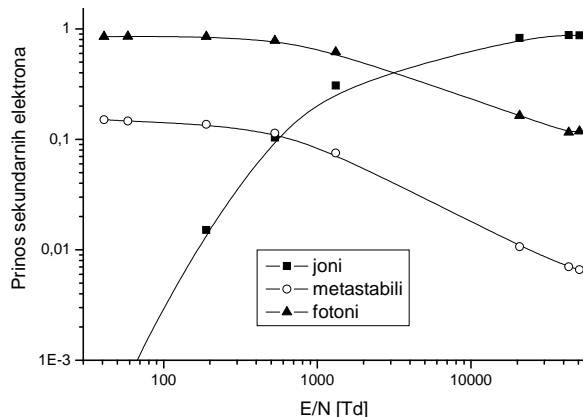
E-pošta: smarija@ipb.ac.rs

Rad primljen: 21. decembar 2009.

Rad prihvaćen: 29. decembar 2009.



Slika 4. Prinos sekundarnih elektrona u funkciji E/N za različite tipove čestica, za čiste površine.
Figure 4. Secondary electron yield as a function of E/N for different types of particles, clean surfaces.

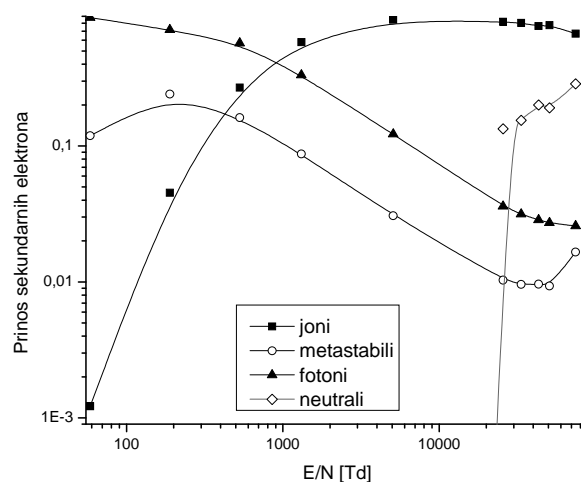


Slika 5. Prinos sekundarnih elektrona u funkciji E/N za različite tipove čestica, za neočišćene površine.
Figure 5. Secondary electron yield as a function of E/N for different types of particles, dirty surfaces.

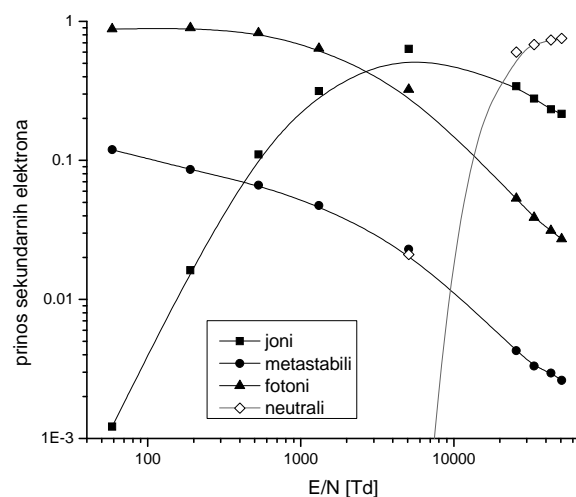
Nestajanje metastabila je usled „kaljenja“ (*quenching-a*) i pri prenosu količine kretanja (*momentum transfer-a*). Iz koda beležimo broj metastabila koji su udarili u katodu. Konačan prinos sekundarnih elektrona od metastabila dobijamo množenjem broja metastabila koji su došli do katode sa koeficijentom $\gamma = 0,02$. Grafici su dati na slikama 6 i 7 za očišćene i neočišćene površine, redom.

U narednom koraku uključili smo i refleksiju jona od katode i anode. Koeficijent refleksije iznosi $R = 0,5$. Rezultati dobijeni na ovaj način prikazani su na slikama 8 i 9 za čiste i neočišćene površine, redom. Uključivanjem refleksije jona od katode i anode očekivano je da se poveća uticaj jona na produkciju sekundarnih elektrona. Upoređivanjem slika 6 i 8 možemo zaključiti da na većim E/N , tj. manjim pritiscima, postoji blagi porast prinosa sekundarnih elektrona od strane jona. Slično razmatranje važi i u slučaju neočišćenih površina, što se ponovo zaključuje posmatranjem slika 7 i 9. Što se tiče metastabila, možemo primetiti da je prinos sekundarnih

elektrona od ovog tipa čestica nešto manji nego u slučaju kada nema refleksije. Ovo možemo objasniti na sledeći način: refleksija dovodi do povećanja broja sudara i samim tim povećanja broja jona. Samim tim imamo više elektron-jon sudara, tj. joni „troše“ elektrone. Kako znamo da metastabili nastaju direktnim pobuđivanjem elektrona na metastabilno stanje u sudarima elektron-atom pozadinskog gasa, to i prethodno razmatranje povlači manji broj metastabila.



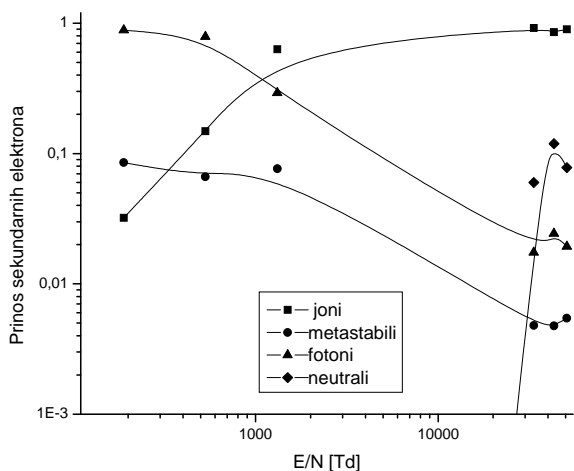
Slika 6. Prinos sekundarnih elektrona u funkciji E/N za različite tipove čestica, za čiste površine.
Figure 6. Secondary electron yield as a function of E/N for different types of particles, clean surfaces.



Slika 7. Prinos sekundarnih elektrona u funkciji E/N za različite tipove čestica, za neočišćene površine.
Figure 7. Secondary electron yield as a function of E/N for different types of particles, dirty surfaces.

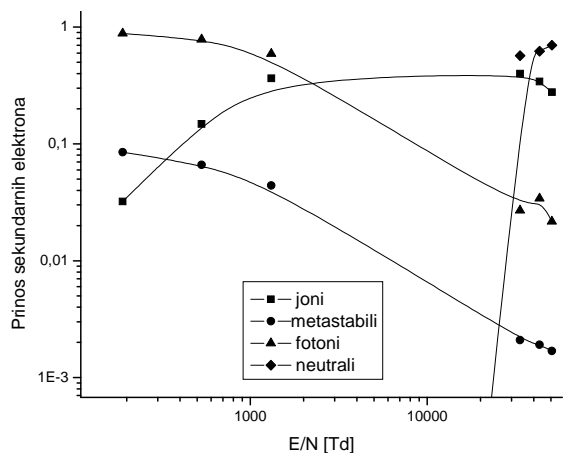
Ukoliko uporedimo prikazane rezultate sa graficima koje su dali Phelps i Petrović [4] možemo doći do određenih zaključaka. Prvi model je (gde je preraspodela metastabila na katodama 50%), kao što se očekivalo, dao rezultate koji dosta odstupaju od analitički

predviđenog rešenja u pomenutom radu. Međutim, može se ipak uočiti očekivani oblik krivih prinosa sekundarnih elektrona.



Slika 8. Prinos sekundarnih elektrona u funkciji E/N za različite tipove čestica, za čiste površine.

Figure 8. Secondary electron yield as a function of E/N for different types of particles, clean surfaces.



Slika 9. Prinos sekundarnih elektrona u funkciji E/N za različite tipove čestica, za neočišćene površine.

Figure 9. Secondary electron yield as a function of E/N for different types of particles, dirty surfaces.

Drugi model (metastabili su uključeni u Monte Karlo kod) značajno je bolji. Samim uključivanjem metastabila u Monte Karlo kod očekivali smo bolje slaganje, što se i pokazalo opravdanim. Konkretno, kriva koja predstavlja prinos sekundarnih elektrona od metastabila pokazuje dobro poklapanje u regionu srednjih E/N . Na manjim E/N , tj. većim pritiscima, model još uvek nije dobar, mada za očišćene površine postoji određen pad koji se i očekuje.

Kao dodatak, prikazan je i slučaj kada je uključena refleksija jona od elektroda. Dobijeni su rezultati koji su i očekivani u slučaju povećanja broja jona u pražnjenju.

Na osnovu prikazanih rezultata možemo uočiti, u skladu sa očekivanjima, da na malim vrednostima E/N

fotoni dominiraju u proizvodnji sekundarnih elektrona, dok je, na visokim vrednostima E/N , najveći doprinos neutrala. Za srednje vrednosti redukovano električnog polja, ne sme se zanemariti doprinos jona i metastabila u generisanju sekundarnih elektrona.

Uspeli smo da dobijemo zadovoljavajuće slaganje sa analitičkim rezultatima iz rada Phelps i Petrović [4]. Bez obzira na prikazane rezultate, postoji još dosta prostora za usavršavanje modela. Ono na čemu treba raditi je pre svega model metastabila. U sadašnji model uključena je samo produkcija metastabila direktnim pobuđivanjem na metastabilno stanje i u sudarima brzi neutral-pozadinski gas. Neophodno je uključiti u Monte Karlo kod još i kaskade, tj. relaksiranje pobuđenih stanja argona na metastabilna stanja kao još jedan proces produkcije metastabila.

Na čemu još treba raditi jeste i model fotona. Ideja je da se i fotoni uključe u Monte Karlo kod kao zaseban tip čestica i da se kao takvi prate tokom pražnjenja.

ZAKLJUČAK

U ovom radu učinjeni su početni koraci ka dobijanju modela koji će omogućiti izračunavanje parcijalnih prinosa sekundarnih elektrona za pojedinačne tipove čestica, korišćenjem Monte Karlo koda, koji je razvijen u Laboratoriji za gasnu elektroniku Instituta za fiziku u Zemunu. Ovaj model je dovoljan za više vrednosti E/N dok se za niže vrednosti mora još razviti model transporta fotona i formiranja molekularne emisije, a generalno se model tretiranja metastabila mora donekle poboljšati.

Zahvalnica

Ovaj rad je omogućen sredstvima Ministarstva za nauku i tehnološki razvoj, broj projekta: 141025. Autori duguju veliku zahvalnost Prof. dr Zoranu Lj. Petroviću na koncipiranju ideje i korisnim sugestijama tokom izrade ovog rada.

LITERATURA

- [1] Y.P. Raizer, Gas Discharges Physics, Springer, Berlin, 1991.
- [2] T. Makabe, Z.Lj. Petrović, Plasma Electronics: Applications in Microelectronic Device Fabrication, Taylor & Francis, New York, 2006.
- [3] M.A. Liberman, A.J. Lichtenberg, Plasma Discharges and Materials Processing, Wiley, New York, 1994.
- [4] A.V. Phelps, Z.Lj. Petrović, Plasma Sourc. Sci. Technol. **8** (1999) R21–R44.
- [5] Z.Lj. Petrović, V.D. Stojanović, J. Vac. Sci. Technol. A **16** (1998) 329–336.
- [6] Z.Lj. Petrović, Z. Ristivojević (to be submitted).
- [7] A.V. Phelps, Phys. Chem. Ref. Data **20** (1991) 557.
- [8] A.V. Phelps, J. Appl. Phys. **76** (1994) 747–753.
- [9] B.M. Smirnov, Physics Of Weakly Ionized Gases, Mir Publishers, Moscow, 1981.

SUMMARY**GAS DISCHARGES MODELING BY MONTE CARLO TECHNIQUE**

Marija Savić, Marija Radmilović-Rađenović

Institute of Physics Belgrade, Pregrevica 118, 11080 Belgrade, Serbia

(Scientific paper)

The basic assumption of the Townsend theory – that ions produce secondary electrons – is valid only in a very narrow range of the reduced electric field E/N . In accordance with the revised Townsend theory that was suggested by Phelps and Petrović, secondary electrons are produced in collisions of ions, fast neutrals, metastable atoms or photons with the cathode, or in gas phase ionizations by fast neutrals. In this paper we tried to build up a Monte Carlo code that can be used to calculate secondary electron yields for different types of particles. The obtained results are in good agreement with the analytical results of Phelps and Petrović (*Plasma Sources Sci. Technol.* **8** (1999) R1).

Ključne reči: Sekundarna emisija elektrona • Model Phelps–Petrović • Monte Karlo kod

Key words: Secondary electron emission • Phelps–Petrović model • Monte Carlo code

Breakdown Phenomena in Water Vapor Microdischarges

M. RADMILOVIĆ-RADJENOVIĆ, B. RADJENOVIĆ* AND M. SAVIĆ

Institute of Physics, Pregrevica 118, 11080 Belgrade, Serbia

The gas breakdown at the large gap sizes is reasonably well understood. However, the breakdown phenomenon in microgaps is still not sufficiently explored. The high electric fields realized in small gaps combined with the lowering of the potential barrier, seen by the electrons in the cathode as ion approaches lead to ion-enhanced field emission leading to deviations from the standard Paschen law. In this paper, semi-empirical expressions for the breakdown voltage based on the fitting of numerical solutions of the DC breakdown criteria in microdischarges have been derived. In the standard breakdown criteria the secondary emission coefficient that incorporates the enhancement of the secondary electron emission has been included. The obtained expressions can be used for determination the pressure and the gap dependence of the breakdown field strength in the water vapor, separately.

PACS numbers: 52.50.Qt, 52.65.Rr, 52.80.Pi

1. Introduction

In the past few decades the field of microdischarges have become more common in everyday life. Microplasmas encompass the advantages of low-pressure plasmas with the advantages of being micro [1–4]. Due to their portability and the non-equilibrium character of the discharges, microplasmas are finding application in many research disciplines, from the optimizing the plasma screens [5], localized silicon etching [6], tunable UV source [7], gas spectroscopy [8, 9], spectroscopy of water impurities [10], up to localized treatment of materials and assembly of nanostructures [11]. On the other hand, plasma-based microsystems can find application in bio microelectromechanical system (bio-MEMS) sterilization, small-scale materials processing and microchemical analysis systems [12]. However, integrability requires not only a reduction in size, but also an understanding of the physics governing the new small-scale discharges.

Making the gap small is the easiest way to obtain a big force, which is restricted by the electric field of breakdown [13, 14]. It is necessary to be aware of the breakdown voltage in microgaps. When changing the size of plasmas, there are scaling laws that are helpful in determining the operating parameters of various sizes of plasmas. The fact that microdischarges operate under conditions, where boundary effects dominate, indicates the importance of establishing scaling laws in a such small gaps. The best way is perhaps to start from the low pressure discharges and to employ the standard scaling laws [15]. The motivation for our studies, resulting from the fact that the electrical breakdown in microgaps occurs at voltages far below the pure Paschen curve mini-

mum and that the modified Paschen curve should be used instead for micron and sub-micron gaps [16]. Electrons from the field emission are one of the possible reasons why the breakdown and sparks occur in a vacuum, which of course is not possible if one only considers the Townsend avalanche mechanisms for the gas phase and the surface ionization that are normally used to generate the Paschen curve [17].

Microplasma can be generated in a wide range of the pressure. In the large scale systems, the experimentally observed Paschen law has been successfully explained by the Townsend theory [18]. The Paschen's law is based on the observation that, over a large range of the pressures and electrode separations, the probability of the ionization per collision in the gas and the probability of the production of electrons by ions by a secondary process are both dependent on the average kinetic energy of the electrons and ions and therefore on the reduced electric field E/N (the electric field E to the gas number ratio N) [19]. The Townsend mechanism by which successive ionizations of the gas molecules induce the gas breakdown describes the process satisfactorily at large separations [20]. The significant parameter is pd (the product of the gap distance and the pressure P). Typically, the Townsend's mechanism (and by extension Paschen's law) applies at pd products less than 1000 Torr cm, or gaps around a 1 cm at 1 atm [21].

The mechanism of the electrical breakdown is, however, completely different in microgaps [2, 3, 4, 14, 15]. A rapid fall of the breakdown voltage with decreasing the gap size may be attributed to the onset of the ion-enhanced field emission in microgaps. Violations of the similarity law take place for the left hand branch of the curve, for such pd values where the electron mean free path is comparable with the gap. When the electron mean free path is comparable with the electrode separa-

* corresponding author; e-mail: bradjeno@ipb.ac.rs

ration the electrical breakdown is based on the cathode-induced breakdown model.

Water vapour in the atmosphere is the key trace gas controlling weather and climate. It also plays a central role in atmospheric chemistry, influencing the heterogeneous chemical reactions that destroy stratospheric ozone. The effects of water vapour are large in the upper troposphere and lower stratosphere, but there are few measurements of water vapour concentrations and its long-term variation in this altitude only region. The influence of water vapour on the breakdown voltage of uniform field gaps has been investigated by Ritzl [22], who was found that the breakdown voltage in air increases by 2% for a change in the partial pressure of water vapour. Later on, some results indicated that the presence of water vapour raised the breakdown voltage by 2.7% above that of dry air [23]. Allen and Phillips [24] investigated the effect of humidity on the spark breakdown voltage. Recently, measurements have been performed for low-pressure breakdown in water vapor [25].

In this paper, high-pressure breakdown field strength in water vapor has been theoretically studied [26]. The expressions for the DC breakdown criteria including the ion-enhanced secondary emission coefficient has been numerically solved for water vapor in order to determine the breakdown voltage versus the gap spacing and the pressure, respectively. The results of this research can be applied in the construction of compact pulse power generators for bioelectric applications.

2. Semi-empirical expressions

Combining the expressions for the electron yield [13]:

$$\gamma = K e^{-D/E}, \quad (1)$$

and for the ionization coefficient [27]:

$$\alpha/p = A e^{-Bp/E}, \quad (2)$$

with the expression for the DC breakdown criteria:

$$\gamma (e^{\alpha d} - 1) = 1, \quad (3)$$

we obtain the transcendental equation [28]:

$$K e^{-D/E} \left(e^{A p d e^{-B p/E}} - 1 \right) = 1, \quad (4)$$

where the material dependent constant D can be calculated using the expression:

$$D = 6.85 \times 10^7 \phi^{3/2} / \beta, \quad (5)$$

knowing a field enhancement factor β and the work function of the metal ϕ expressed in eV. On the other hand, from the experimental values of the slope of the $\log \gamma$ versus $1/E$, the values of D were also determined for some materials, for example, aluminum, stainless steel and conventional steel (as can be seen, from Table I in Ref. [13]). In this paper we have used the value of 9.3×10^8 V/m that corresponds to the aluminum. Contrary, determination of the constant K that appears in Eqs. (1) and (4) may be quite difficult, especially if there are additional complications due to electron attachment, ionization by metastables, ect. [14]. In practice, the constant K can be found from the ratio of the field emis-

sion current density to the positive ion current density onto the cathode. A and B are gas dependent constants that can be found elsewhere [27]. The expressions for the breakdown field strength will be determined by solving transcendental Eq. (4) numerically by using the package Mathematica and then by fitting these solutions.

3. Results and discussion

For a fixed pressure, the transcendental Eq. (4) has been numerically solved by varying the interelectrode distance d . The obtained numerical solutions for the breakdown field strength E against the gap size d are shown in Fig. 1. These values can be fitted by a simple formula:

$$E = a d^{-1} + b \times d^c, \quad (6)$$

where the fitting coefficients a , b and c , for the a few pressures are listed in Table I.

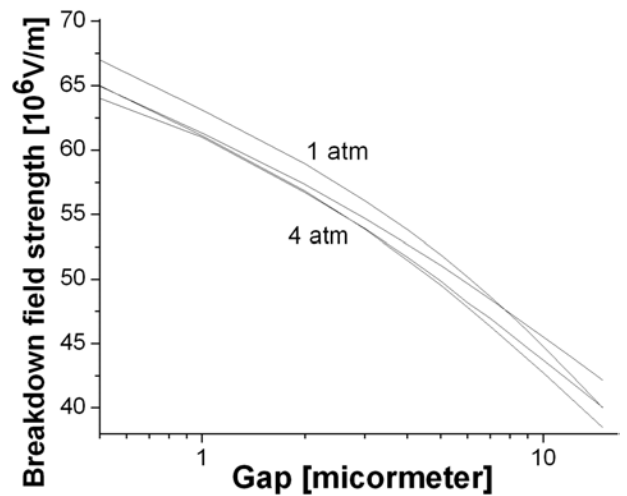


Fig. 1. The breakdown field strength versus the gap spacing for pressure in the range from 1 atm up to 4 atm. The gap was varied between $0.5 \mu\text{m}$ up to $15 \mu\text{m}$.

TABLE I

Fitting coefficients for the Eq. (6) for various values of the pressure.

Pressure [atm]	a	b	c
1	-26.122	90.012	-0.281
2	-20.662	82.597	-0.267
3	-14.906	76.304	-0.228
4	-11.456	73.16	-0.196

As can be seen from Fig. 1, the breakdown field strength defined as the ration of the breakdown voltage and the gap size strongly depends on the interelectrode separation. For gaps less than $5 \mu\text{m}$, the breakdown phenomena are attributed to the ion-enhanced field emission [14]. At large separations, however, processes in

TABLE II
The Values of the fitting coefficients m and n , for a few gap sizes, in Eq. (7).

Gap [μm]	m	n
0.5	90.188	-0.0442
1	85.898	-0.0456
2	83.266	-0.052
4	82.527	0.0574

the gas cause breakdown rather than secondary electron emission.

In a similar way, for a fixed gap sizes, the transcendental Eq. (4) has also been solved by varying the gas pressure, in order to obtain the pressure dependence of the electric field strength. Numerical solutions are presented in Fig. 2 and fitted by using expression:

$$E = m \cdot p^n, \quad (7)$$

with fitting coefficient m and n given in Table II.

Figure 2 clearly illustrates the weak dependence of the breakdown field strength on the pressure, even for the gaps of the order of a few micrometers. Such trend in the curves presented in Fig. 2 can be explained by the exponential dependence of the ion-enhanced field emission on the electric field and not on the pressure.

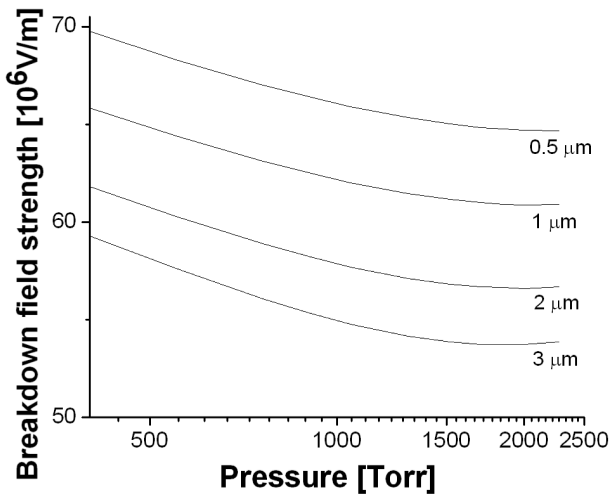


Fig. 2. The breakdown field strength as a function of the gas pressure for the gaps from 0.5 to 3 μm .

4. Conclusion

This paper contains theoretical studies of the breakdown field strength in the microgaps. Departures from the large scale similarity laws are expected with the onset of field emission on such small gaps indicating that Townsend mechanism is not sufficient to explain the breakdown mechanism. The semi-empirical expressions

for the breakdown field strength suggested here are based on the fit of the numerical solutions of the breakdown criteria including field emission effects in microgaps. The new breakdown field curve obtained, when the field emissions are accounted for, retains the right branch of the conventional Paschen curve, i.e. field emissions can be neglected in large gaps. The left branch, however, is substituted by a rapid decrease of the breakdown voltage and increases in the breakdown field strength below the minimum of the conventional Paschen curve. This reduction in the breakdown voltage is observed for gap sizes smaller than 5 μm and is a direct consequence of the onset of field emissions.

The results of our studies should be useful for determining minimum ignition voltages in microplasma sources as well as the maximum safe operating voltage and critical dimensions in other microdevices.

Acknowledgments

The authors acknowledge financial support of the Ministry of Science of the Republic of Serbia 141025.

References

- [1] J.M. Thores, R.S. Dhariwal, *Nanotechnology* **10**, 102 (1999).
- [2] M. Radmilović-Radjenović, J.K. Lee, F. Iza, G.Y. Park, *J. Phys. D, Appl. Phys.* **38**, 950 (2005).
- [3] M. Radmilović-Radjenović, B. Radjenović, *Contrib. Plasma Phys.* **47**, 165 (2007).
- [4] M. Radmilović-Radjenović, B. Radjenović, *Plasma Sources Sci. Technol.* **16**, 337 (2007).
- [5] S.S. Yang, J.K. Lee, S.W. Ko, H.C. Kim, J.W. Shon, *Contrib. Plasma Phys.* **44**, 536 (2004).
- [6] H. Wang, G. Li, L. Jia, L. Li, G. Wang, *Chem. Commun. (Camb)* **7**, 3786 (2009).
- [7] P. Kurunczi, J. Lopez, H. Shah, K. Becker, *International Journal of Mass Spectroscopy* **205**, 277 (2001).
- [8] T. Svensson, M. Andersson, L. Rippe, J. Johansson, S. Folestad, S. Andersson-Engels, *Opt. Lett.* **33**, 80 (2008).
- [9] M. Saito, T. Hiraga, M. Hattori, S. Murakami, T. Nakai, *Magn. Reson. Imaging* **23**, 607 (2005).
- [10] L. Que, C.G. Wilson, Y.B. Gianchandani, *J. Microelectromech. Syst.* **14**, 185 (2005).
- [11] A.K. Chakraborty, A.J. Golumbskie, *Annual Review of Physical Chemistry* **52**, 537 (2001).
- [12] W.K.T. Coltro, *Química Nova* **30**, 1986 (2007).
- [13] W.S. Boyle, P. Kisliuk, *Phys. Rev.* **97**, 255 (1955).
- [14] M. Radmilović-Radjenović, B. Radjenović, *Plasma Sources Sci. Technol.* **17**, 024005 (2008).
- [15] Z.Lj. Petrović, N. Škoro, D. Marić, C.M.O. Mahony, P.D. Maguire, M. Radmilović-Radenović, G. Malović, *J. Phys. D, Appl. Phys.* **41**, 194002 (2008).
- [16] L.H. Germer, *J. Appl. Phys.* **30**, 46 (1959).
- [17] P. Kisliuk, *J. Appl. Phys.* **30**, 51 (1959).
- [18] F. Paschen, *Wied. Ann.* **37**, 69 (1889).

- [19] L.B. Loeb, *Fundamental Processes of Electrical Discharges in Gases*, J. Wiley and Sons, Inc., New York (1939).
- [20] J.M. Meek, J.D. Craggs, *Electrical breakdown of gases*, Oxford University Press, (1953).
- [21] M.A. Lieberman, A.J. Lichtenberg, *Principles of Plasma Discharges and Materials Processing* 2nd ed. Wiley Interscience, Hoboken, NJ: Wiley, (2005).
- [22] H. Ritz, *Archiv fur Elektrotechnik* **26**, 219 (1932).
- [23] W. Kohrman, *Ann. d. Phys.* **18**, 379 (1956).
- [24] K.R. Allen, K. Phillips, *Nature* **183**, 174 (1959).
- [25] D. Marić, N. Škoro, G. Malović, Z.Lj. Petrović, Proceedings of the 29th ICPIG, Cancun Mexico, (12–17 July 2009), PA8-5 (2009).
- [26] M. Radmilović-Radjenović, B. Radjenović, Contributed papers of 24th Summer School and International Symposium on the Physics of Ionized Gases, Novi Sad, Serbia (25–29 August 2008) 379 (2008).
- [27] D. Marić, M. Radmilović-Radjenović, Z.Lj. Petrović, *EPJ D* **35**, 313 (2005).
- [28] M. Radmilović-Radjenović, B. Radjenović, *Europhys. Lett.* **83**, 25001 (2008).